NASA Tech Briefs

National
Aeronautics and
Space
Administration

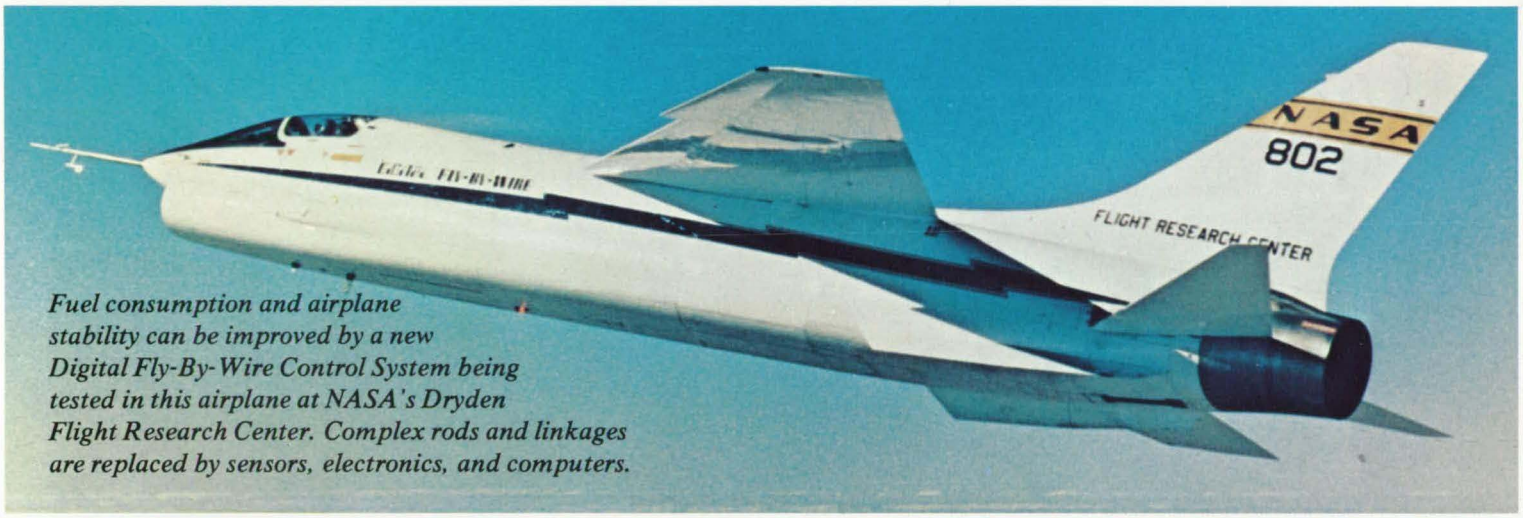

Fuel consumption and airplane stability can be improved by a new Digital Fly-By-Wire Control System being tested in this airplane at NASA's Dryden Flight Research Center. Complex rods and linkages are replaced by sensors, electronics, and computers.

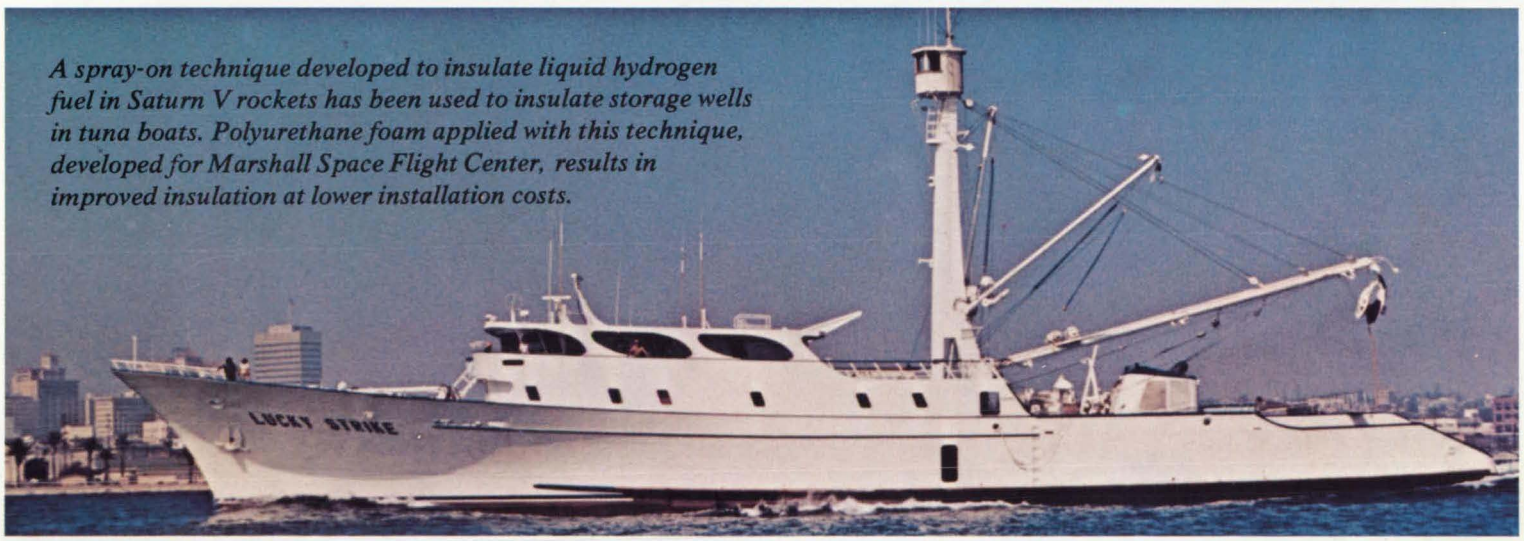

A spray-on technique developed to insulate liquid hydrogen fuel in Saturn V rockets has been used to insulate storage wells in tuna boats. Polyurethane foam applied with this technique, developed for Marshall Space Flight Center, results in improved insulation at lower installation costs.

Clean-room technology employing laminar flow techniques has been adapted to produce air purifiers for toll booths in Washington State. Booth operators are protected from poisonous exhaust fumes with draft-free high-volume purifiers.

Vol. 3, No. 1

SPRING 1978

About the NASA Technology Utilization Program

The National Aeronautics and Space Act of 1958, which established NASA and the United States civilian space program, requires that "The Administration shall provide for the widest practicable and appropriate dissemination of information concerning its activities and the results thereof."

To help carry out this objective the NASA Technology Utilization (TU) Program was established in 1962. It offers a variety of valuable services to facilitate the transfer of aerospace technology to nonaerospace applications, thus assuring American taxpayers maximum return on their investment in space research; thousands of spinoffs of NASA research have already occurred in virtually every area of our economy.

The TU Program has worked for engineers, scientists, technicians, and businessmen. And it can work for you.

NASA Tech Briefs

Tech Briefs is published quarterly and is free to any U.S. citizen or organization. It is both a current-awareness medium and a problem-solving tool. Potential products ... industrial processes ... basic and applied research ... shop and lab techniques ... computer software ... new sources of technical data ... concepts ... you will find them all in NASA Tech Briefs. The first section highlights a few of the potential new products contained in Tech Briefs. The remainder of the volume is organized by technical category to help you quickly review new developments in your areas of interest. Finally, a subject index makes each issue a convenient permanent reference file.

Further Information on Innovations

Although many articles are complete in themselves, others are backed up by Technical Support Packages (TSP's). TSP's are available without charge and may be ordered by simply completing the enclosed TSP Request Card. Further information on some innovations is available for a nominal fee from other sources, as indicated at the ends of the articles. In addition, Technology Utilization Officers at NASA Field Centers will assist you directly when necessary. (See page A4.)

Patent Licenses

Many of the inventions described are under consideration for patents or have been patented by NASA. Unless NASA has decided not to apply for a patent, the patent status is described at the end of each article. For further information about the Patent Program see page A8.

Other Technology Utilization Services

To assist engineers, industrial researchers, business executives, city officials, and other potential users in applying space technology to their problems, NASA sponsors six Industrial Applications Centers. Their services are described on page A6. In addition, an extensive library of computer programs is available through COSMIC, the Technology Utilization Program's outlet for NASA-developed software. (See page A5.)

Applications Program

To help solve public-sector problems in such areas as safety, health, transportation, and environmental protection, NASA TU Applications Teams, staffed by professionals from a variety of disciplines, work with Federal agencies, local governments, and health organizations to identify critical problems amenable to technical solutions. Among their many significant contributions are a rechargeable heart pacemaker, a lightweight fireman's breathing apparatus, aids for the handicapped, and safer highways.

Reader Feedback

We hope you find the information in NASA Tech Briefs useful. A reader feedback card has been included because we want your comments and suggestions on how we can further help you apply NASA innovations and technology to your needs. Please use it, or if you need more space, write us a letter.

NASA Tech Briefs

National Aeronautics and Space Administration

SPRING 1978
Volume 3, Number 1

COVERS: The photographs on the front and back covers illustrate recent developments by NASA and its contractors that resulted in commercial and nonaerospace spinoffs. You can use the TSP Request Card at the end of this issue to learn more about the Digital Fly-By-Wire Control System [Circle 80], Spray-On Foam Insulation Technique [Circle 81], Air Purification System [Circle 82], and Filament-Wound Pressure Vessels [Circle 83].

About This NASA Publication

NASA Tech Briefs, a quarterly publication, is distributed free to U.S. citizens to encourage commercial application of U.S. space technology. For information on publications and services available through the NASA Technology Utilization Program, write to the Director, Technology Utilization Office, P. O. Box 8757, Baltimore/Washington International Airport, Maryland 21240.

"The Administrator of National Aeronautics and Space Administration has determined that the publication of this periodical is necessary in the transaction of the public business required by law of this Agency. Use of funds for printing this periodical has been approved by the Director of the Office of Management and Budget through December 31, 1978."

Change of Address

Change of Address: If you wish to have NASA Tech Briefs forwarded to your new address, use one of the Subscriptions cards enclosed in the back of this volume of NASA Tech Briefs. Be sure to check the appropriate box indicating change of address.

Communication Concerning Editorial Matter

For editorial comments or general communications about NASA Tech Briefs, you may use the self-addressed Feedback card in the back of NASA Tech Briefs, or write to: The Publications Manager, Technology Utilization Office (Code KT), NASA Headquarters, Washington, DC 20546. Technical questions concening specific articles should be directed to the Technology Utilization Officer of the sponsoring NASA Center (addresses listed on page A4.)

NASA TU SERVICES

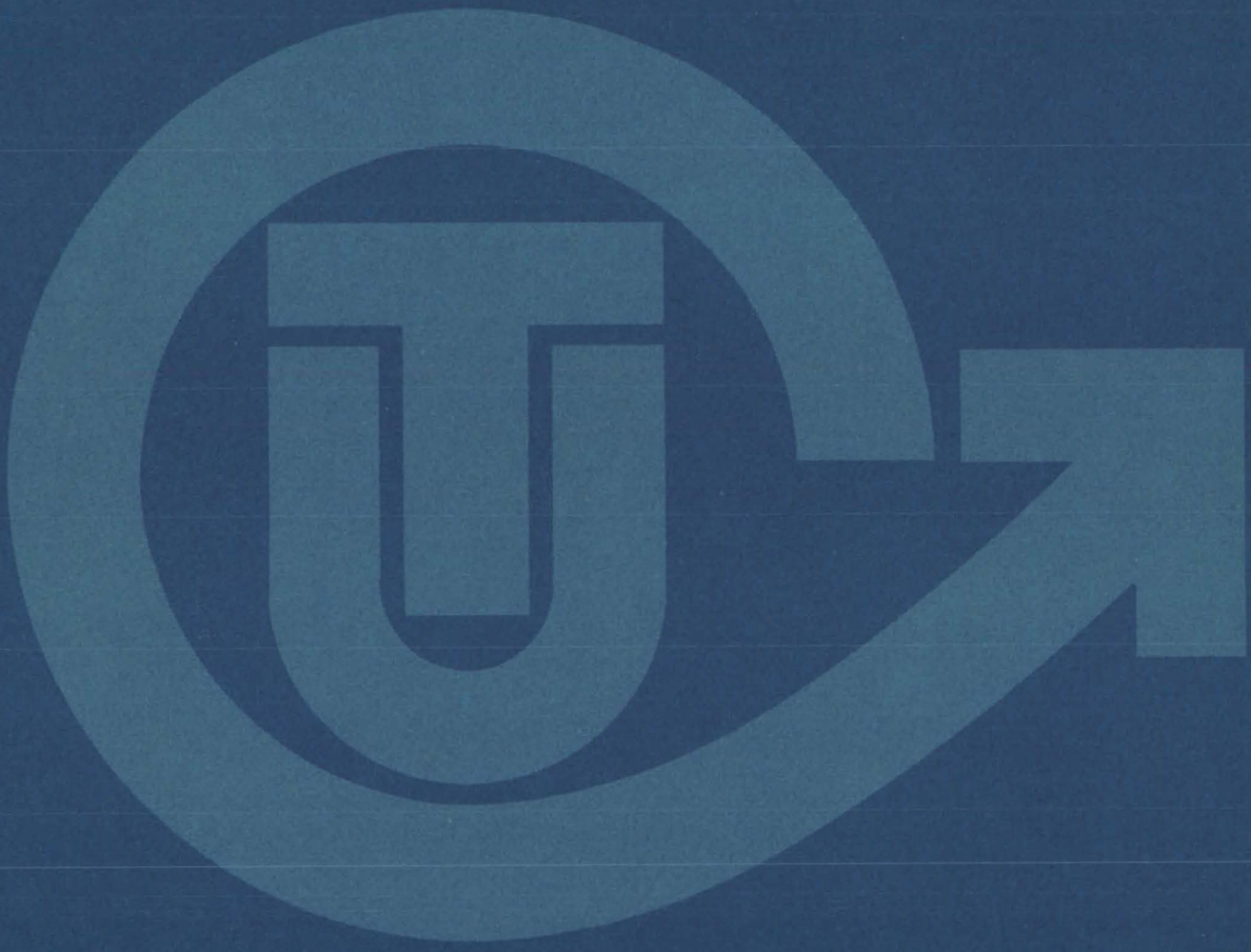

THE NASA TECHNOLOGY UTILIZATION OFFICERS

They will help you apply the innovations described in Tech Briefs.

The Technology Utilization Officer (TUO)
Each NASA Center has a Technology Utilization Officer — An applications engineer whose job is to help you make use of new technology developed at his center. He brings you the NASA Tech Briefs and other special publications, sponsors conferences, and arranges for expert assistance in solving technical problems.

Technical Assistance
Working together with NASA Scientists and Engineers and the Industrial Applications Centers, the center TUO's can answer specific questions about innovations and related NASA technology.

Technical Support Package (TSP's)
For many of the innovations described in Tech Briefs, the center TUO has prepared additional material that will help you in detailed evaluation and actual use or construction of the new technology. You may get TSP's free of cost by using the TSP Request Card or writing the center TUO.

Who to Contact. Of course, many technical questions about Tech Briefs are answered in the TSP's, but when no TSP is available, or you have further questions, write the Technology Utilization Officer at the center that sponsored the research at the address listed below.

Charles C. Kubokawa
Ames Research Center
Code AU: 240-2
Moffett Field, CA 94035
(415) 965-5554

Donald S. Friedman
Goddard Space Flight Center
Code 702.1
Greenbelt, MD 20771
(301) 982-6242

John T. Wheeler
Johnson Space Center
Code AT3
Houston, TX 77058
(713) 483-3809

Raymond J. Cerrato
John F. Kennedy Space Center
Code SA-RTP
Kennedy Space Center, FL 32899
(305) 867-2780

John Samos
Langley Research Center
Mail Stop 139A
Hampton, VA 23665
(804) 827-3281

Paul Foster
Lewis Research Center
21000 Brookpark Rd.
Cleveland, OH 44135
(216) 433-4000, Ext. 6832

Aubrey D. Smith
Marshall Space Flight Center
Code AT01
Marshall Space Flight Center, AL 35812
(205) 453-2224

John C. Drane
NASA Resident Legal Office-JPL
4800 Oak Grove Drive
Pasadena, CA 91103
(213) 354-6420

Gilmore H. Trafford
Wallops Flight Center
Wallops Island, VA 23337
(804) 824-3411, Ext 201

Louis Mogavero, Chief
Technology Utilization Branch
Code ETU-6
NASA Headquarters
Washington, DC 20546
(202) 755-2220

COSMIC

(Computer Software Management & Information Center)

AN ECONOMICAL SOURCE OF COMPUTER PROGRAMS DEVELOPED BY THE GOVERNMENT.

COSMIC is sponsored by NASA to give you access to over 1400 computer programs developed by NASA and the Department of Defense, and selected programs from other government agencies. It is one of the Nation's largest software libraries.

COSMIC charges very reasonable fees for programs to help cover part of their expenses—and NASA pays for the remainder. Programs generally cost from $500 to $1000, but a few are more expensive and many are less. Documentation is available separately and very inexpensively.

COSMIC collects and stores software packages, insures that they are complete, prepares special announcements (such as Tech Briefs), publishes an indexed software catalog, and reproduces programs for distribution. COSMIC helps customers to identify their software needs, follows up to determine the successes and problems, and provides updates and error corrections. In some cases, NASA engineers can offer guidance to users in installing or running a program.

COSMIC programs range from management (pert scheduling) to information science (retrieval systems) and computer operations (hardware and software). Hundreds of engineering programs perform such tasks as structural analysis, electronic circuit design, chemical analysis, and design of fluid systems. Others determine building energy requirements, optimize mineral exploration, and draw maps of water-covered areas using NASA satellite data. In fact, the chances are, if you use a computer, you can use COSMIC.

COSMIC is eager to help you get the programs you need. For more information about services or software available from COSMIC, fill out and mail the COSMIC Request Card in this issue.

COSMIC: Computer Software Management and Information Center

Suite 112, Barrow Hall, University of Georgia, Athens, Georgia 30602 Phone: (404) 542-3265

WHERE IS THE WORLD'S LARGEST BANK OF TECHNICAL DATA

?

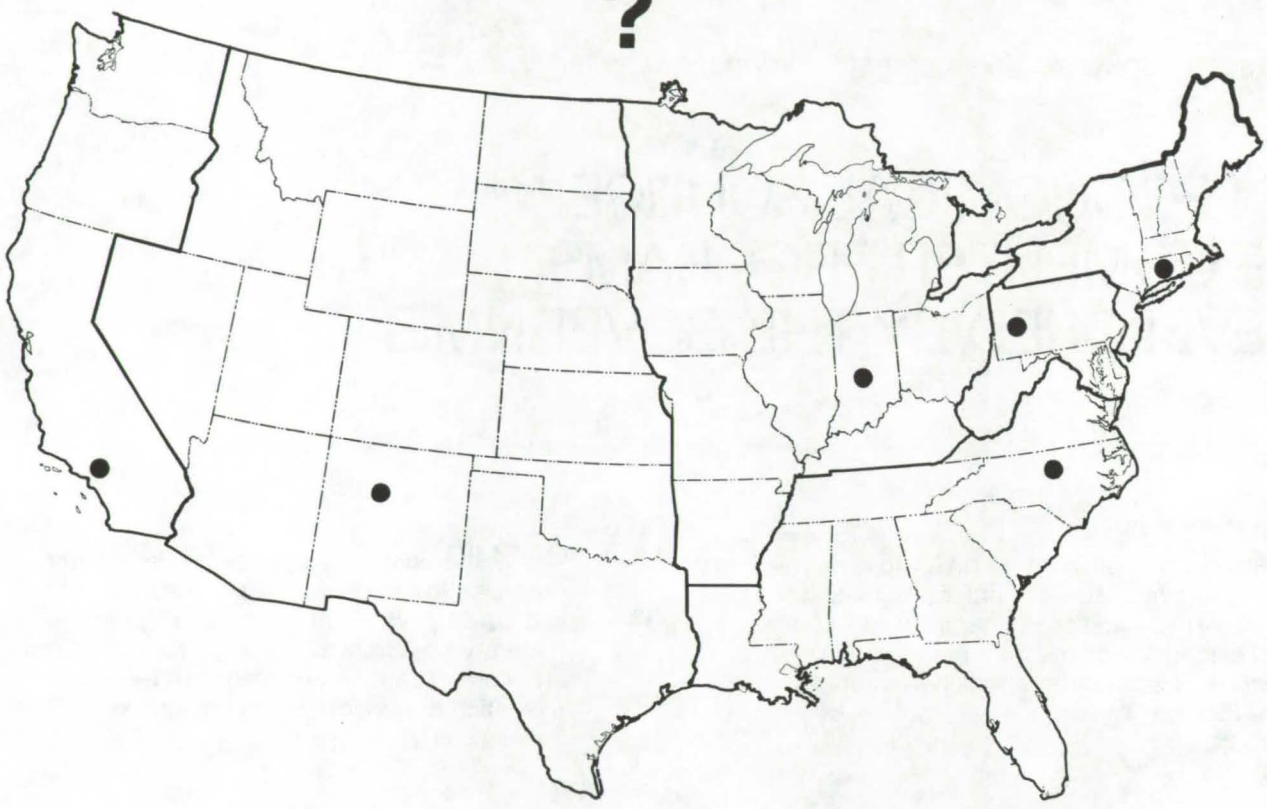

It's in Indianapolis and Pittsburgh, it's in Storrs, Connecticut and Research Triangle Park, North Carolina; and it's in Albuquerque and Los Angeles.

NASA IAC's — INDUSTRIAL

You can get more information and more data on more technical subjects through NASA's network of IAC's than anywhere else in the world. About 8,000,000 documents and growing at the rate of 50,000 more each month!

Major sources include:

- 750,000 NASA Technical Reports
- Selected Water Resources Abstracts
- NASA Scientific and Technical Aerospace Reports
- Air Pollution Technical Information Center
- NASA International Aerospace Abstracts
- Chem Abstracts Condensates
- Engineering Index
- Energy Research Abstracts
- NASA Tech Briefs
- Government Reports Announcements

and many other specialized files on food technology, textile technology, metallurgy, medicine, business, economics, social sciences, and physical science.

The IAC's are one of the most economical ways of staying competitive in today's world of exploding technology. The help available from the network ranges from literature searches through expert technical assistance.

Literature Searches
Help in designing your search, typically from 30 to 300 abstracts in as narrow or broad an area as you need, and complete reports when you need them. The most complete "search before research" available!

Current Awareness
Consult with our applications engineers to design your personal program — selected monthly or quarterly abstracts on new developments in your speciality. It's like having your own journal!

Technical Assistance
Our applications engineers will help you evaluate and apply your literature-search results. They can help find answers to your technical problems and put you in touch with scientists and engineers at NASA Field Centers.

To obtain more information about how NASA's IAC's can help you —
Check the IAC box on the TSP Request Card in this issue,
Or write or call the IAC nearest you.

APPLICATIONS CENTERS

How to get reports and other documents discussed in this issue of Tech Briefs

Many of the innovations in Tech Briefs are described in detail in reports available at a reasonable cost through one or more of the IAC's. To order a report, call or write the IAC referenced at the end of the Tech Brief article at the address below. Be sure to list the titles and accession numbers (N76-..., N75-..., etc.) of those you wish to purchase.

Aerospace Research Application Center (ARAC)
Indiana University-Purdue University at Indianapolis
1201 E. 38th St.
Indianapolis, IN 46205
E. Guy Buck, Director
(317) 264-4644

Knowledge Availability Systems Center (KASC)
University of Pittsburgh
Pittsburgh, PA 15260
Dr. Edmond Howie, Director
(412) 624-5211

New England Research Application Center (NERAC)
Mansfield Professional Park
Storrs, CT 06268
Dr. Daniel U. Wilde, Director
(203) 486-4533

North Carolina Science & Technology
Research Center (NC/STRC)
P. O. Box 12235
Research Triangle Park, NC 27709
Peter J. Chenery, Director
(919) 549-0671

Technology Application Center (TAC)
University of New Mexico
Albuquerque, NM 87131
Stanley A. Morain, Director
(505) 277-4000

Western Research Application Center (WESRAC)
901 Exposition Boulevard, Room 205
University of Southern California
University Park
Los Angeles, CA 90007
Radford King, Director
(213) 741-6132

NASA INVENTIONS AVAILABLE FOR LICENSING

Over 3,500 NASA inventions are available for licensing in the United States - both exclusive and nonexclusive.

Nonexclusive Licenses

Nonexclusive licenses for commercial use are encouraged to promote competition and to achieve the widest use of inventions. They must be used by a negotiated target date but are usually royalty free.

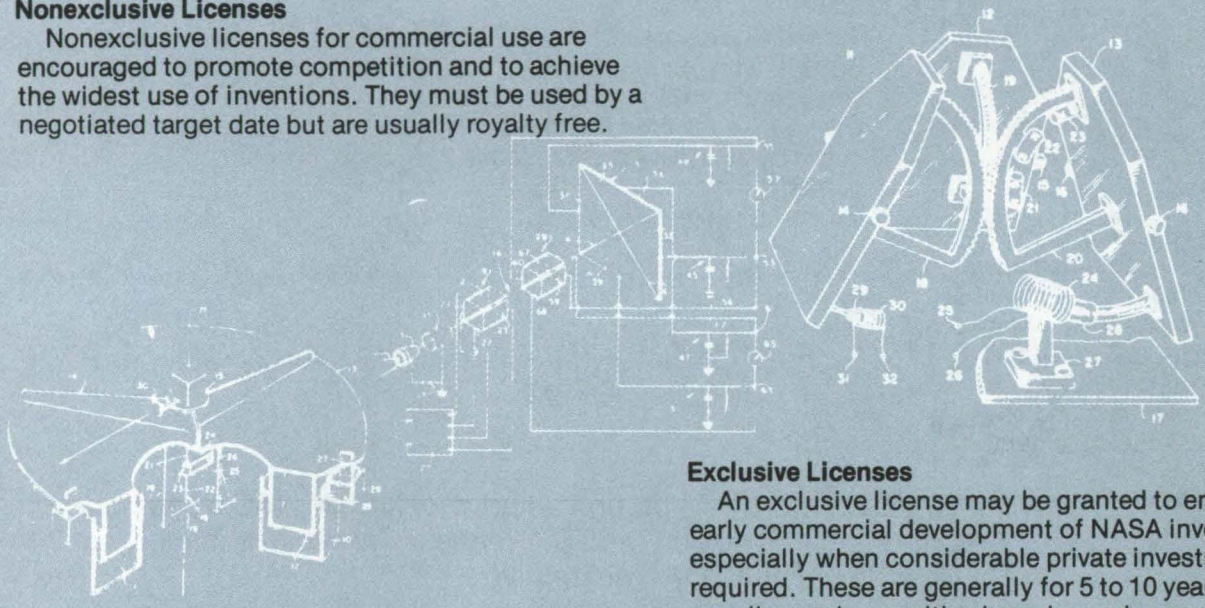

Exclusive Licenses

An exclusive license may be granted to encourage early commercial development of NASA inventions, especially when considerable private investment is required. These are generally for 5 to 10 years and usually require royalties based on sales or use.

The NASA patent licensing program also provides for licensing of NASA-owned foreign patents. In addition to inventions described in Tech Briefs, "NASA Patent Abstract Bibliography," containing abstracts of all NASA inventions, can be purchased from: National Technical Information Service, Springfield, Va., 22161. This document is updated semi-annually.

Patent Licenses and the NASA Tech Brief

Many of the inventions reported in Tech Briefs are patented or are under consideration for a patent at the time they are published. When this is the case, the current patent status is described at the end of the article; otherwise, there is no statement about patents. **If you want to know more about the patent program or are interested in license for a particular invention, write the Patent Counsel at the NASA Field Center** that sponsored the research. Be sure to refer to the NASA reference number in parenthesis at the end of the Tech Brief.

Robert F. Kempf
NASA Headquarters, Code GP-4
400 Maryland Ave., S.W.
Washington, DC 20546
(202) 755-3932

Darrell G. Brekke
Ames Research Center
Mail Code: 200-11A
Moffett Field, CA 94035
(415) 965-5104

John O. Tresansky
Goddard Space Flight Center
Mail Code: 204
Greenbelt, MD 20771
(301) 982-2351

Marvin F. Matthews
Lyndon B. Johnson Space Center
Mail Code: AM
Houston, TX 77058
(713) 483-4871

James O. Harrell
John F. Kennedy Space Center
Mail Code: SA-PAT
Kennedy Space Center, FL 32899
(305) 867-2544

Howard J. Osborn
Langley Research Center
Mail Code: 279
Hampton, VA 23665
(804) 827-3725

Norman T. Musial
Lewis Research Center
Mail Code: 500-311
21000 Brookpark Road
Cleveland, OH 44135
(216) 433-4000

Leon D. Wofford, Jr.
Marshall Space Flight Center
Mail Code: CC01
Marshall Space Flight Center, AL 35812
(205) 453-0020

Monte F. Mott
NASA Resident Legal Office
4800 Oak Grove Drive
Pasadena, CA 91103
(213) 354-2700

NEW PRODUCT IDEAS

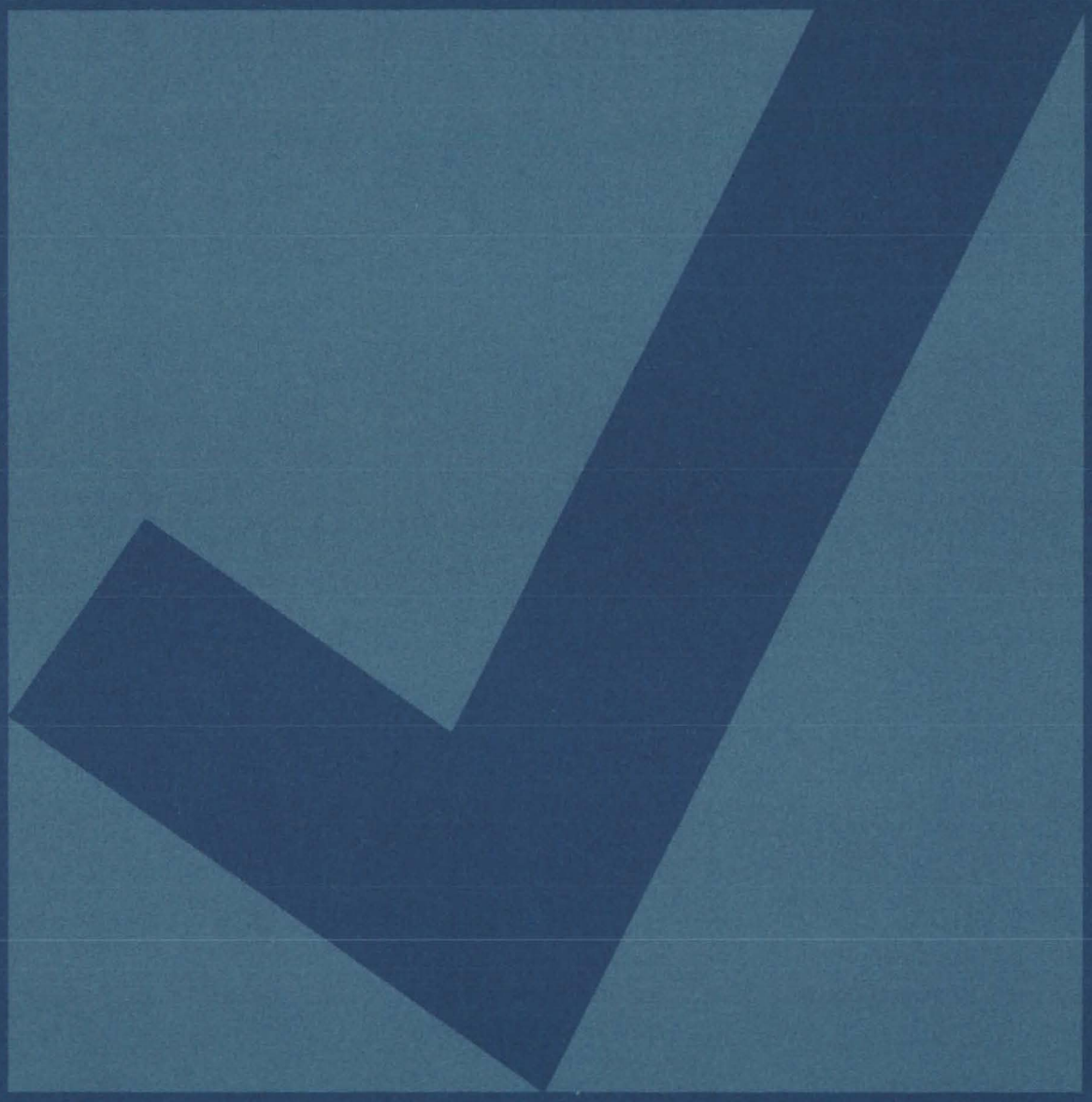

NEW PRODUCT IDEAS are just a few of the many innovations described in this issue of NASA Tech Briefs and having promising commercial applications. Each is discussed further on the referenced page in the appropriate section in this issue. If you are interested in developing a product from these or other NASA innovations, you can receive further technical information by requesting the TSP referenced at the end of the full-length article or by writing the Technology Utilization Office of the sponsoring NASA center (see page A4). NASA's patent-licensing program to encourage commercial development is described on page A8.

Safety Tent

A safety tent for enclosing a cryostat located inside a building prevents toxic or explosive vapors from entering the building atmosphere. A similar design could be used for other applications in which hazardous vapors are generated in enclosed areas. The tent is supported by a lightweight sectional framework that is sized for convenient storage. The covering is made from a clear transparent vinyl for maximum transmission of light. A collar that attaches to a hose leading to an airblower is included. Casters support the frame posts to allow the tent to be moved easily from one area to another.
(See page 88.)

Tool Simplifies Weld Preparation in Aluminum

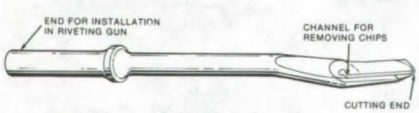

A special cutting tool prepares aluminum for welding quickly, easily, and cleanly. The tool, a chisel that is installed in a pneumatic riveting gun, has a V-shaped cutting end that slopes slightly to the rear for easy penetration of the material. It contains a channel for efficient removal of the cuttings. The tool can be used to cut a V-groove that allows the weld zone to penetrate the base material; it can also dislodge cracked or porous material. The midsection of the tool is bent slightly for easier access to the work.
(See page 139.)

Instrument for Measuring Organics in Water

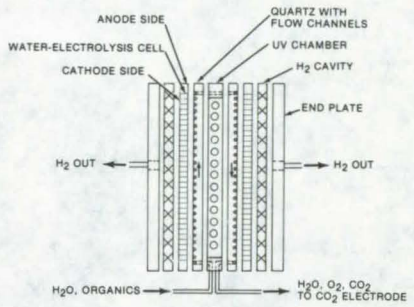

An instrument for determining the total organic carbon concentration in water uses no corrosive reagents or gases. Instead a continuous ultraviolet photolysis process converts organic compounds to carbon dioxide. A CO_2 electrode is used to measure the CO_2 content. The only reagent necessary is oxygen, generated in situ by electrolyzing some of the water. In addition to applications in the aerospace industry, the system has potential uses in pollution monitoring and in laboratory analyses.
(See page 55.)

Dip-Molded T-Shaped Cannula

A new cannula, fabricated out of polyetherurethane, has been designed for long-term service. The improved cannula is T-shaped to collect blood from both directions, thus replacing the two conventional cannulas that are usually required and eliminating the need for a large surgical wound. It is fabricated by using a new dip-molding process that can be adapted to other elastomeric objects having complex shapes. The dimensions of the cannula were chosen to optimize its blood-flow properties and to reduce the danger of excessive clotting, making it suitable for continuous service up to 21 days in the vein or artery of a patient.
(See page 68.)

Low-Intensity X-Ray and Gamma-Ray Imaging Device

A new low-dosage, low-power, X-ray system can be made completely self-contained, allowing fluoroscopy and radiography to be carried out in field and remote locations. The new device, known as a "Lixiscope," can be used with a conventional X-ray machine turned down to a low level, or, it can be operated with a radioisotope source for hand-held portable applications.

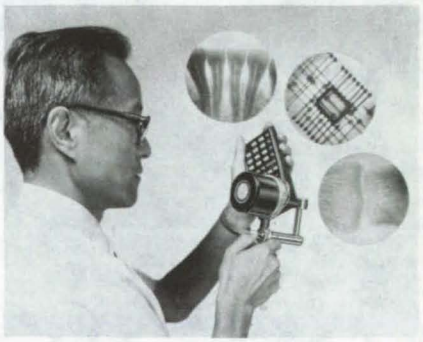

Originally developed for X-ray astronomy, the Lixiscope obtains its high sensitivity by using intermediate stages of photoelectron conversion and electron amplification to generate an image suitable for direct viewing or for recording on film.
(See page 67.)

Flat-Plate Heat Pipe

A new heat pipe has its working fluid sealed between two flat panels rather than in the conventional cylindrical housing. A metal wick is installed between the planes to provide a continuous fluid path in cooperation with capillary grooves on the inside surfaces of the plates.

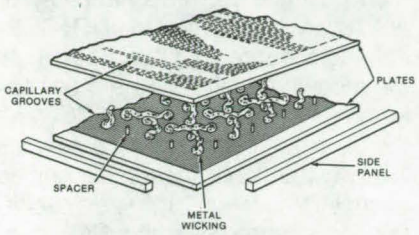

The new heat pipe is easily coupled to flat surfaces such as integrated circuit substrates, mirrors, and electronic cold plates and would be more effective than conventional heat pipes when removing heat in these applications.
(See page 43.)

"Nonfloating" Universal Joint

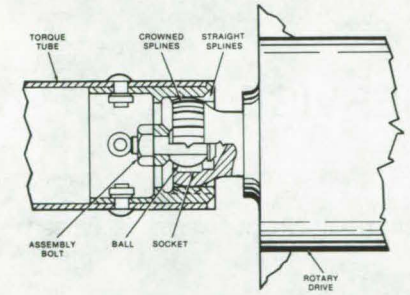

A new coupling uses a ball and socket within a crowned spline to form an exceptionally-tight universal joint. The novel design is lightweight and durable and requires a minimum of parts. Since the joint does not use elastomers or other cushions to limit play, it will function over a wide range of temperatures. The joint may be used to connect a drive motor to a driven shaft, while allowing for misalinements, or as a coupling between sections of a segmented torque tube. Other applications are possible where rotary motion is to be transmitted with high axial and radial stability.
(See page 115.)

Portable Spark-Gap Arc Generator

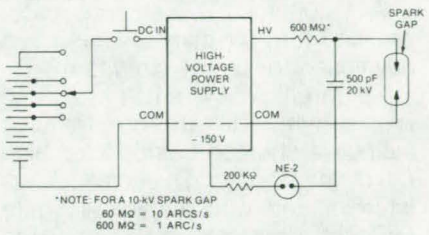

A self-contained spark generator that simulates the electrical noise caused by the discharge of static charge can be a useful tool when checking sensitive components and equipment. In a test setup, the device can introduce repeatable noise pulses as the behavior of the component is monitored. The generator uses only standard commercial parts and weighs only 4 pounds; a portable dc power supply is used. Two configurations of the generator have been developed; one is a free-running arc source, and the other delivers a spark in response to a triggering pulse.
(See page 10.)

Fire-Retardant Foams

A new family of polyimide resins are being developed as foams with exceptional fire-retardant properties. The foams are potentially useful for seat cushions in aircraft and ground vehicles and for applications such as home furnishings and building-construction materials. The basic formulations can be modified with reinforcing fibers or fillers to produce celular materials for a variety of applications. By selecting the reactants, the polymer structure can be modified to give foams with properties ranging from high resiliency and flexibility to brittleness and rigidity.
(See page 59.)

Electrically-Conducting Thermal-Control Coating

A new coating, comprised mainly of zinc and aluminum oxides, is characterized by high thermal emittance, low thermal absorption, and high electrical conductivity. Originally developed to protect spacecraft, the coating can be used to prevent charge buildup on components in other applications. The mixture is stable under ultraviolet and X-ray radiation and under bombardment by ionizing particles. It can be applied to aluminum, stainless steel, epoxy/fiberglass, and other substrates. When exposed to the equivalent of 1,000 Sun-hours illumination, the coating remained stable and retained its optical properties.
(See page 52.)

Self-Sterilizing Canister

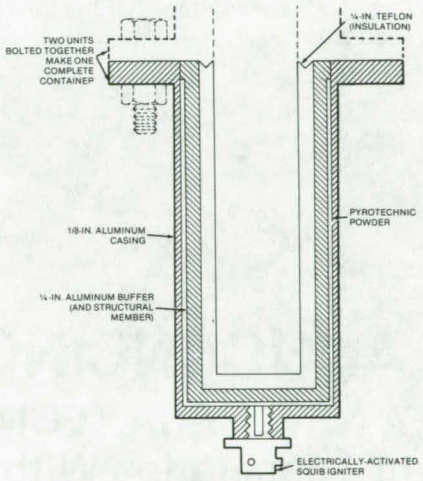

A self-sterilizing canister, originally conceived for remote sterilization of spacecraft packages, could be used terrestrially to handle samples in biologically hazardous environments. The multiwalled canister includes an inner layer of pyrotechnic powder. For sterilization, an electrically activated squib ignites the powder, raising the temperature of the outer surface of the canister to 230° C for several minutes. A thermal-buffer inner layer prevents the inside temperature from exceeding 100° C, to protect the contents from damage. Samples in field hospitals and other emergency situations could also be handled by this equipment.
(See page 70.)

Long-Lasting Solid-Polymer Electrolytic Hygrometer

A new hygrometer, suitable for operation under high g loads and prolonged exposure to vacuum, uses an oxidation-resistant fluorocarbon polymer to absorb the moisture from a gas sample. The water content of the sample is measured by monitoring conductance changes in the solid polymer. The oxidation resistance of the polymer gives this device a longer lifetime under continuous use than other solid or liquid electrolytic hygrometers. It is easily fabricated by installing a hollow tube of the polymer in a glass container and winding platinum electrodes on the inner and outer surfaces of the tube.
(See page 92.)

Gate-Assisted Turn-Off Thyristor

A 1,000-volt, 200-ampere gate-assisted turn-off thyristor has been developed for power circuits requiring high efficiency, small size, and low weight. Its design features include a shunted cathode for high dV/dt capability. The cathode is interdigitated with a dynamic gate for fast, low-loss switching. The operating frequency exceeds 20 kHz with an overall energy dissipation of less than 12 mJ per pulse for a typical 20-microsecond half-sine waveform. The device has a turn-on time of 2 microseconds and a turn-off time as short as 3 microseconds with only 2 amperes of gate drive.
(See page 6.)

Modified Chemiluminescent Analyzer for NO_X

The installation of a molybdenum NO-to-NO_X converter in a chemiluminescent gas analyzer and the use of an air purge allow accurate measurements of NO_X in exhaust gases containing as much as 30 percent carbon monoxide. Measurements using a conventional analyzer are highly inaccurate for NO_X if as little as 5 percent CO is present. In the modified analyzer, the molybdenum has high tolerance to CO, and the air purge substantially quenches NO_X destruction. In tests, a modified chemiluminescent analyzer accurately measured NO and NO_X concentrations for over 4 months with no degradation in its performance.
(See page 54.)

ANNOUNCING . . .

A NEW NASA TECHNOLOGY UTILIZATION SERVICE in Cooperation With STATE GOVERNMENTS

NASA recently inaugurated a State Technology Applications Center (STAC) program with the opening of facilities in Florida and Kentucky.

The purpose of the experimental STAC program is to provide technical information services to state and local government agencies as well as to industry within each state.

The STAC's differ from the NASA Industrial Applications Centers (see page A7) primarily in that the STAC's are integrated into existing state technical assistance programs and serve only the host state, whereas the Industrial Applications Centers serve multistate regions.

The STAC's have access to several commercial data bases, as well as the NASA data base, and they normally charge a fee for their services.

Persons wishing **further information** should write to:

In Florida

NASA/Florida State Technology Applications Center (STAC)
311 Weil Hall
University of Florida
Gainesville, Florida 32611

or phone, Gainesville: (904) 392-6760
Orlando: (305) 275-2706
Tampa: (813) 974-2499

or contact the local State Department of Commerce Business Development Representative

In Kentucky

NASA/University of Kentucky State Technology Applications Program (STAP)
109 Kinkead Hall
University of Kentucky
Lexington, Kentucky 40506

phone: (606) 258-4632

Electronic Components and Circuits

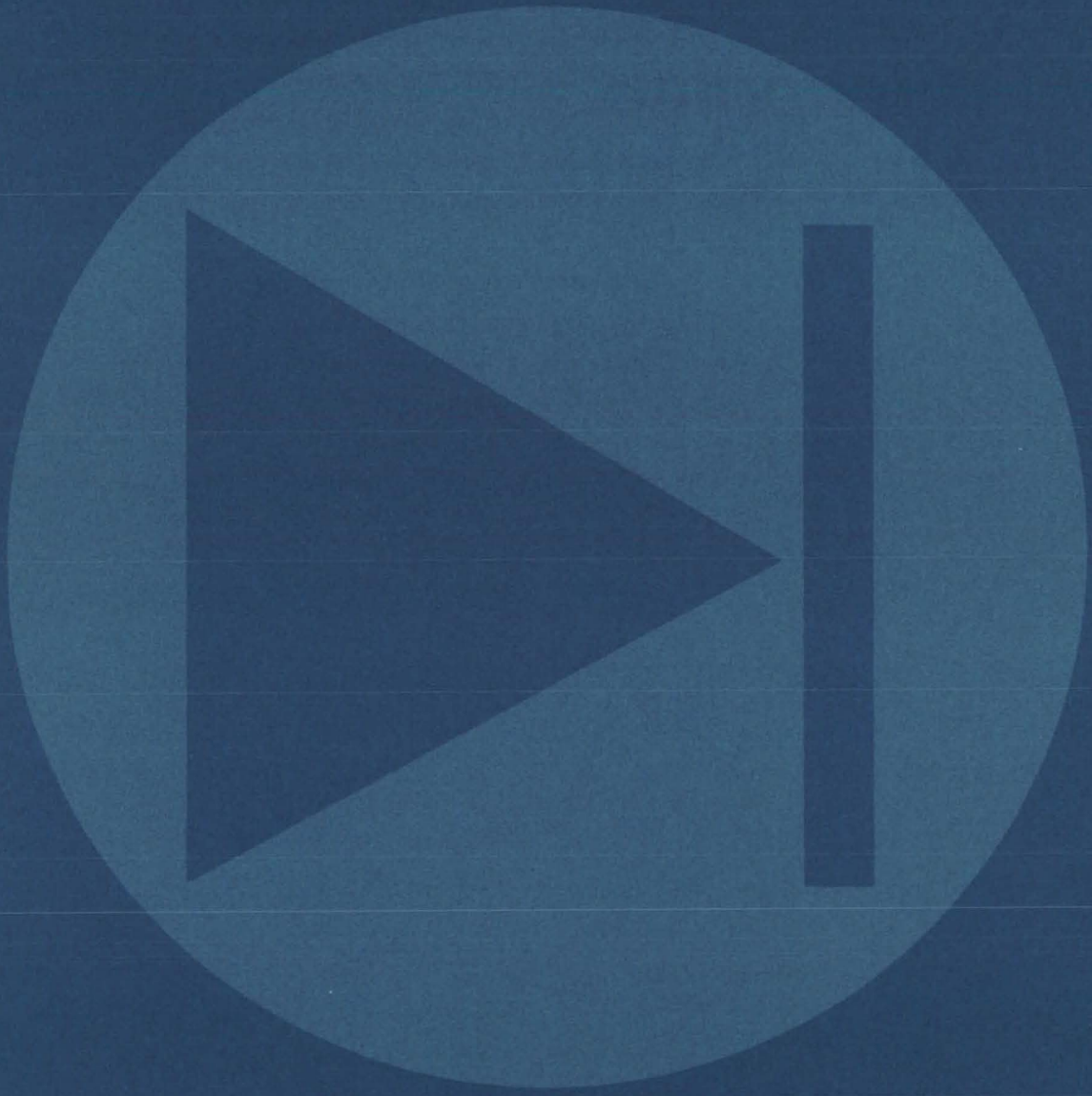

Hardware, Techniques, and Processes

Automated Tester for MOS Devices

Programed electronics
perform online diagnostic checks.

NASA's Jet Propulsion Laboratory, Pasadena, California

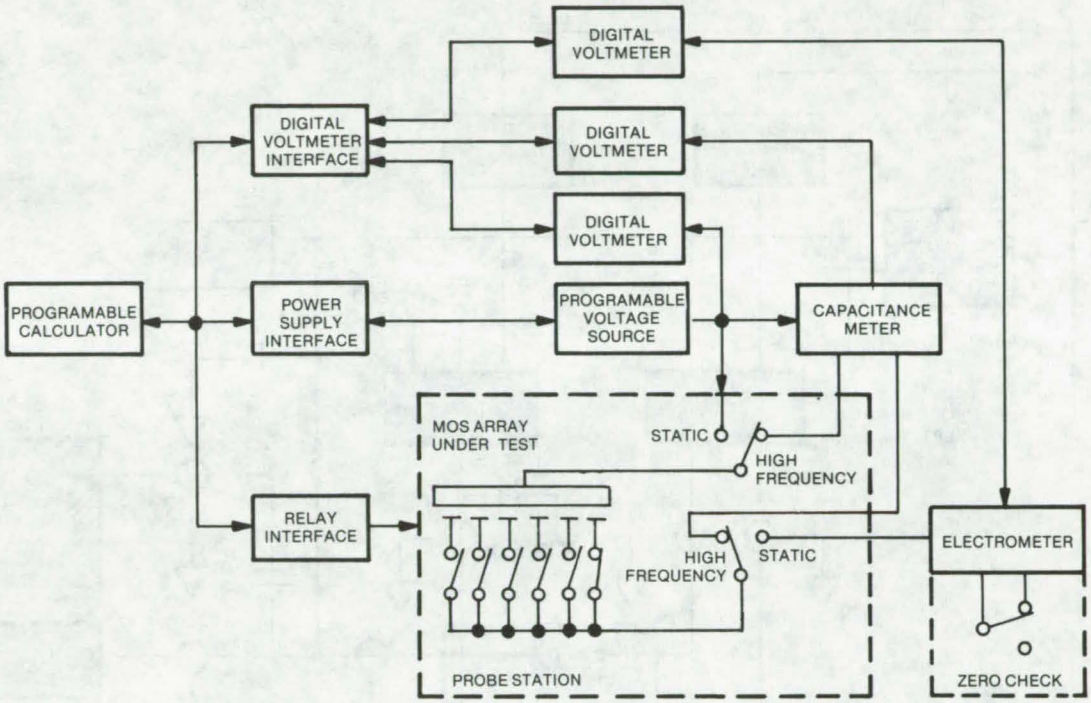

Programed Electronics perform fast, accurate diagnostic checks of MOS devices. The relay interface controls relays that switch between the test operations and between the elements to be tested; the power supply interface directs the voltage sources to apply voltages at the appropriate times; and the voltmeter interface commands the digital voltmeters to take readings, to reset, and to transfer the readings to the calculator memory for processing.

An automated system that diagnoses MOS structures can speed production and quality-control testing of MOS integrated circuits. The flexible system is more accurate than manual testers. Its programed electronics investigate transistor and cell characteristics to rapidly compile the data needed for screening. The system can handle many test specimens while holding to rigid and repeatable setup parameters.

In its present form, the tester makes four types of measurements: (1) surface-state density by static and high-frequency (1 MHz) capacitance-voltage (C-V) measurement, (2) capacitance-time (C-t) measurement, (3) bias stress-temperature (B-T) capacitance-voltage measurement, and (4) hole trapping by avalanche injection [see page 4 of this issue, "Measuring Oxide Trapping Parameters in MOS Structures" (NPO-14120)]. Wafer- and packaged-chip test stations are capable of applying both hot (300° C) and cold (liquid nitrogen) temperature stress and bias and current stresses. Future modifications will provide radiation stress and other stress factors.

A block diagram of the system is shown in the figure. The programable calculator commands digital power supplies and relays to switch between samples and the different test operations and to read data from test instruments. Digital voltmeters and an electrometer are used to make the elementary voltage, current, and charge measurements. The calculator processes the data and gives either a printout or a graphical output. Test programs are stored on tape cassettes as routines that define the order of measurements.

The system tests automatically in a fraction of the time required for manual testing, and with greater precision. Both the time and precision can be altered, and test procedures can be quickly modified by changing the program.

This work was done by Richard H. Cockrum of Caltech for **NASA's Jet Propulsion Laboratory.** *For further information, Circle 1 on the TSP Request Card.*
NPO-14088

Measuring Oxide Trapping Parameters in MOS Structure

A simple technique, avalanche injection, works for both electrons and holes.

NASA's Jet Propulsion Laboratory, Pasadena, California

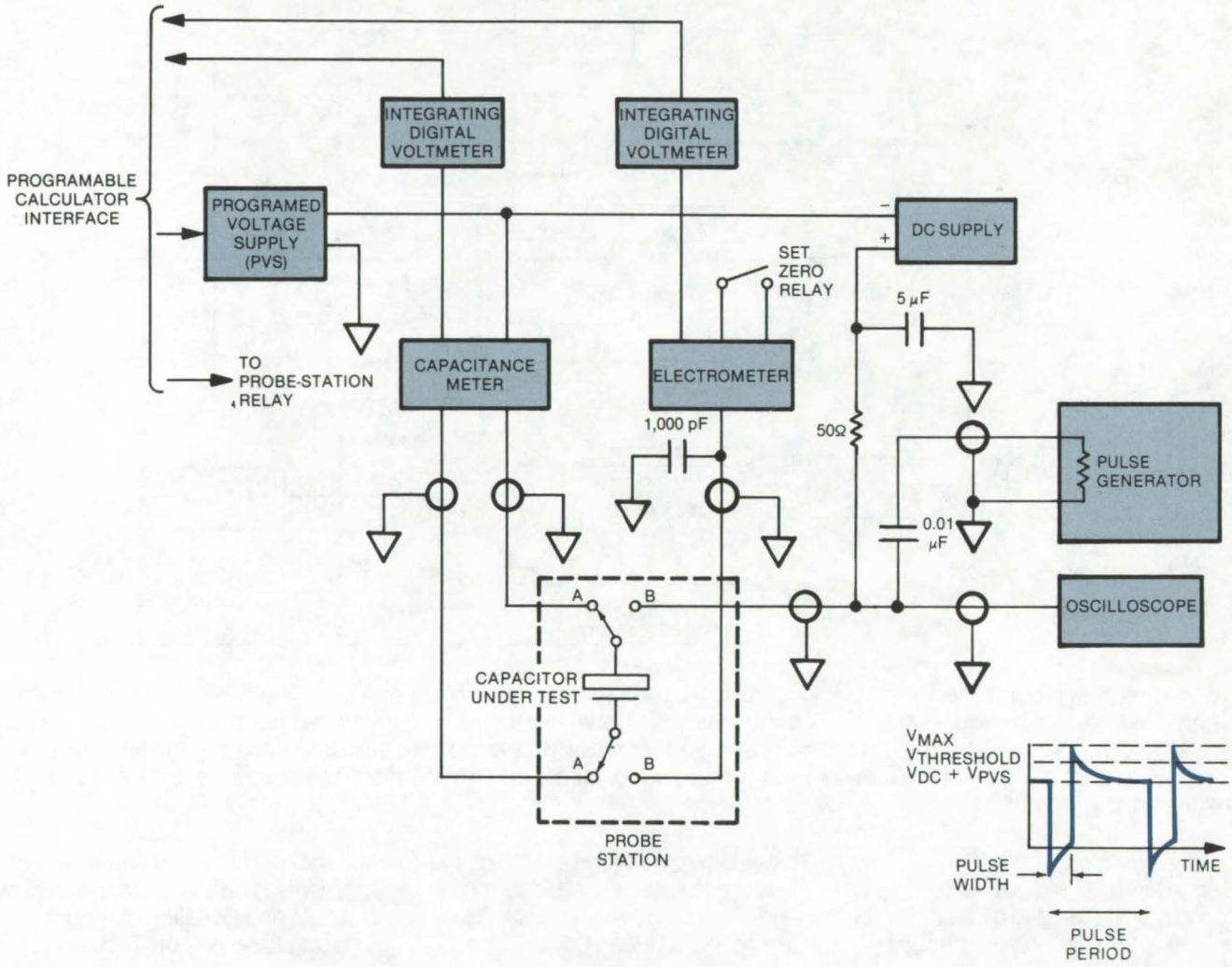

Oxide Trapping Parameters Are Determined by measuring shifts in the C-V curve of a MOS capacitor due to avalanche injection of carriers. When the relay is in position A, the test device "sees" only the voltage impressed by the programed voltage source; in position B, the sum of the programed source, dc supply, and pulse generator is applied to produce the waveform shown in the inset. The polarity of V_{max} is positive for hole injection from n-type silicon and is negative for electron injection from p-type silicon.

The controlled injection of electrons or holes into the oxide layer of a MOS capacitor can be used to measure oxide trapping parameters such as trap cross section and trap density. The capacitor test structures require moderately heavily doped silicon (approximately 2×10^{17} cm^{-3}) and a thick field oxide at the boundary of the capacitor gate oxide to guard against localized avalanche breakdown. The method is implemented with the test system described on page 3 of this issue in "Automated Tester for MOS Devices" (NPO-14088), in which all measurements and data analyses are carried out under program control.

The trapping of carriers at defect sites in the oxide is a serious

problem when MOS circuit elements are exposed to ionizing radiation. Such radiation can generate electron-hole pairs in the oxide. Generally, the more mobile electrons are drawn off into the external circuit, but the holes can be trapped, setting up a charge that shifts the threshold voltage. Some electron trapping can also occur, and this partially offsets hole trapping. Since these mechanisms can cause degradation and ultimate failure of the MOS device, reliable trapping measurements are required to predict its radiation tolerance or "hardness."

The automated test system described on page is modified by adding the interface electronics and instrumentation shown in the figure. A capacitance meter measures capacitance changes caused by the avalanche injection of carriers. The charge that is not trapped is collected at the metal electrode and is measured by an electrometer. A programable voltage supply and a pulse generator apply the required voltages during the test.

Initially, the relay is set to position A, and the device capacitance-voltage (C-V) curve is measured. The point of maximum slope (defined by $d^2C/dV^2 = 0$) is determined and is used as a reference for measuring later voltage shifts at the same capacitance. The relay is switched to position B, and the programed applied voltage source is set to exceed the threshold for avalanche injection. The charge accumulating on the gate of the capacitor is then measured every second until it reaches a predefined value; the voltage is reduced below threshold, and the final charge is recorded. Finally, the relay is switched back to position A, and the voltage shift is measured at the reference capacitance.

This process is repeated until the total injected charge reaches a selected value. The measured voltage shifts and charge values are stored in a computer memory after each measurement.

The carrier trapping measured equations can be solved for the trapping efficiency in terms of the trap parameters, and measured number of injected carriers. To solve the equations, it is assumed that the trapping efficiency is small (as is typically the case) and that the injected carriers move at the thermal velocity. The voltage between pulses is adjusted to be below threshold but large enough so that this condition is satisfied.

A linear regression analysis determines the trapping parameters that best fit the measured trapping efficiency. These data can also be analyzed to determine if different trap mechanisms are active or only a single process is occurring.

This work was done by Joseph Maserjian of Caltech for **NASA's Jet Propulsion Laboratory.** *For further information, Circle 2 on the TSP Request Card.*
NPO-14120

Nylon Screws Make Inexpensive Coil Forms

Coils may often be made by laying windings in threads of right-sized screws.

Lyndon B. Johnson Space Center, Houston, Texas

Standard nylon screws can serve as inexpensive and readily available forms for winding coils. They may often eliminate the need for relatively-expensive custom coil forms. Moreover, the screws come in a great variety of sizes, and they are uniform enough to have been used successfully for coils needed in breadboarding electronic equipment.

The diameter and the pitch of the screw and the separation of its threads are the key parameters to consider in trying to meet the design requirements of a coil. The copper wire for the coil is simply placed in the spiral thread so that the coil inner diameter and the spacing between turns can be reproduced easily just by choosing the right screw. If a screw of the right length is not available, it is easy to trim a longer one to the length that is desired. One drawback, however, is that it is not possible to tune the coil by adjusting the spacing between windings, a technique sometimes used with air-core coils.

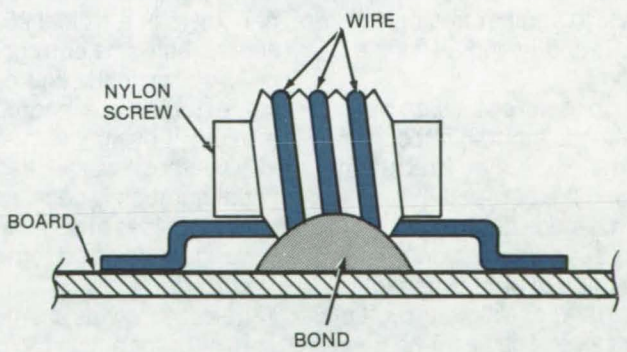

Nylon Screw Acts as the Coil Form with copper wire laid down in the spiral thread. The completed coil may be bonded to a printed-circuit board.

This work was done by Gerard Aucoin and Charles Rosenthal of TRW, Inc., for **Johnson Space Center.** *No further documentation is available.*
MSC-16912

Gate-Assisted Turn-Off Thyristor

High efficiency and reliability are combined with small size and weight.

Lewis Research Center, Cleveland, Ohio

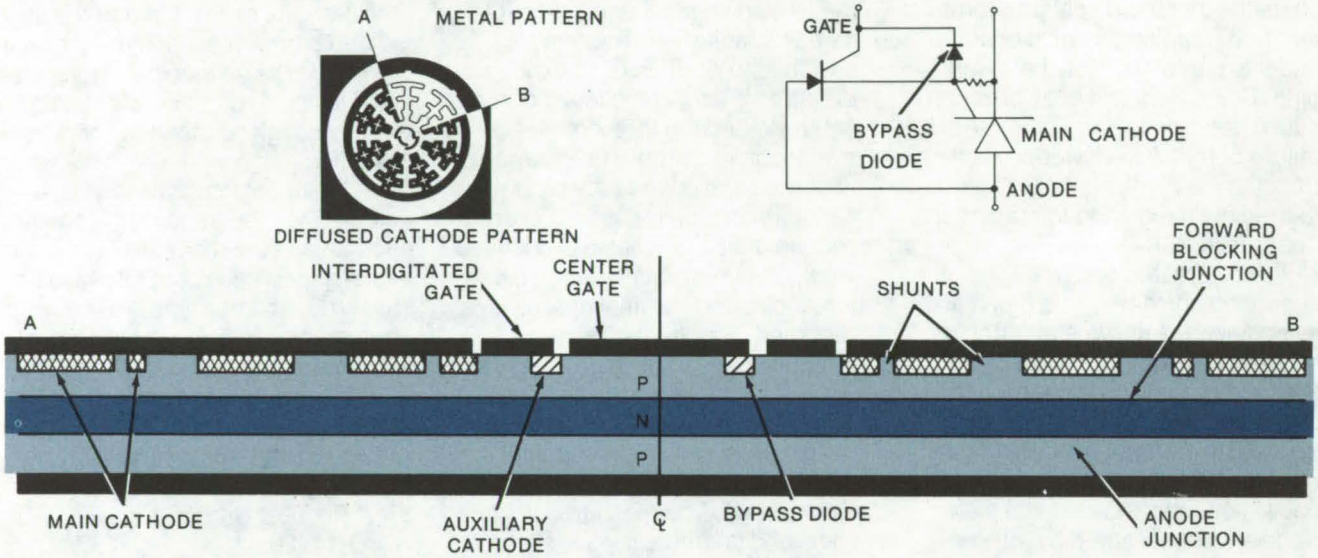

Gate-Assisted Turn-Off Thyristor incorporates a digitated and shunted cathode. A bypass diode integrated into the thyristor allows dynamic gating to be combined with gate-assisted turn-off.

A 1,000-volt, 200-ampere gate-assisted turn-off thyristor (GATT) has been developed for circuitry requiring high efficiency and high reliability as well as small size and weight. The GATT is being used in a 3-kW series inverter circuit for the conversion of dc power from one voltage level to another and can be used for both space and terrestrial applications.

The design features include a shunted cathode interdigitated with a dynamic gate, electron irradiation for optimizing the carrier lifetime level, and a bypass diode. The bypass diode is necessary to permit the combination of both dynamic turn-on and gate-assisted turn-off in the same device. The GATT has a turn-on time of two microseconds, and a turn-off time as short as 3 microseconds with only two amperes of gate drive for a few microseconds.

The size, weight, and power loss of solid state power-conditioning equipment can be reduced through the use of small circuit components if the circuit operating frequency can be increased. High efficiency requires that the switching losses in thyristors be held to a minimum. This newly developed GATT performs to meet these requirements. Its operating frequency capability exceeds 20 kHz with an overall energy dissipation of less than 12 mJ per pulse for a typical 20-microsecond half-sine current waveform.

As shown in the figure, the following features were incorporated in the new GATT design:

- The cathode was digitated. This configuration is necessary both for fast, low-loss turn-on and for effective, gate-assisted turn-off behavior.
- The cathode was shunted. Shunting provides for a high dV/dt capability (time rate of applied voltage) whether or not there is a gate-assist bias present, and it eliminates current crowding of the type that causes failures in transistors and gate turn-off thyristors. In addition, shunts direct the current paths in such a manner that the effect of the gate-assist bias is more reliable and requires a lower drive voltage. Shunts make the device more tolerant of process-induced nonuniformities and thereby make it easier to manufacture.
- A bypass diode was necessary to combine the advantages of dynamic gating and gate-assisted turn-off. The figure shows the bypass diode circuit that was integrated into the thyristor element. When forward bias is applied to the gate, it causes current to flow through the auxiliary cathode in the usual manner, and little current flows through the high resistance under the bypass diode. When a reverse gate-assist bias is applied to the gate, most of the current flows through the bypass diode and little flows through the high resistance under the auxiliary cathode. In order to prevent electrons emitted by the bypass diode from firing the thyristor, the carrier lifetime is decreased in this local area by selective electron irradiation.
- A precisely controlled, easily variable dose of electron irradiation was used to control minority carrier lifetime. The combination of this

high-energy electron irradiation and gate-assist current provides for simple, precise tailoring of the device characteristics to the intended application.

This work was done by Lewis R. Lowry, Derrick J. Page, and Earl S. Schlegel of Westinghouse Electric Corp., for **Lewis Research Center.** *Further information may be found in NASA CR-134951 [N77-31405] "Development of a 1,000V 200A Low-Loss, Fast-Switching, Gate-Assisted Turn-Off Thyristor", which may be obtained at cost from the New England Research Application Center [see page A7].*

Title to this invention has been waived under the provisions of the National Aeronautics and Space Act [42 U.S.C. 2457(f)], to the Westinghouse Electric Company, Pittsburgh, Pennsylvania 15235. LEW-12535

S-Band Complex-Weight Module for Adaptive Processing

Computer aided design was used for MIC module.

Langley Research Center, Hampton, Virginia

Adaptive processing is a relatively new technique whereby a signal from an antenna is manipulated electrically. Its advantages include interference rejection, cross-polarization rejection, and beam steering. Adaptive processing requires an electronic device called a "complex weight" that must be able to shift the phase of the incoming signal by 180° and vary its amplitude for all possible angles. The "weight" can consist of doubly balanced mixers or active mixers, or one can use voltage-controlled attenuators or variable gain blocks that are 180° out of phase.

A 1.7-to-2.2-GHz IF complex weight for an adaptive Ku-band cross polarization separator has been developed in the form of an adaptive microwave-integrated-circuit (MIC) module. The configuration selected for this S-band complex weight consisted of four passive attenuators. The control circuitry is external to the module. Each attenuator responds to a positive voltage: its attenuation is reduced as the voltage is increased. The use of two quadrature hybrids in each weight provides the 180° phase shift. The complex weight is produced by placing two weights in quadrature separated by another 90° hybrid (see figure).

Computer aided design was used extensively for the individual piece parts and also for the total complex weight. The requirements for the components were that they be broadband, approximately 500 MHz at S-band, and that they exhibit phase and amplitude tracking to one another. All circuits were fabricated using thin-film MIC techniques on polished Al_2O_3 substrates. The conductor material was gold with nichrome as the thin-film resistor material.

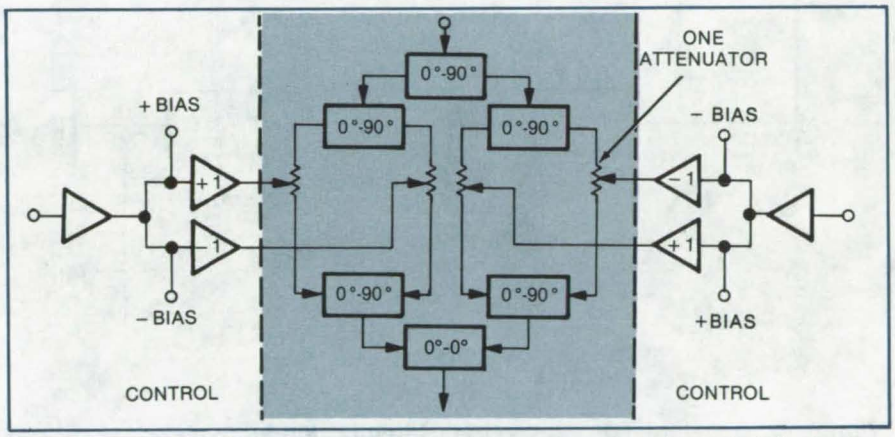

S-Band Complex Weight for adaptive processing has been fabricated as a microwave integrated circuit. The two control circuits are not part of the module. The overall weight is made complex by placing the two weights in the module above in quadrature and separating them by another 90° hybrid.

Because the attenuators are separated by 180°, their crossover (where two attenuators null each other) may be set anywhere in the attenuation range. Three possible attenuator crossover points were computer modeled: maximum, minimum, and midrange attenuations. Use of the maximum attenuation point as the crossover for the attenuators in each weight gave the most-linear amplitude and phase response and gave the best cancellation over frequency for the "off" condition of the weight.

This versatile microwave functional component, when interfaced with a suitable control component, is potentially capable of producing 25 dB rejection of interference over a bandwidth of 500 MHz. Performance improves with decreased bandwidth. Versatility stems from the numerous control methods available in the broadening field of adaptive processing.

This work was done by A. J. Gianatasio, J. B. Schappacher, D. G. Scott, and M. R. Williams of Harris Corp., for **Langley Research Center.** *For further information, Circle 3 on the TSP Request Card. LAR-12197*

Adaptive Polarization Separation Experiments

Adaptively-controlled-RF and wide-band-IF correction networks are developed

Langley Research Center, Hampton, Virginia

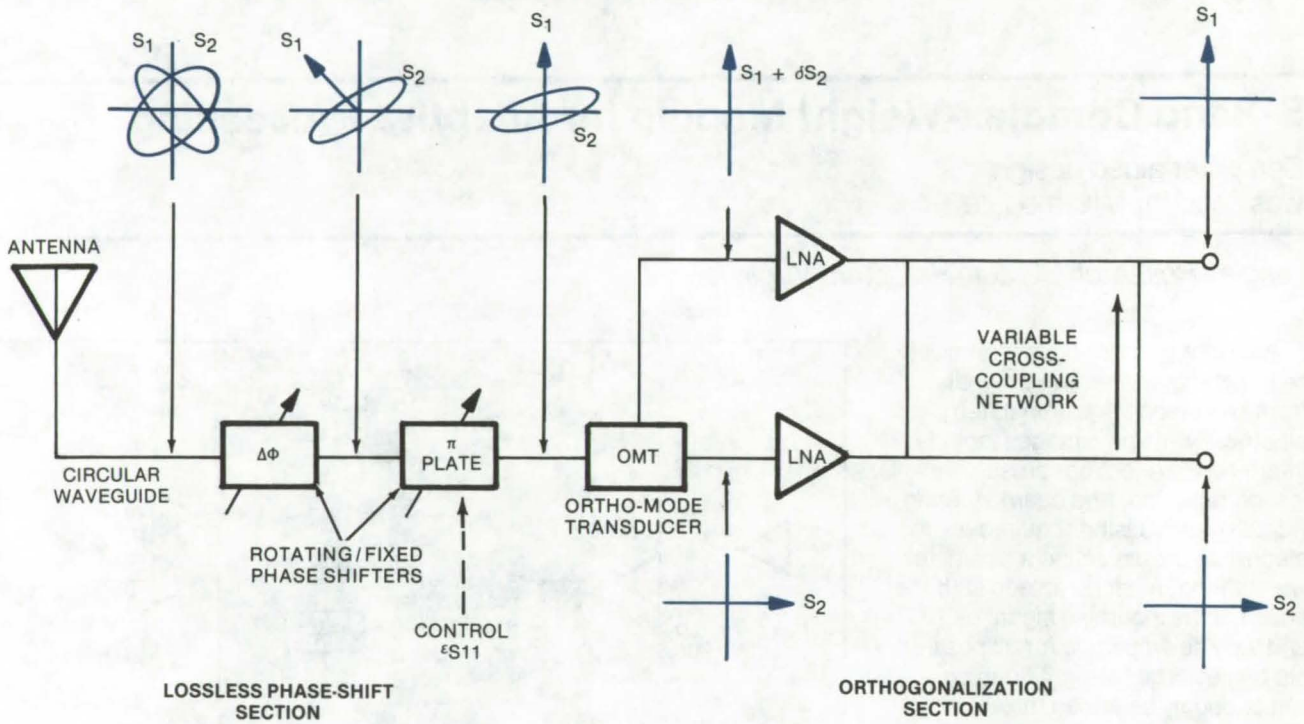

Figure 1. Baseline RF Correction Network lends itself to adaptive control for the correction of varying uncontrolled polarization of the transmitted signal.

It is reasonable to expect that future communications systems will be allocated only a very limited spectrum in desirable frequency bands, while bandwidths of signals will be increasing. Several approaches, such as more-efficient analog-to-digital conversion, more-efficient modulation techniques, and dual polarization, can be used to increase the data capacity of the available spectrum.

With dual polarization, different channels are established for each of two orthogonal polarizations transmitted. Dual polarization systems are particularly attractive when the modulation used is efficient in terms of bit rate per unit bandwidth. With a perfectly operating system, the effective data capacity for a given bandwidth is doubled. However, cross-polarization interference causes some degradation of the channel capacity of the communications links. This interference can be reduced with a cross-polarization "cancellation" or "correction" network. In order for a polarization correction network to respond to variations in cross polarization (due to such factors as changing weather), the correction network should be automatic, or adaptive, so as to track the varying cross polarization.

RF waveguide cancellation networks have been the primary approach to cross polarization cancellation in the past; however, these were not adaptively controlled networks. Previous IF cancellation networks, even if adaptively controlled, operated only over narrow bandwidths. The RF/IF experiments performed in this program have led to the design of a wideband adaptively controlled polarization cancellation network.

A new RF cancellation network approach was designed that lends itself to simple, direct, analog adaptive control. The block diagram is shown in Figure 1. The two incoming signals are assumed to be originally transmitted as horizontal and vertical polarization, respectively. Upon polarization due to rain, antennas, and other factors, they become two elliptically polarized signals as shown. This system was constructed and tested successfully with the adaptive control yielding residual cross polarization -35 to -40 dB below the main channel level for input cross polarization as large as -7 dB.

An IF cancellation network was constructed that significantly

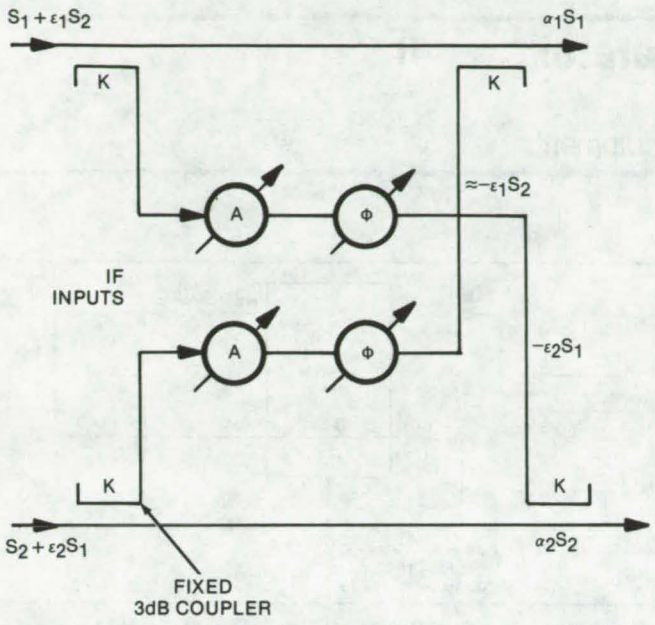

Figure 2. IF Cancellation Network works over a 500-MHz bandwidth to compensate for the effects of cross-polarization.

cancels polarization over very wide bandwidths (500 MHz) and is adaptively controlled. The block diagram is shown in Figure 2. It is a straightforward cross-coupling network that cross couples each signal into the other channel to cancel the cross polarization in that channel. The performance of the IF network, although expectedly not as good as that of the RF network, is a major improvement considering the wide bandwidth. Cancellation to approximately -36 dB rms cross polarization was obtained over a 500 MHz bandwidth; -40 dB rms over 250 MHz, was obtained for a severe rain cross polarization of -20 dB. For greater input cross polarization, the output cross polarizations are higher.

This work was done by C. A. Baird, A. J. Gianatasio, G. M. Pelchat, G. G. Rassweiler, D. G. Scott, R. F. Varley, and L. R. Young of Harris Corp. for **Langley Research Center.** *For further information, Circle 4 on the TSP Request Card.*
LAR-12196

Curve Tracer Checks CMOS IC's

Transfer characteristics are displayed instantaneously for rapid failure analysis.

Goddard Space Flight Center, Greenbelt, Maryland

A conventional transistor curve tracer can speed up the failure analysis of CMOS integrated circuits by displaying the transfer characteristic while the device is subjected to vibration or environmental testing. Failures that show up as a change in the threshold voltage or transfer characteristic are quickly detected by this method. Previously, a time-consuming point-by-point plot of the characteristic was required; with the curve tracer, the same information is displayed instantaneously.

To make a test, the collector supply of the curve tracer is connected to the V_{DD} input of the integrated circuit, the base step generator (set on "volts") and offset functions are connected to the control-voltage input to be tested, and the emitter terminal of the curve tracer is connected to the V_{SS} input. All other inputs of the integrated circuit are set to definite logic levels; usually they can be connected directly to V_{SS}. To display the transfer characteristic, the curve tracer is set to monitor collector current versus base volts.

The method is applicable to simple gates as well as to more complicated devices. It may also be useful for other digital integrated circuits.

This work was done by F. Kizer of **Goddard Space Flight Center.** *No further documentation is available.*
GSC-12209

Portable Spark-Gap Arc Generator

Electrical noise due to static discharge is simulated for bench checks of electronic equipment.

Lewis Research Center, Cleveland, Ohio

A self-contained spark-gap arc generator has been developed to simulate the electrical noise from the discharge of a static charge. The arc potentials are variable from 3 to 15 kV with the energy per arc 0.01 to 0.25 joules or greater.

Investigations into anomalies observed in spacecraft operating at or near synchronous altitudes have disclosed that, as a result of charged-particle impingement, certain spacecraft surfaces were being charged to potentials as high as 11,000 volts. The electrostatic discharge of these charged surfaces to other spacecraft structures or equipment produces RFI (Radio Frequency Interference) which can disturb nearby electronic components. Thus, equipment was needed to test spacecraft components for susceptibility to RFI generated by arc discharges.

Two configurations were developed; one is a free running arc source (Figure 1); and the second unit is triggered (Figure 2). Each unit uses standard commercial parts, measures 3 by 5 by 10 in. (7.6 by 12.7 by 25.4 cm), and weighs 4 lbs (1.8 kg). The circuits shown employ a high-voltage low-inductance RF-type ceramic capacitor and a spark gap for rapid switching. This system provides a realistic simulation of the high voltage, low inductance of charged spacecraft surfaces. The arcs generated produce RFI with a nominal 30 MHz ringing and 200-nanosecond duration. For tests where a nonoscillatory transient is desired, a 12-ohm resistor can be put in series with the spark gap to critically damp the discharge.

The circuit (Figure 1) functions as follows. The energy storage capacitor is charged through a high value resistance, from the high-voltage power supply. When the voltage across the storage capacitor reaches the breakdown voltage of the spark gap, the spark gap triggers and discharges the capacitor. The spark gap switches from a nonconducting state to a conducting state in a few nanoseconds. The inductance of the capacitor spark-gap circuit loop and the capacitor capacitance form a resonant LC circuit. Minimizing the circuit loop length is required to maintain the low inductance needed for proper simulation. With the circuit resistance and arc losses, the oscillation decays to zero in 200 nanoseconds, the spark gap then returns to the nonconducting state, and the cycle repeats.

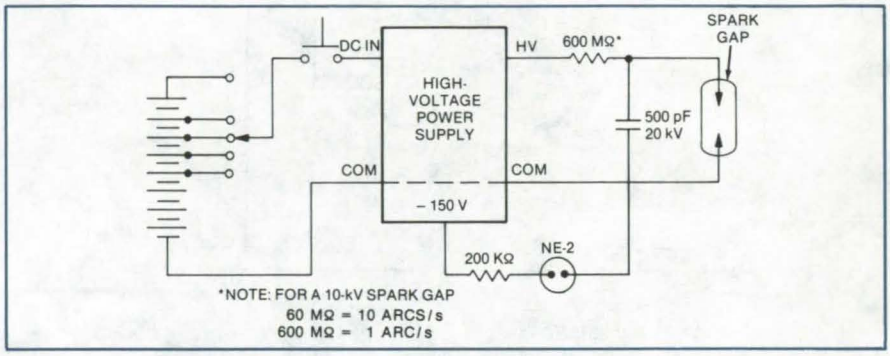

Figure 1. Free-Running Arc Source simulates electrical noise caused by static discharge. The spark gap switches to the conducting state in a few nanoseconds once its breakdown voltage is reached. It returns to the nonconducting state in about 200 nanoseconds.

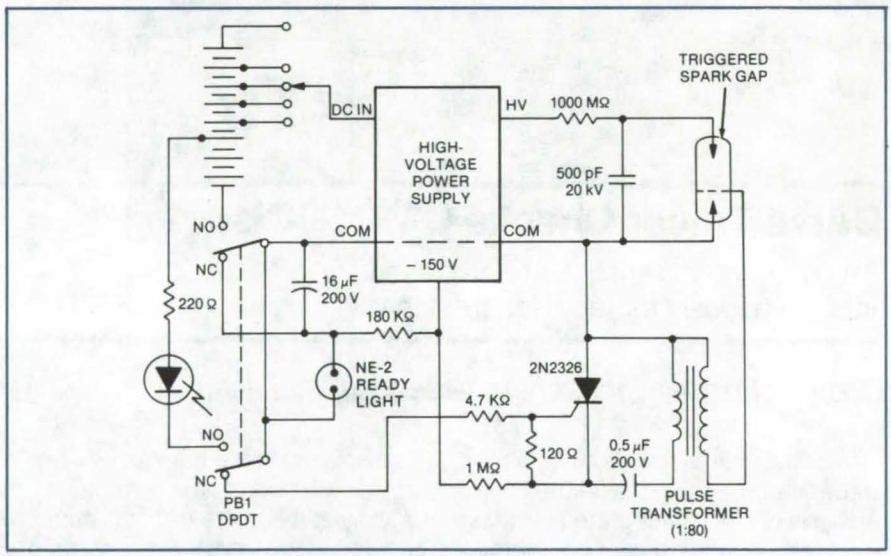

Figure 2. Triggered Pulse initiates arc-gap breakdown in this variation of the circuit in Figure 1. The high-voltage supply is set at 80 percent of the gap breakdown potential.

Operation for the triggered spark gap circuit shown in Figure 2 is similar to above, except that the high-voltage supply output is set at 80 percent of the spark-gap self-breakdown potential. A trigger pulse is then used to break down the gap and establish the arc.

The units are constructed to operate with various spark gaps by adjusting an internal tap on the battery cells for a given spark-gap

voltage rating.

The capacitor to spark gap lead length is kept to a minimum, typically less than 6 in. (15 cm) total arc-circuit loop length. (Minimum inductance is important for proper simulation.)

The battery consists of 10 series-connected AA cells, sufficient for thousands of discharges. The high-voltage power supply has a high-voltage output 1,000 times the dc input voltage.

Tests have been conducted with voltages ranging from 8 kV to 15 kV and capacitor sizes of 500 to 2,500 $\mu\mu$F. For a 10 kV spark gap and a 500 $\mu\mu$F capacitor, the energy dissipated per arc is 0.025 joules. This level of energy is sufficient to induce tens of volts into an electrical cable when the arc-to-cable spacing is less than 12 in. (30 cm).

Of the several methods employed to generate arc noise, this approach proved most successful for the following reasons:

1. Portability — The dc power source not only permits ease of use without an encumbering ac cord, but eliminates possible interference which may be caused by arc noise coupling to test equipment via the ac line.
2. Repeatability — For a given test set-up, identical noise pulses are induced in the harness or equipment tested for each arc discharge while other methods using arc discharges in air were not consistently repeatable.

This design can be used for testing any device for susceptibility to arc-generated noise (especially from static discharge).

This work was done by Louis R. Ignaczak of **Lewis Research Center.** *No further documentation is available.*
LEW-12886

Coaxial Isolator Has Versatile Interface

Its connectors can be changed to meet the user's requirements.

Lyndon B. Johnson Space Center, Houston, Texas

Coaxial ferrite isolators are conventionally manufactured with permanently installed connectors. When integrated into a small electronic assembly, the isolator requires two cables, each with its own connector, for the electrical interface. The space needed to accommodate these cables and connectors can easily exceed that of the isolator itself.

Rather than installing permanent connectors, a new approach that increases system-packaging flexibility was developed for S-band isolators aboard the Space Shuttle. The isolators are constructed with removable connectors that can be changed to meet the user's requirements. For example, a right-angle connector could be installed, or the connector type might be changed from male to female. If necessary, the connectors can be eliminated entirely and replaced with adapters for solder-tab interconnection. Moreover, the removable connectors allow the system to be designed and tested with standard test equipment.

For the S-band isolators, the removable connectors are attached to an adapter flange that matches a flange on the connector body. The adapter is installed on the isolator at the location of the connector. With this arrangement, the transition can be right at the housing wall. No additional cable or connectors, or any soldering, are required.

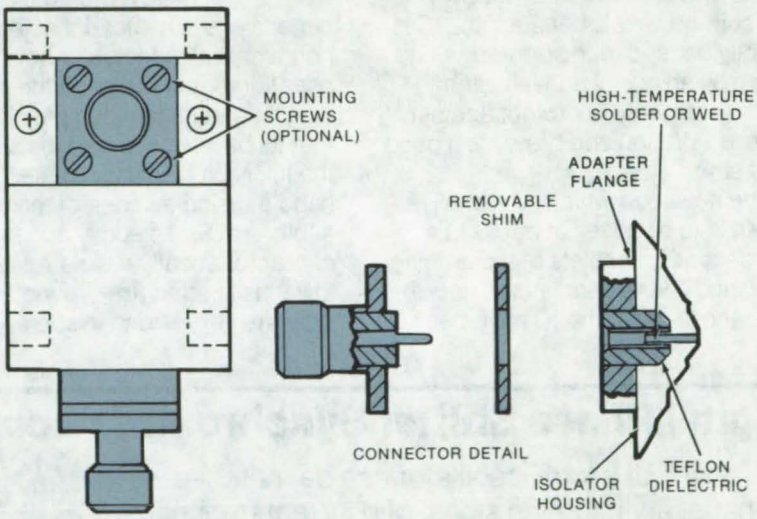

Typical Isolator Configuration shows installation of the removable connectors. Right- and left-hand circulation versions can accommodate virtually any packaging configuration.

An advantage of the technique is that it reduces development scheduling problems. Isolators can be procured before the package design is firm and then readily reconfigured to meet the final design requirements. In addition, the changes to existing designs to incorporate the removable connectors are minimal. The small adapter plates that are added increase size only modestly; weight increase is negligible. Mounting holes can be tapped in the isolator case, so that it can be inverted if necessary.

This work was done by David L. Olsson of TRW, Inc., for **Johnson Space Center.** *No further documentation is available.*
MSC-16908

Simple Tool Removes IC Flat Packs

Handtool pulls hybrid packages from circuit boards without damaging the board or package.

Lyndon B. Johnson Space Center, Houston, Texas

A new tool makes it easy to remove hybrid integrated-circuit flat packs from printed-wiring boards. The simple, easy-to-use tool does not damage the IC or the board. Thus the board can be reused with a replacement circuit, and the old circuit can be analyzed for faults and, if possible, repaired.

Hybrid IC packs have a flat rectangular ceramic substrate covered by a flat metal can from which the leads to the "outside world" protrude. These circuit packs often represent considerable value in materials and labor, and it is therefore desirable to retrieve faulty packs and repair them. Removal is difficult, however, because the IC is usually bonded to the printed-wiring board by an epoxy adhesive that holds it securely to protect against severe vibration and provides a good heat sink.

The new tool, which makes it possible to remove flat packs in a few seconds, consists of a clamping head and a long handle (see figure). After the leads of the IC have been desoldered from the printed-wiring board, the clamping head is slipped over the pack. The internal dimensions of the head match the pack dimensions. The head, however, contains a slight internal bevel. The user tightens a screw on the handle, which tightens the clamping head so that its beveled lips grip the sides of the IC. Next, the user rotates the handle, using an edge of the pack as a fulcrum. Since epoxy adhesives characteristically have a relatively low tensile strength — even though they are very strong in shear, the bond between pack and board is easily broken, and the pack can be removed.

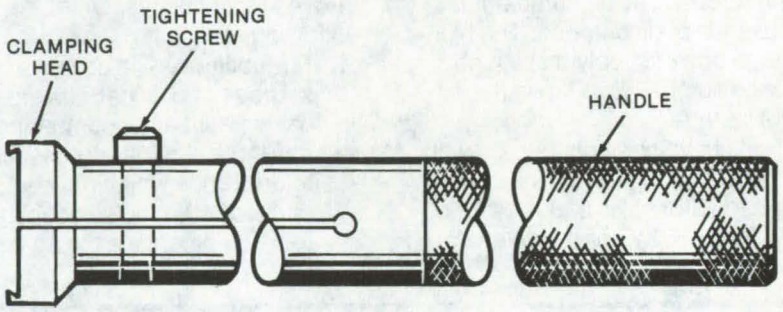

Handtool for Removing IC Flat Packs has a bifurcated handle that can be tightened so that the clamping head grips the pack securely.

It is important that the internal depth of the clamping edges is less than the height of the IC package top above its leads — otherwise the sharp edges could bend or break the leads.

This work was done by Jacob Eggebeen of Sperry Rand Corp. for **Johnson Space Center.** *No further documentation is available.*
MSC-16058

Digital Phase Shifter Synchronizes Local Oscillators

The phase of a local oscillator can be matched to that of an incoming signal of different frequency.

Lyndon B. Johnson Space Center, Houston, Texas

A digital phase-shifting circuit synchronizes a local oscillator with an incoming signal that may have a different frequency. The circuit was developed to replace conventional phase-locked-loop circuitry and to provide more accurate and stable phase synchronization.

Such a circuit is needed, for example, in single-channel data-communication systems, in which a local clock must adjust into synchronism with the incoming data stream. The new circuit has been used in such an application — a Manchester II decoder — to keep phase relationships accurate to one cycle in 1 MHz. Another possible application is in a hybrid digital/analog phase-locked loop, in which the circuit can correct the inherent phase error.

The figure shows the circuit used as a synchronous frequency multiplier. An external time source provides time codes at precise 1-millisecond intervals; and the circuit generates a synchronous output stream of 1-microsecond pulses.

The 16.000-MHz clock drives the synchronous 4-bit up counter. Two of the counter outputs drive the 8-bit shift register. The shift-register outputs are 1-MHz signals spaced at phase intervals of 45°.

The crux of the problem is to select the one signal from the eight that is closest in phase to the incoming signal. The selection can be

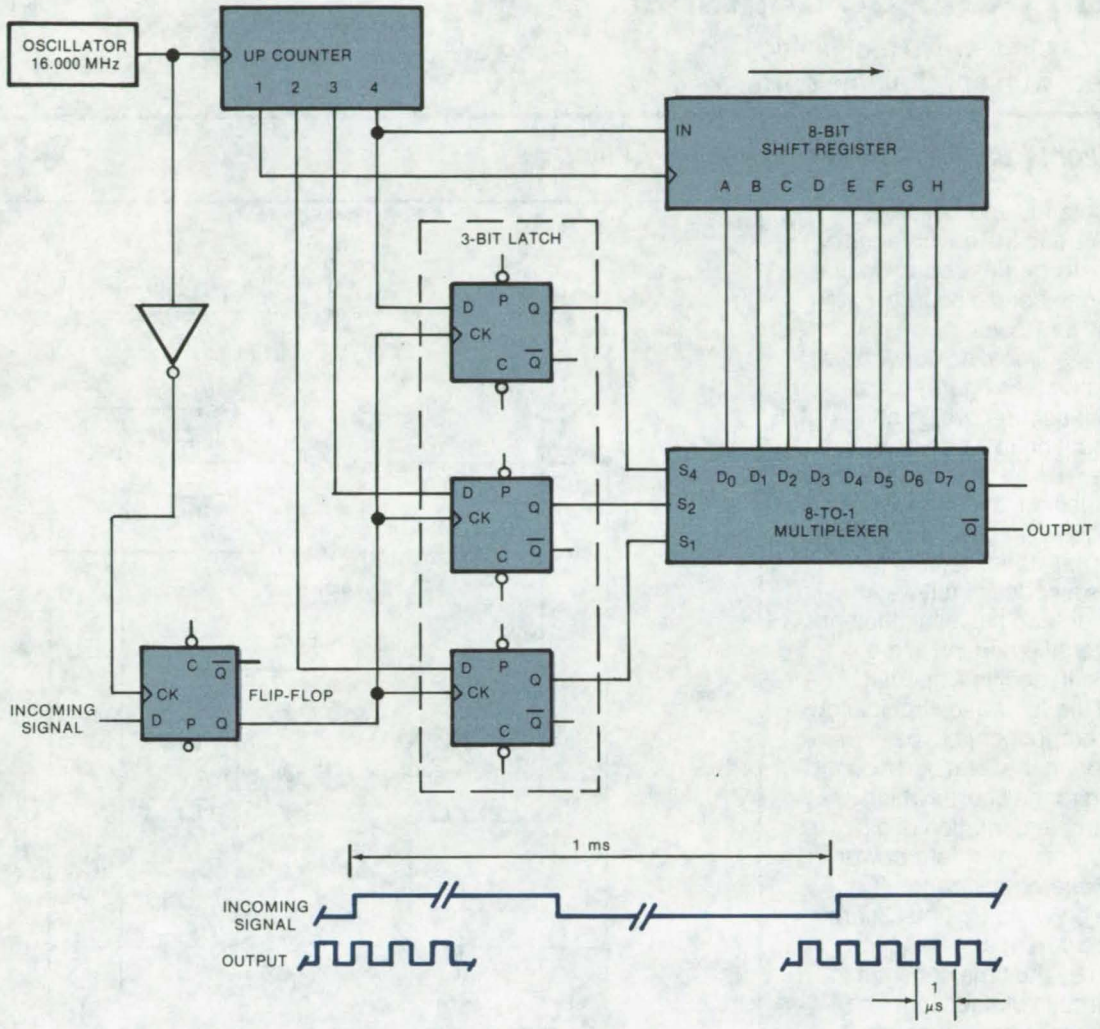

The 1-MHz Synchronizer Output is phase locked with the lower-frequency (1-kHz) incoming signal. The counter and shift register provide eight 1-MHz signals spaced at 45° phase intervals. The rising edge of the incoming signal latches the multiplexer output to the input signal that is closest to it in phase.

made because the three most significant bits (MSB's) of the counter always indicate which data to the multiplexer will undergo a negative transition. For example, when the three MSB's represent four, the data input D_4 to the multiplexer is the only one that will undergo a negative transition. When the three MSB's represent five, D_5 becomes the only input to go through a negative transition, and so forth.

A positive-going transition of the output of flip-flop 4 (the synchronized incoming signal) latches the current three MSB's of the counter into flip-flops 1, 2, and 3, which causes one of the eight 1-MHz shift-register outputs to be selected by the multiplexer. (The synchronization performed by flip-flop 4 is necessary so that flip-flops 1, 2, and 3 can be clocked only when the counter is known to be in a nontransitional state.) This selected 1-MHz signal becomes the circuit output until the next positive transition of the incoming signal, after which the selection process is repeated. Thus, the signal with the closest possible phase relationship to the incoming signal is always the output.

In the application illustrated in the figure, the minimum possible phase difference is desired. For other applications, specific phase shifts (such as 90°) can be accommodated by rearranging the connections from the shift register to the multiplexer.

For greater precision, it is possible to halve the total phase error by adding another counter stage, doubling the clock frequency, doubling the shift-register length, and using a 16-to-1 multiplexer. For even greater precision, additional halvings are possible. However, unless custom integrated circuits are used, the large number of packages required may be impractical.

This work was done by Saiyed M. Ali of Rockwell International Corp. for **Johnson Space Center.** *For further information, Circle 5 on the TSP Request Card.*
MSC-16695

Efficient DC-to-DC Converter

Advantages of full-wave rectification are utilized, with only half the parts.

Dryden Flight Research Center, Edwards, California

High efficiency and low parts count are among the advantages of a new, transformerless dc-to-dc converter that can handle source voltages as low as 1.5 volts.

As in conventional dc converters, the new circuit (see figure) consists of a chopper section, which converts the input dc to a square wave, followed by a bridge-rectifier stage. In the new design, the chopper has been configured to give nearly-ideal switching charcteristics, and the bridge uses a series of full-wave stages rather than the less-efficient half-wave rectifiers found in previous circuits. In addition, special features of the full-wave circuit allow redundant components to be eliminated, lowering the total parts count.

Referring to the figure, which shows the implementation of a 5-V to minus-13-V converter, four power transistors alternately switch (Q_1 and Q_3 are on while Q_2 and Q_4 are off, and vice versa) at a frequency determined by the time constant in the base circuits of each leg. The chopper output, between points A and B, has a peak-to-peak amplitude that is twice as large as the input voltage. Note that only the saturation resistance of the transistors (typically less than 0.1 V) is present in the output circuit at any time.

The rectifier accepts the two out-of-phase square-wave signals from the chopper and generates the rectified, amplified signal shown. It is constructed by placing two half-wave rectifier stacks side-by-side. Normally each half-wave section would consist of two diodes and two capacitors; however, the capacitor that would be positioned along the centerline of the full-wave combination is eliminated since only dc voltages are present there. One diode also becomes redundant and can be removed (and replaced by a solid wire). The resulting full-wave circuit has no more parts than the half-wave version, yet achieves higher conversion efficiency. (An overall efficiency of 80 percent is obtained for the entire circuit.)

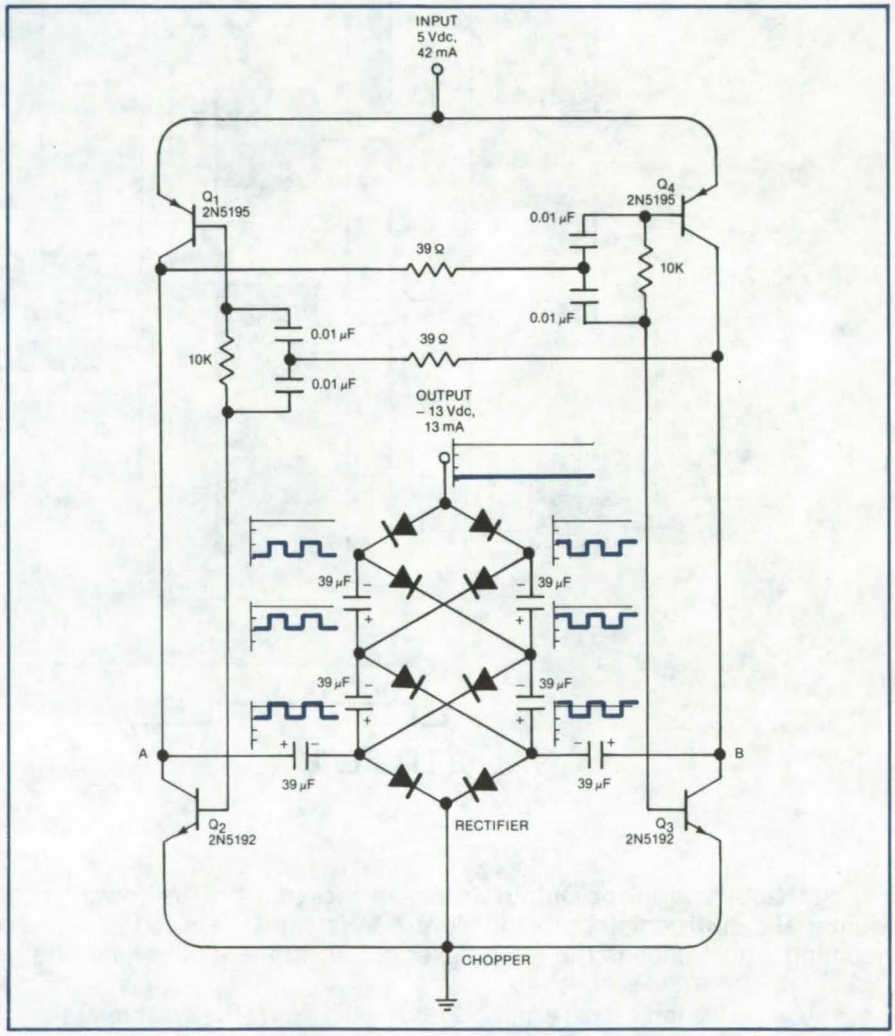

An Efficient DC-to-DC Converter couples a low "on" resistance chopper with a full-wave rectifier stack. A conversion efficiency of 80 percent is obtained for the two-stage combination.

The circuit can also be adapted for use as a dc-to-ac converter or as a combination dc-and-ac source. For light-loading conditions, Darlington transistor pairs can be used to improve the efficiency. In other applications, field-effect transistors can be substituted for the bipolar transistors shown, although this will increase the circuit "on" resistance.

This work was done by James M. Black of **Dryden Flight Research Center.** *For further information Circle 6 on the TSP Request Card.*

Inquiries concerning rights for the commercial use of this invention should be addressed to the Patent Counsel, NASA Resident Legal Office-JPL [see page A8]. Refer to FRC-11014.

Electronic Systems

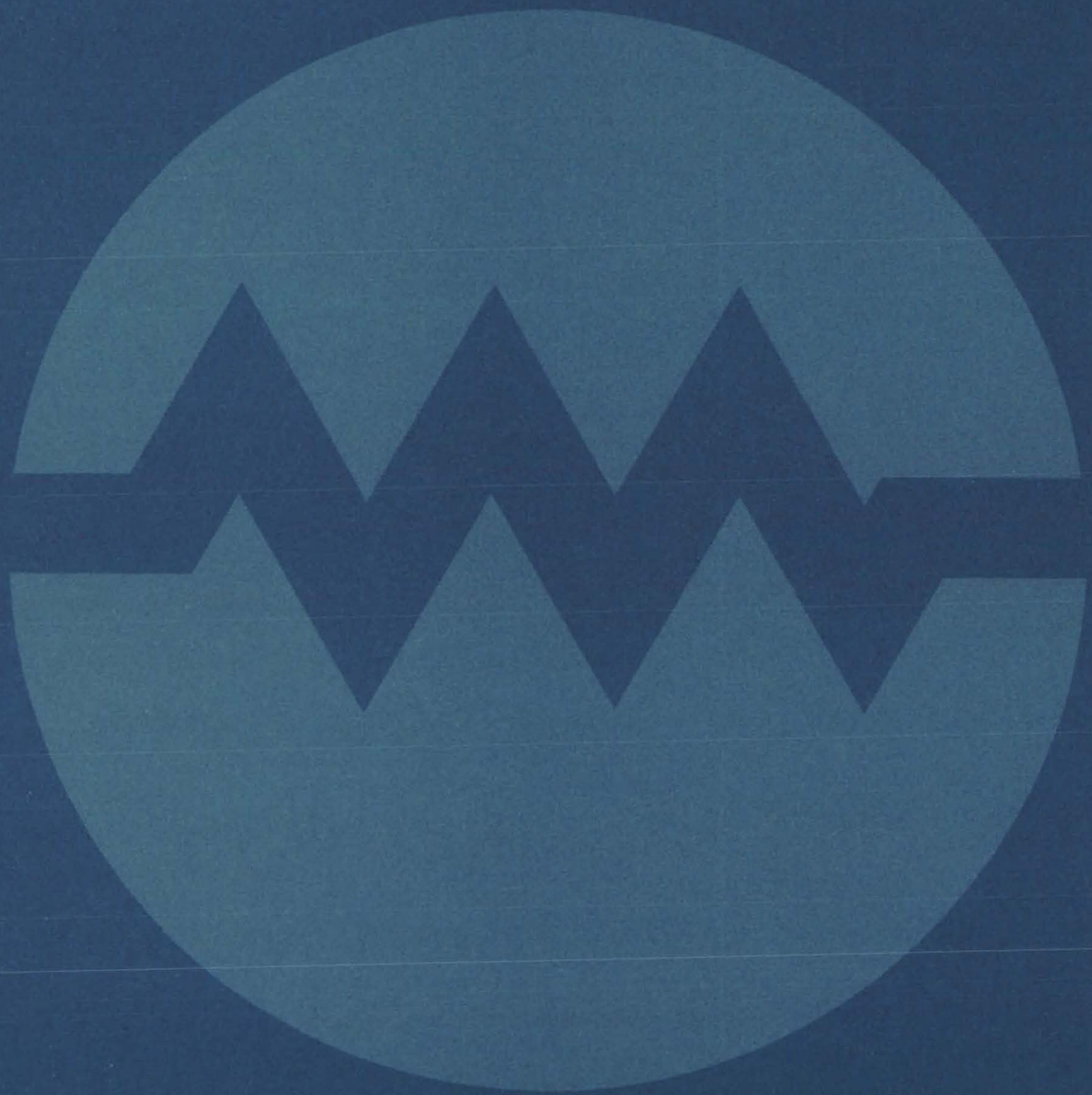

Hardware, Techniques, and Processes

Video Scrambler/Descrambler

Relatively simple circuits can insure privacy in TV transmissions.

Lyndon B. Johnson Space Center, Houston, Texas

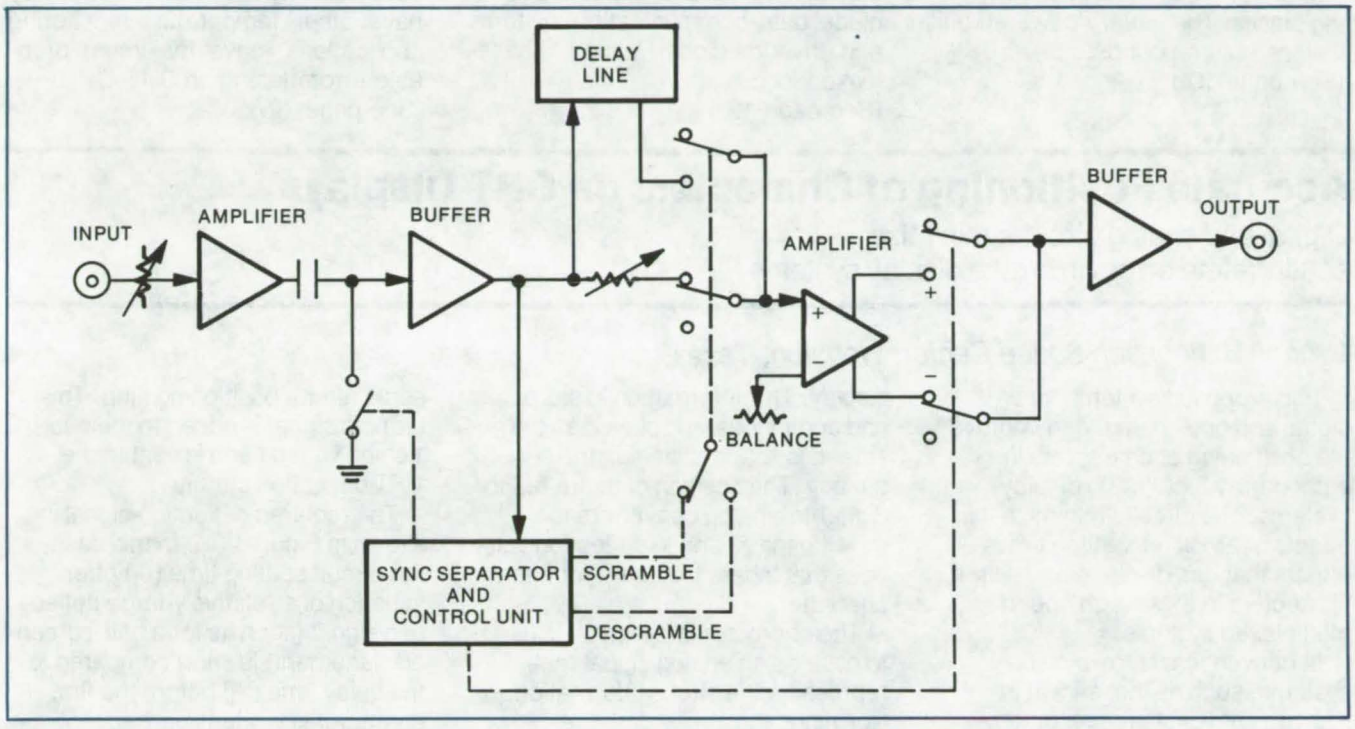

Video Scrambler/Descrambler has a coaxial delay line that retards alternate video fields by 4 microseconds. Blocks of two, four, or eight horizontal lines are then inverted and passed to the output. Even fields are retarded by the scrambler circuit; odd fields are retarded by the descrambler to realine the picture.

A video scrambler that operates on baseband signals uses relatively-simple delay and inversion circuitry to alter a television signal so that it is unrecognizable when picked up on a TV monitor. A descrambler that uses essentially the same circuit restores the signal and allows the original video information to be retrieved. When installed in a TV communications network, the circuits allow only authorized parties to have access to the transmitted information. In one application, the scrambler/descrambler was used to preserve the confidentiality of medical data that were transmitted via satellite for remote examinations of patients in Alaskan villages.

A block diagram of the circuits is shown in the figure. The scrambler accepts the input video and provides amplification, clamping, and sync separation. A coaxial delay line retards the video and sync by 4 microseconds, or about 7.5 percent of the picture width. This delayed signal passes through the circuit on even fields only. The undelayed signal is switched in during the video portions of odd fields; the delayed signal is switched back for the sync interval. The switching causes the active video of the composite to appear advanced on alternate fields.

Next, the signal proceeds to inversion circuitry that inverts alternate blocks of two, four, or eight horizontal lines (as set by an internal patch). The sync is not affected by this processing. Finally, the signal is buffered and passed to the output to give a scrambled picture that is chopped into horizontal bars and jitters horizontally.

The descrambler uses identical circuitry except that the control unit passes the delayed signal on odd fields only; this realines the video and removes the jitter. The inversion circuitry reinverts the groups of lines to restore the original picture.

The input to the scrambler is connected to a 75-ohm 1-volt peak-to-peak video source; its output drives a 75-ohm coaxial cable. The scrambler is completely automatic and requires no operating controls. The descrambler has one control, a "balance" that offsets misalinements or nonlinearities in the transmission link. The balance is adjusted for minimal horizontal bars while the output is observed on a monitor.

This work was done by Phillip C. Lipoma and Kenneth H. Vorhaben of Lockheed Electronics Co., Inc., for **Johnson Space Center.** *For further information, Circle 7 on the TSP Request Card.*
MSC-16843

Portable Spark-Gap Arc Generator

A portable spark generator can assist in checking systems that are sensitive to the discharge of static electricity. It provides controlled, repeatable noise pulses in a free-running mode or, in an alternate configuration, in response to triggering pulses. The battery-powered unit weighs only 4 pounds.
(See page 10.)

Digital Phase Shifter Synchronizes Local Oscillators

A new digital phase-shifting network may be used as a synchronous frequency multiplier for applications such as phase-locking two signals that may differ in frequency. The circuit has variable phase-shift capability. Possible applications include data-communication systems and hybrid digital/analog phase-locked loops.
(See page 12.)

Body /Bone-Marrow Differential-Temperature Sensor

A differential-temperature sensor, developed to compare bone-marrow and body temperatures in leukemia patients, uses a single stable amplifier to monitor the temperature difference recorded by thermocouples. The system, which may have other temperature-monitoring applications, gave maximum probable errors less than 0.1° C.
(See page 72.)

Accurate Positioning of Characters on CRT Displays

Digital and analog circuits minimize settling-time errors in stroke display systems.

Lyndon B. Johnson Space Center, Houston, Texas

Two proposed systems, one digital and one analog, can improve the positioning of characters in cathode-ray tube (CRT) display systems. The circuits minimize the effects of amplifier settling times — effects that can displace and distort characters in these high-speed multiplexed systems.

In conventional stroke display systems, such as that shown in Figure 1, a digital processor generates position and character information needed to generate the display. This information is stored and continuously displayed as the screen is scanned at high frequency. The position data are fed to digital-to-analog converters to develop the X- and Y-deflection voltages that locate the beam for each character.

The character information is used to develop an analog signal that represents the stroke information. Normally, the stroke data are delayed for a period equivalent to the time needed for the beam to settle after a positioning step. This graphic signal is added to the positioning voltage and is sent to the CRT deflection circuitry.

The required deflection signal is shown in Figure 2(a). In this case, the circuit settling time (t_S) after initiation of a relatively-large deflection signal (such as for a half-screen displacement) is short compared to the delay time (t_d) before the first character is written. Subsequent characters will then all be written at the proper positions. If, on the other

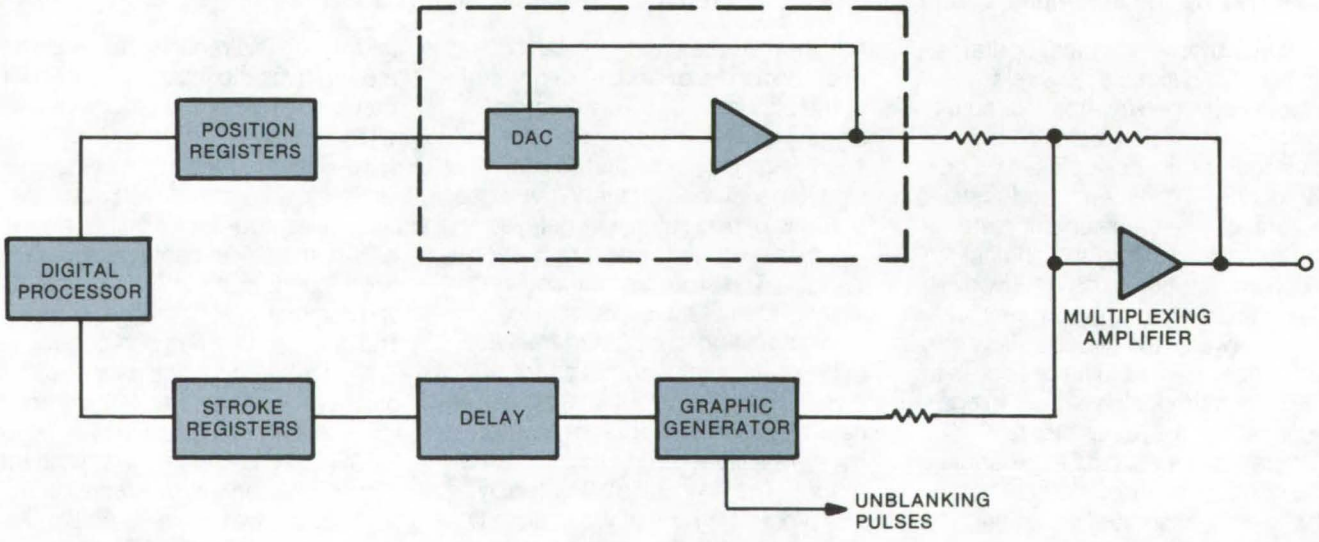

Figure 1. A **Conventional Stroke Display Circuit** generates position and character signals that are multiplexed and fed to the CRT deflection circuitry. This circuit can give positional inaccuracies if amplifier settling times are long.

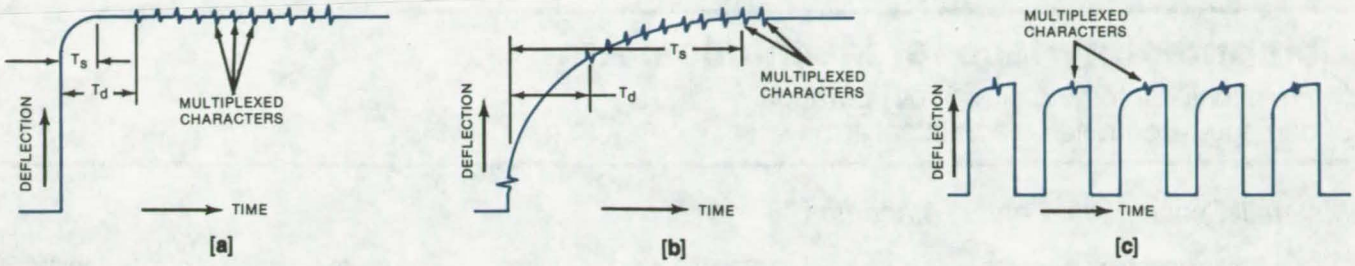

Figure 2. **Ideal Deflection Characteristic,** seen in (a), is contrasted with actual characteristic, (b), obtained when the circuit of Figure 1 is used and settling times are large. The characteristic generated by the proposed circuits is shown in (c).

hand, the settling time is larger than the delay time, the deflection voltage will continue to increase between characters, as in Figure 2(b), and the position of the characters will be displaced from their proper locations.

To produce the deflection characteristic shown in Figure 2(a), the circuits must respond rapidly, settle out fast, and accurately hold dc levels for relatively long periods of time. To accomplish this, high-slew-rate amplifiers must be used, and the circuits must be packaged to minimize capacitive effects. Also, the components must be selected carefully, to reduce dielectric hysteresis.

One technique for minimizing settling-time effects is to operate the amplifier over a narrower bandwidth by keeping the operating frequency relatively constant. If a relatively-fixed-frequency ac mode is used, the circuit can be simplified, and the characteristics can be controlled more easily.

The proposed circuits accomplish this by returning the deflection voltage to zero after each character by gating the deflection circuit off during the character-fetch phase [Figure 2(c)] of the display cycle. In this way, each character is written at the same point on the settling curve; thus little deflection error develops between characters, and the graphics will be positioned properly.

The two methods for implementing this scheme are

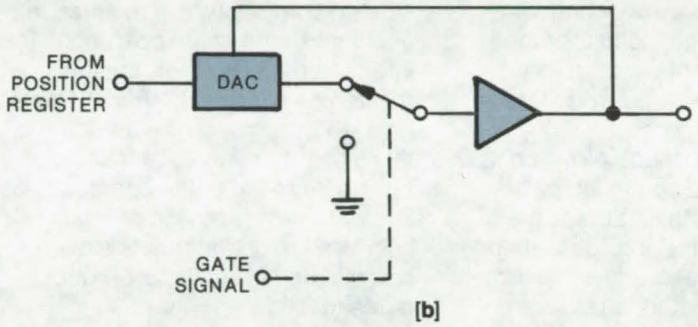

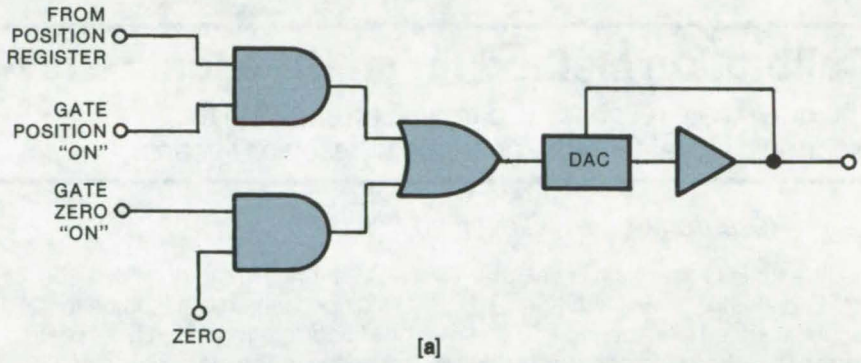

Figure 3. **Settling-Time Errors Are Minimized** by gating the deflection circuit with the digital network shown in (a) or with the analog circuit shown in (b). The gate circuit drops the deflection voltage to zero during each character fetch.

shown in Figure 3. The digital version (a) uses a combination of AND and OR gates to switch the DAC input to zero during the character fetch. The second design (b) uses a single-pole double-throw analog switch in much the same way as the digital switch in the first method. In both cases, the gate signal can be easily derived from the timing pulses already present in the display subsystem.

This work was done by John R. Damian of IBM Corp. for **Johnson Space Center.** *For further information, Circle 8 on the TSP Request Card.*
MSC-16505

Computer Interface for Mechanical Arm

Man/machine interface simplifies operation of computer-controlled mechanical arm.

Marshall Space Flight Center, Alabama

A new man/machine interface commands a computer-controlled mechanical arm. This remotely-controlled mechanical arm has six degrees of freedom and is controlled through a "supervisory-control" mode, in which all motions of the arm follow a set of preprogramed sequences. The program is stored beforehand in a computer.

The entire set of arm movements is monitored and controlled by the operator behind the interface panel. The interface panel includes a television screen that displays the arm movements; a cathode-ray tube (CRT) that displays, in simple language, the exchange being accomplished, the activity being conducted, and the action required of the operator; and a set of keys to punch in the next sequence of movements.

For simplicity, only a few prescribed commands are required to accomplish the entire operation. The interface panel controls can be mastered very quickly. Recent tests have shown that, on the average, it takes only 10 minutes of training time to learn the entire operation. System safety is thus improved because the operator needs no complicated checklists or procedures to follow.

This type of an interface can be used in a number of applications. For example, it can operate a computer-controlled arm to handle radioactive or explosive materials or command an arm to perform functions in hostile environments. A modified version using the displays may be applied in medicine.

This work was done by W. L. DeRocher and R. O. Zermuehlen of Martin Marietta Corp. for **Marshall Space Flight Center.** *For further information, Circle 9 on the TSP Request Card.*

Inquiries concerning rights for the commercial use of this invention should be addressed to the Patent Counsel, Marshall Space Flight Center [see page A8]. Refer to MFS-23849.

Calibration Method for an Ultrasonic Gray-Scale Recorder

The gray-scale response is directly correlated to the electronic signal for more accurate ultrasonic C-scans.

Lewis Research Center, Cleveland, Ohio

Ultrasonic C-scanning is one principal nondestructive evaluation technique used in inspection. The current practice is to generate either a black and white or gray tone "C-scan" to show flaws. In the use of gray tone C-scans, there is a need to relate the gray level to the signal strength received as quantitatively as possible. Currently a qualitative judgement is made of the darkness of a scan and an estimate is made of the signal strength transmitted. The present methods are time consuming and have limited accuracy. A calibration method is needed which produces a comparator scale based on signal strength which may be matched with the "C-scan" record of the recorded signal.

A calibration method has been developed which is based on the direct correlation of the gray scale response to the electronic signal used. This calibration takes the form of a density scale with the different levels of gray corresponding to a percentage of signal transmission.

To perform this calibration, the transducers are positioned just as for a through-transmission ultrasoinc C-scan, but no specimen is used between the transducers. The spacing between transducers is set at the same distance as for actual specimens. The gain is set to give a signal strength of 100 percent as measured on the oscilloscope when the ultrasonic beam is passing through the water path only. With the recorder turned on, an area about 1/2 by 5 in. (1.3 by 13 cm) of an imaginary specimen is scanned. The recorder is preset so that it gives the maximum intensity recording at this 100 percent signal intensity. The gain is then adjusted to give a signal setting of 90 percent on the oscilloscope. Another 1/2 by 5 in. (1.3 by 13 cm) area is scanned and recorded alongside the previous 100 percent area. The procedure is repeated using signal strength settings of 80 percent, 70 percent, 60 percent and so on down to 10 percent. This procedure gives a recording similar to the one shown in Figure 1.

This recording then becomes a standard. To use the standard for

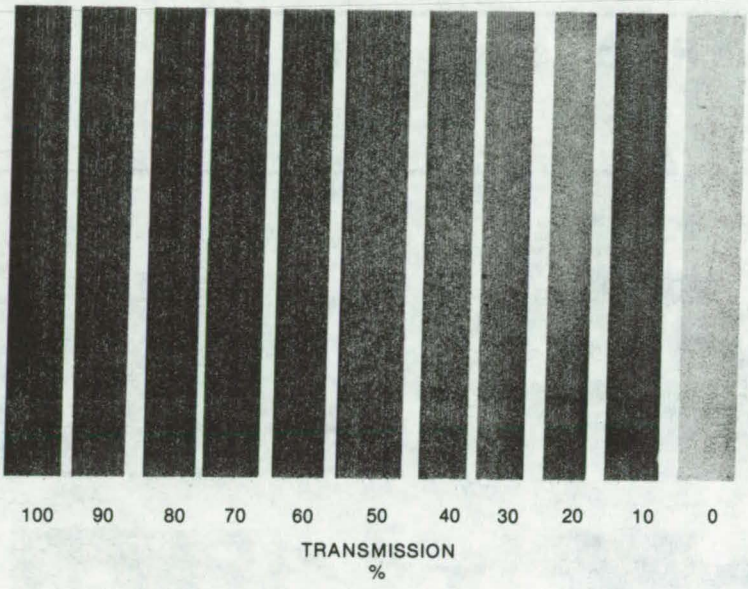

Figure 1. The **Optical Density** of each reference area is measured, preferably with a reflective metering device, to generate this reference curve of reflective-intensity versus transmission.

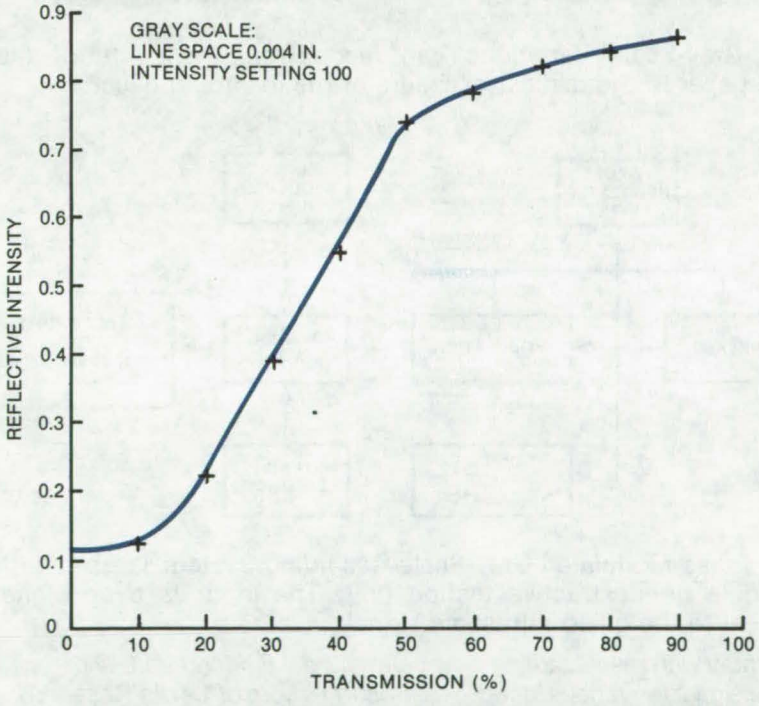

Figure 2. **Intensity-Versus-Transmission Curve** for a gray-scale recorder is obtained with the transducers positioned for a through-transmission ultrasonic C-scan, but with no specimen between the transducers.

determining the ultrasonic transmission of an unknown part, the optical density of each 1/2 by 5 in. (1.3 by 13 cm) reference area is measured (preferably with a reflective-type metering device) and a reference curve of reflective intensity versus transmission is plotted as shown in Figure 2. Next, the unknown specimen is placed in a fixture between the two transducers using the same setup and settings used to develop the reference curve and the entire part is scanned. Transmission of any area can be determined by measuring the recorded density of that area and reading the transmission value off the curve.

This calibration method can be used to determine the transmission of an unknown specimen. The method could also be used to shift the recording range to a more desirable one, i.e., more linear with respect to transmission versus intensity. The high transmission range is sometimes of more interest than the lower ranges, and the recording range could be artificially shifted to make it linear with respect to intensity in this higher range.

This calibration method could also be used for other types of ultrasonic C-scans, such as pulse-echo.

This work was done by Paul E. Moorhead of **Lewis Research Center.** *No further documentation is available.*
LEW-12782

High-Resolution Gray-Scale Recorder

Accurate gray-scale recordings from low-voltage signals.

Lewis Research Center, Cleveland, Ohio

An electronic circuit has been developed which makes it possible to obtain gray-scale recordings with good contrast and linearity over the entire recording density range for an ultrasonic testing unit.

Ordinarily the output signal of an ultrasonic unit is not suitable for gray recordings because the voltage is too low. Simple amplification of the signal results in nonlinearity and poor contrast in the recording. This new specially-developed electronic circuit produces a square wave of constant voltage but of varying width. The frequency of the square-wave pulses can be adjusted to determine the optimum pulse frequency. After determining this best frequency, it is held constant (a frequency of approximately 1 kHz works well with this unit).

In operation, the voltage and frequency of the square wave are held constant. The density of the recording is controlled by varying the pulse width proportional to the incoming voltage signal. This signal is amplified and sent to the recording pen. This yields recording densities varying continuously from the darkest possible with the recording paper being used to the color (whiteness) of the recording paper as shown in Figure 1. A block diagram of the circuitry is shown in Figure 2.

This electronic circuit is presently being used for gray-scale recordings of C-scans in ultrasonic nondestructive testing; it could be used with any instrumentation where a recording in shades of gray with respect to intensity of signal for various locations on a specimen or part is desired.

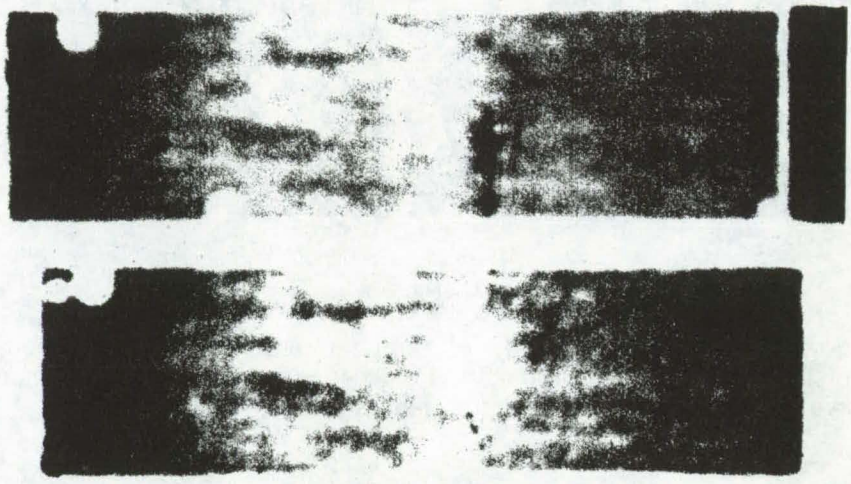

Figure 1. **Gray-Scale Variations** can range from the white of the recording paper to the darkest exposure of the recording paper.

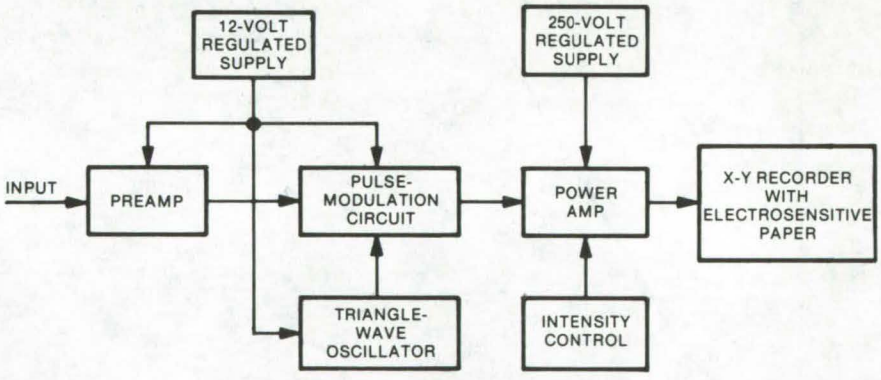

Figure 2. **Pulse-Modulated Gray-Scale Recording System** is used with an ultrasonic nondestructive testing unit. The input is a dc signal proportional to the gated ultrasonic signal.

This work was done by Thomas M. Davis, Paul E. Moorhead, and Robert L. Sorg of **Lewis Research Center.** *No further documentation is available.*
LEW-12783

Multiple-Input Land-Use System Concept

Interactive system would simplify the storage, retrieval, and manipulation of demographic information.

NASA's Jet Propulsion Laboratory, Pasadena, California

There is a growing need for a comprehensive geographic-information system that can be used for natural resource analysis and land-use planning. Ideally the system would accept any input format including photographs, thematic maps, and tabular data. Existing systems that rely on digital maps extracted from remotely sensed images such as satellite photographs have limitations because they are not interfaced easily with other geocoded information. Those systems that use grid-cell codes are difficult to update and are restricted in their range of applications because of their inherent tabular format.

A proposed computerized system for land use overcomes these difficulties and allows interaction between the user and stored digital images extracted from virtually any information source. The system would simplify the incorporation of new data and the comparison of data sets. It would also facilitate the interrogation of particular areas of interest within the data base.

A block diagram of the proposed system is shown in the figure. Demographic information in any format is converted to frames of digital data, each of which is arranged as a raster scan. The frames are registered by pixel alinement to conform to a single format and are assembled into a comprehensive data base of registered "images." A major advantage of the raster format is that x and y coordinates are implicit in the scan and thus do not have to be entered as separate coded data; z values can be treated as Boolean layers in a three-dimensional data space. The images could be extended to include more area or more variables without reformatting the data. Updated images could be introduced simply by replacing a data plane.

Perhaps the greatest flexibility offered by this system is in the interrogation of particular areas and in cross-referencing between data planes. As seen in the figure, the user would first extract the relevant data region from the major file; then the area of immediate interest (an administrative district for example) would be accessed by generating a binary mask that outlines the area. Multiplication of the binary mask with the frame would select data from the defined area.

The use of pixels as grid cells has other advantages. For example, a histogram of pixel values could be used to derive area percentages within a raster scan; or, table-stretch algorithms could be applied to manipulate pixel values within a frame or between two frames to generate a third.

This work was done by Frederic C. Billingsley, Nevin A. Bryant, and Albert L. Zobrist of Caltech for **NASA's Jet Propulsion Laboratory.** *For further information, Circle 10 on the TSP Request Card.*
NPO-13903

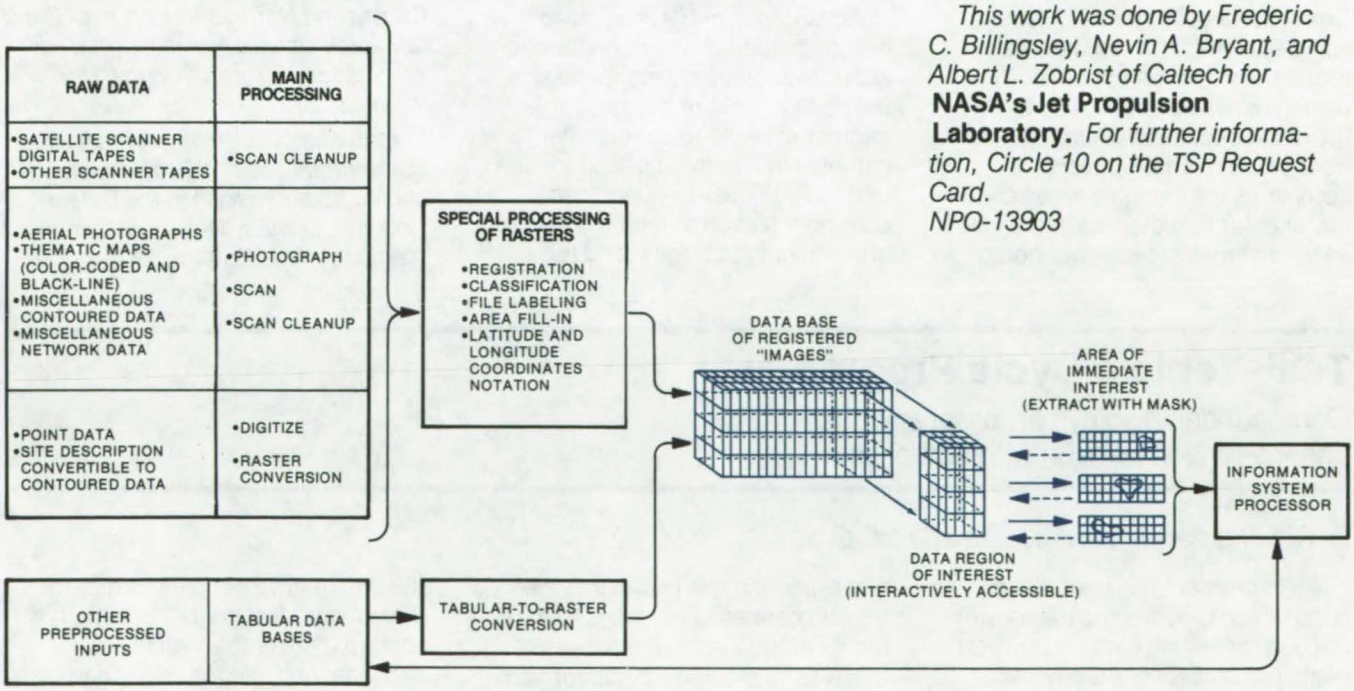

Image Based Information System would accept data in a variety of formats and convert it to registered raster-scan images with a single format. The images could then be manipulated by the system processor to read out desired information. Existing methods of digital-image processing could be modified to develop the necessary software and hardware needed to implement the system.

Microstrip Backfire Antenna

Microstrip resonator is improvement over dipole-fed and waveguide-fed backfire designs.

Langley Research Center, Hampton, Virginia

Short backfire antennas have been effectively employed for various applications over the past several years. The radiated field from a backfire antenna is similar to that from a multielement endfire antenna that has a radiation pattern with field maxima in a direction normal to the large reflector. Thus, short backfire antennas, whether dipole-fed or waveguide-fed, are much smaller and weigh much less than multielement arrays that have similar radiation characteristics. In this same respect to weight and size, the waveguide-fed backfire design was an improvement over the dipole-fed design. Now the microstrip backfire antenna described in the illustration is a further improvement over both designs.

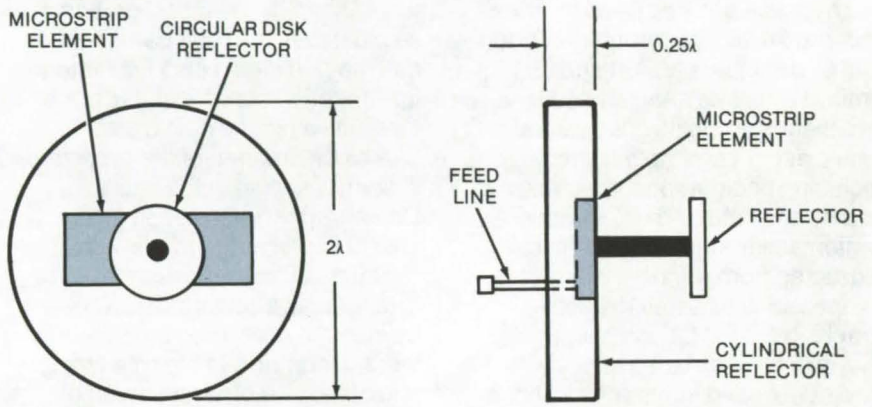

A Thin Microstrip Resonator in the new design replaces the waveguide to provide pattern and gain characteristics similar to those of the waveguide-fed design with much less physical area, thus reducing weight and size of the antenna assembly without degrading the performance.

Tests were conducted, including impedance, radiation patterns, and gain, to determine optimal design for the microstrip backfire antenna. Optimum directivity was obtained using a flush (or offset) mounted rectangular microstrip resonator having dimensions of $0.4\lambda\varepsilon_r$ by $0.9\lambda\varepsilon_r$. A circular reflector placed in front of the microstrip resonator completes the backfire assembly. A rectangular reflector the same size as the microstrip resonator could also be used. The basic microstrip resonator design is a suitable substitute for the waveguide configuration.

Advantages of the microstrip design include simpler construction with a reduction in weight and size over other backfire designs. The microstrip backfire concept has potential in a number of applications that include dual-frequency and dual-polarization antenna systems, array-thinning designs, and feed designs for larger parabolic reflectors.

This work was done by Thomas G. Campbell of **Langley Research Center** *and Norman V. Cohen of Old Dominion University. For further information, Circle 11 on the TSP Request Card.*

Inquiries concerning rights for the commercial use of this invention should be addressed to the Patent Counsel, Langley Research Center [see page A8]. Refer to LAR-12172.

Test-Vehicle Cycle Programer

Compact unit displays preprogramed test speeds for comparison with actual speed.

Lewis Research Center, Cleveland, Ohio

An instrument has been developed which reduces the manpower needed for testing electric powered vehicles. Society of Automotive Engineers test procedures require operating an electric vehicle in a selected stop-and-go driving cycle and repeating this cycle until the vehicle ceases to meet the requirements of the cycle. The results of these tests provide a basis for comparing the performance of various electric vehicles. A typical cycle is to accelerate from zero to 20 mph (32 km/h) in 19 seconds, cruise at 20 mph for 19 seconds, coast for 4 seconds, brake to a halt in 5 seconds, and idle for 25 seconds before starting the next cycle. For this type of testing, it was necessary to have a human timer work with the

driver. The Test Vehicle Cycle Programer, Figure 1, eliminates the need for this extra person.

The heart of the system is a programable read only memory (PROM), Figure 2, which has the required test profiles permanently recorded on plug-in cards. A clock oscillator with a timing resolution of 0.5 seconds drives a timing counter which addresses the profile memory. The PROM generates a DC analog signal which drives a speedometer displayed on one scale of a dual meter whose second scale displays the vehicle actual speed. The vehicle operator controls vehicle speed to match the desired speed. The accuracy of the displayed speed generated by the test vehicle cycle programer is about 1.0 mph (1.6 km/h) within typical meter accuracy and readibility.

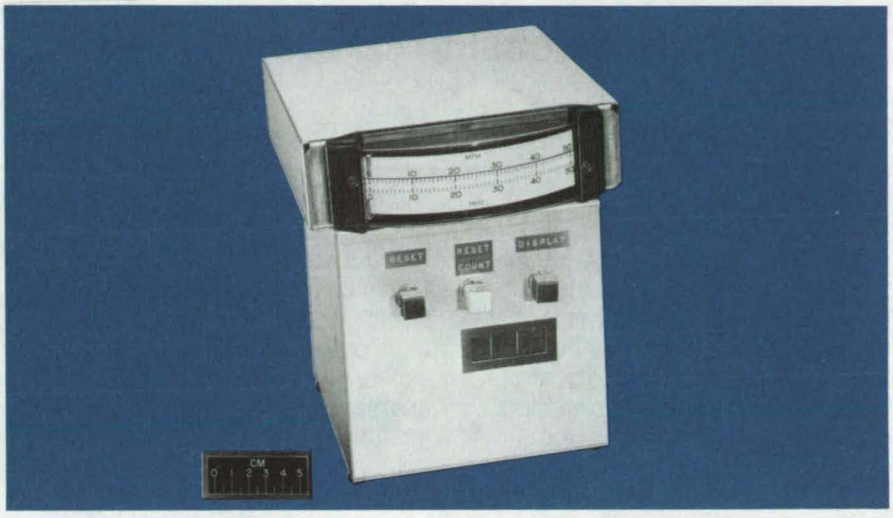

Figure 1. **Test-Vehicle Cycle Programer** has a dual scale that allows the operator to compare his actual speed with the preprogramed test speed.

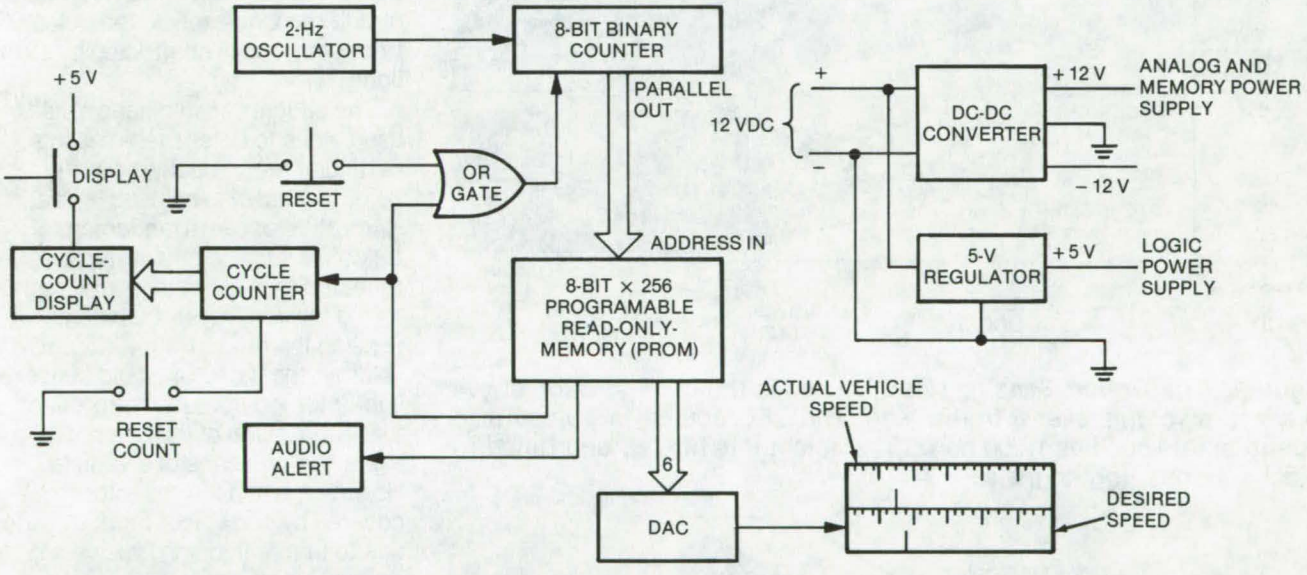

Figure 2. **Clock and Counter** step a programable read-only memory (PROM) through the test cycle. Audio tones alert the driver to the start of a new cycle and to a speed transition within a cycle.

One second prior to each speed transition such as acceleration-to-constant-speed or constant-speed-to-coast, a buzzer sounds for one-half second to forewarn the operator of a change. A longer duration signal of one second is used after the idle period to emphasize the start of a new cycle. The PROM controls the recycle start time as well as the buzzer activation.

Three switches are incorporated into the test vehicle cycle programer. One switch resets the programer back to the start of a cycle in case of a false start. A second switch activates a digital display which stores the total number of cycles completed. The third switch resets the stored number of cycles completed to zero.

The cycle programer is powered by the test vehicle's 12-volt battery through a 5-volt regulator and a 12-volt dc to dc converter.

Features of the test vehicle cycle programer include a large meter, a buzzer, packaging to allow a ready interchange of memories with different profiles, small size, minimal current drain, and reverse supply voltage protection.

This work was done by Daniel J. Lesco and Richard F. Soltis of **Lewis Research Center.** *For further information, Circle 12 on the TSP Request Card.*
LEW-12977

Optical Traffic-Sensing Concept

Photosensor does not depend on the interruption of ambient light.

NASA's Jet Propulsion Laboratory, Pasadena, California

Recent studies have shown that traffic flow on highways can be improved if pertinent information about traffic status is made available to the motorist or is used to control traffic signals. A scaled-up version of an optical proximity detector (described in "Optical Proximity Detector," NPO-13306, *NASA Tech Briefs,* Vol. 2, No. 1, p. 50) has been proposed as a versatile traffic sensor that could replace or augment existing systems (such as inductive loops). The photosensor, which does not depend on ambient light, has several features that protect it against spurious or ambiguous inputs. It could be implemented in several forms to cope with different roadway conditions.

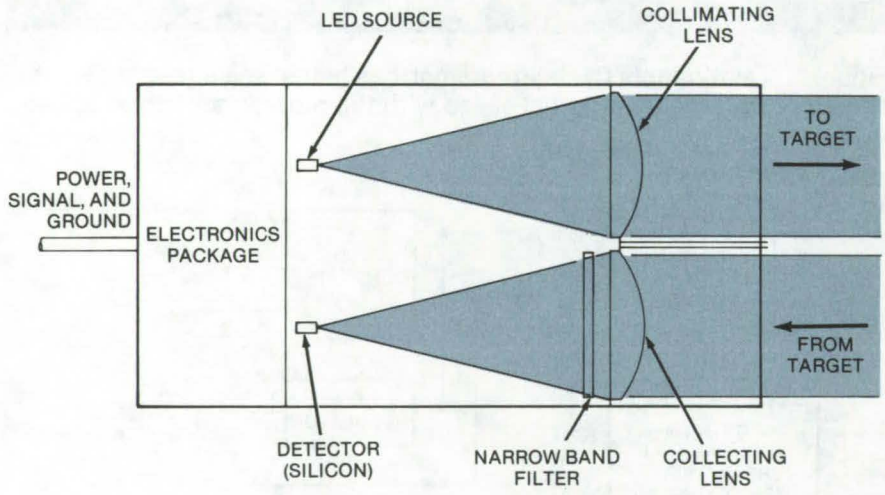

Figure 1. The **Optical Sensing Head** is used in the configuration above to sense a volume over a traffic lane. The LED source is pulsed at a repetition rate such as 1,200 hertz. The detector is filtered and tuned to reject spurious light signals.

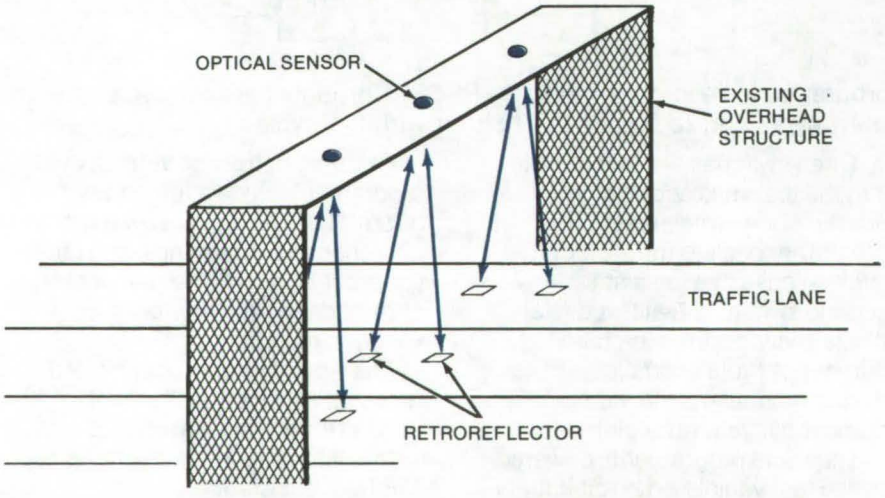

Figure 2. An **Optical Traffic-Status Sensing System** is shown in an overhead arrangement using an existing structure to mount the sensing heads. By processing the output of the two adjacent retroreflectors in a lane, vehicle speed and even vehicle length and spacing can be determined.

The optical sensing head is shown in Figure 1. Passing vehicles would reflect the beam of the LED which is pulsed at a convenient frequency near 1 kHz. The LED output is picked up by a silicon PIN photodiode. A phase-sensitive detection circuit responds only to the pulse frequency and is unaffected by stray light.

The optical sensing head could be used alone to detect vehicles in a particular area - such as a traffic lane. It could also be used with a retroreflector (an arrangement of reflective surfaces that returns reflected rays along the same path as the incident rays). Instead of sensing the return from a vacant volume, the detector would sense light returned from the retroreflector. Interruption of the beam would signal the presence of a vehicle. However, when the reflector is covered by snow, ice, mud, or water due to rain or flooding, this version is probably ineffective, and the proximity sensing arrangement may be more reliable.

One possible arrangement of the sensing system is shown in Figure 2. Other arrangements would depend on the structures that exist or can be built at a particular location.

This work was done by Alan R. Johnston and Katsunori Shimada of Caltech for **NASA's Jet Propulsion Laboratory.** *For further information, Circle 13 on the TSP Request Card.*
NPO-13603

Voice-Output Solar Energy Reporter

Continuous telephone access to local Sunfall data.

Lewis Research Center, Cleveland, Ohio

The output of any particular solar energy installation depends on the amount of solar energy input at the proposed location. For a given location, National Weather Service records are typically used, where available, to estimate how much solar energy will be received. Such records are generalized, however, and as the use of solar energy grows, accurate and complete day-to-day information is needed on how much solar energy is actually available at the location of interest.

The Voice-Output Solar Energy Reporter automatically obtains daily measurements of locally available solar energy and reports the information on request over a commercial telephone line. The system is designed for users who can knowledgeably interpret the measurements; e.g., news-media weather reporters who can explain the meaning of the data to the general public and designers of solar-energy systems. A prototype system has been successfully tested in the Cleveland, Ohio, area for over six months providing data for a local television station daily report of the "Solar Energy Index."

Referring to the figure, the system uses a commercially available pyranometer transducer to sense Sunlight intensity, an integrator to accumulate measurements over the daytime period, and a commercially available voice synthesizer to report the results in English language through an automatic response telephone interface.

The system measures Sunlight intensity continuously and integrates the measurement over two different time periods. The minor integration period, 3.6 seconds, measures immediate solar intensity in arbitrarily selected units of kilowatts per 500 square feet. The major integration period, nominally Sunrise to Sunset, generates a daily "Solar Energy Index" measured again in arbitrary units of kilowatt-hours per 500 square feet. [The units have been selected to represent a practical collection module 20 by 25 ft (6.1 by 7.6 m) in size.] The Index is clear measurement of the amount of solar energy available at the location. Users of the Index must, of course, calculate conversion efficiencies based on how the energy is utilized; e.g., conversion to heat with solar collectors may be up to 60-percent efficient, while conversion to electricity with solar cells is typically 10- to 15-percent efficient.

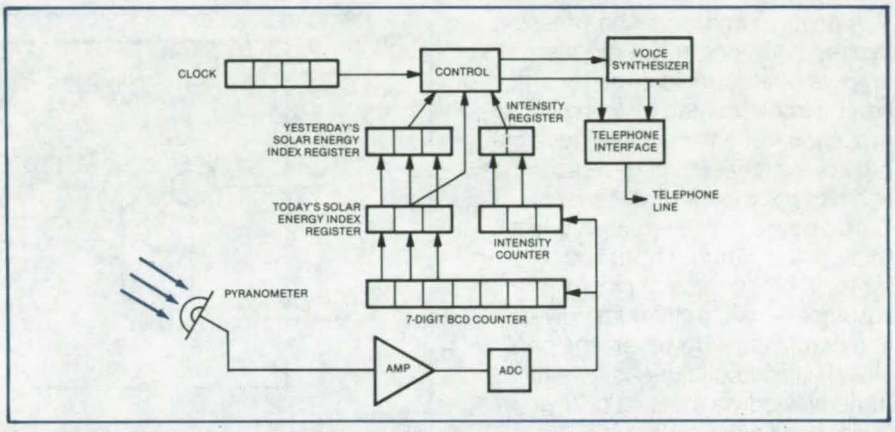

Voice-Output Solar Energy Reporter combines commercially available equipment to sense solar energy and measure instantaneous intensity and accumulated energy at a remote site. Data are encoded in voice form and stored for retrieval at any time by commercial telephone.

The system is accessible by telephone at any time through a compatible telephone interface which provides automatic ring and answer functions; i.e., a Bell System Model 1001B data coupler or equivalent. When the telephone is answered, the voice synthesizer vocally reports the measured results in decimal numbers. Three measurements are reported: yesterday's "Solar Energy Index," the current value of today's "Solar Energy Index," and the current solar intensity. A 24-hour electronic clock automatically transfers today's "Index" to yesterday's register at a pre-set time and resets the integrator to start a new day's measurement.

Digital readouts on the front panel provide, also, for direct and continuous reading of all three measurements.

Except for the pyranometer, the telephone line, and a 117-volt ac power source, the system is entirely self-contained. When the unit is once matched to a particular pyranometer at a fixed location and orientation, internal calibration adjustments should not be necessary. The integrator has a built-in self-zero correction which eliminates any drift in the measurement circuits. Zero offset is corrected automatically every 3.6 seconds.

This work was done by Burdell L. Detterman and Robert L. Miller of **Lewis Research Center.** *For further information, Circle 14 on the TSP Request Card.*

Preliminary drawings can be reproduced and made available at cost if requested.

Inquiries concerning rights for the commercial use of this invention should be addressed to the Patent Counsel, Lewis Research Center *[see page A8].* *Refer to LEW-12947.*

Simplified Data Compressor

Image data are compressed for transmission by simple, economical circuitry.

NASA's Jet Propulsion Laboratory, Pasadena, California

A novel image-data compression system demands only a modest amount of electronic circuitry and can be implemented by using microprocessor technology. The system provides a low-cost compressor that exhibits good performance.

The new compressor is intended for sending pictures from space — for example, photos of planet surfaces — with minimum power and bandwidth. However, the principle is also applicable to facsimile transmission via satellite or over telephone lines.

The compressor uses a microprocessor and various IC's for memory, buffering, and control. The total power consumption is only 3.55 watts.

Like previous compressors, the new unit applies a mathematical transform (in this case, the Hadamard transform) to samples of data from each line of the image and then applied differential pulse-code modulation (DPCM) to the transform coefficients. Unlike previous units, the new version preprocesses the image signal by multiplying blocks of

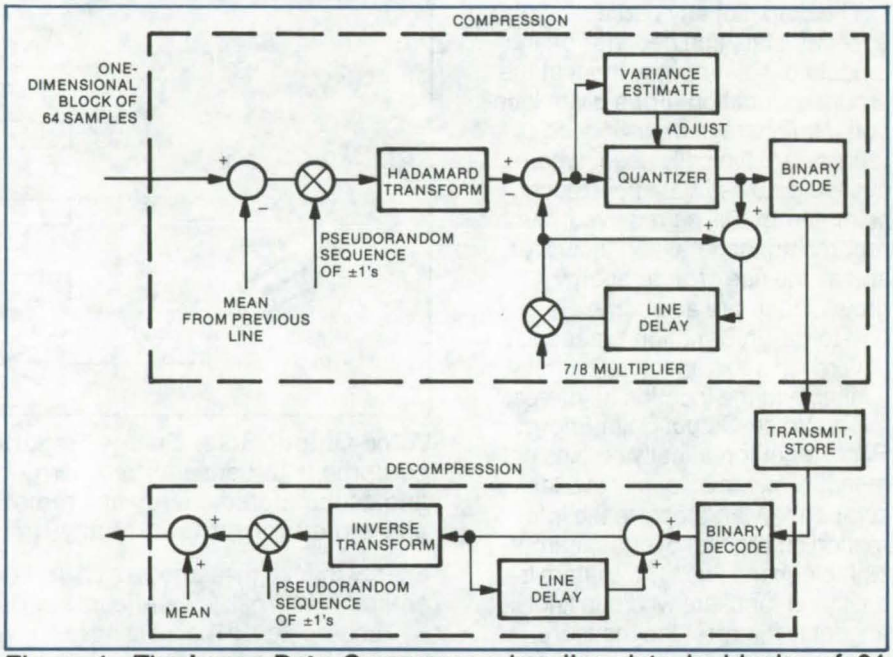

Figure 1. The **Image-Data Compressor** handles data in blocks of 64 samples. The mean from a previous line is subtracted, and a pseudorandom sequence of positive and negative 1's multiplies the samples of each block. A Hadamard transform applied to the blocks yields 64 transform coefficients. Each coefficient is compared with an approximation to the corresponding coefficient of the previous line, and the difference is quantized. The quantized values are transmitted or stored. The procedure is reversed to reproduce the image.

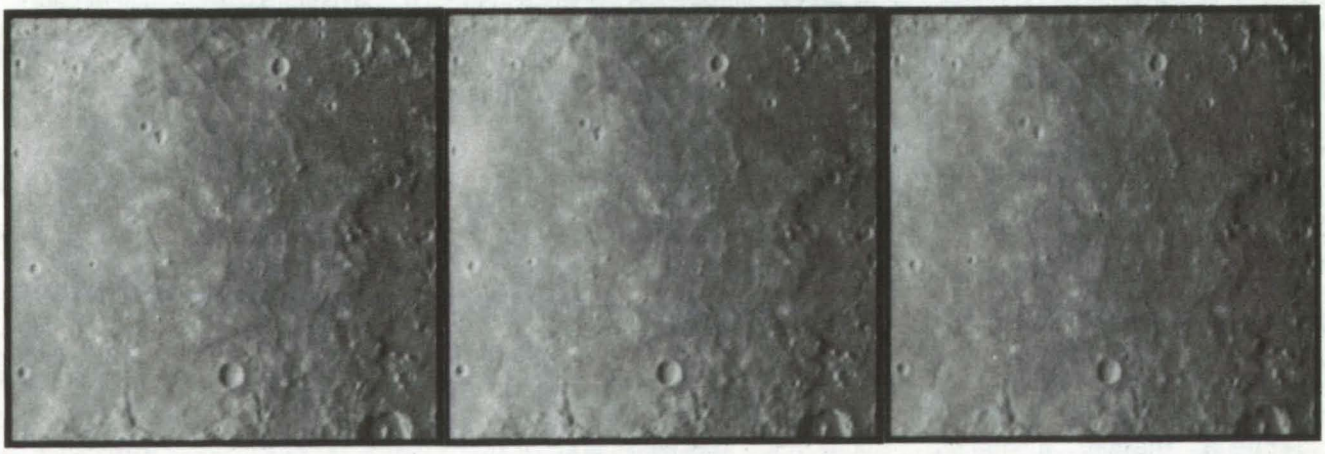

[a] [b] [c]

Figure 2. The **Original Image** (a) coded at 8 bits per pixel, is hardly distinguishable from that reproduced from the compressed version at 2.1 bits per pixel (b). Compression at 1.1 bits per pixel (c) creates a poorer image, but would still be acceptable for many applications.

incoming data by a pseudorandom sequence of positive and negative 1's (Figure 1). As a result, the transform coefficients have similar statistical characteristics, and the same DPCM coder can be used for all of them. The compression process is simpler, and less circuitry is required. Also, the process is reversible — it functions just as well as a decompressor on the receiving end.

The data compressor operates with a maximum image line length of 2,048 picture elements (pixels) at 8 data bits per pixel. The maximum incoming data rate is 80,000 pixels per second.

The unit compresses the data to either 1.1 bits per pixel or 2.1 bits per pixel. The 2.1-bit compression (Figure 2b) provides an excellent image that is difficult to distinguish from the original (Figure 2a). The 1.1-bit compression (Figure 2c) produces a poorer image but nevertheless one that offers a better rate/quality tradeoff than many other compression techniques. The unit is almost immune to data errors; random errors at rates up to 1 per 1,000 have negligible effect on quality.

This work was done by Robert F. Rice, Vance C. Tyree, and Chialin Wu of Caltech for **NASA's Jet Propulsion Laboratory.** *For further information, Circle 15 on the TSP Request Card.*
NPO-14041

Preventing Radio-Paging System Tieup

A time-delay relay limits message time of emergency radio-paging system, thereby preventing its inadvertent tieup.

Lyndon B. Johnson Space Center, Houston, Texas

Emergency radio-paging systems are tied in with the standard telephone network. They are commonly used in large facilities where key people frequently move around and are difficult to reach by telephone. These people carry belt-mounted paging receivers that are reached by radio transmitter through a standard telephone system. A person simply dials a three-digit number on his telephone unit to communicate with a particular receiver. The system is designed to handle one telephone at a time because the messages are relatively short.

One problem with this system is that it can be easily tied up if a telephone caller depresses a hold button or forgets to hang up while he is still on the air. This problem is resolved with an automatic time-delay relay.

The relay is connected with the telephone circuit as shown in the figure and permits adjustable message time between 30 and 55 s. After that interval, the relay opens, making the line free for another paging regardless of what the previous caller did with his telephone.

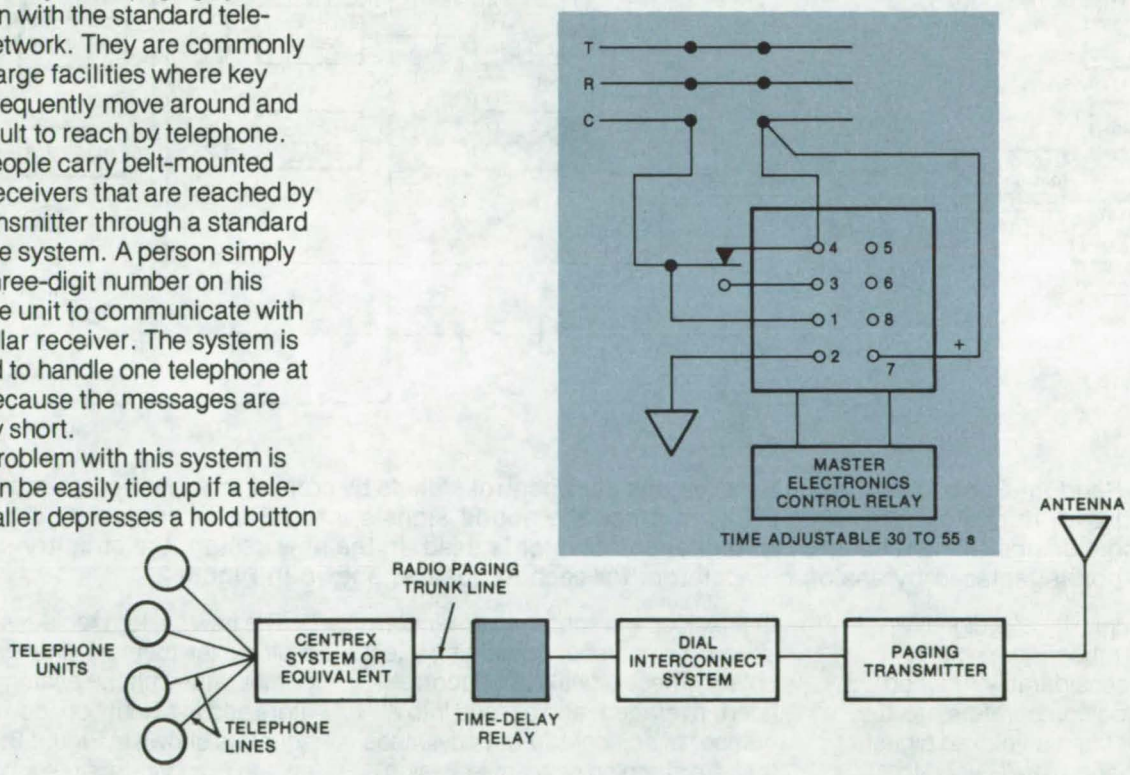

Emergency Radio-Paging System Uses Time-Delay Relay to prevent system tieup. As shown in the magnified detail, the "C" lead closes to energize the relay to permit a message to go through. At the end of the time delay, the "C" lead opens, releasing the switch train ahead of the circuit to the radio-paging amplifier.

This work was done by Jose P. Jasmin of Rockwell International Corp. for **Johnson Space Center.** *No further documentation is available.*
MSC-19696

Hybrid Random-Sound Test-Control System

Analog and digital circuits are combined in a simple and versatile controller.

NASA's Jet Propulsion Laboratory, Pasadena, California

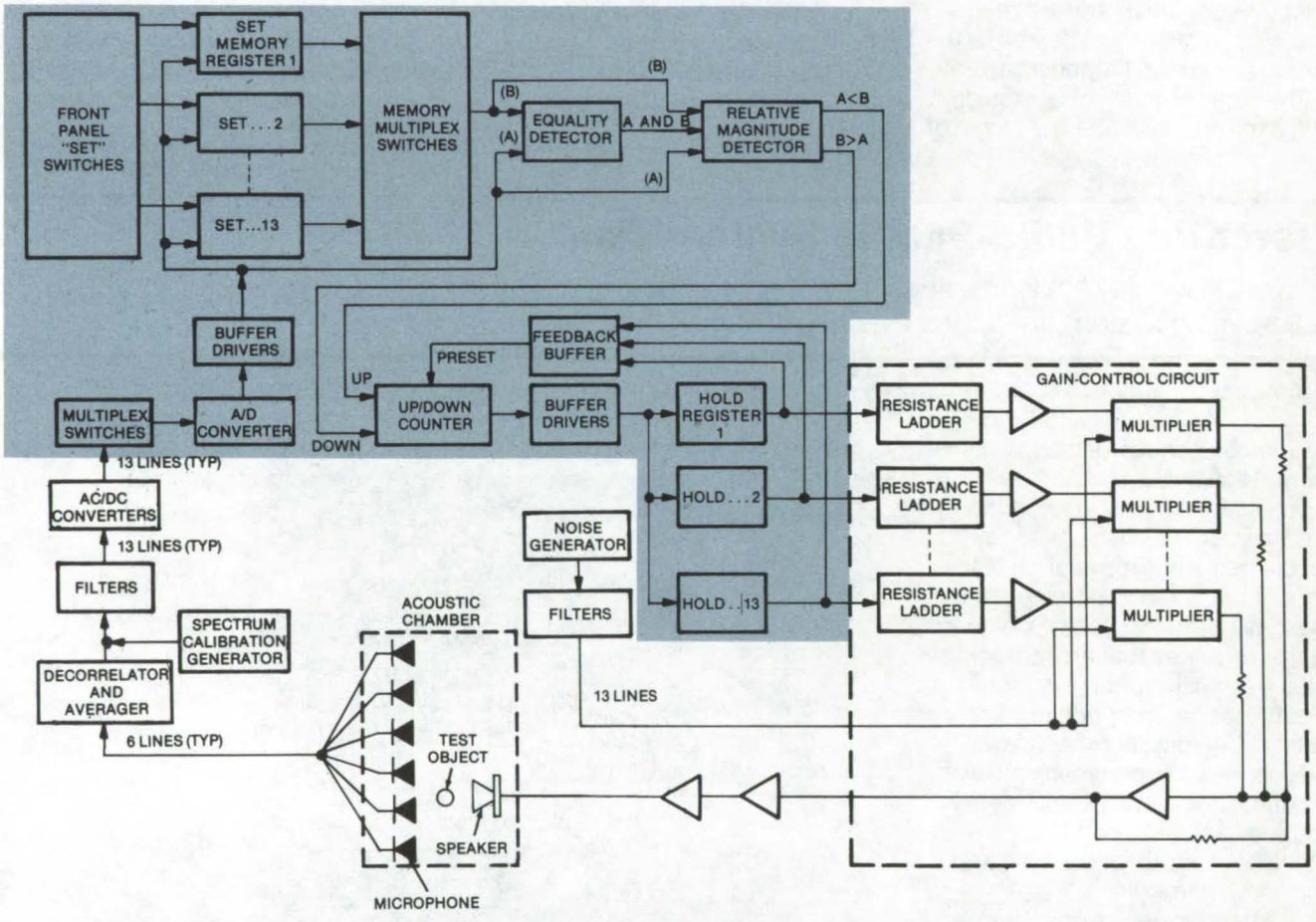

Figure 1. **Random-Sound Test Controller** develops gain-control signals by comparing detected sound levels in each band with reference "set" levels. Filters block the sound signals into adjacent frequency bands. In a conventional design, shown here, an all-digital comparator is used. In the new design, the circuitry shown in the color box is replaced by analog comparators for each frequency, shown in Figure 2.

The complexity of a digitally-controlled random-sound test system is considerably reduced when analog comparators are substituted for the multiplexed digital circuitry that is usually used to compare actual and reference sound levels. Digital processing is retained in other portions of the controller. The hybrid system is simpler than its all-digital counterpart as well as having flexibility and versatility not possible when digital techniques are used alone.

A typical digital sound-test system (Figure 1) has several microphones that pick up the spectrum of random sound in a chamber containing a test object. These signals are decorrelated, averaged, and divided into a number of adjacent frequency bands that are sampled by a time-division multiplexer. Each sound level is converted to a digital word and is compared with a reference that is stored in a memory register. The reference levels are changed by digital panel switches. A counter is stepped up or down in response to each comparison to increase or decrease the gain for that frequency band.

The new system replaces the multiplexer memory and digital comparator with the analog comparators and individual up/down counters shown in Figure 2. The analog comparators respond to the relative values of the detected and reference signals in each frequency band. If the detected signal is less than the reference, the corresponding counter is clocked "up"; if it is greater, the counter is clocked "down." The counter outputs directly couple to the resistance ladders in the gain-control circuit.

By eliminating the multiplexing

network and single clock used in the digital system, the new design allows the servocontrol rate for each band to be adjusted independently. This is desirable since the response times of the frequency bands are different. The servocontrol rate is easily adjusted for each channel by changing the clock frequency of its up/down counter. The higher the frequency, the faster the servo-system will adjust to changing signal levels.

Since a separate comparator is used for each channel, theoretically there is no limit to the number of channels; in the original design the number was limited by the multiplexer inputs and the speed of the A/D converter. In addition, online changes in the control level for any channel can be made by adjusting the reference potentiometer while the system is operating. This obviates the need for the "spectrum calibration generator" shown in Figure 1.

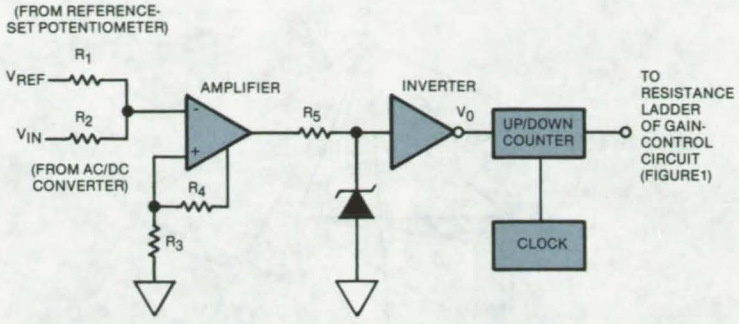

Figure 2. **Analog Comparators** for each frequency band replace the digital comparator (color box) of Figure 1. When V_{in} exceeds V_{ref}, V_o goes to logical "0," which puts the counter in the "count-up" mode. This increases the gain for that frequency band, ultimately increasing V_{in}. The feedback mechanism holds the sound level within ± 1 dB of the set level.

An additional benefit of the modified system is the ability to introduce hysteresis in the analog comparator response by varying resistors R_3 and R_4. This allows compensation for time lags in non-linear systems such as anisotropic acoustic chambers.

This work was done by Raymond C. Woodbury of Caltech for **NASA's Jet Propulsion Laboratory.** *For further information, Circle 16 on the TSP Request Card.*
NPO-13900

Self-Navigating Robot

Rangefinding equipment and onboard navigation system determine the "best" route from point to point.

NASA's Jet Propulsion Laboratory, Pasadena, California

An autonomous self-navigating robot, with laser/stereo-TV "vision" and the "intelligence" to decide how to get where it is going with the least expenditure of energy, has been converted from science-fiction fantasy to hardware reality by scientists at NASA's Jet Propulsion Laboratory. With its onboard navigation system and rangefinding and touch sensors, the JPL robot can be deposited in an unknown environment and find its way around obstacles, taking the most efficient route to a desired goal. Along the way, its "eyes" periodically pan the surroundings and update its memory as to the positions of obstacles, passable regions, and other features that might affect its movement. Its odometer and gyrocompass keep track of its current position and generate signals that are used to keep the robot on the current path.

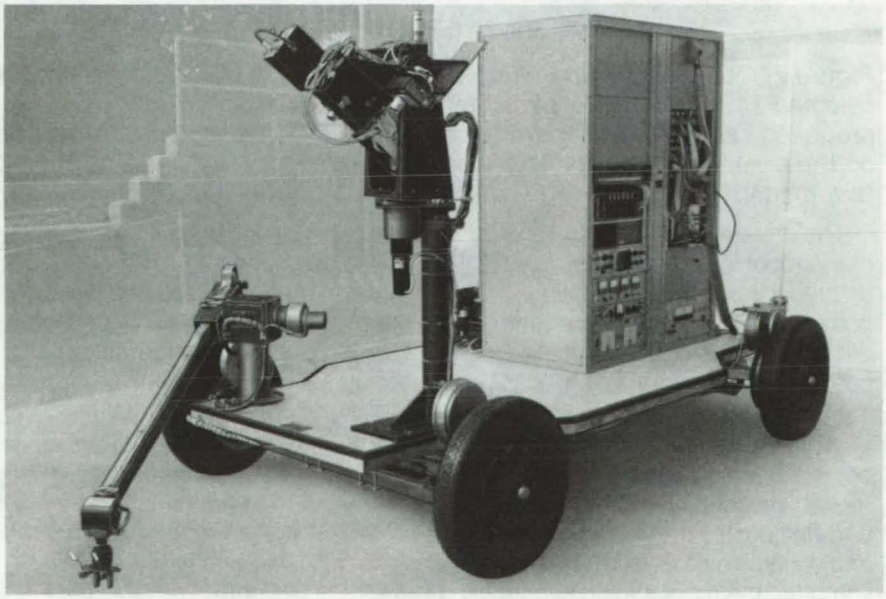

Figure 1. The **JPL Research Robot** has two TV cameras and a laser for scanning and mapping its environment. An arm for collecting rock samples is seen in the foreground.

(continued next page)

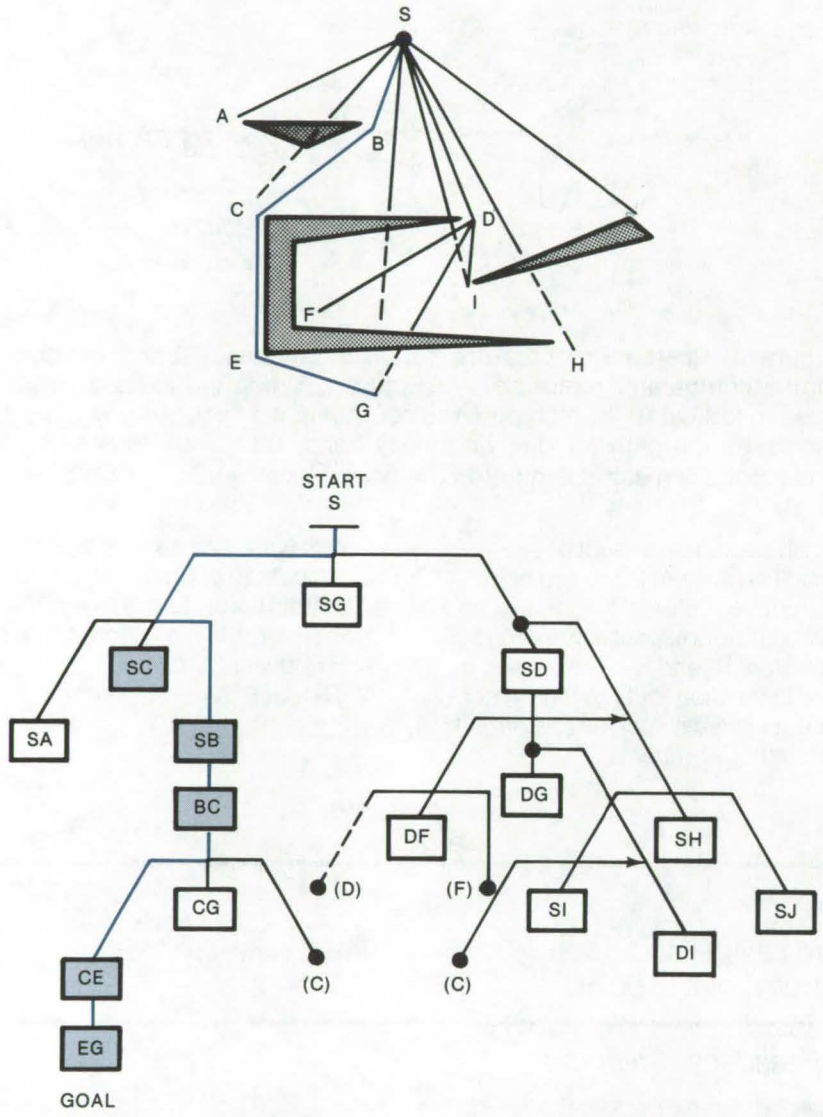

Figure 2. The Best of All Possible Paths (in color) from start to goal is selected from candidate paths by the robot navigation system. Each proposed segment is checked for obstacles (implied by an intersection on the tree) and is evaluated for cost. Distance is a measure of cost in this model.

The present experimental version of the robot is connected by an umbilical cord to its controlling computer network. However, the decreasing size of powerful microcomputers now enable all processing to be done onboard.

While its travels have thus far been limited to a laboratory test-model landscape, where it has been carrying out tasks such as finding and collecting selected rock samples, the robot should eventually find many terrestrial and space applications. Its abilities to work in environments that would be hazardous to people and to handle dangerous materials could be exploited, for example, in finding and transporting explosives and radioactive samples.

The ability of the robot to navigate is sharpened by other "smart" features, including its "maze-solving" and "wall-following" capabilities, its "awareness" of how its own size, shape, and turning radius can effect its maneuverability, and special "path-pruning" computations that reduce the number of potential paths, while the robot searches for the one that is most efficient.

The JPL robot operates as a hierarchy of concurrent processes that are distributed through its computer network. Its navigation system includes an "executive," which is the controlling section, a path-planning module, and a guidance system. To plan a path, the system memory maintains a terrain model of the robot's environment as sensed by its laser and TV vision system. The model is partitioned into small segments, and the ground features (i.e., traversable, nontraversable, or unknown regions), are recorded in a compact numerical representation.

The path planner finds the most direct, unobstructed route that would require the minimum expenditure of energy. At present, distance is used as a measure of energy expense, although other measures, such as time or power consumption (which would depend on the topography of the path), may be used in the future.

The terrain model is structured so that if an obstruction to the direct path is detected, alternate paths that avoid the obstruction are proposed. For example, in traveling from point S to point G in Figure 2, the robot selected the best path (in color) after considering the alternatives shown in the "search tree." In this notation, a line cutting a tree link implies an obstruction of the physical link and that the alternate paths originate from the same point as the original link. Associative memory methods are used to detect and prevent repetition in the search, and cost estimates are associated with each proposed segment.

This work was done by Alan M. Thompson of Caltech for **NASA's Jet Propulsion Laboratory.** *For further information, Circle 17 on the TSP Request Card.*
NPO-14190

Physical Sciences

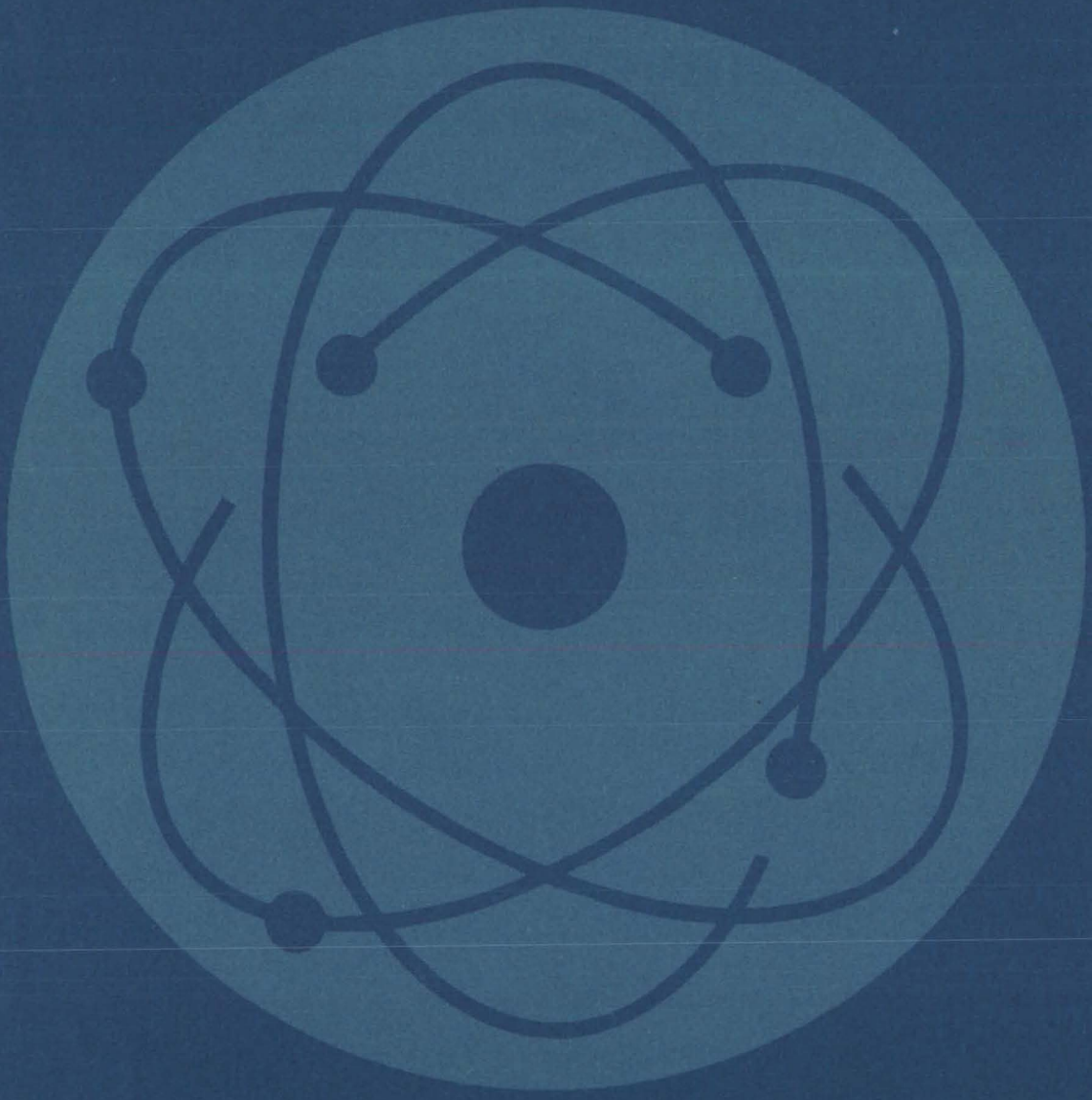

Hardware, Techniques, and Processes

Books and Reports

Improved Optical Filter

Partial polarizers increase the selectivity of birefringent filters.

Goddard Space Flight Center, Greenbelt, Maryland

A new birefringent optical filter uses partial-polarizing elements to improve the suppression of unwanted wavelengths. The new filter, which is tunable over a wide range, was originally designed for satellite observations of solar phenomena. It should be useful in other applications that demand precision tunable optical filters.

The simplest form of a conventional (Lyot) birefringent filter uses a polarizer and a sequence of doubly refracting elements each followed by a polarizer. The thicknesses of the birefringent elements form a geometric progression. This assembly produces a sequence of spaced transmission bands; however, since not all wavelengths between the transmission bands are suppressed, colored filters must be added to remove secondary transmission maxima.

The new filter is assembled as a sequence of modules. Each module (see figure) includes: a "perfect" entrance polarizer, a first birefringent crystal with fast and slow axes at 45° to one polarizer axis, a partial polarizer, a second birefringent crystal that is half the length of the first with the fast axis rotated 90° with respect to the first, and a final perfect-polarizing element. With the partial polarizer, the assembly acts as a superposition of Lyot filters for which the transmitted electric field strengths near the secondary maxima are opposite in phase and cancel. If the ratio of polarized to unpolarized light is equal to 9, the first secondary maximum can be decreased by a factor of 24.

The filter is tuned by rotating the exit and entrance polarizers in unison. An alternative design is tuned by sandwiching the entrance and exit polarizers between pairs of rotatable half-wave plates. The plates can be controlled by stepping motors commanded by a computer.

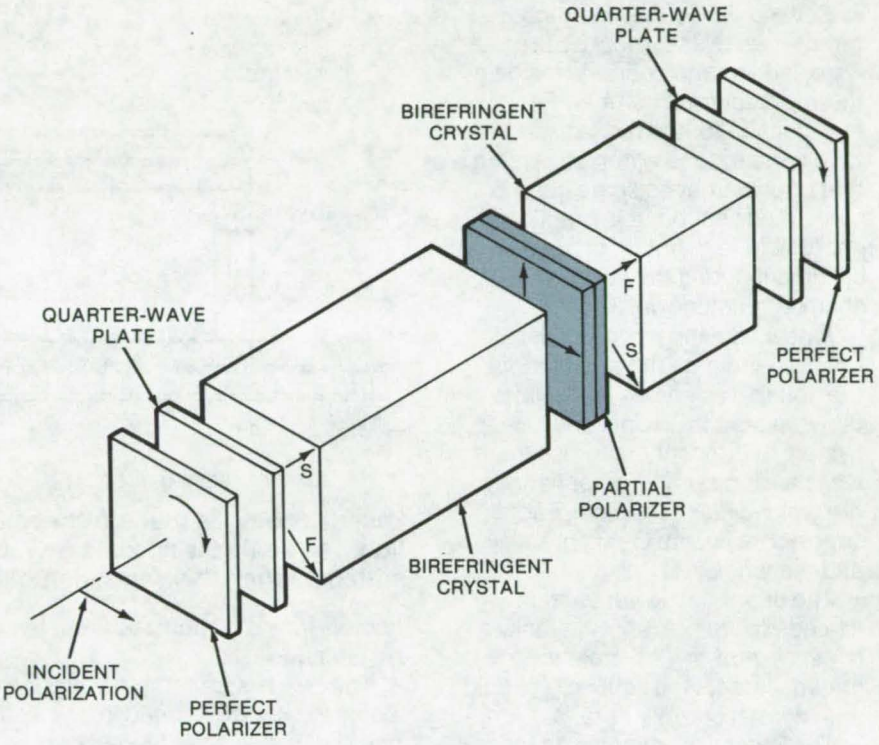

This Improved Optical Filter includes a partial polarizer between birefringent elements. A plastic film on the partial polarizer compensates for any polarization rotation by the partial polarizer. The thickness of the film is determined empirically. The two quarter-wave plates change incident, linearly polarized light into elliptically polarized light.

The separation of the transmission bands may be increased by coupling several modules, with the length of the first birefringent element of each module equal to two-thirds of the length of the second element of the preceding module. In this configuration, each exit polarizer serves as the entrance polarizer for the succeeding module.

A four-module filter has been built. In this filter, the longest crystal is 79.312 mm in length. At a wavelength of 5,324 Å, the filter gives a half width of 0.09 Å; it is tunable from 4,500 to 8,500 Å.

This work was done by Alan M. Title of Lockheed Missiles & Space Co., Inc., for **Goddard Space Flight Center.** *For further information, Circle 18 on the TSP Request Card.*

This invention is owned by NASA, and a patent application has been filed. Inquiries concerning nonexclusive or exclusive license for its commercial development should be addressed to the Patent Counsel, Goddard Space Flight Center [see page A8]. Refer to GSC-12225.

Housing Protects Laser in Vacuum

An airtight housing encloses a laser for easy alinement and operation in a high-vacuum chamber.

Goddard Space Flight Center, Greenbelt, Maryland

Several difficulties are encountered when a laser must be precisely positioned and operated inside a thermal vacuum chamber. First, the high voltage for the laser discharge tube can produce corona or arcing that often damages some components; and second, it is practically impossible to maintain precise laser alinement during the vacuum chamber pumpdown.

A new housing has been developed to eliminate these problems; the housing as shown in the illustration is sealed to enclose the laser system at atmospheric pressure. Its walls and upper and lower flanges are welded stainless steel. Each flange contains an O-ring groove and tapped holes.

The upper and lower vacuum-sealed covers are 6AL4V, titanium honeycomb 1 in. (2.5 cm) thick. This material meets the lightweight, rigid, and thermal stability criteria.

The lower cover serves as a mounting and reference plane for the laser and the laser beam bender. Both covers are bolted to the flanges. The upper cover provides access for instrumentation and laser maintenance.

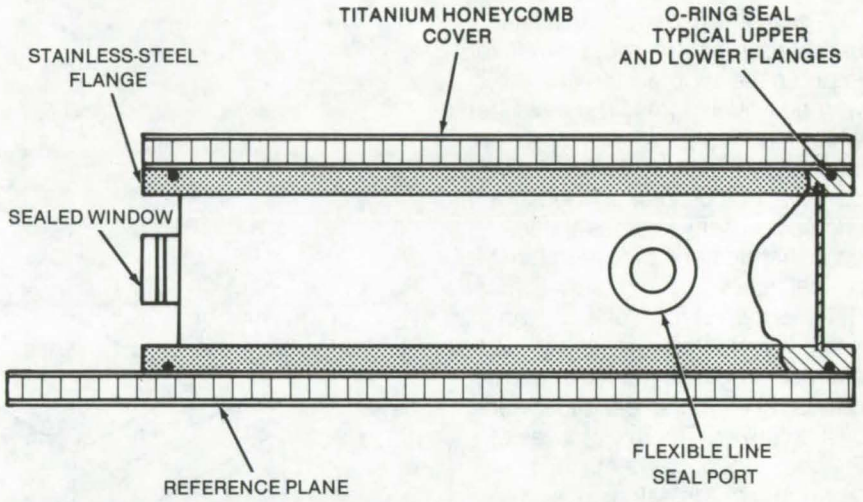

Laser Housing is made from type 304 stainless-steel welded construction. The sealed window is BK7, or equivalent, glass. The beam is transmitted through this window into the vacuum chamber.

The beam is transmitted through a sealed window located in one housing wall. A seal flanged port located in another wall serves as an interface for flexible line coupling. The flexible line runs through the vacuum chamber to the outside, maintaining the laser enclosure at atmospheric pressure.

This work was done by Vincent G. Canali of **Goddard Space Flight Center.** *For further information, Circle 19 on the TSP Request Card.*
GSC-12241

Directional Laser Velocimeter With Doppler Velocity Simulator

Directional ambiguity eliminated with optical adaptation of microwave technique.

Langley Research Center, Hampton, Virginia

A serious limitation in laser velocimetry has been the problem of directional ambiguity. Techniques demonstrated in the past for the removal of directional ambiguity have employed color, polarization, or frequency shifting. A newly developed technique uses phase-shift networks at the optical and baseband frequencies and, as such, is an optical adaptation of previously-existing microwave technology.

A diagram of the optical layout of the laser velocimeter (LV) is shown in Figure 1. The laser illuminates the sample volume, which is replaced here by a laser-Doppler velocity simulator consisting of a rotating glass block and a mirror. The simulator has been developed as a fundamental instrument for testing and analyzing LV's. The beam is refracted through the glass block and is reflected back by the mirror through essentially the same optical path. The simulator is simple to construct and has reversible motion with a component in the direction of the illuminating laser beam. The returned beam is collinear with the incident beam and provides Doppler shifts of 5 MHz or greater.

The backscattered radiation is collected and split into two equal intensity beams, each of which is incident on a photodiode detector. The transmitted beam is sampled by low-reflectance beam splitters, and

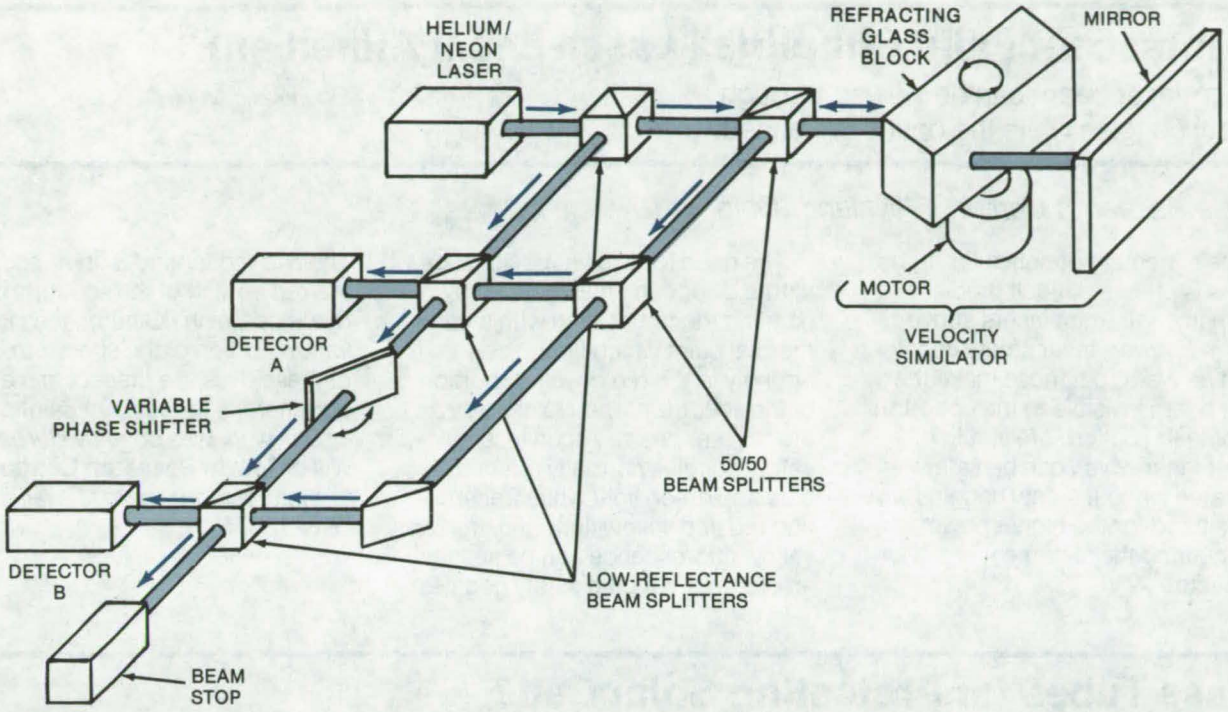

Figure 1. The **Direction-Sensitive Laser Velocimeter** is shown above with a velocity simulator developed for test purposes.

the sample beams are heterodyned with the backscattered light. The phase shifter produces an effective phase delay of 90° between the sampled transmitter beam to detector A and the sampled transmitter beam to detector B. Figure 2 shows a typical output for a velocity simulator rotating at 45 rps.

This newly developed technique for direction sensing in reference-beam laser-Doppler velocimeters has been tested (along with the newly developed velocity simulator), and immediate application is planned for wind-tunnel velocity measurements. An alternate configuration produces finite fringes that move in one direction or the other as the measured particle approaches or recedes.

This work was done by John M. Franke of **Langley Research Center.** *For further information, Circle 20 on the TSP Request Card.*

Inquiries concerning rights for the commercial use of this invention should be addressed to the Patent Counsel, Langley Research Center [see page A8]. Refer to LAR-12176 and LAR-12177.

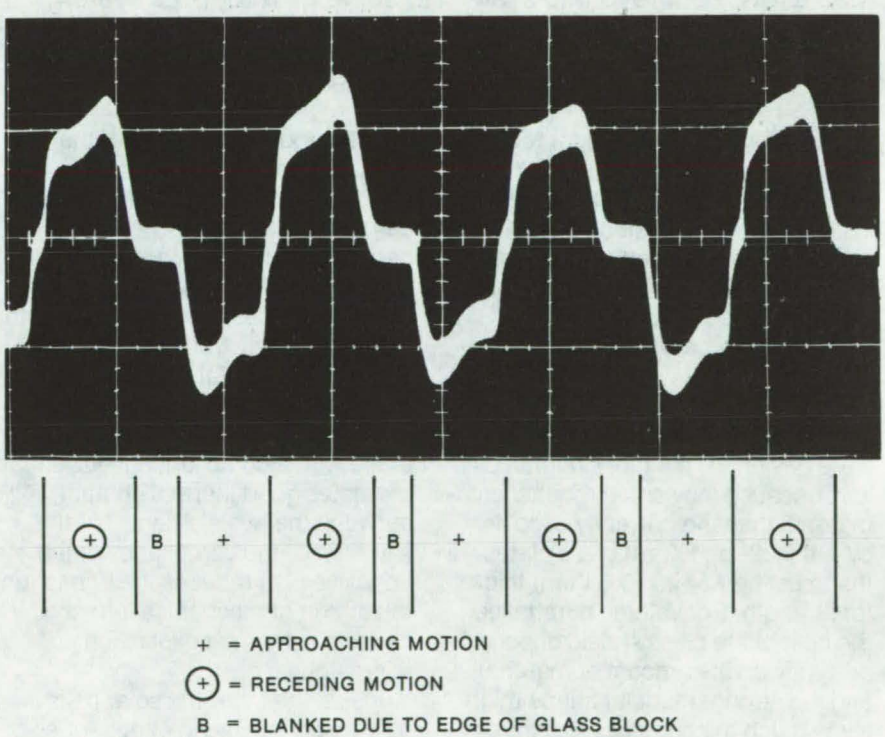

Figure 2. The **Output of the Direction-Sensitive Velocimeter** is an electronic signal that differentiates between approaching and receding motion. As the refracting block rotates, the mirror appears to approach, stop, and recede. The output is not a perfect square wave because of inherent characteristics of the electronic processing system.

Fluorescent Paint Simplifies Laser-Beam Alinement

Argon-laser beam can be viewed through safety goggles while the optics are alined.

Lewis Research Center, Cleveland, Ohio

The alinement of optics for argon lasers is often a difficult problem. Normally, for argon lasers above 1.0 mW power, laser safety goggles must be worn, but these make the laser beam invisible to the operator. To aline the optics safely, a low power laser which can be safely operated without safety goggles is substituted for the higher power laser during the alinement procedure.

The need for a lower power substitute laser can be eliminated by painting the target area with a commercial paint which fluoresces strongly in the red or yellow portion of the spectrum when excited by an argon laser beam. Argon laser safety goggles normally attenuate blue and green light while transmitting red and yellow light, thus red or yellow fluorescence can be seen by an operator wearing safety goggles.

The dye rhodamine B fluoresces in the red portion of the spectrum; the dye rhodamine 6G fluoresces in the yellow portion of the spectrum. Both of these dyes are present in many commercial fluorescent paints.

This work was done by Herbert A. Will of **Lewis Research Center.** *No further documentation is available. LEW-12571*

Glass Tubes for Protecting Solar Cells

Tubes might be less expensive enclosures than parallel plates and also allow a photovoltaic system to serve as a thermal system.

NASA's Jet Propulsion Laboratory, Pasadena, California

Photovoltaic solar cells for terrestrial use might be protected more easily and cheaply by putting them inside glass tubes instead of sealing them hermetically between a pair of flat glass sheets. This approach has been proposed as a method of protecting the cells against environmental effects of wind, rain, snow, hail, and blowing sand.

In the application for which they were designed, the tubes might cost less because they could require less material than the currently used 4- by 4-ft (1.2- by 1.2-m) glass plates that must be 1/4 in. (0.64 cm) thick for strength. For volume purchases, the cost of the glass should depend primarily on the amount of material, and the stronger tubular shape might allow much thinner glass and thus cost less.

The cells would be placed at the center of the glass tube, as shown in Figure 1. There, they "sit" atop a formed copper-foil pedestal that also makes electrical contact to the (positive-polarity) bottom of the cells. The foil pedestal also conducts heat away from each solar cell to the glass envelope. The negative, or top, contact is made at either end of the cell. This contact may also be designed and shaped to draw heat away from the semiconductor material.

The structural bond between the circuit and the glass envelope is made with a compliant adhesive that promotes good thermal contact between the two elements. At the same time, the compliancy of the adhesive also reduces the impact on the circuit of mechanical stresses caused by thermal expansion mismatches.

Inside the tube, the solar cells may be connected in either series or parallel, although the parallel connection is easier to implement and is mechanically superior. Output from cells measuring 2 by 2 cm would be approximately 0.35 A/in. (0.14 A/cm) of length, with each

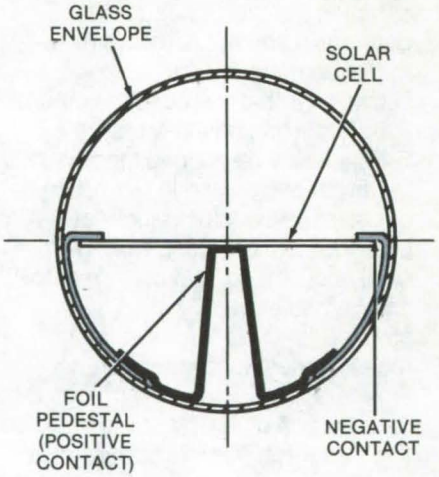

Figure 1. **Glass-Tube Mounting** for solar cells employs a pedestal made of copper foil that also provides the positive contact. The negative contact is made to the top of the semiconductor cell. For one test system, the tubes were 1 in. (2.5 cm) in diameter and 4 ft (1.2 m) long.

solar-cell element generating 0.46 Vdc.

It is also possible to match the electrical performance of each tube to an electrical storage medium such as nickel/cadmium cells. For example, eight cells 6 in. (15 cm) long, connected in series via overlapping tabs on the positive and negative interconnects, would deliver 2 A at 3.68 Vdc. The solar cells could be coupled to a three-cell storage battery integrated into the tube itself. The result would be a freestanding power source.

Terminations within the tube, shown in Figure 2, are made much as for a standard cylindrical battery cell, although both polarity connections are on the same end of the tube instead of at opposite ends. Springfinger contacts to these terminations permit the cell to be rotated mechanically to track the path of the Sun across the sky. Such tracking would increase the power output from the solar cells because they would receive more direct solar radiation during the course of a day.

It would also be possible to put many of the tubes in parallel on a movable platform so they could all track the Sun together. With the tubes ganged in this way, air circulated through and around them could absorb the solar energy not converted to electricity. Not only would the air cool the tubes but it could also be used as a source of heat.

This concept has recently been used to construct a few test panels, which are now being evaluated. Although performance and cost data are not yet available, the system has initially been shown to function much as predicted.

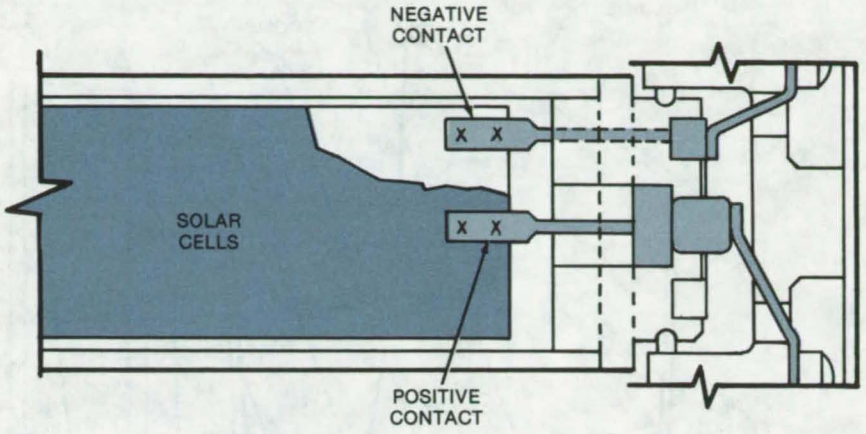

Figure 2. Connections to the Solar Cells are made at one end of the glass tube, which can also be rotated to track the path of the Sun across the sky. The connection shown above is for one tube in an array of several side-by-side tubes.

This work was done by Benjamin Shelpuk of RCA Corp. for **NASA's Jet Propulsion Laboratory.** *No further documentation is available.*

This invention is owned by NASA, and a patent application has been filed. Inquiries concerning nonexclusive or exclusive license for its commercial development should be addressed to the Patent Counsel, NASA Resident Legal Office-JPL [*see page A8*]. *Refer to NPO-14200.*

High-Temperature Solar Converter

Three-dimensional absorber and adjustable reflector are efficient in direct or diffuse Sunlight.

Goddard Space Flight Center, Greenbelt, Maryland

By using a three-dimensional arrangement of absorbers and an adjustable parabolic reflector, a new solar-energy converter achieves the high temperatures in direct Sunlight that are typical of solar concentrators yet remains efficient when there is a strong component of diffuse light, such as on cloudy days. The converter requires no solar-tracking mechanism, thereby saving weight and cost.

As seen in the figure, two focusing parabolic reflectors concentrate Sunlight on three absorbers in a "pi" configuration within an evacuated glass cylinder. The focus of each parabola is located on the profile of the other, as shown. Each focus serves as a pivot point around which its parabola can be turned to adjust the upper aperture of the reflector. This allows the concentration ratio to be varied between 2 and 10.

The collector plates are finned aluminum tubes with an absorbing "dark-mirror" coating (consisting of Al, SiO, and Cr). The collector fluid flows down a central tube, to a rear manifold, then back along the collector through the aluminum tubes. The fluid leaves through a front manifold. This simplifies the external heat-transfer loop, particularly when several collectors are used in combination. Spiral turbulators are included in the absorber ducts to reduce laminar flow and to improve heat transfer to the interior of the collector fluid.

The converter can be used with either a gaseous or liquid heat-transfer medium. The "pi" cross-section collector is intended for use with a liquid; a triangular arrangement is best for gases. The collector tubes could also be configured with combinations of flat and curved fins

(continued next page)

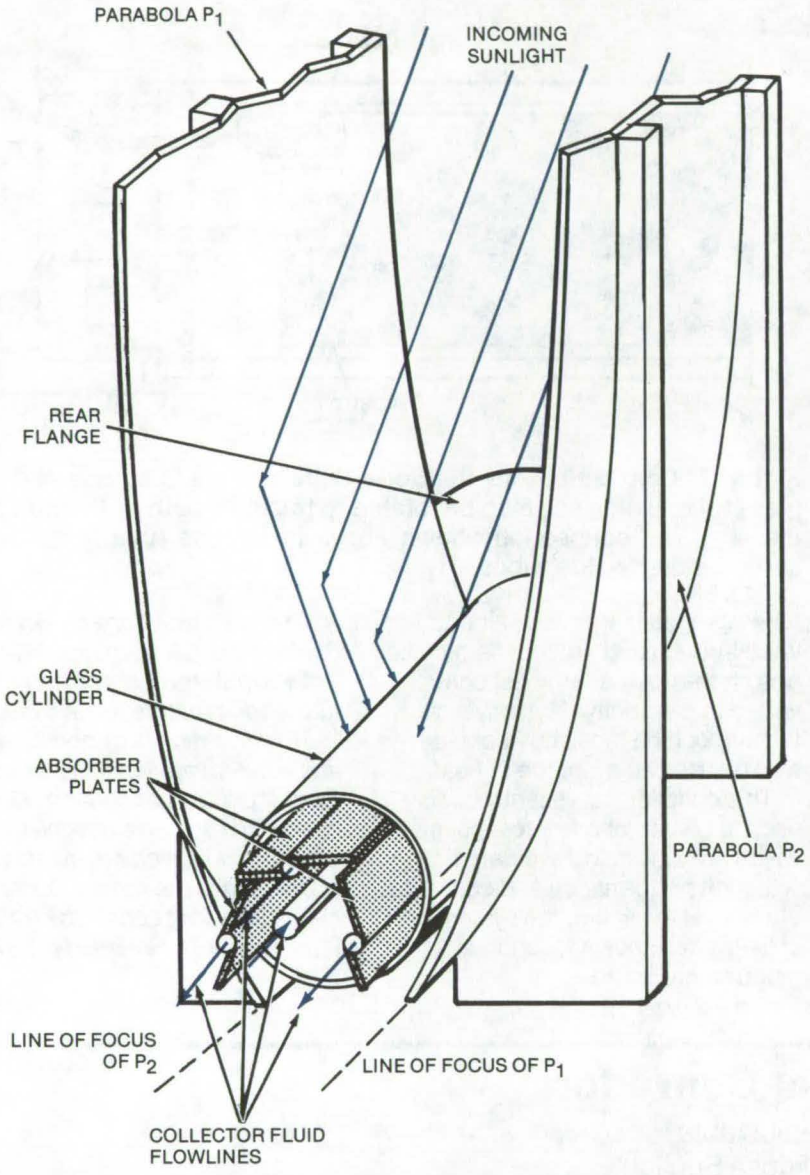

This **High-Temperature Solar Converter** has a parabolic concentrator that directs Sunlight on a three-dimensional absorber assembly within an evacuated glass cylinder. No tracking mechanism is required. The concentrator aperture is adjustable (mechanism not shown) to modify concentration in direct or diffuse Sunlight. The range of adjustment is small.

to maximize the amount of solar radiation that comes in perpendicularly to the collector surfaces.

A prototype of the liquid-collector version has a glass tube 6 in. (15.24 cm) in diameter. The collector plates have fins 2 in. (5.08 cm) wide on tubes 1/2 in. (1.25 cm) in diameter. A 3/4-in. (1.91-cm) central tube is used for the inlet flow. The liquid has a boiling point above 350° F (177° C) and a freezing point below -10° F (-23° C). It remains in the liquid phase during the operation of the converter.

This work was done by Gerard Ascher of **Goddard Space Flight Center.** *For further information, Circle 21 on the TSP Request Card.*
GSC-12234

Double-Sided Solar-Cell Package

A cost-effective solar-cell package is proposed for development of a practical solar-cell system.

NASA's Jet Propulsion Laboratory, Pasadena, California

One of the major difficulties in the fabrication of silicon solar cells has been in obtaining silicon wafers thin enough; i.e., 4 mils (0.1 mm) or less for adequate performance levels. A proposed alternative is to use silicon wafers of practical thickness between 6 to 8 mils (0.15 to 0.20 mm) that are illuminated on both sides. Figure 1 shows two possible double-sided solar-cell configurations that allow the solar energy to reach both sides of the cells.

An important question about a contact arrangement that will permit

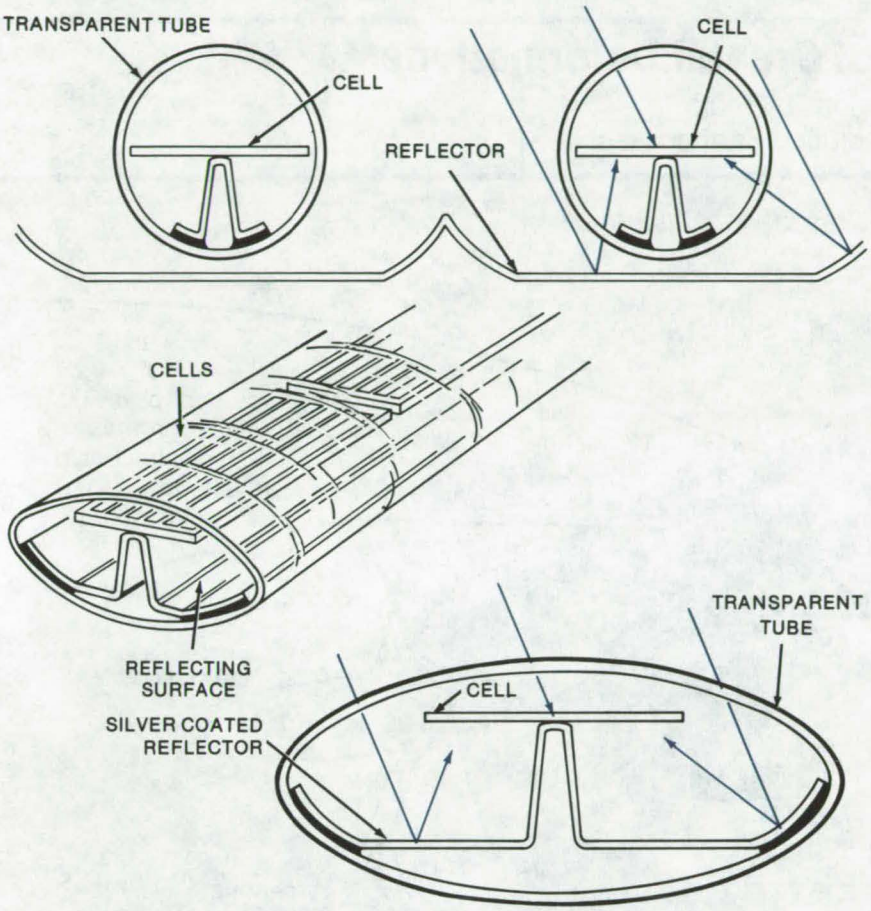

Figure 1. **Proposed Double-Sided Cell Packages** use reflectors to illuminate the back faces. The top configuration shows adjacent cells spaced in such a way that equivalent area is occupied by a reflector allowing a full solar flux to be incident on the back face. The bottom configuration shows a tube package using silver coating to provide a similar system.

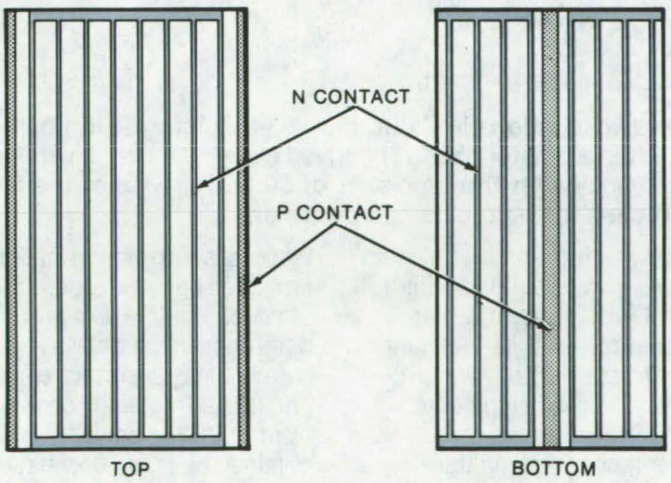

Figure 2. In the **Proposed Contact Arrangement,** after the junction is diffused into all exposed surfaces of the silicon, an etching process is completed in the areas indicated in grey. These areas are metalized to make contact to the base material of the cell. By connecting the three contact stripes, the electrical resistance due to base-material sheet resistivity becomes acceptable.

the collection of photon-generated electrons from both sides of the cell is resolved as shown in Figure 2. Calculations show that if a low-resistivity (0.2 ohm/cm) material can be used, the contact spacing of 1 cm will be adequate. Current at the illuminated surfaces is collected by using a metal grid similar to that used on standard cells, except that the grid is in a front-to-back wrap-around with the exception of areas where the junction has been etched through. The base contact is made by bonding the center stripe to a mounting pedestal, which also acts as one electrical contact.

Since the cells are enclosed in inexpensive plastic tubes, a forced-air-cooling loop is proposed to maintain cell temperature at adequate levels. The loop must include a desiccant to remove moisture from the nonhermetic enclosures to prevent cell corrosion.

This work was done by Benjamin Shelpuk of RCA Corp. for **NASA's Jet Propulsion Laboratory.** *No further documentation is available.*

This invention is owned by NASA, and a patent application has been filed. Inquiries concerning nonexclusive or exclusive license for its commercial development should be addressed to the Patent Counsel, NASA Resident Legal Office-JPL *[see page A8].* *Refer to NPO-14199.*

Real-Time Monitoring of Crustal Deformations

Monitoring Earth's crustal deformations by radio interferometry may be useful in predicting Earthquakes.

NASA's Jet Propulsion Laboratory, Pasadena, California

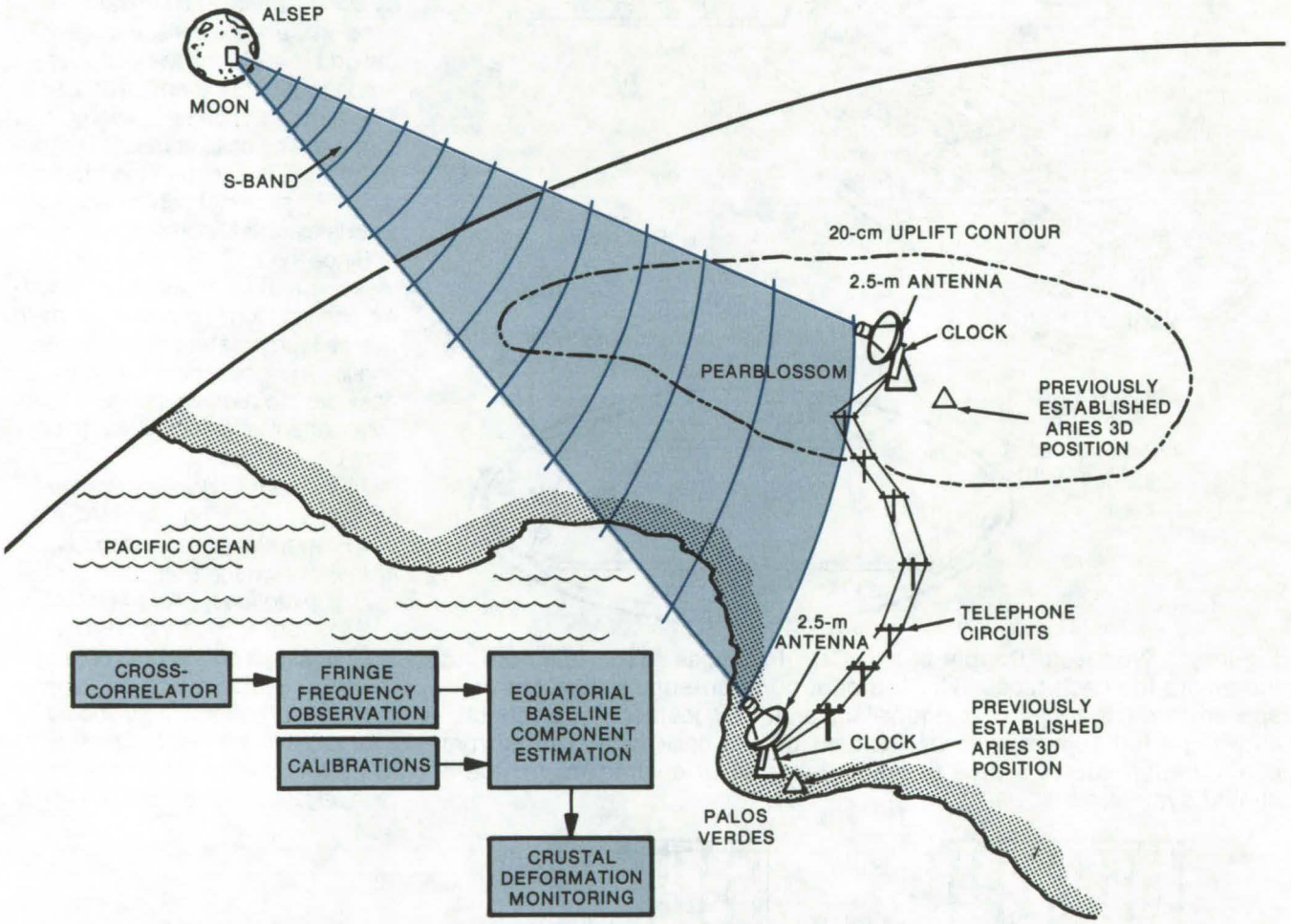

Crustal Deformation Monitoring System setup at two locations in California: A 3-kHz information bandwidth is used for transmission over the telephone lines. Interferometer phase is derived every 10 s over an 800-s interval that makes it possible to extract the fringe frequency with the precision of 50 to 100 μHz of the S-band. A 50-μHz data quality every 800-s time interval implies a 10-cm baseline precision.

The real-time monitoring system with two radio interferometer systems is used to detect the crustal bulging of the Earth's surface, which may be directly related to Earthquakes.

One of the interferometer systems includes two 2.5-m-diameter antennas positioned at two different geographical areas. The antennas receive S-band signals from the Moon, transmitted by ALSEP (Apollo Lunar Surface Experiments Package) stations left on the lunar surface during Apollo flights.

The second interferometer system is ARIES (Astronomical Radio Interferometric Earth Surveying) that utilizes quasars as a time-invariant frame of reference. The two ALSEP antennas are located at the established ARIES sites.

As the antennas pick up the S-band signals from the Moon, the signals are time-tagged by digital code or by L-band signals from GPS (Global Positioning System), using synchronized atomic clocks at both stations (see figure). The signals are then transmitted by telephone lines to a cross-correlation station. The time tags permit the determination of telephone-line delays so that the difference in the delays is compensated before the cross-correlation. The fringe frequency observation from ALSEP or delay from GPS are obtained by cross-correlation and used to estimate crustal deformation.

By incorporating two interferometer configurations, the entire system combines the advantages of both. First, the advantage of ARIES'

time-invariant quasar interferometer is utilized, and second, the real-time capability of ALSEP is used. The system frequency requirement is $\Delta f/f = 2 \times 10^{-13}$, with period T = 800 s.

This work was done by Peter F. MacDoran of Caltech for **NASA's Jet Propulsion Laboratory.** *For further information, Circle 22 on the TSP Request Card.*

This invention is owned by NASA, and a patent application has been filed. Inquiries concerning nonexclusive or exclusive license for its commercial development should be addressed to the Patent Counsel, NASA Resident Legal Office-JPL [see page A8]. Refer to NPO-14124.

Flat-Plate Heat Pipe

"Sandwich" transfers heat efficiently in flat-plate geometries.

Goddard Space Flight Center, Greenbelt, Maryland

Conventional cylindrical heat pipes are not efficient for removing heat from flat surfaces since the evaporator of the heat pipe is not easily coupled to the flat surface. Fluid transfer loops or a flat heat sink attached to the evaporator may be used to improve the coupling; however, these methods require additional hardware and are less efficient than direct coupling.

A new flat heat pipe removes heat efficiently from flat plates and is suitable for applications such as electronic "cold" plates, high-power integrated-circuit substrates, and laser mirrors. The new heat pipe, shown in the figure, has metal transfer wicks — either wire felt or sintered powdered metal — sandwiched between metal plates containing capillary grooves. The working fluid is sealed between the metal panels. As in conventional heat pipes, the fluid evaporates at places where heat is applied and condenses at spots where heat is to be removed, giving up its latent heat of vaporization. The capillary grooves are etched or machined on the inner surfaces of the plates. The metal transfer wicking intersects the grooves on both surfaces to allow fluid flow from plate to plate. There is a continuous vapor path to all points on the plates.

Low-vapor-pressure fluids such as water or methanol are the best working fluids when operating near ambient temperatures. Ammonia and other high-vapor-pressure fluids used with cylindrical heat pipes would be difficult to contain without deforming the flat plates. Other fluids exhibiting low vapor pressures can be used at higher or lower temperatures.

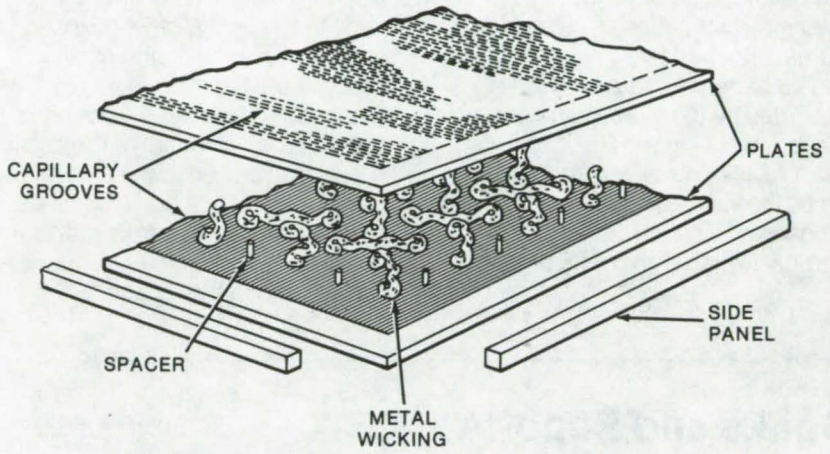

Flat-Plate Heat Pipe has metal transfer wicking and a working fluid sealed between parallel plates containing capillary grooves. The plates can be made of any of the structural metals and joined to the side panels by soldering, welding, brazing, or diffusion bonding.

A typical flat-plate heat pipe with methanol as the working fluid can transport an input heat flux of 2.8 watts/cm^2 while remaining essentially isothermal (varying by only 3° to 5° C over the panel surface). Conductances are approximately 0.7 watt/cm^2-° C at the evaporator and 0.3 watt/cm^2-° C at the condenser. Higher values are possible with water as the working fluid.

This work was done by George L. Fleischman and Bruce D. Marcus of TRW, Inc., for **Goddard Space Flight Center.** *For further information, Circle 23 on the TSP Request Card.*

This invention is owned by NASA, and a patent application has been filed. Inquiries concerning nonexclusive or exclusive license for its commercial development should be addressed to the Patent Counsel, Goddard Space Flight Center [see page A8]. Refer to GSC-11998.

Video Method for Studying Optical Fields

A TV system and an oscilloscope can determine the point-by-point intensity distribution of a two-dimensional optical field.

Marshall Space Flight Center, Alabama

A clever approach for making quantitative measurements of the point-by-point intensity distribution in a two-dimensional optical field uses a TV camera, a TV receiver, and a standard laboratory oscilloscope. By using the lag characteristics of a vidicon, the technique also allows a detailed study of the intensity distribution of pulsed (e.g., 20-ns) light patterns.

The pattern to be examined is recorded by the vidicon and is displayed, by using the RF output, on the television receiver. At the same time, the video signal is displayed on an oscilloscope, by using the vertical sweep signal as a trigger. For TV cameras with random interlace, horizontal and vertical sweep triggers should be provided to the camera externally.

Single horizontal lines in the optical field can be observed by using the "B sweep delay" feature present on most oscilloscopes to isolate one horizontal line. By varying the delay, any horizontal line can be displayed on the oscilloscope. To determine exactly which line is being displayed, a wire from the "A gate" terminal of the oscilloscope is attached to the antenna of the TV receiver. A black line that corresponds to the horizontal line being observed on the oscilloscope will appear on the TV set.

The lag (persistence due to bright illumination) present in all vidicons could be used to display patterns from pulsed lasers, for example the output of a Michaelson-Morley interferometer illuminated by a pulsed ruby laser (pulse duration approximately 15 ns). In this case, the technique can be used to determine the coherence length of the laser.

This work was done by R. S. Mezrich of RCA Corp. for **Marshall Space Flight Center.** *For further information, Circle 79 on the TSP Request Card.*
MFS-23103

Books and Reports

These reports, studies, and handbooks are available from NASA as Technical Support Packages (TSP's) when a Request Card number is cited; otherwise they are available from one of NASA's Industrial Application Centers or the National Technical Information Service.

Solar-Energy Bibliography

A compilation of current and past research

A bibliography of information describing the Marshall Space Flight Center solar-energy research program is available. The bibliography lists over 100 ongoing projects, Tech Briefs, papers and periodicals, and technical reports and patents pertaining to work performed at the center and by its contractors. Each item includes a brief summary or abstract of the work, its publication date (except for ongoing research), and a listing of other materials related to that work. A comprehensive subject index is also included.

Typical entries in the "Ongoing Research" section are:

- Development of a Solar Powered Residential Air Conditioner,
- Design, Fabrication, Testing, and Delivery of a Solar Collector, and
- An Investigation of Fresnel Lens Utilization in Collecting Solar Energy for Power Generation.

Items under "Papers and Periodicals" include:

- Status of Marshall Space Flight Center Solar House and
- Solar Energy Recorder — For Converter Site Selection.

Among "Tech Briefs" cited are:

- Selective Coating for Collecting Solar Energy on Aluminum,
- Printed-Circuit Solar-Cell Array, and
- Universal Solar-Cell Terminal.

"Technical Reports and Patents" is the largest section of the bibliography and includes entries such as:

- Solar Energy Power System — Using Freon,
- Mechanical Thermal Motor, and
- Corrosion Inhibitors for Solar Heating and Cooling Systems.

This report was compiled by Stephen Gargus of **Marshall Space Flight Center.** *Further information may be found in NASA TM-X-73398 [N78-13554], "Solar Energy Bibliography," a copy of which may be obtained at cost from the New England Research Application Center* *[see page A7]*.

Inquiries concerning rights for the commercial use of this invention should be addressed to the Patent Counsel, Marshall Space Flight Center *[see page A8]*. *Refer to MFS-23823.*

Materials

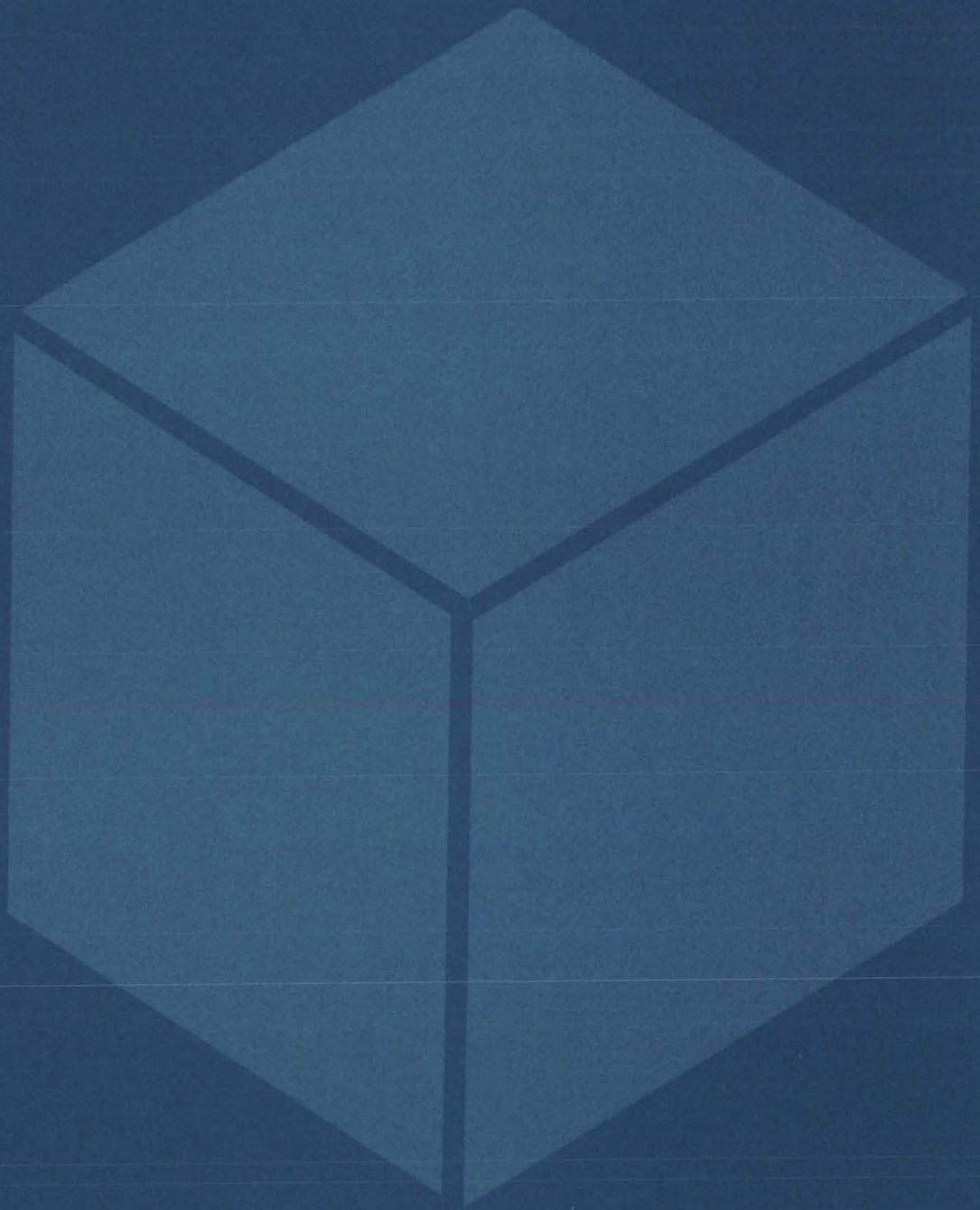

Hardware, Techniques, and Processes

Books and Reports

Microbial Desulfurization of Coal

Laboratory experiments show bacteria can remove sulfur from coal.

NASA's Jet Propulsion Laboratory, Pasadena, California

Present-day processes for the desulfurization of coal require large amounts of hydrogen and other raw materials directly derived from petroleum. Hydrodesulfurization when used for sulfur removal requires large capital costs for equipment. The reactors used in this process are operated at high temperatures and pressures and frequently require major overhaul due to rapid corrosion.

Recent experiments indicate that several sulfur-oxidizing bacteria strains have been very efficient in desulfurizing coal. This process occurs at room temperature and does not require large capital investments or high energy inputs. To date, favorable results have been obtained using two strains of the bacterium *Thiobacillus ferrooxidans,* and it is believed that other bacterial strains of the sulfur-oxidizing type, such as *T. thiooxidans,* would likewise be suitable.

The experiments were conducted using *T. ferrooxidant* strains 13,598 and 19,859 (from the American Type Culture Collection). Each reaction flask contained 5 ml of the bacterium in a *Thiobacillus* medium mixed in 15 ml of water acidified to 3.5 pH and 1.0 g of coal ground to a 270 mesh. The water was acidified by adding 0.45 ml of 1 N sulfuric acid to a liter of distilled water.

The mixtures in the reaction flasks were agitated for prolonged periods at room temperature in open air, using a conventional laboratory shaker. The course of the reaction was monitored by periodically removing portions of the coal and analyzing for sulfur content. Simultaneously, a series of control samples containing identical ingredients without bacteria was similarly agitated and analyzed.

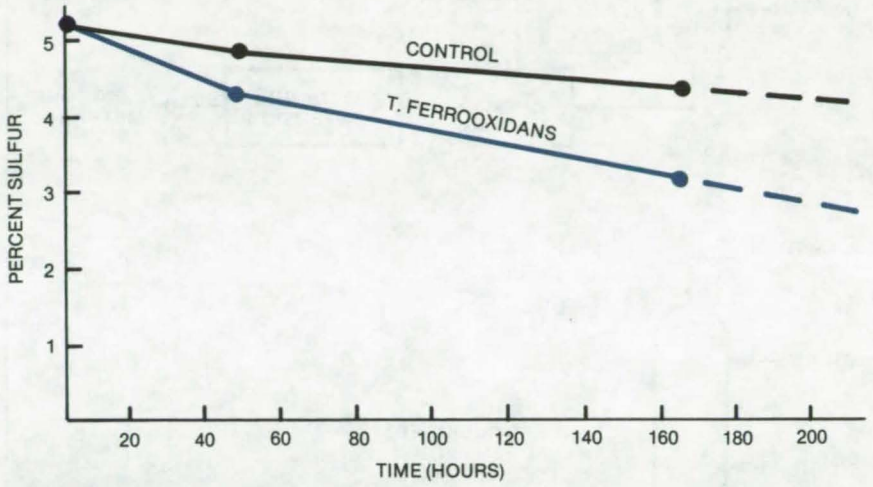

Sulfur Removed With Bacteria was tested in the laboratory, by treating Illinois bituminous coal No. 6 with *T. ferrooxidans.*

Results have indicated that the bacteria reduced the sulfur content significantly. Samples with initial sulfur levels of 5.12 percent lost approximately 40 percent of their sulfur content down to the range of 3.05 to 3.19 percent in 4 to 7 days (see figure).

The new process may expand the use of abundant reserves of high-sulfur bituminous coal, which is currently restricted due to environmental pollution. On a practical scale, this process may be integrated with modern coal-slurry transportation lines.

This work was done by Minoo N. Dastoor and John J. Kalvinskas of Caltech for **NASA's Jet Propulsion Laboratory.** *For further information, Circle 24 on the TSP Request Card.*

Inquiries concerning rights for the commercial use of this invention should be addressed to the Patent Counsel, NASA Resident Legal Office-JPL [see page A8]. Refer to NPO-14227.

Hydrogen Enrichment of Synthetic Fuel

Synthetic gas may be produced at lower cost and higher efficiency by using an outside source of hydrogen.

Marshall Space Flight Center, Alabama

A catalytic shift reaction is used in coal gasification to produce synthesis gas (e.g., methanol). The reaction, which is necessary to generate additional amounts of H_2, one of the key ingredients of synthetic gas, is described by the following equation:

$$CO + H_2O \rightarrow CO_2 + H_2$$

This scheme is expensive because it requires installation of the shift reactor and a continuous supply of catalyst. In addition, it reduces

(continued next page)

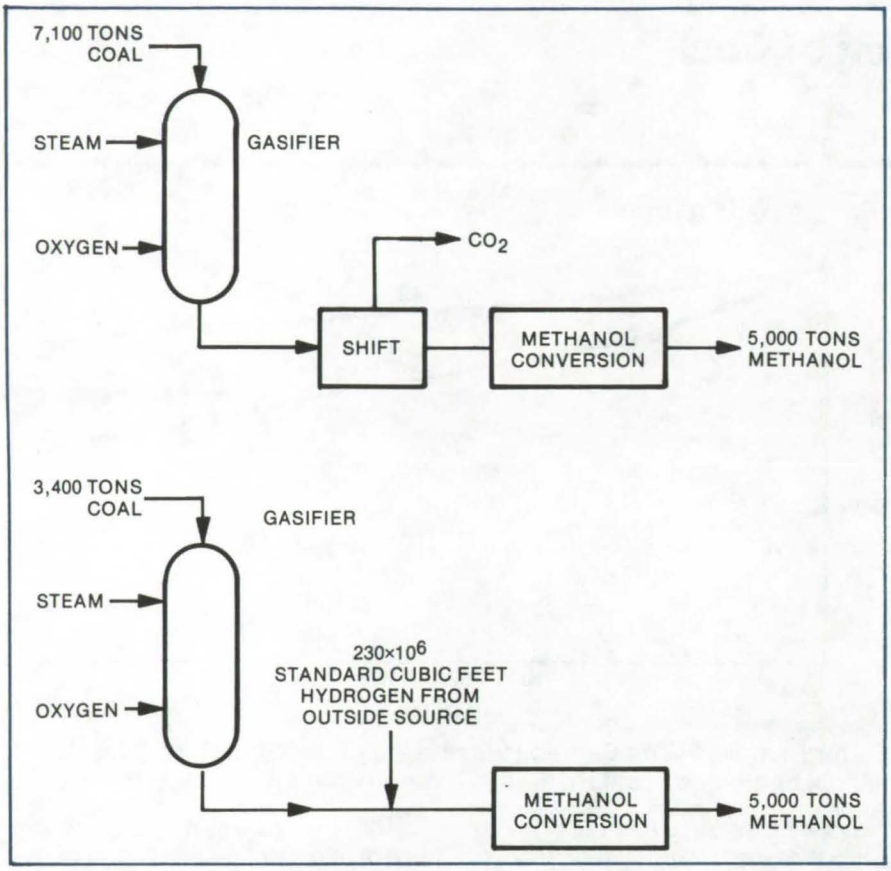

A **Standard Shift Reaction** (above) is compared with direct hydrogen supply from an outside source (below). The new process increases the efficiency by using less coal and water to provide an equal amount of synthetic gas.

the amount of valuable CO in the stream and generates useless CO_2, which is scrubbed from the process and vented into the atmosphere.

An alternative approach is to replace the reactor with an outside source of H_2 (see illustration). In the new method, H_2 is added directly to the stream, allowing easy adjustment of the H_2-to-CO ratio to increase process efficiency. In this way CO is not wasted.

The new method is compatible with the same temperatures and pressures as the shift reaction. Best results are obtained at temperatures below 1,400° F (665° C).

This work was done by C. Gillis Jay of the Institute of Gas Technology for **Marshall Space Flight Center.** *For further information, Circle 25 on the TSP Request Card.*

MFS-23279

Polyimide Adhesives for Titanium and Composite Bonding

Meta-linked diamines in molecular structure produce superior bonding.

Langley Research Center, Hampton, Virginia

High temperature polymers are in growing demand for application in composite structures for aircraft because of their light weight and excellent resistance to fatigue and corrosion. Mach 3 aircraft will experience skin temperatures between 500° and 600° F (260° and 315° C). Currently available commercial adhesives used for bonding in these applications are less than satisfactory at such extreme temperatures. Most aromatic polyimides are intractable due to their all-para linkages in the diamine portions of the structure. Bismaleimide adhesives are unstable over 500° F (260° C). Even the commercially-available high-temperature condensation polyimide adhesives have serious drawbacks such as creepage and evolution of large amounts of volatiles. A new approach at Langley Research Center has resulted in the synthesis of addition polyimide adhesives with exceptional high temperature capabilities that show excellent potential for bonding titanium metal, polyimide/graphite composites, and combinations of these materials.

The new thermosetting adhesives are a result of structural modification of the addition polyimide prepolymers through the incorporation of meta-linked diamines into the molecular backbone. The amic acid prepolymers were prepared by reacting a meta-substituted aromatic diamine with either 3,3′,4,4′-benzophenone tetracarboxylic acid dianhydride (BTDA) or 4,4′-oxydiphthalic anhydride (ODPA). Nadic anhydride (NA) was used as an end capping agent to produce an average molecular

weight of 1300. The aromatic diamines (Ar) used were m,m′-methylenedianiline (m,m′-MDA) and m,m′-diaminobenzophenone (m,m′-DABP). The amic acid prepolymers were imidized either as a solid by heating to 200° C or in solution heated to 150° C. The general imide prepolymer is shown in Figure 1.

The meta-substituted prepolymers, because of high solubility in a variety of solvents and because of low melt-flow temperatures, offer distinct processing advantages over para-substituted counterparts. The incorporation of meta-linked diamines in the addition polyimide structure has proved to be the major factor contributing to the increased adhesive bonding strengths of these polymers. The room-temperature adhesive properties of the unformulated meta-substituted addition polyimides are compared in the table in Figure 2 to those of the para-substituted polymers. In all cases the meta-linked polymers are decidedly superior to the para-linked polymers. Aluminum powder added to the adhesive resin (LARC-13) enhances the strengths at high temperature as shown in the table in Figure 3, where a bonding pressure of only 50 psi (345×10^3 N/m^2) was used.

The change from para to meta-oriented diamines in the molecular structure of addition polyimide prepolymers has resulted in an easily processible class of materials exhibiting excellent adhesive properties at temperatures up to 600° F (315° C). These adhesives, compatible with the type materials used in high performance aircraft and spacecraft structures, should also prove highly desirable in many other applications involving similar adherends.

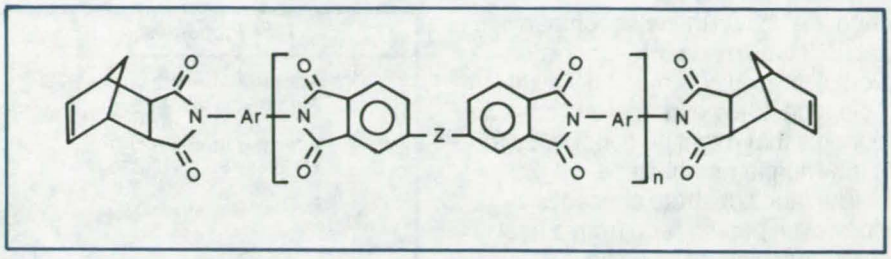

Figure 1. **Imide Prepolymer** used for thermosetting adhesives.

MATERIAL	LAP SHEAR STRENGTH (PSI)
BTDA/m,m′-MDA/NA (LARC-13)	2800
BTDA/p,p′-MDA/NA	580
BTDA/m,m′-DABP/NA	2130
BTDA/p,p′-DABP/NA	1270
ODPA/m,m′-MDA/NA	2480
ODPA/p,p′-MDA/NA	1280
ODPA/m,m′-DABP/NA	2990
ODPA/p,p′-DABP/NA	1270

Figure 2. **Comparison of Room-Temperature Adhesive Properties** of meta-substituted addition polyimides (titanium to titanium) with those of analogous para-substituted polymers.

ADHERENDS	TEMPERATURE (°F)	LAP SHEAR STRENGTH (PSI)
Titanium to Titanium	RT	3000
	500°	2750
	550	2300
	600°	1500
Composite to Composite	RT	5000
	500°	3050
	600°	1650

Figure 3. **Adhesive Properties of LARC-13 Containing 30 Percent Aluminum.**

This work was done by Anne K. St. Clair and Terry L. St. Clair of **Langley Research Center.** *For further information, Circle 26 on the TSP Request Card.*

Inquiries concerning rights for the commercial use of this invention should be addressed to the Patent Counsel, Langley Research Center [see page A8]. Refer to LAR-12257.

Flame-Retardant Adhesive Tape

Nonflammable tape adheres well, can be written on, and has other properties making it an extra-safe general-purpose tape.

Lyndon B. Johnson Space Center, Houston, Texas

A new nonflammable adhesive tape has been formulated and prepared in limited-production quantities. Made from commercially available materials, the tape meets rigorous performance specifications, making it potentially useful in high-temperature environments where conventional flammable tapes may be hazardous.

Some of the specifications of the

(continued next page)

tape are shown in the accompanying table. It was made after an evaluation of several commercially available tapes, and of numerous components that might be candidates for a new nonflammable tape.

The tape substrate chosen is a nonwoven paper made from a heat-resistant nylon, frequently used in fabric form for electrical insulation. The adhesive is based on a commercially-available silicone, pressure-sensitive adhesive, to which flame retardants are added to make it completely nonflammable. The final composition uses a mixture of decabromobiphenyl oxide and antimony trioxide as a retardant.

In order to allow the tape to be unwound from a roll, a proprietary acrylic emulsion is used. After evaluating several materials, aluminum was selected as the material for the core around which the tape is wrapped.

The entire tape was manufactured in limited quantities in a pilot-scale coater. Two 25-ft (7.6-m) lengths of tape were fabricated on rolls 15 in. (38 cm) wide. These were later cut up into individual rolls approximately 2 in. (5 cm) wide.

A more complete description of the pilot process, specific materials used, and quantitative data on the tape formulation can be found in the report referenced below.

Tape Properties	Test Results
Adhesive Strength on Aluminum (180° Peel)	0.7 to 0.9 lb/in. (125 to 160 g/cm)
Adhesive Strength on Stainless Steel (180° Peel)	0.6 to 0.8 lb/in. (103 to 145 g/cm)
Unwind Resistance	1.5 to 2.0 lb (680 to 905 g)
Tensile Strength	42 lb/in. (7,500 g/cm)
Elongation at Break	7% to 8%
Tear Strength, Elmendorf	--
Tear Strength, Tongue	0.7 to 0.9 lb (320 to 410 g) (Machine Direction)
Color	Light (off-white)
Printability	Printable With Pencil and Ballpoint Pen
Flammability	Self-extinguishing after bottom ignition in 24% oxygen, 76% nitrogen, atmospheric pressure

Specifications for the nonflammable tape insure good adhesion, easy tear, and other properties making an excellent general-purpose tape.

This work was done by Arthur D. Little, Inc., for **Johnson Space Center.** *Further information may be found in NASA CR-151224 [N77-19251]. "Development and Production of a Flame Retardant, General Purpose, Pressure Sensitive Adhesive Tape" [$4.00]. A copy may be purchased [prepayment required] from the National Technical Information Service, Springfield, Virginia 22151.*
MSC-16721

New Adhesive Withstands Temperature Extremes

Polyfunctional epoxy resin remains intact at temperatures up to 200° C and down to -195° C.

Goddard Space Flight Center, Greenbelt, Maryland

An adhesive that was originally developed to attach polyimide film to rigid polyimide surfaces and metals for high-temperature components aboard satellites is useful at both high and low temperatures. The new adhesive does not char when soaked at 200° C nor does it lose its adhesion at temperatures near -189° C. It also exhibits low-vacuum volatility and low shrinkage.

To formulate the adhesive, a resin, a hardener, an accelerator, and a solvent are combined in the correct order at specified temperatures. The system uses a polyfunctional epoxy resin [see (a) in figure] that has high aromatic content, low equivalent weight, and a more dense (compact) polymer than the conventional bisphenol A type [see (b) in figure].

The epoxide resin, at 100 parts by weight (pbw), is heated to about 135° C and is combined with 39 pbw of diamyl diphenyl sulfone hardener. When the mixture cools to 100° C, 0.5 pbw of boron trifluoride monoethylamine accelerator is added. Finally, at about 60° C, up to 60 pbw

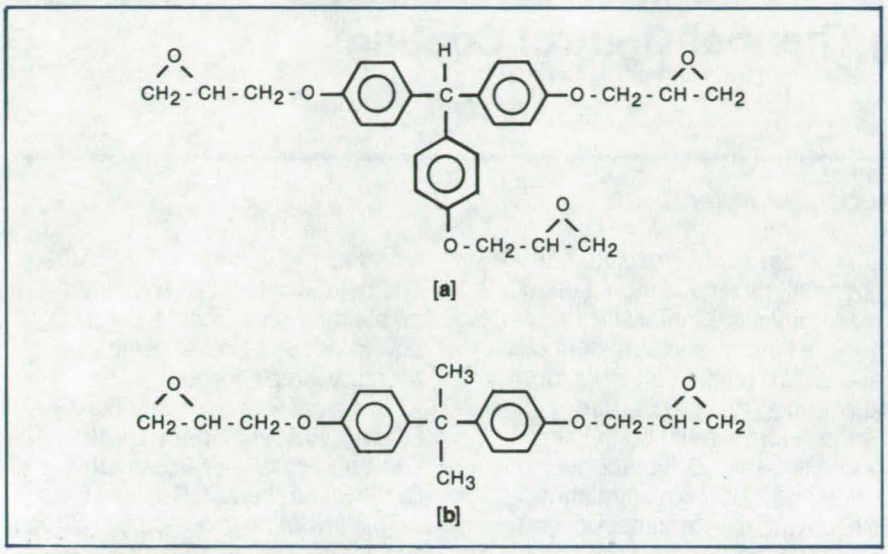

Triphenol Methane Backbone Epoxide (a) gives better high-and low-temperature properties than the bisphenol backbone epoxide shown in (b). Low shrinkage characteristics allow flexible polyimide foam to be joined to polyimide film without distorting the resulting laminate. Aluminum on polyimide film has also been successfully bonded to the polyimide foam.

of methyl ethyl ketone, acetone, or other ketone solvent are added to give the desired workability. The materials must be stirred constantly to maintain homogeneity as each new component is added.

The adhesive requires little pressure to obtain good contact between the bonded components. Full cures are achieved by heating the assembled laminate for 2 hours at 150° C and then for another 24 hours at 200° C.

This work was done by John J. Park and Benjamin Seidenberg of **Goddard Space Flight Center.** *For further information, Circle 27 on the TSP Request Card.*
GSC-12345

Boron Trifluoride Coatings for Plastics

A durable, uniform coating can be applied by the plasma glow-discharge deposition of boron trifluoride.

Ames Research Center, Moffett Field, California

Plastic optical components fabricated from organic resins such as acrylics and polystyrenes have a number of advantages over traditional glass and crystalline materials including their lighter weight, better resistance to thermal shock and mechanical stress, ease of processing, and lower cost. However, these plastics are particularly vulnerable to abrasion, scratching, and environmental conditions that may impair or even completely destroy their optical capabilities.

Attempts to correct these defects have usually involved the application of a scratch-resistant material over the plastic component by dip coating, electron-beam coating, ultraviolet polymerization, or even varnishing (after which the solvent is allowed to evaporate). In general the protective layers applied by these methods are not uniform, do not have good adhesive properties, and are expensive.

Tough, durable coatings can be deposited on plastics by using plasma glow-discharge methods. Boron trifluoride is the primary coating material, although it can be applied simultaneously with organic polymers or used as a base material for other coatings to increase adhesion.

To apply a coating, the component is supported near the center of a plasma glow-discharge reactor. The reactor is evacuated, and the boron trifluoride is allowed to flow in at the proper rate and pressure. Radio-frequency power is applied, and the deposition takes place through low-temperature plasma glow discharge. Although a range of power settings and pressure combinations can be used, optimum values are around 9.3 to 20 N/m^2 pressure and 30 to 75 watts power.

The boron trifluoride can be applied alone or used as a base on which organic polymer coatings can be deposited; or, an organic monomer gas may be deposited simultaneously with the boron trifluoride to give special properties such as increased abrasion resistance, antireflectivity, and adhesion. The coating can be further treated in a gas plasma of oxygen, ammonia, or nitrogen to react with the coating substance and, by forming chemical resistant linkages, improve the properties of the coatings.

This work was done by Ronald M. Kubacki of Bell & Howell Co. for **Ames Research Center.** *For further information, Circle 28 on the TSP Request Card.*

This invention is owned by NASA, and a patent application has been filed. Inquiries concerning nonexclusive or exclusive license for its commercial development should be addressed to the Patent Counsel, Ames Research Center [see page A8]. *Refer to ARC-11057.*

Electrically-Conducting Thermal-Control Coating

An inorganic conducting coating resists ionizing and ultraviolet radiation.

Goddard Space Flight Center, Greenbelt, Maryland

A new coating, originally developed to protect spacecraft, is characterized by low thermal absorption, high thermal emittance, and high electrical conductivity. It can be used where such thermal properties are necessary and where charge buildup due to ionic or electric fields must be avoided. The coating is stable under ultraviolet and under bombardment by ionizing particles, such as electrons and protons. It can be applied to a variety of substrates, including aluminum, mild steel, stainless steel, and epoxy/fiberglass.

The coating mixture consists of a fired oxide comprised principally of zinc oxide, aluminum oxide, and, optionally, a small amount of cobalt oxide, an alkali-metal silicate vehicle binder, and sufficient water to create a mixture suitable for application to the substrate.

For a formulation containing approximately 98.5 percent zinc oxide and 1 percent aluminum oxide, with the remainder cobalt oxide, the absorptance and emittance were respectively 0.58 and 0.87, and the area resistance was less than $1.7\times10^{3}\ \Omega\text{-m}^2$. The measurements were made at a pressure of 1×10^{-5} torr ($1.3\times10^{-3}\ \text{N/m}^2$) after the coatings were stored under vacuum for 24 hours. The optical properties remained stable through exposure to 1,000 equivalent Sun-hours, using a mercury lamp source.

This work was done by Michael C. Shai of **Goddard Space Flight Center.** *For further information, Circle 29 on the TSP Request Card.*

This invention is owned by NASA, and a patent application has been filed. Inquiries concerning nonexclusive or exclusive license for its commercial development should be addressed to the Patent Counsel, Goddard Space Flight Center [see page A8]. Refer to GSC-12207.

Wrought Nickel-Base Superalloy

High-temperature alloy is suitable for powder metallurgy.

Lewis Research Center, Cleveland, Ohio

An improved wrought nickel-base superalloy for advanced temperature use has been obtained by modification of NASA IIB-11 (see NASA Tech Brief 74-10003). This new alloy, IIB-11E, is better suited to cost-saving powder-metallurgy manufacturing methods and has improved phase stability during long-time heating. Compositional changes in IIB-11E are reduced carbon, from 0.13 to 0.06 weight percent, and slightly reduced refractory metal concentrations. Fewer carbides in this initially-fine-grained powder-metallurgy alloy allow easier grain growth, which is necessary for high-temperature strength. Reduced refractory metals have eliminated the embrittling μ-phase which precipitated in the original alloy during long time heating. The IIB-11E composition in weight percent is 0.06 carbon, 4.5 aluminum, 0.75

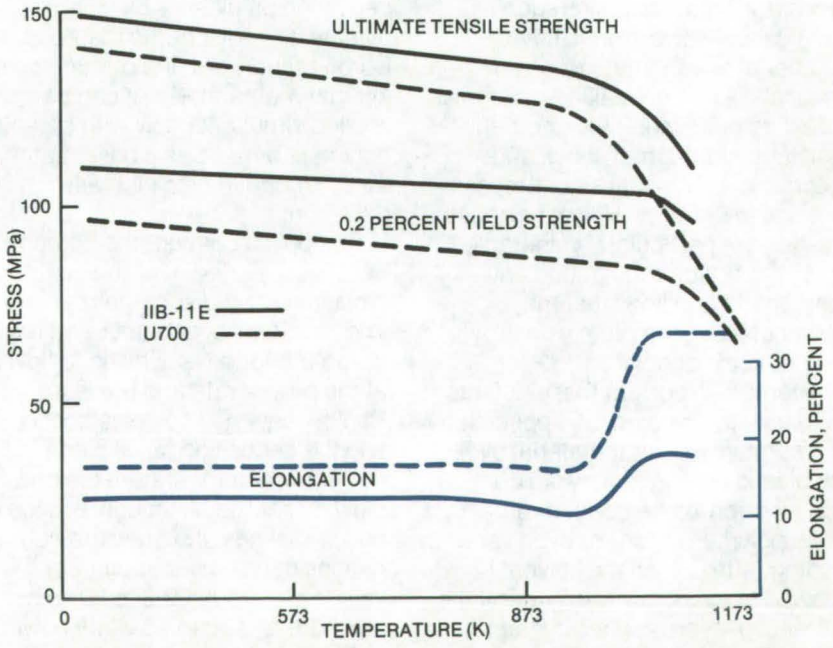

Figure 1. Tensile Properties of IIB-11E produced from prealloyed powder are compared with those of conventionally produced U700.

titanium, 6.6 tantalum, 0.7 hafnium, 8.5 chromium, 2.0 molybdenum, 7.1 tungsten, 0.5 vanadium, 9.0 cobalt, 0.01 boron, 0.01 zirconium, and the balance nickel. Its density is rather high, 8.75 g/cm^3.

IIB-11E has been fabricated by cross-rolling billets of hot-isostatically compacted prealloyed powder. It is heat treated by solution treating at 2,250° to 2,275° F (1,506 to 1,519 K) and then furnace cooled to 2,100° F (1,422 K) before rapidly cooling in air. It is aged 16 hours each at 1,600° and 1,400° F (1,144 and 1,033 K).

Tensile properties of IIB-11E are compared with those of an older conventionally-produced wrought superalloy (U-700) in Figure 1. IIB-11E has modestly higher strength but lower ductility than the older alloy. Stress-rupture strengths of the same two alloys are shown as a function of Larson-Miller parameter, P, in Figure 2. IIB-11E clearly has a considerable advantage in rupture strength.

IIB-11E is considered an excellent candidate material for advanced-operating-temperature gas-turbine disks. It should also be considered for high temperature static structures.

This work was done by Robert V. Miner, Jr. and Fredric H. Harf of **Lewis Research Center** *and William B. Kent of Universal Cyclops Corp. Similar alloys, NASA IIB-7 and NASA IIB-11, are described in NASA Tech Briefs 74-10002 and 74-10003. Further information may be found in NASA CR-135131 [N77-20208], "Development of an Extra-High-Strength Powder-Metallurgy Nickel-Base Superalloy," copies of which may be obtained at cost from the New England Research Application Center [see page A7]*
LEW-12844

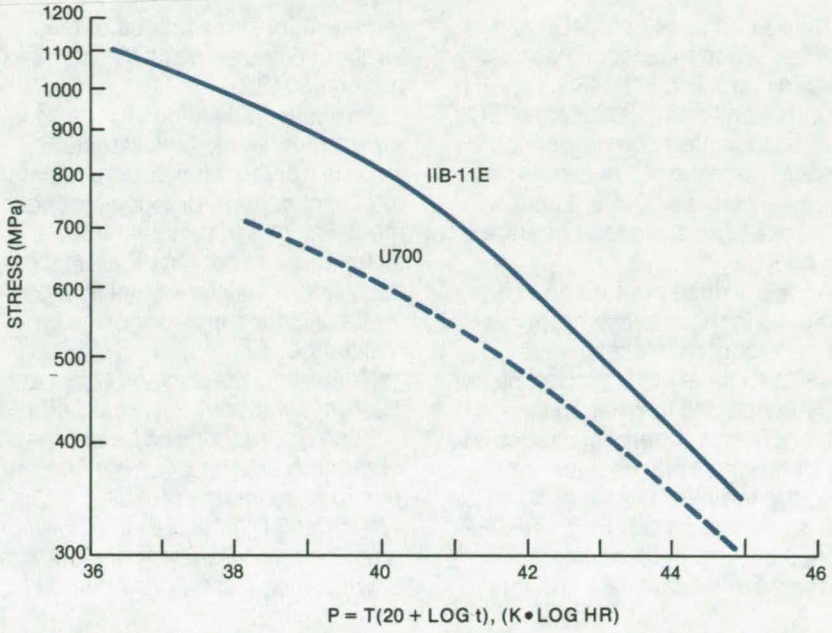

Figure 2. Rupture Stress, as a function of Larson-Miller parameter, of IIB-11E produced from prealloyed powder is compared to that of conventionally produced U700.

Low-Chromium Stainless Steels

Lower chromium content is possible without sacrificing performance.

Lewis Research Center, Cleveland, Ohio

Chromium has been identified as being a potential shortage material within the United States. All of the chromium used in this country is imported, with the exception of a small amount reclaimed from scrap. The majority of U.S. chromium consumption is in stainless steel production and specifically in 304SS (18 percent Cr). In fact, approximately 830,000 tons of 304SS are produced each year. To significantly reduce this use of chromium, two modified composition 304 stainless steel alloys have been developed with chromium contents reduced from 18 percent to 12 percent. These two new low-chromium-content alloys have oxidation, corrosion resistance, tensile strength, ductility, and temperature performances fully comparable to the present high-chromium-content 304SS alloys. This one-third reduction in chromium content can save many tons of chromium annually. Based on the annual production of stainless steel, it is estimated that the savings in chromium would be about 50,000 tons per year.

The compositions of these modified 304SS alloys include the normal alloying elements contained in 304SS alloys with the exception of 12 percent chromium + 2 percent aluminum + 2 percent molybdenum in one alloy, and 12 percent chromium + 2.65 percent silicon (0.65 percent silicon in commercial 304SS) in a second alloy.

High temperature [1144 K (1,600° F)] cyclic oxidation tests have shown that based on weight change, spalling characteristics, and X-ray diffraction, the two

(continued next page)

modified-composition 304SS alloys have oxidation resistances comparable to commercial 304SS.

Corrosion tests in a $CuSO_4$-H_2SO_4 solution indicated comparable corrosion resistance of the experimental alloys and 304SS based on metallography, surface appearance, and ductility.

An austenitic structure can be achieved in these alloys by increasing the 8 percent nickel contained in 304SS to a level of 10 percent nickel or by increasing the maganese content from 1.1 percent in 304SS to 5.1 percent for the modified alloy. Over the temperature range 77 to 810 K (-321 to 1,000° F), the experimental alloys exhibit comparable strengths and ductilities, and the temperature-dependence of their strength is the same as the commercial 304SS.

Possible applications for these low-chromium stainless steels include transfer lines for chemicals, heat exchangers, cryogenic containment vessels, automobile trim, and a very large variety of other applications where stainless steel is used for its oxidation and/or corrosion resistance.

This work was done by Charles A. Barrett, Charles A. Gyorgak, and Joseph R. Stephens of **Lewis Research Center.** *Further information may be found in NASA TN-D-8459 [N77-23241], "Oxidation and Corrosion Behavior of Modified-Composition, Low-Chromium 304 Stainless Steel Alloys", which may be obtained at cost from the New England Research Application Center [see page A7] and in "Substitution for Chromium in 304 Stainless Steel", Proceedings of Conference, Environmental Degradation of Engineering Materials, October 10-12, 1977, College of Engineering, Virginia Polytechnic Institute and State University, Blacksburg, Virginia 24061.*

This invention is owned by NASA, and a patent application has been filed. Inquiries concerning nonexclusive or exclusive license for its commercial development should be addressed to the NASA Patent Counsel, Lewis Research Center [see page A8]. Refer to LEW-12543.

Modified Chemiluminescent NO Analyzer Accurately Measures NO_x

Inaccuracy due to CO content is eliminated by a molybdenum converter and an air purge.

Lewis Research Center, Cleveland, Ohio

It has been observed that chemiluminescent analysis of oxides of nitrogen in gas samples containing significant amounts of carbon monoxide can be highly inaccurate. The cause of this inaccuracy has been identified, and corrective measures have been determined.

Analysis of exhaust gases from combustion sources is important to many research programs and investigations. Measurement of the various oxides of nitrogen is often of particular interest. The most common instrument for measuring oxides of nitrogen is the chemiluminescent analyzer. This instrument has quite specific response to nitric oxide (NO). It can also be utilized to measure higher oxides of nitrogen (NO_x) by adding a NO_x to NO converter accessory. The amount of NO_x in the sample gas is the difference between the amount of NO measured with the sample gas bypassing the converter, and the amount of NO measured with the sample gas flowing through the converter. In practice, it was noted that whenever five percent or more of carbon monoxide (CO) was present in the sample gas, the converted NO measurement was less than the unconverted NO measurement and hence the NO_x determination was highly inaccurate.

A test program established that (1) both NO_x and NO were being destroyed in the converter in the presence of CO and the corresponding absence of oxygen (O_2); (2) the NO_x destruction was lessened when the converter was located within the analyzer rather than in the sample gas stream before the analyzer inlet; (3) between the commonly used converter materials, stainless steel and molybdenum, molybdenum converters have the highest tolerance to CO; and (4) the addition of either O_2 or air to the sample gas to insure an O_2 concentration of at least five percent in the gas stream passing through the converter substantially quenched the NO_x destruction.

In accordance with these findings, a chemiluminescent analyzer equipped with a molybdenum converter located within the analyzer and with an air purge was used; it accurately measured NO and NO_x in sample gases containing thirty percent CO and did so over a four-month period with no degradation of accuracy or performance.

These effects were observed in chemiluminescent analyzers with evacuated reaction chambers and the modifications devised are recommended for that type of instrument.

This work was done by Robert L. Summers of **Lewis Research Center.** *Further information may be found in NASA TM-X-73480 [N76-30319], "NO_x Destruction by CO in NO_x to NO Converters of Chemiluminescent NO Analyzers," copies of which may be obtained at cost from the New England Research Application Center [see page A7]. LEW-12850*

Measurement of Total Organic Concentration in Water

A continuous one-step electrophotolysis oxidation system measures total organic carbon present in water samples.

Lyndon B. Johnson Space Center, Houston, Texas

In a new process and instrument for the determination of the total organic carbon (TOC) concentration in water, organic compounds are oxidized to carbon dioxide by ultraviolet photolysis. This process has advantages over commonly used methods as it does not require corrosive reagents or gases, thereby eliminating their associated storage and dispersing systems. The only reagent necessary, oxygen, is generated in situ by the electrolysis of water.

The device, shown in Figure 1, consists of two water-electrolysis cells positioned on either side of a flat-grid, ultraviolet light source. The cells are arranged so that the anodes, which produce the oxygen, face a UV source. The UV source and anodes are separated only by a quartz plate equipped with flow channels. As a water sample enters the flow channels, it is irradiated by the UV radiation. At the same time, some of the water is electrolyzed in the electrolysis cell to produce oxygen. The UV irradiation catalyzes the oxidation of any organic compounds present. The reaction stream is channeled to a CO_2 electrode sensor where total CO_2 content is measured. To eliminate interference from dissolved CO_2, another CO_2 measurement is made upstream of the electrophotolysis cell. The difference between CO_2 measurements represents the amount of CO_2 produced in the oxidation reaction and can be used to calculate the amount of organic carbon present in the original sample.

Although this process has been developed for use in the aerospace industry, wide-range applications exist in environmental sciences, such as water pollution control and water quality monitoring. In addition, the system could be suitably adapted to permit batch analysis for laboratory use.

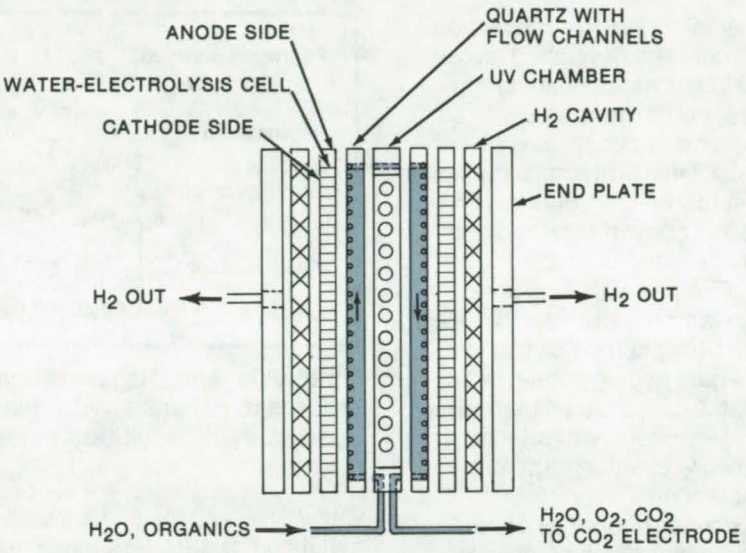

Figure 1. A Continuous One-Step Electrophotolysis oxidation system measures organic carbon present in water samples by means of ultraviolet photolysis and water electrolysis. The water-electrolysis cells employ a solid ion-exchange membrane/electrolyte. Hydrogen produced in the process is vented away as a waste product. Tie bolts are used to hold the cell ports together as an integral unit.

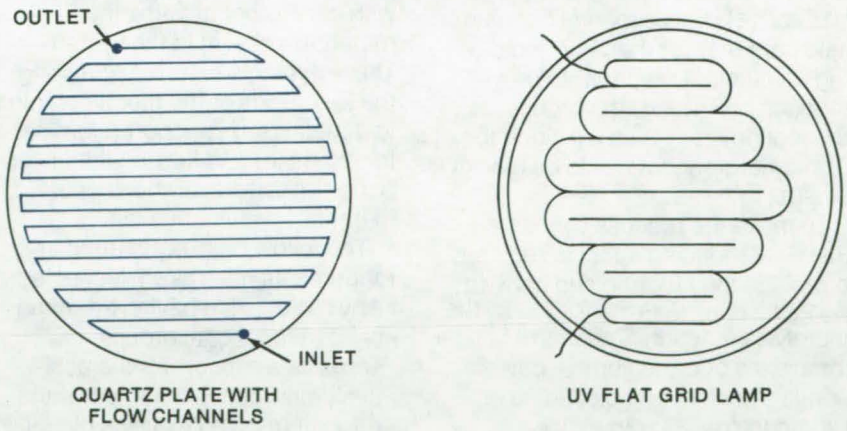

Figure 2. Flow Channels in the quartz plate (left) match the flat-grid, ultraviolet light source (right). The serpentine flow path through the quartz plate provides a long exposure time to the UV radiation to insure complete oxidation.

This work was done by Eugene Winkler of **Johnson Space Center.** *No further documentation is available.*

Inquiries concerning rights for the commercial use of this invention should be addressed to the Patent Counsel, Johnson Space Center [see page A8]. Refer to MSC-16497.

Solar Photolysis of Water

A possible cyclic process for producing hydrogen from water, using Sunlight

NASA's Jet Propulsion Laboratory, Pasadena, California

If an efficient energy-conversion process could be developed, solar energy, the most abundant energy resource, could provide us with an environmentally acceptable alternative to fossil fuels. Practical methods are presently being sought to harvest and convert solar radiation to a concentrated, storable form of energy. One possibility involves splitting water molecules under the action of Sunlight (photolysis) to produce pure hydrogen gas; once formed, the gas could be burned with oxygen to form water — an exceptionally clean, energy-producing reaction.

A proposed scheme for generating hydrogen through photolysis uses an aqueous solution of europium ions in their +2 oxidation state (Eu^{+2}). The Eu^{+2} loses an electron in the presence of light of the appropriate wavelength to form the +3 ion (Eu^{+3}) and liberates both hydrogen and hydroxide ions according to reaction (1). Experimental quantum yields are greater than 0.2, indicating an efficient reaction. However, although promising, the process is not economically feasible since the Eu^{+2} photoreagent would be quickly exhausted.

To make the process cyclic, a chemical reducing agent is required to replace the electron and convert the Eu^{+3} back to Eu^{+2} for use in the photolysis reaction. Organometallic complexes of ruthenium — particularly ruthenium and bipyridine or 4,4-dicarboxy-2,2-bipyridine (denoted by RuL_3^{+2}) — can reduce the Eu^{+3} in the photoassisted regeneration sequence represented in equations 2 and 3.

Certain undesirable side reactions (equations 4 through 6) can occur between the Eu^{+2} and oxygen (formed in the reaction of RuL_3^{+3} with water) and the Eu^{+2} and the metal complex. Unless these reactions are suppressed, any batch regeneration process will not produce significant amounts of Eu^{+2}.

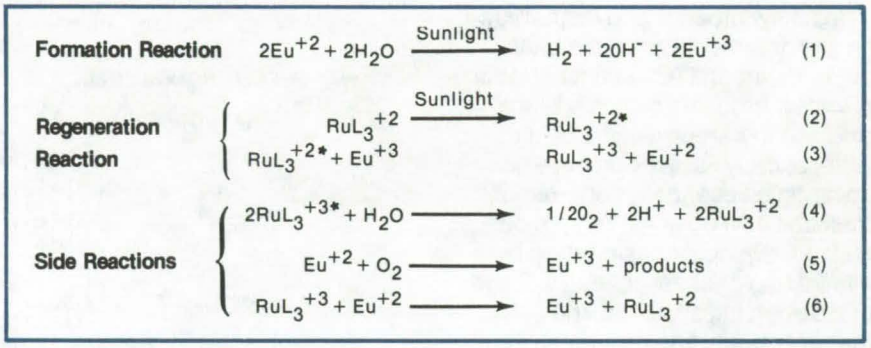

Photolysis and Regeneration Reactions could be used in a cyclic process to generate hydrogen gas from water, using Sunlight (see text). Species marked with an asterisk are in an excited state.

Several proposed process-flow systems might prevent these side reactions by separating the regeneration products before they react with each other or with other materials present in the system. These systems envision attaching the Eu^{+3} ions or the metal complex to a metal oxide support (alumina, for example) and flowing the unsupported species over the supported material.

The following experimental arrangements have been suggested:

- Any metal oxide having attached oxygen functional groups may serve as a support for the positively-charged Eu ions, while the ruthenium complex flows over it. A quick flow rate of RuL_3^{+2} will prevent any reaction between oxygen and the Eu^{+2} and also quickly remove RuL_3^{+3}. This cycle is completed by removing the RuL_3^{+2} solution, replacing it with water, and continuing the reduction.
- The metal oxide supports the ruthenium complex. Acidified Eu^{+3} (the product of the reduction of water) can be passed over the supported RuL_3^{+2}, and the resulting +3 ruthenium complex can be treated with water to yield oxygen and +2 ruthenium complex.
- Ruthenium and europium are both bonded to metal oxide surfaces, and the pH or hydrogen-ion concentration is regulated to determine which reaction occurs. The regeneration step may be initiated at a pH of 5 to minimize or prevent direct reduction of the supported ruthenium complex by hydrogen as H^+ or H_2^+.

This work was done by Porter R. Ryason of Caltech for **NASA's Jet Propulsion Laboratory.** *For further information, Circle 30 on the TSP Request Card.*

This invention is owned by NASA, and a patent application has been filed. Inquiries concerning nonexclusive or exclusive license for its commercial development should be addressed to the Patent Counsel, NASA Resident Legal Office-JPL [see page A8]. *Refer to NPO-14126.*

Low-Cost High-Purity Silicon Production

High-purity silicon is obtained by the low-temperature reaction of silicon tetrafluoride with metallic sodium.

NASA's Jet Propulsion Laboratory, Pasadena, California

An economical process can produce high-purity silicon crystals, suitable for use in solar cells. The process starts from silicon tetrafluoride (SiF_4), an easily purified by-product of fertilizer production, and reduces it with metallic sodium. The reaction is strongly exothermic and can be initiated at relatively low temperatures (175° C), making it potentially suitable for development into a low-cost commercial process.

Silicon that was produced by the reaction was examined spectroscopically and was found to be very pure; impurities such as Ti, V, Zr, and Cr, which are detrimental to solar-cell performance, were not present.

The reaction of SiF_4 with metallic sodium

$$SiF_4 + 4Na \rightarrow Si + 4NaF$$

is accompanied by the side reaction

$$2NaF + SiF_4 \rightarrow Na_2SiF_6$$

The end product, sodium fluorosilicate, is mixed with the silicon, but is readily leached out with acidic solutions. The sodium fluoride that is not consumed can be used to generate more silicon tetrafluoride.

Important advantages of this method over current techniques of silicon production, such as those using electric furnaces to react silica and carbon or the reduction of silicon tetrachloride by an active metal such as sodium or magnesium, are its exothermic character and comparatively low process temperatures. These could lead to significant savings in equipment and energy costs.

This work was done by Vijay K. Kapur of Stanford Research Institute for **NASA's Jet Propulsion Laboratory.** *For further information, Circle 31 on the TSP Request Card.*

NPO-14198

Ultra-High-Strength Boron Fibers

Chemical etching significantly improves fiber properties by removing surface flaws and redistributing internal stress.

Lewis Research Center, Cleveland, Ohio

For many structural applications where low density, high strength, and high stiffness are required, boron on tungsten (B/W) fibers make satisfactory composites with resin or aluminum matrices. However, for structures which must absorb large amounts of energy due to impact (e.g., compressor blades), the fracture characteristics of these commercial B/W fibers are significantly less than optimum.

Experimental and theoretical studies of the failure modes, internal stress distributions, and deformation characteristics of the as-received B/W fibers have aided in the development of a fracture model which explains how this fiber can be modified to achieve significantly better fracture properties. Tensile strength and strain-to-failure can be increased by 50 percent and the coefficient of variation (COV) reduced to five percent by removing surface flaws from the fibers and by redistributing residual internal stresses which are normally present. These improvements lead to an increase in the impact energy absorption capability of the fiber of approximately 200 percent.

Controlled chemical etching is a simple method for removing surface flaws and effecting beneficial changes in internal stress distributions. Failure mode studies have indicated that initial fracturing in as-received fibers occurs over a broad stress range (large COV). Failures in the lower part of this stress range are due to surface flaws. Once these surface flaws are eliminated by removing a few micrometers of the fiber surface, fracture is induced by flaws near or in the tungsten-boride core. Fibers with smoothed surfaces reach a higher average fracture stress with a significantly lower COV. Further etching removes additional compressive layers of the B-sheath and produces an axial contraction of the remaining boron and its core with a corresponding increase in stress and strain-to-failure from flaws in the sheath and tungsten-boride core.

Chemical etching of the commercial 203-micrometer diameter B/W fiber has achieved average tensile strength and strain-to-failure of 740 ksi (5×10^9 N/m^2) and 1.3 percent, respectively. Since the

(continued next page)

fiber deforms elastically near 68° F (20° C), the values correspond to a fracture energy density of 33×10^6 j/m^3. Therefore, this simple etching technique, which produced a stronger fiber with a lower COV, can also more than double the capability of the fiber to absorb impact energy. It is believed that the etching process can easily be adapted to rapid commercial manufacturing.

These improved ultra-high-strength boron fibers (high-strength, high-modulus, low-density material) can be used as reinforcement in many lightweight composite applications such as structural components of aircraft, trains, and automobiles, structures for space applications, and composite rotors for energy storage.

This work was done by Donald R. Behrendt, James A. DiCarlo, Hubert H. Grimes, and Robert J. Smith of **Lewis Research Center.** *Further informaton may be found in:*

NASA TN-D-8219 [N76-22313], "Changes in Boron Fiber Strength Due to Surface Removal by Chemical Etching,"

NASA TM-X-73402 [N76-21293], "Longitudinal Residual Stresses in Boron Fibers," and

NASA TM-X-73627 [N77-23207], "Techniques for Increasing Boron Fiber Fracture Strain."

Copies of these reports may be obtained at cost from the New England Research Application Center [see page A7].

LEW-12739

Partial Interlaminar Separation for Composites

Perforated film between laminae increases strength of composite.

Langley Research Center, Hampton, Virginia

Partial separation of laminated layers has been found to improve significantly the toughness and impact resistance of epoxy-matrix composites. Epoxy-matrix composites, used in aerospace structures and for other structural applications, have outstanding strength properties but are sensitive to flaws and to accidental damage. The fracture toughness of multidirectional epoxy-matrix composites is relatively low because the interlaminar bond, which is necessary for cohesion and for prevention of local buckling, allows crack front stress fields to develop. These are strong enough to propagate cracks perpendicular to the filament direction. Intermittent separation of the laminae reduces the crack front stress fields, significantly increasing the fracture toughness.

A partial interlaminar separation system consisting of a perforated Mylar film is used to partially break the bond between laminae. The partial separation diffuses the local stress concentrations near a crack, reducing the crack front stress fields and allowing the main load-carrying fibers to reach a higher average stress before fracture.

During fabrication, the perforated film is placed between individual laminae. The film should have a regular hole pattern and may be punched with circular holes or may be gang punched like a computer card. Hole size should be 1 to 10 times the laminae thicknesses, covering 20 to 80 percent of the film area. The epoxy matrices are joined through the holes but are separated elsewhere by the film. The separation system may be applied between all laminae or some laminae, over the whole structure or over parts of it in strips or patches. To retain superior strength, the interlaminar film should not extend to the edge of a panel but should be stopped at a distance from the edge equal to or slightly less than the critical crack length of the unmodified composite.

Tests made using graphite/epoxy panels separated by 0.01-mm-thick

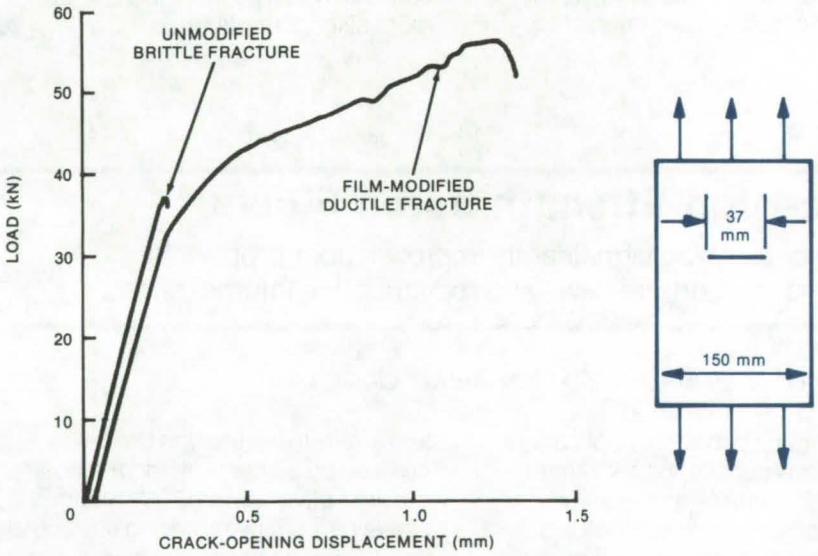

Fracture Tests made on a partially separated laminate of the dimensions shown above are compared to tests made on a conventional laid-up panel. The fracture strength of the modified panels is improved about 50 percent.

Mylar film containing a 50-percent hole area showed a sharp improvement in strength properties. Fracture tests on 150-mm-wide graphite/eposy panels with 37-mm central slots indicate that the fracture strength of modified panels is up to 50 percent higher than that of unmodified panels. The accompanying figure shows the relation between the applied load and the crack opening at the center of the slot for the unmodified composite (brittle fracture) and the modified composite (ductile fracture).

Fracture toughness, tensile strength, and impact resistance tests show, in addition to the increase in fracture strength, an absorbed energy at fracture of the modified panel five times greater than that of the unmodified panel, an ultimate strain four times greater, and an impact resistance of approximately 50 percent greater with the addition of the perforated Mylar film.

A previous method of overcoming fracture problems in similar composites was to employ softer fibers in strips as a means of intercepting cracks, but this technique has the disadvantage of making the structure heavier. The partial interlaminar separation system has the advantage of a significantly lower additional weight to the structure with a superior demonstrated effect on the strength properties of the composite.

This work was done by Wolf Elber of **Langley Research Center.** *Further information may be found in NASA TM-X-78643, "Toughening of Graphite-Epoxy Composites by Interlaminar Perforated Mylar Films," a copy of which may be obtained at cost from the North Carolina Science & Technology Research Center* [see page A7].

Inquiries concerning rights for the commercial use of this invention should be addressed to the Patent Counsel, Langley Research Center [see page A8]. *Refer to LAR-12065.*

Fire-Retardant Foams

A family of polyimide foams has potential applications in homes and vehicles.

Lyndon B. Johnson Space Center, Houston, Texas

A new family of polyimide resins are being developed as foams with exceptional fire-retardant properties. The foams are potentially useful for seat cushions in aircraft and ground vehicles and for applications such as home furnishings and building-construction materials. They are thermally stable and release virtually no smoke or toxic combustion products when exposed to high temperatures (see table). Additional research that will optimize their mechanical properties for commercial use is underway for the most promising formulations.

To make the foams, at least one heterocyclic diamine and at least one low-basicity aromatic diamine are reacted under controlled conditions with an aromatic tetracid possessing low-acidity content. The polyimide precursor that forms (initially a heavy syrup) is subsequently dried and pulverized. The resulting powder is spread over an aluminum foil and heated until it melts, releasing gaseous byproducts that cause it to expand as a foam.

The polyimide foams have been produced with densities from 16 to 640 kg/m^3; they can be modified with reinforcing fibers or fillers to produce cellular materials for specific applications. In addition, by selecting the reactants and their molecular ratios, the basic polymer structure can be modified to give foams with properties ranging from high resiliency and flexibility to brittleness and rigidity.

Work on these materials is continuing and will be reported in a further issue of *NASA Tech Briefs.*

Property	Resin #29	Resin #25
Density (kg/m^3)	22.56	20.32
Tensile Strength (N/m^2)	90.3×10^3	67.56×10^3
Elongation (Percent)	23.9	19.8
Tear Resistance (N/m)	181.0	171.0
Odor		
Room Temperature	Not detectable	Not detectable
160° F (71° C)	Not detectable	Not detectable
Resilience		
Rebound Value	58.0	54.0
Oxygen Index	44.4	43.8
Smoke Density (DMS Uncorrected)		
Nonflaming (Percent)	1.0	0.0
Flaming (Percent)	0.5	0.0
Toxic Products of Combustions (Tentative)		
HCl (ppm)	None present	None present
HF (ppm)	None present	None present
H_2S (ppm)	None present	None present
HCN (ppm)	1.0	1.0
Thermostability		
Loss at 400° F (204° C)	No Loss	No Loss

Typical Mechanical and Fire-Retardant Properties of polyimide-based foams: These 2 formulations, out of 33 initially tested, were selected for development as seat-cushion material.

This work was done by John Gagliani of International Harvester Co. for **Johnson Space Center.** *Further information may be found in NASA CR-147496* [N76-18278], *"Fire Resistant Resiliant Foams,"* [$4.50]. *A copy may be obtained* [prepayment required] *from the National Technical Information Service, Springfield, Virginia 22151. MSC-16222*

Abrasion-Resistant Antireflective Coating for Polycarbonate

Treatment with oxygen glow discharge improves abrasion resistance.

Ames Research Center, Moffett Field, California

Among many plastics, polycarbonate remains one of the top choices in the fabrication of safety glasses and shields and space helmet visors. Although other plastics have better abrasion resistance and transparency, polycarbonate features high impact resistance and dimensional stability that often tip the scale in its favor.

Recent experiments with silane-coated polycarbonate samples have shown new improvements in polycarbonate transparency and abrasion resistance. Following a plasma-polymerization technique similar to that reported in Vol. 1, No. 2 of *NASA Tech Briefs* ("Abrasion-Resistant Coatings for Plastic Surfaces", ARC-10915), treatment in an oxygen glow discharge has been shown to further enhance abrasion resistance and transmission.

Samples post-treated in oxygen demonstrated a 5-percent improved transmission at 550 nm wavelength as compared to the uncoated samples. Improvement in abrasion resistance was also shown by measuring the percentage of haze resulting from abrasion (see table).

Haze Resulting from Abrasion of Polycarbonate Substrates

Sample Description	Percent Haze	Notes
Uncoated Polycarbonate	5.2±0.8	Average haze for 10 samples
Coated Polycarbonate	4.1±0.5	Average haze for 3 samples
Coated and O_2-Treated Polycarbonate	2.5±0.2	Average haze for 6 samples
Uncoated and Unabraded Polycarbonate	2.3±0.1	Average haze for 10 samples
Coated and Unabraded Polycarbonate	2.2±0.1	Average haze for 3 samples

Plasma-polymerized vinyltrimethoxy silane films were deposited on transparent polycarbonate substrates inside a plasma reactor. The films were deposited by using a pulsed-mode plasma generator with a pulse duration of 1.5 ms on and 1.5 ms off and with peak-to-peak voltage and current of 400 V and 0.6 A, respectively.

Liquid vinyltrimethoxy silane monomer vapor was supplied from a reservoir held in a thermostated water bath at a temperature of 23.4°±0.1° C. Monomer flow was adjusted to a constant flow rate of $3.2\times10^{-9}m^3$(STP)/s. The polycarbonate substrates were 1 by 1 by 0.25 in. (2.5 by 2.5 by 0.64 cm) and were held in a 1.75-in. (4.45-cm) square frame that insured uniform film thickness over the entire substrate surface.

Following the deposition, some samples were post-treated in an oxygen glow discharge for 600 s, using 99.5 percent pure oxygen. In this procedure, continuous-wave plasma operation was used with peak-to-peak voltage and current of 390 V and 0.58 A, respectively.

The coated samples were later analyzed for abrasion, using a standard fresh rubber eraser. Other tests included spectra measurements and elemental analysis with spectrometers and spectrophotometers.

This work was done by T. Wydeven of **Ames Research Center.** *For further information, Circle 32 on the TSP Request Card.*

This invention is owned by NASA, and a patent application has been filed. Inquiries concerning nonexclusive or exclusive license for its commercial development should be addressed to the Patent Counsel, Ames Research Center [see page A8]. *Refer to ARC-11047.*

Electroplating and Stripping Copper on Molybdenum and Niobium

Plating and stripping procedures have been optimized and specified.

Lewis Research Center, Cleveland, Ohio

It was desired to both electroplate and subsequently strip copper from molybdenum (Mo) and niobium (Nb). Since general standard plating techniques produced poor quality coatings, general procedures were optimized and specified to give good results with Mo and Nb.

Procedure:

Cleaning of Specimens Prior to Electroplating

Mechanically clean the specimen thoroughly. Rinse the specimen thoroughly in CH_3CCl_3 (NA-500). Ultrasonically clean the specimen in high purity CF_3CCl_3 at least two times, for at least 15 minutes each time. Rinse the specimen thoroughly in C.P. acetone. For a Nb specimen, immerse the specimen in concentrated (6-10M) NaOH for a few minutes and rinse with water.

Electroplating of Specimens

Prepare an electroplating bath

containing 83.5 g concentrated H_2SO_4 and 67 g $CuSO_4 \cdot 5H_2O$ (technical grade is satisfactory) dissolved per liter of solution, made up with distilled water. As the anode, prepare a piece of clean copper with an area approximately equal to or greater than that of the specimen to be plated. (The anode may be cleaned by rinsing with an organic solvent, stripping with fairly concentrated HNO_3, and rinsing with water.) Mount the anode horizontally in the plating bath. Mount the specimen to be plated horizontally above and approximately parallel to the anode. The anode-to-specimen distance is not critical; distances of 1/4 to 1 in. (0.63 to 2.5 cm) have been found to work quite satisfactorily. With the plating bath stirred vigorously, allow the specimen to soak about 5 minutes in the plating solution at room temperature. (Make sure no metallic component of the specimen which permits electroless copper plating, e.g., iron, contacts the plating solution.)

Use a current-voltage controlling dc power supply for plating, with the cathode lead attached to the specimen being plated and the anode lead attached to the copper anode. With vigorous stirring continued and the plating bath at room temperature, apply plating voltage to not more than a maximum of 0.7 V. Typical satisfactory current densities during plating, based on the specimen area, are: 25 mA/cm² for a Mo specimen and 95 mA/cm² for a Nb specimen. For a constant current density, the plating voltage will decrease during plating. Continue plating to the desired thickness, as estimated by assuming near unity current efficiency and knowing the plating time and specimen current density during plating. At the conclusion of the electroplating, immediately rinse the plated specimen thoroughly with water and dry it by rinsing with C.P. acetone. The copperplate should have a uniform bright appearance, uniform thickness on all surfaces and edges, and excellent adherence and resistance to physical removal. The copper-plating solution is not depleted or contaminated during the plating process and may be repeatedly reused.

The described electroplating procedure has been used to produce excellent copperplates up to 0.05 mil (1.3×10^{-3} mm) thick on arc-cast (pure) Mo specimens and up to 1 mil (2.5×10^{-2} mm) thick on pure Nb foil. In addition, intricate molybdenum grid assemblies have been copper plated with very good results. No reason is apparent why this technique cannot be used to produce much thicker plates of similar quality on both Mo and Nb specimens.

Stripping of Electroplated Copper

Mechanically clean the plated specimen (either Mo or Nb) thoroughly. Further clean the specimen thoroughly with organic solvents as required to remove all foreign matter from the plated surfaces.

For stripping a plated Mo specimen at a moderate rate, prepare a 5.2 M (0.33 concentration) HNO_3 stripping solution. Holding the specimen so that the major plated surface is horizontal and facing down, immerse the specimen in the stripping solution (at room temperature) with agitation. Precautions should be taken against spraying of the solution during this operation. Continue the stripping until the copper plate is visibily removed from the specimen and a brown coloration is seen in the solution, indicating the Mo is being significantly attacked. Immediately withdraw the specimen and rinse it copiously with water. For thicker copper plates, use two or more fresh batches of stripping solution (to the above end point). The quoted strength of stripping solution completely strips a copperplate on Mo approximately 0.02 mil (0.5×10^{-3} mm) in thickness in about 20 seconds at room temperature. For faster stripping (or thicker copperplates), a 6.3-M (0.4-concentration) HNO_3 stripping solution may be used. This strips the above copperplate in about 3 to 5 seconds. For slower stripping, a 3.9-M (0.25-concentration) HNO_3 stripping solution may be employed; this requires about 8 minutes to completely strip the above copper plate.

The brown/black Mo oxide coating produced on the Mo specimen during the above stripping procedure may be readily removed by immersing the specimen for about 1 minute or less in concentrated HCl containing about 0.5 M HNO_3, with the operation done at room temperature. After rinsing in water, the Mo specimen should have regained its original dull, light gray appearance, and its surface may appear somewhat etched. With care exercised during the stripping operations, however, the loss of Mo from the specimen should be negligible, and, if desired, the specimen may be repeatedly replated with copper and stripped by the above procedures.

To strip a clean copper-plated Nb specimen, simply immerse the specimen in concentrated HNO_3 at room temperature, taking care that the solution is diluted as required for a safe reaction rate. Continue the stripping until the copper is completely removed from the specimen; then rinse it in water. The HNO_3 does not attack the Nb.

This work was done by John L. Power of **Lewis Research Center.** *No further documentation is available.*
LEW-12151

Custom Blending of Lamp Phosphors

The spectral output of fluorescents can be precisely adjusted.

Lyndon B. Johnson Space Center, Houston, Texas

The spectral output of fluorescent lamps can be precisely adjusted by using a new computer-assisted analysis for custom blending the lamp phosphors. The "customized" fluorescents can serve as supplementary lighting and as "fill-in" lamps to eliminate shadows in applications that demand a specified spectral output.

The new technique was developed to fabricate lamps for in-studio lighting of camera models in flight simulators. The simulators have a main bank of metal halide lamps; however, since rear lighting is used, the main bank produces shadows of the camera itself. This is a serious problem when illuminating closeups. Auxiliary fluorescents are commonly used in front of the camera to offset this shadowing since fluorescent tubing gives bright, even illumination at close range. However, unless the secondary lighting has the same spectral output as the main lamps, a difference in color will be seen. In flight simulators, even small color differences can give pilots false cues for judging their altitudes and distances.

With the new technique, the spectrum of the main bank of lamps is measured and stored in a computer memory along with the emission characteristics of commonly available phosphors. The computer then calculates the ratio of the green and blue intensities and the ratio of the red and blue intensities for each phosphor according to the manufacturer's specifications and plots them as coordinates on a graph. The same ratios are calculated for the measured spectrum. If a straight line can be drawn through the points corresponding to two phosphors and also through the ideal response, then some mixture of the two will match the ideal. Likewise, if a triad of three points joined by lines encloses the ideal, a mixture of the three can be blended to match the ideal.

To find the proper mix, it is assumed that the blend will emit radiation with a distribution that is proportional to the relative quantities of the components. Once the proper mix has been determined, it is applied as a coating to the fluorescent tubing.

This work was done by Robert E. Klemm of The Singer Co. for **Johnson Space Center.** *For further information Circle 33 on the TSP Request Card.*
MSC-16692

Books and Reports

These reports, studies, and handbooks are available from NASA as Technical Support Packages (TSP's) when a Request Card number is cited; otherwise they are available from one of NASA's Industrial Application Centers or the National Technical Information Service.

Cure-Rate Data for Silicone Adhesive

Mixing with as little as 0.07 percent catalyst increases the mobility of low-outgassing adhesive.

By decreasing the amount of catalyst below 0.1 percent, the cure rate for a commercially-available silicone adhesive (General Electric #566) can be altered to yield longer working times. Since this adhesive has low-outgassing properties and does not require a bakeout, it is often used in high-vacuum systems. When combined with 0.1 percent catalyst, however (the amount that is usually recommended), its relatively low pot life gives working times that are too short for many production applications. Its range of uses can be broadened by adjusting the amount of catalyst and thereby increasing the flow time.

The technique of altering mobility by adjusting the amount of catalyst is well known; however, no flow data have been available until now for catalyst concentrations less than 0.10 percent in this system. A report that describes work with concentrations down to 0.07 percent is now available and should be useful when applying the adhesive in terrestrial and space applications. The cured silicone retains its low-outgassing properties, as well as its snap, elongation, and resilience.

A syringe was used to measure out the small amount of catalyst — for example, a 100-gram batch of polymer requires less than 0.1 gram of catalyst — accurately and repeatedly. The equipment, cleaning and drying agents, and procedures for calibrating the syringe to dispense accurate weights of catalyst as a function of volume are described in detail in the report. Calibrating each syringe to account for slight differences in a parameter as bore diameter, for example, is important for maintaining the correct weight-to-volume ratio. The syringes used to dispense the tiny amount of catalyst are quite small, with

capacities down to 0.05 milliliter. Moreover, each syringe should be chosen so that the volume of catalyst dispensed is close to its maximum capacity.

Flow rate tests, after allowing 45 minutes for catalysis, were run on 100-gram batches of the silicone. Concentrations of 0.10, 0.09, 0.08, 0.075, and 0.07 percent catalyst B were added to the silicone resin. The mobility increased greatly in the 0.075- and 0.07-percent ranges, approximately doubling at 0.07 percent catalyst, as compared to 0.01 percent catalyst.

Each of the silicone batches with these catalyst concentrations was also subjected to an outgassing test at 125° C for 24 hours. The batches had excellent, low-outgassing characteristics. They showed no deterioration or increase in condensable production as catalyst concentration decreased, an indication of good cure.

Likewise, tests for hardness of the silicone material also showed good results. Elongation, resilience, and snap were good for each of the samples. There was no gross hysteresis observable on recovery from stretching nor was there any decrease in hardness.

This work was done by Carroll Clatterbuck and Aaron Fisher of **Goddard Space Flight Center.** *To obtain a copy of the report, Circle 34 on the TSP Request Card.*
GSC-12330

Fire- and Smoke-Retardant Polyesters and Elastomers

Study compares effectiveness of inorganic fillers.

Fire- and smoke-retardant plastics and elastomers find many applications in mass transit systems ranging from seat cushion materials to cable coatings. These polymers contain materials such as phosphates, antimony, boron, or halogen compounds, which are used to improve the fire safety of plastic material. A problem with these flame retarded polymers is that during fire they may emit large quantities of smoke and toxic gases. These can cause limited visibility and dangerous panic in a crowded mass transit vehicle that may delay exit of the passengers and lead to loss of life.

In an effort to find better retardants a study has been carried out to determine what filler materials would be most effective in improving the fire- and smoke-retardant characteristics of plastic products. An NBS (National Bureaus of Standards) Smoke Density Chamber was used to test polyester, polyurethane, and elastomer samples that were mixed with a number of fillers. The tests were conducted at standard exposure conditions of 2.5 W/cm^2 radiant heat flux with and without pilot flames. In a flaming test, six small flames about 1/2 in. (1.3 cm) were allowed to contact the lower portion of the sample. The heat flux was sufficient to raise the surface temperature of an asbestos block placed in front of the heat source to approximately 400° C. The test exposure times were as long as 20 min.

The quantity of smoke generated inside the chamber was measured by using a light-transmission meter set 3 ft (91 cm) from a vertical light source. Many tests were terminated sooner than 20 min when the smoke density value exceeded 500, or light-transmission value of less than 0.015 percent.

The test results indicate that the most effective fire- and smoke-retardant fillers are inorganic hydrates and carbonates that release water and/or carbon dioxide. The most effective filler tested was hydrated sodium silicate ($Na_2SiO_3 \cdot 9H_2O$). Its effectiveness is due to its high water content and the formation of a viscous molten glass when heated. The glass tends to inhibit polymer combustion and to promote the formation of char residue. However, because it is water-soluble and because it evolves water at temperatures below 100° C, this filler may not find practical applications in plastics.

Perhaps a better filler is $Mg(OH)_2$, which has been very effective under both flaming and nonflaming tests. This compound is not water-soluble and begins to evolve water at a temperature of approximately 350° C. At this time, $Mg(OH)_2$ is probably the best choice as a filler for flame- and smoke-retardant cable coverings and undercoating formulations.

This work was done by Shirley Y. Chung, John D. Ingham, Daniel D. Lawson, and Michael Mosesman of Caltech for **NASA's Jet Propulsion Laboratory.** *To obtain a copy of the report, Circle 35 on the TSP Request Card.*

Inquiries concerning rights for the commercial use of this invention should be addressed to the Patent Counsel, NASA Resident Legal Office-JPL [see page A8]. Refer to NPO-14053.

Mossbauer Studies of Bulk and Thin-Film FeTe

Film properties are examined as a function of thickness and substrate material.

A systematic Mossbauer study of bulk and thin-film iron tellurium (FeTe) has been carried out and is desribed in a report that is now available. In the study, the dependence of the Mossbauer parameters on film thickness and film substrate (amorphous Mylar and crystalline aluminum) was measured and related to the FeTe structure.

For bulk FeTe the Mossbauer spectrum exhibits an isomer shift (IS) and a quadrupole shift (QS) that indicate a quadrupole structure. The charge state is Fe^{2+} with a strongly-covalent hybridized bond. The film-thickness study showed that there is a dependence of the IS and QS values on thickness below 1,000 Å; above that, the values are equal to those obtained in the bulk sample.

It is postulated that the thickness dependence is due to dangling bonds. In the thinnest films, ions do not fill in gaps created in the initial stages of film formation. Their low mobility causes them to stick to the substrate randomly. As the deposition continues, ions fill in the dangling bonds caused by these

(continued next page)

gaps. By raising the substrate temperature to increase the ion mobility, it should be possible to lower the critical thickness above which the film behaves like a bulk sample.

Crystal-structure distortion and the preferential orientation of monocrystals were observed to decrease with increasing film thickness. FeTe spectra from the two substrate materials were found to be very different in both their shapes and IS values, indicating that the crystal structure (or lack of it) of the substrate strongly influences the nature of the deposited film.

The report also describes the film deposition technique (flash deposition) and the Mossbauer apparatus.

This work was done by Kamna Aggarwal, W. T. Escue, and R. G. Mendiratta of **Marshall Space Flight Center.** *Further information may be found in NASA TM-X-73380 [N77-23965], "Bulk and Thin Films of FeTe: A Mossbauer Study," a copy of which may be obtained at cost from the New England Research Application Center* *[see page A7]*.
MFS-23773

Fast-Drying Coating

Nonflammable coating meets strict outgassing requirements.

A report now available describes a new water-based latex fluoropolymer coating that meets the demanding requirements of the space program; it may also have industrial applications. The coating dries to the touch in about 1 hour, and it dries fully at normal room temperature and humidity in 24 hours.

The new nontoxic coating has excellent optical properties and can be pigmented in many different colors. It bonds well, can be applied by conventional methods, weathers well, and is self-extinguishing.

The fluoropolymer system consists of a terpolymer of vinylidene fluoride and two perfluoro-olefins. The coating composition comprises latex blends of the fluorocarbons, acrylic resins, stabilizers, modifiers, a variety of inorganic pigments, and other additives. Suitable latex primers have also been developed from an acrylic latex base.

The report describes work done by E. J. Bartoszek of Pennwalt Corp. and was prepared for **Johnson Space Center.** *It is identified as NASA CR-147499 [N76-18237], "Special Purpose Spacecraft Interior Coating." A copy may be obtained for* **$***4.00 [prepayment required] from the National Technical Information Service, Springfield, Virginia 22151.*
MSC-16056

Life Sciences

Hardware, Techniques, and Processes

Low-Intensity X-Ray and Gamma-Ray Imaging Device

Low-dose, low-power, rugged X-ray fluoroscopic system is completely self-contained.

Goddard Space Flight Center, Greenbelt, Maryland

A new X-ray and gamma-ray imaging device, originally developed for X-ray astronomy applications, makes it possible to perform fluoroscopy and radiography at reduced dosages. In certain applications, the entire fluoroscopic and radiographic system can be made fully portable (see Figure 1), allowing medical diagnostics to be performed in field and remote locations.

The new device, known as a Lixiscope (low-intensity X-ray image scope), is capable of imaging objects that are positioned in front of a low-intensity X-ray or gamma-ray source. The X-ray or gamma-ray shadow image is converted to a visible-light image. This visible-light image is then intensified through intermediate photoelectron conversion and electron amplification to a level suitable for viewing. While the Lixiscope can be used with a conventional X-ray machine turned down to a very low level, it can also be operated with its own source (such as a radioisotope) or small radiation generator for hand-held portable applications.

As shown in Figure 2, the converter is a layer of luminescent material, such as a rare-earth phosphor (for X-rays) or a high-efficiency scintillator (for gamma rays). The intensifier has a microchannel plate (MCP) amplifier positioned between a photocathode and a phosphor screen; it is capable of visible-light gain in excess of 10^4. The intensifier output can be viewed directly or recorded on visible-light sensing devices; e.g., film and TV cameras.

The phosphor layer or scintillator, shielded from external light, converts the incoming radiation to visible-light photons that are piped into the high-vacuum chamber of the intensifier by a fiber-optics faceplate. The diameter of the fibers is less than 5 μm. The loss of resolution is minimal because of the close coupling of the converter to the fiber-optics plate and the small size of the fibers.

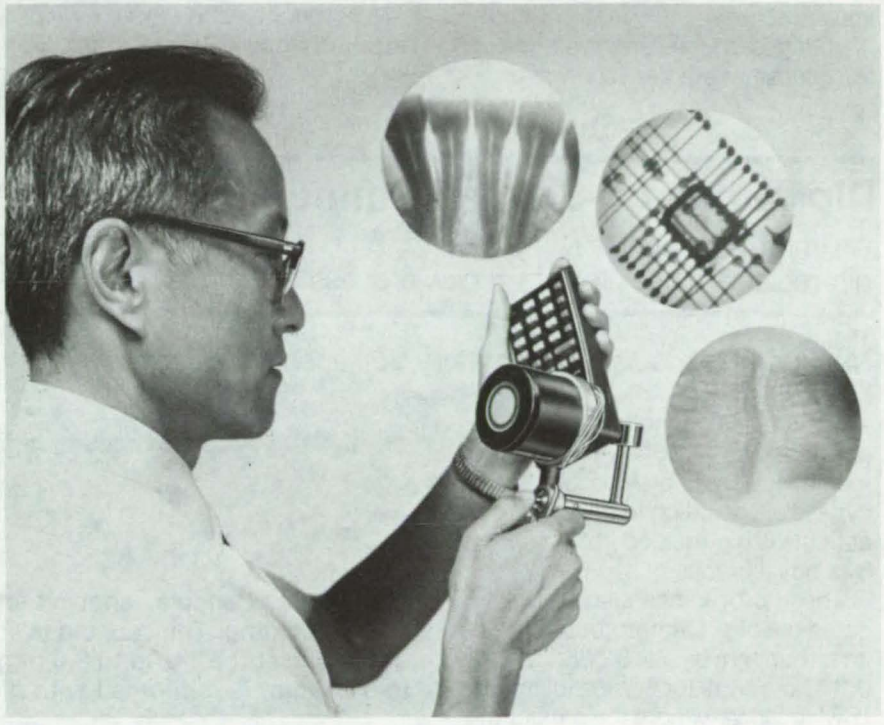

Figure 1. New **Portable Low-Intensity X-ray Imaging Device** carries its own radiation source and image intensifier. The hand-held unit has potential uses in medicine and microelectronics (see insets) and in other radiographic applications.

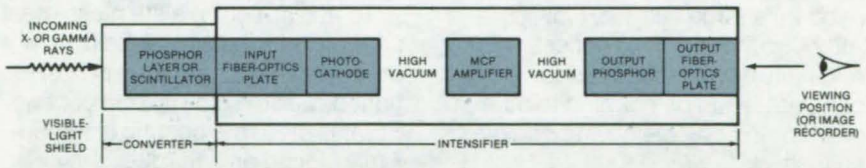

Figure 2. The **Lixiscope Inner Workings** are shown in this schematic. Its cylindrical housing is made out of ceramic, glass, or other material suitable for electrical insulation and vacuum isolation.

Photocathode material with high efficiency at the output wavelength of the converter is deposited on the vacuum side of the fiber-optics plate. The photocathode generates large numbers of electrons in response to the incoming light. These photoelectrons are accelerated across a gap to the microchannel plate amplifier. The output electrons are accelerated toward an aluminized phosphor screen that is deposited on the vacuum-side surface of the output fiber-optics faceplate. There, the electrons are

(continued next page)

converted back to visible light; the aluminized layer prevents light feedback to the photocathode. Since the input and output faceplates also act as vacuum seals, no additional "windows" are necessary. This improves efficiency and makes it easy to couple to virtually any type of image recorder.

Voltages for the various stages of the intensifier are derived from a 3-volt battery. The voltage supply and protective circuitry are encased in silicone rubber around the intensifier. The visible-light image intensifier tube containing the microchannel plate was developed by the U.S. Army Night Vision Laboratory, Fort Belvoir.

This work was done by Lo I Yin of **Goddard Space Flight Center.** *For further information, Circle 36 on the TSP Request Card.*

This invention is owned by NASA, and a patent application has been filed. Inquiries concerning nonexclusive or exclusive license for its commercial development should be addressed to the Patent Counsel, Goddard Space Flight Center [see page A8]. Refer to GSC-12263.

Dip-Molded T-Shaped Cannula

An improved cannula is dip-molded in one piece by a new process.

NASA's Jet Propulsion Laboratory, Pasadena, California

A T-shaped cannula that was developed as part of an experimental system to provide long-term bypass oxygenation to respiratory patients is dip-molded in one piece by a novel process.

The improved cannula is fabricated out of polyetherurethane with an ultrathin (typically 0.038- to 0.076-cm) wall for compatibility with flowing blood without the danger of excessive clotting. It is suitable for continuous service for up to 21 days. The T-shape collects blood from both directions, thus replacing the two conventional cannulas that are usually required and eliminating the need for a large surgical wound. Although the molding process was originally developed to fabricate the cannula, it can be adapted to other elastomeric objects having complex shapes.

To form the cannula, a mandrel is dipped in segmented polyetherurethane (SPU) mixed with a solvent. The thickness of this first SPU layer, typically 0.25 to 0.76 mm, is controlled by varying the temperature and concentration of the solution and the rotation rate of the mandrel.

When the wall builds to the desired thickness, the piece is dipped in acetone. This swells the coating and allows the T-arm of the mandrel to be unscrewed and removed. Both sections can then be withdrawn from the mold. To prevent sticking, the mandrel is initially covered with an outer layer of Ryton or other suitable material.

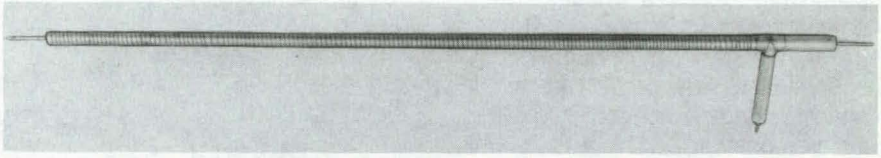

A T-Shaped Cannula, shown here while still on its mandrel, is formed by dip-molding. The cannula is 45.3 cm long. It tapers from a diameter of 9.8 mm at the T-arm to 8.0 mm at its end. Its thin wall, typically 0.25 to 0.76 mm, is reinforced with a metal helix.

To add strength, a stainless-steel wire is preformed into a helix on a second mandrel and then is positioned over the dip-molded coating. For this step, the coating is temporarily placed on a third, slightly smaller, mandrel. Finally, the piece is dipped in SPU to form an outer layer that encases the helix. The long arm is built up to its required thickness during this step, and the T-arm is simultaneously built up to its different thickness, by controlling the process parameters.

To optimize blood-flow properties, one end of the long arm (the shorter end) is given a slightly smaller diameter than the other, and the other end has a gradually tapering diameter. Since these dimensions would make it impossible to withdraw the mandrel, the smaller diameter is formed by inserting an SPU-coated Teflon stub. The end of the cannula is dipped in acetone to receive the stub. When the acetone evaporates, the arm shrinks, forming a tight seal.

This work was done by Howard F. Broyles, Edward F. Cuddihy, and Jovan Moacanin of Caltech for **NASA's Jet Propulsion Laboratory.** *For further information, Circle 37 on the TSP Request Card.*

Inquiries concerning rights for the commercial use of this invention should be addressed to the Patent Counsel, NASA Resident Legal Office-JPL [see page A8]. Refer to NPO-14073.

Improved Control of Medical X-Ray Film Exposure

New optical arrangement
gives greater sensing accuracy.

NASA's Jet Propulsion Laboratory, Pasadena, California

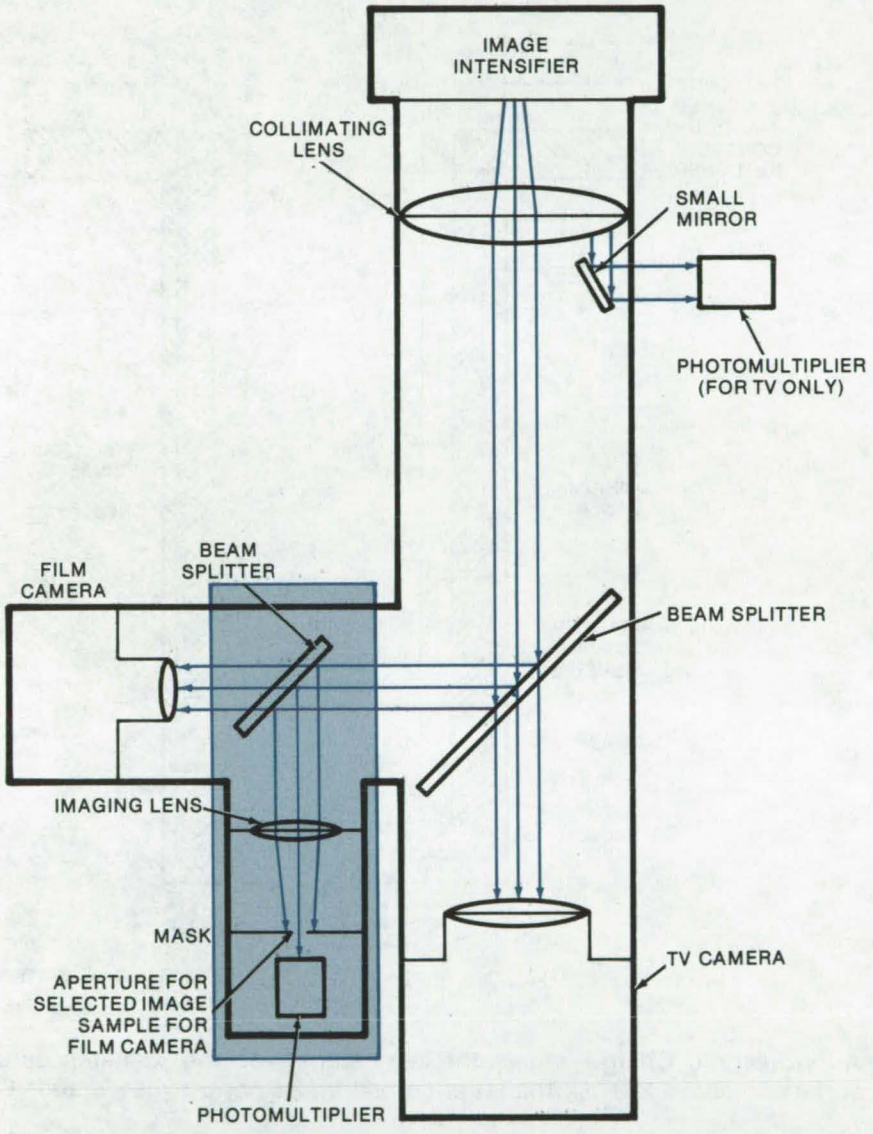

This **X-Ray Motion Picture System** uses the sensing optics shown in the color box to control the film exposure. The small mirror and photomultiplier at the upper right had previously been used to control both the film and TV image; they are now used only to adjust the TV-picture quality.

Motion picture X-ray systems use an image intensifier to increase the brightness of a conventional X-ray fluorescent screen image. The light from the intensifier is collimated and sent to a motion picture camera and a TV system by means of a beam splitter. The TV system allows the operator to center the tissue of interest in the screen field while the film camera records the image.

In these X-ray systems the film exposure is often determined by a sensing system that samples a small portion of the light from the collimated beam. Since collimating the light beam averages the brightness level over the entire image, it is difficult to determine the optimum exposure for the particular portion of the image that is of interest. Often the exposure is unsatisfactory, and the patient must be subjected to another X-ray dose to obtain a better picture.

To solve this problem the exposure sensing system has been relocated near the motion picture camera. As seen in the figure, a second beam splitter directs a portion of the light through an aperture (or an adjustable diaphragm) to a photomultiplier. The aperture allows the photomultiplier to see only the section of the image that is centered on the area of interest and allows a more accurate determination of the exposure level.

This work was done by C. Martin Berdahl of Caltech for **NASA's Jet Propulsion Laboratory.** *For further information, Circle 38 on the TSP Request Card.*

This invention is owned by NASA, and a patent application has been filed. Inquiries concerning nonexclusive or exclusive license for its commercial development should be addressed to the Patent Counsel, NASA Resident Legal Office-JPL *[see page A8].* *Refer to NPO-13808.*

Self-Sterilizing Canister

Electrically-activated pyrotechnic charge heats the outer surface, yet does not damage contents.

NASA's Jet Propulsion Laboratory, Pasadena, California

The increasing use of active biological materials for medical and research purposes requires the development of devices that can be used to transfer materials into and out of environments that are biologically hazardous or require severe biological control. A solution to this problem is a canister, the outer surface of which can be sterilized without damaging a sample held in an inner compartment.

As seen in the figure, one version of the canister consists of four concentric layers: an inner layer of Teflon, an aluminum member serving both as a structural member and thermal buffer for the inner layer, a layer of zirconium/barium chromate (or equivalent) powder, and finally, an outer aluminum casing. An electrically-activated explosive charge (squib) ignites the powder. A powder composition that reacts without releasing significant amounts of gas is used, so no venting is needed.

The pyrotechnic powder reacts in the temperature range of 800° to 1,000° C. Once ignited it brings the temperature of the outer surface to a minimum of 230° C for several minutes. The buffer distributes and controls the heat transfer so that the inner surface never exceeds a temperature of 100° C. If necessary, multiple sterilizations or decontaminations are possible with more than one layer of the powder.

The self-sterilizing canister concept has many possible applications in which it can be used to sterilize either the inner or outer surface of a container or both. Although originally conceived as a means for remote sterilization of spacecraft packages prior to their reentry into the Earth's atmosphere, it could also be used to transfer samples into and out of biologically hazardous laboratories. Equipment in field hospitals and in other emergency situations could also be handled with this equipment.

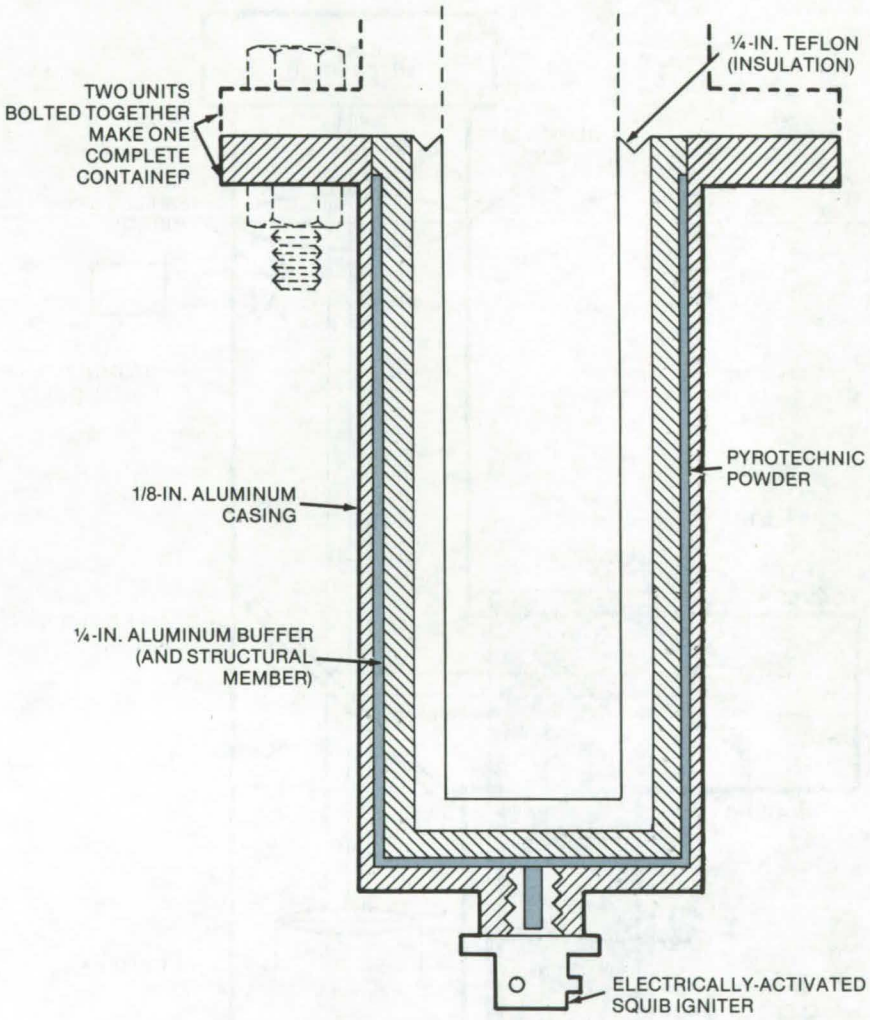

A Pyrotechnic Charge raises the temperature of the canister outer surface to above 230° C; the inner compartment never exceeds 100° C.

This work was done by Lien C. Yang of Caltech for **NASA's Jet Propulsion Laboratory.** *For further information, Circle 39 on the TSP Request Card.*

Inquiries concerning rights for the commercial use of this invention should be addressed to the Patent Counsel, NASA Resident Legal Office-JPL [see page A8]. Refer to NPO-14237.

Controlled Freezing of Biological Samples

Precisely controlled freezing of blood-cell and biological-tissue samples enhances the viability and the yield of the frozen cell population.

Goddard Space Flight Center, Greenbelt, Maryland

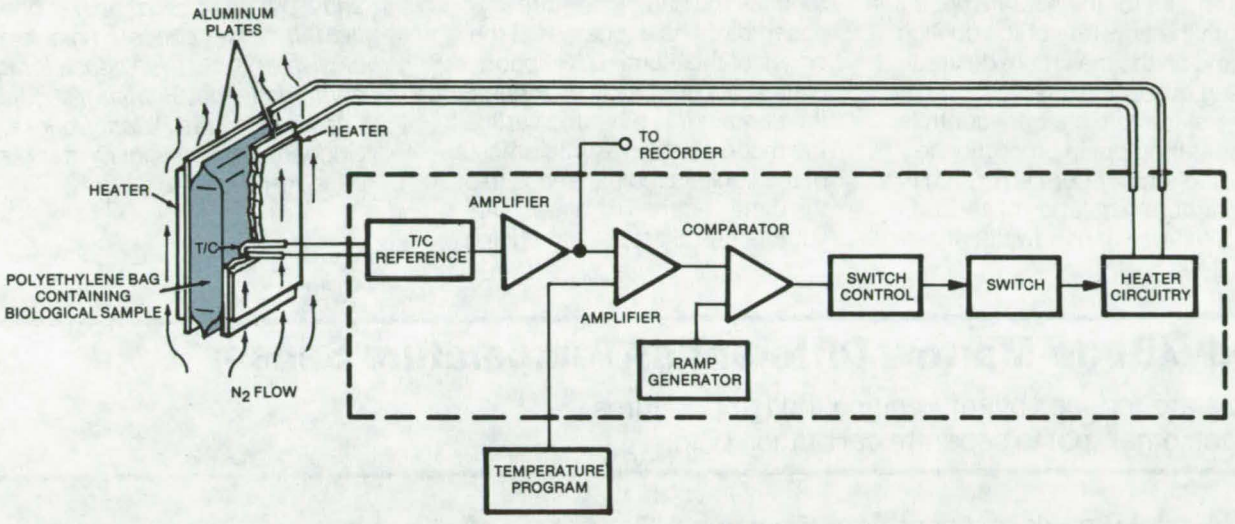

The Controlled-Temperature Freezing Apparatus Circuitry consists of a thermocouple that is connected to a semiconductor reference junction. The reference junction is connected to an amplifier that boosts the signal by 1,000. The high-level signal is displayed on a recorder and fed into a second amplifier where it is compared with the signal from the potentiometer or programed dc reference in the bag-temperature programer. The greater the difference in these signals, the greater the output voltage from the second amplifier. The remaining circuitry provides zero-phase, time-proportion control of the heaters such that heater power is directly proportional to this error signal.

The viability of frozen blood cells, tissue samples, and other "living" matter has been known to depend strongly on the freezing rate. Freezing too quickly or too slowly destroys cells.

As generally practiced, the freezing rate is controlled by varying the flow or temperature of a cooling gas such as that derived from liquid nitrogen. This approach works well enough for much of the cooling cycle, but runs into problems when the sample reaches the freezing point. There, large amounts of heat must be removed (the latent heat of fusion), and relatively large changes in the cooling capacity of the gas must be made in relatively short periods of time. The time required for changes in the flow rate or temperature of the cooling gas to affect the sample is too long to control the freezing rate accurately.

This handicap can be overcome with a new system that uses heaters to control the sample temperature and thus the rate heat is removed from the sample. The heaters respond much faster than gas-flow systems, allowing freezing rates to be controlled more precisely.

The apparatus is a sample container assembly, a heater, and an electronics control unit (see figure). Blood cells, bone marrow, or other similar biological tissue are placed in a polyethylene bag that is sandwiched between two hardened aluminum plates. The plates conduct heat readily so that the tissue and container assembly are kept at substantially the same temperature. The outer surfaces of the container assembly are covered with printed-circuit heaters. The container assembly is placed in a cold gas stream inside a freezer and is cooled with the refrigerating fluid at a time-programed rate that is slightly greater than the maximum cooling rate needed at any time during the freezing process.

The temperature of the surface of the container assembly is constantly monitored as representative of the tissue temperature. This temperature is compared to a temperature/time curve; the heaters are turned on or off to keep the tissue at the programed temperature. For instance, the tissue is heated to compensate for any excessive cooling that might result from the refrigerating fluid, or the heater power is automatically reduced when the temperature of the tissue increases due to the supercooling effect that occurs near the freezing point. As the latent heat of fusion is being removed from the tissue at the liquid/solid phase, the heaters can be deactivated.

The sample container is a polyethylene bag (a comparatively-good

(continued next page)

thermal conductor) with a wall thickness of 0.05 mm. A self-sealing port allows the cells to be injected and withdrawn under sterile conditions. The heater thickness is less than 0.2 mm to reduce the thermal resistance path and speed up thermal response. The maximum power requirement for the heaters depends on both the flow rate of the cooling gas and on the maximum desired cooling rate of the tissue.

The electronic circuitry controls the heater output in proportion to detected temperature error. It has a temperature resolution of 1/60° C with a full-power bandwidth of 1/2° C. The circuit allows full heater energization within 0.5 second and has a continuous power output of up to 1,500 watts.

A thermocouple passes through the heater/plate assembly and is permanently mounted on the inside surface of the plate, so that it touches the bag. The entire assembly is held together at the edges of the aluminum support plates by a fiberglass channel. Since the container is mounted vertically, the moderate hydrostatic pressure of the liquid in the bag tends to push the plates apart. The plates are sufficiently stiff to resist bending, and the sample maintains a uniform thickness.

This work was done by Thomas A. Cygnarowicz and Thomas E. Williams of **Goddard Space Flight Center.** *For further information, Circle 40 on the TSP Request Card.*

This invention is owned by NASA, and a patent application has been filed. Inquiries concerning nonexclusive or exclusive license for its commercial development should be addressed to the Patent Counsel, Goddard Space Flight Center [see page A8]. Refer to GSC-12173.

Body/Bone-Marrow Differential-Temperature Sensor

Errors are reduced by referencing the temperatures to each other, not to separate calibration points.

NASA's Jet Propulsion Laboratory, Pasadena, California

Periodic samplings of bone marrow in the hip region can be taken to monitor the condition of patients suffering from leukemia. The in vivo temperature of the marrow, obtained from a marrow sample immediately after extraction, is also being studied as a possible indicator of the disease status.

There is believed to be a correlation between the body and marrow temperatures, but this can be confirmed only be measuring both temperatures at very nearly the same time. However, when temperature measurements are made by separate sensors, each with its own calibration reference, the error can be unacceptably large (on the order of 0.5° C) for these studies.

This error can be reduced by an order of magnitude if the two temperature measurements are referenced to one another. The electronics required to accomplish this are shown in Figure 1. In the

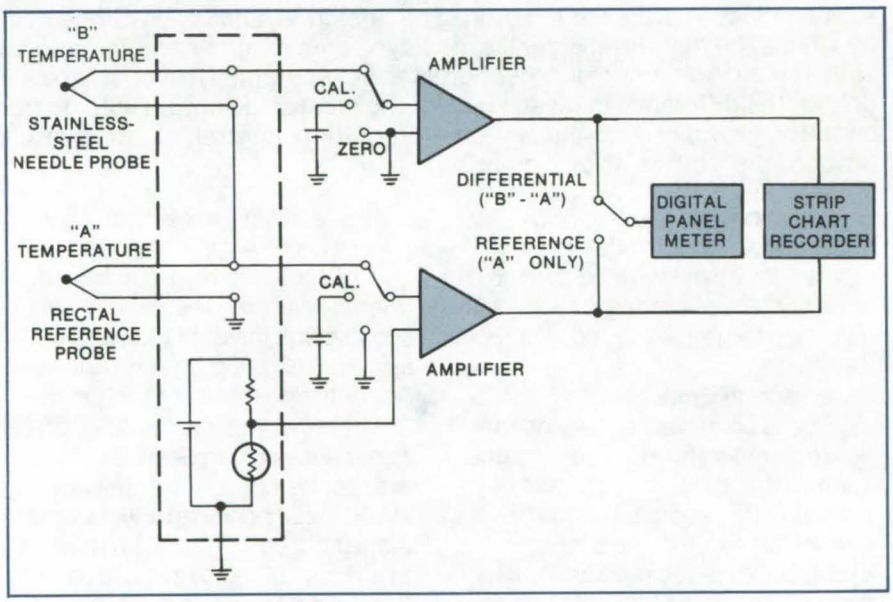

Figure 1. **Bone-Marrow and Body Temperatures Are Referenced** to each other, rather than to separate calibration points. In the reference mode, the output of the rectal probe is amplified; in the differential mode, the difference between the outputs of the needle probe and the rectal reference probe is amplified by a single stable amplifier and is displayed on the panel meter.

reference mode, the output of a rectal body-temperature probe is amplified and displayed on the panel meter. In the differential mode, the difference between the outputs of the bone-marrow sensor and rectal sensor is amplified by one amplifier and displayed. Since a single, stable amplifier is used in making the differential measurement, the effect of unequal drifts of two separate amplifiers is eliminated. Maximum probable errors of less than 0.1° C are possible with this instrumentation.

The tip of the needle probe is maintained at ground potential, while the rectal-probe thermocouple potential is always within a fraction of a millivolt of ground potential. It is electrically insulated from the body by its silicone sheath.

The structure of the bone-marrow probe and sensor is shown in Figure 2. A stainless-steel tube inside a needle contains thermocouple wires. A connector body forms a base for the tube and attaches to a cable leading to an electronics package. The structure of the rectal-temperature sensor is similar except that the rectal probe is covered by a soft silicone sheath for flexibility and safety. The sheath also electrically insulates the probe from the body.

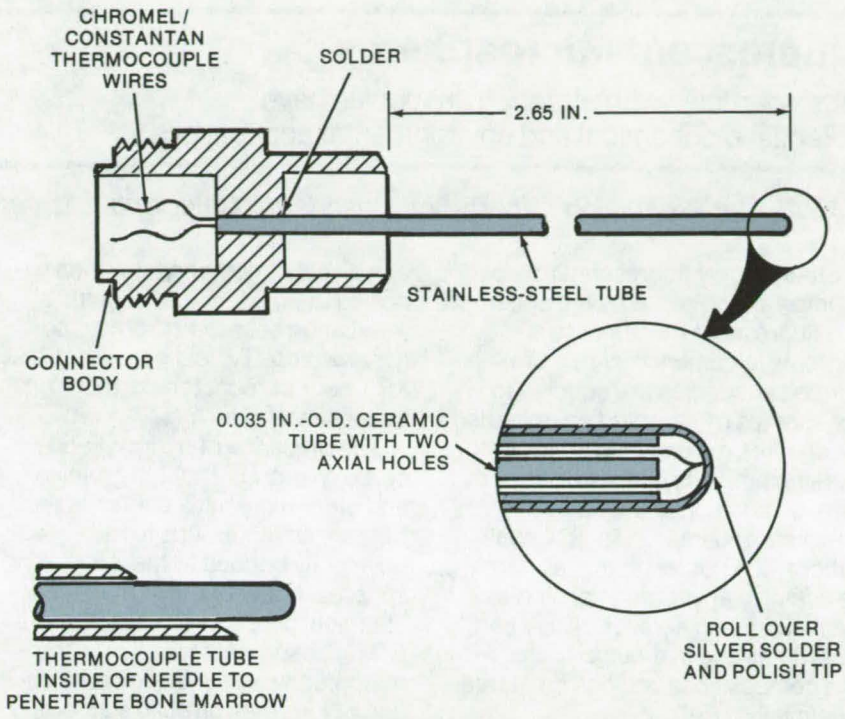

Figure 2. The Probe Portion of the marrow-temperature sensor has a stainless-steel tube that sheathes the thermocouple wires. A ceramic tube with two axial passageways for the wires lies within the stainless-steel tube for insulation.

This work was done by Victor J. Anselmo and C. Martin Berdahl of Caltech for **NASA's Jet Propulsion Laboratory.** *For further information, Circle 41 on the TSP Request Card.*
NPO-14121

Bacillus Cereus Strain MCV as a Debriding Agent

Enzyme-producing bacteria strain is used for eschar debridement.

Langley Research Center, Hampton, Virginia

A biologically active means has proven effective for rapidly removing scar tissue caused by burns or corrosive agents. A specially selected strain of bacteria, *Bacillus cereus* strain MCV, applied to the injury site, releases enzymes which are active against the eschar. These bacteria have a tendency to locate between the eschar and the unburned tissue, thus providing an optimal cell surface area arrangement for enzyme dispersal.

Bacterial activity of *Bacillus cereus* strain MCV produces a variety of enzymes which promote or accelerate cellular breakdown in eschar type tissues. Enzymes from other bacteria such as *Bacillus subtilis* have been used previously, but the results of the current experiments indicate that *Bacillus cereus* strain MCV and its enzymes perform the debridement function in a more efficient manner and leave the injury site in better condition for grafting.

The rapid debridement of the eschar obtained by this technique enhances the probability of success in skin grafting. This procedure may prove especially useful in the treatment of disaster casualties under relatively primitive conditions.

This work was done by Harry P. Dalton, Boyd W. Haynes and Larry L. Stone of the Medical College of Virginia for **Langley Research Center.** *For further information, Circle 42 on the TSP Request Card.*

Inquiries concerning rights for the commercial use of this invention should be addressed to the Patent Counsel, Langley Research Center [see page A8]. Refer to LAR-12287.

Fluorescent Microspheres

Latex particles with attached antibodies have potential biochemical and environmental applications.

NASA's Jet Propulsion Laboratory, Pasadena, California

Stable highly fluorescent microspheres are obtained by the addition of a fluorescent monomer to a hydrophilic comonomer mixture. Purified antibodies are coupled to the spheres by standard chemical procedures making them suitable for marking antigens on the surfaces of cells. In addition to their biochemical and immunological applications, the microspheres also may be useful in environmental studies such as tracing aerosols. They can be synthesized in a range of sizes and compositions and can be stored indefinitely.

Latex spheres, with diameters from 0.3 to 3 microns, are formed by adding a fluorescent monomer, e.g., dansyl allyiamine or an adduct of allylamine and fluorescein isothiocyanate to a mixture of hydroxyethyl methacrylate, methyl methacrylate, methacrylic acid, and ethylene glycol dimethacrylate, then exposing the mixture to a cobalt γ-radiation source to promote polymerization. Typical exposures last for 1 hour at room temperature (in the absence of air).

The presence of hydroxyl and carboxyl groups enables proteins and other molecules containing primary amino groups to be covalently bonded to the latex spheres. Many of the same chemical procedures used in preparing absorbents for affinity chromatography and in the immobilization of enzymes on solid supports can be used to form the antibody/latex conjugates.

Antibodies purified by immunoabsorbent chromatography have been coupled to the spheres by either a cyanogen bromide, carbodiimide, or glutaraldehyde method. The reactions are carried out under conditions that maintain the antigen-binding activity of the antibodies and minimize the aggregation of latex particles. The number of bound antibody molecules can be controlled by varying the concentration of antibodies in the reaction. Antibody/latex conjugates can be separated from unbound antibody molecules by column chromatography, filtration, centrifugation, or electrophoresis.

Human red blood cells and lymphocytes have been labeled with fluorescent microspheres by either a direct or indirect immunological technique. The immunolatex spheres can also be used for detecting and localizing specific cell surface receptors. Hormones and toxins may also be bondable.

This work was done by Alan Rembaum of Caltech for **NASA's Jet Propulsion Laboratory.** *For further information, Circle 43 on the TSP Request Card.*
NPO-13946

Mechanics

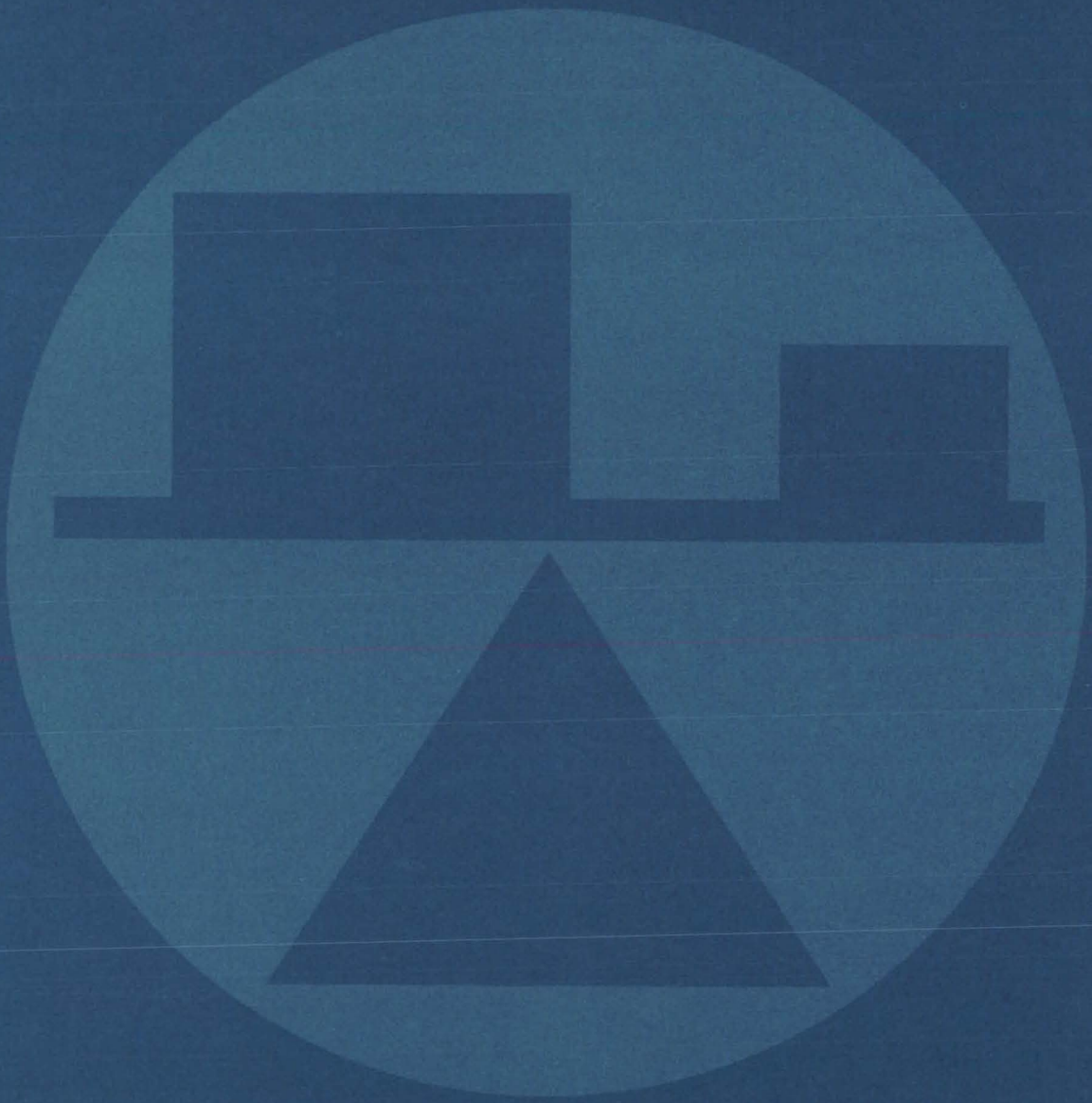

Hardware, Techniques, and Processes

Books and Reports

Computer Programs

Aerodynamic Design Lowers Truck Fuel Consumption

Forebody modifications reduce tractor-trailer fuel consumption by up to 24 percent.

Dryden Flight Research Center, Edwards, California

New energy-saving concepts in truck design are emerging from research being done at Dryden Flight Research Center. The Dryden effort, which evolved from experience with aircraft, has concentrated on developing new shapes with improved aerodynamic flow properties that can reduce the air-drag coefficient of conventional tractor-trailers, without requiring severe design changes or compromising the load-carrying capability.

Tests on a conventional cab-over-engine tractor with a two-axle smooth-walled trailer that was modified to a low-drag configuration (see figure) showed a 37-percent reduction in drag coefficient and a 20- to 24-percent decrease in fuel consumption in controlled tests over the open road at 55 miles per hour (88.5 km/h). These improvements involved no modifications to the engine or drive train and were obtained solely by improving the forebody aerodynamics through the use of sheet-metal fairing and increased corner radii. The measured reduction in aerodynamic drag was more than 50 percent greater than those obtained with previous changes in aerodynamic design.

The drag data were obtained on the low-drag-configuration and control vehicles shown in the figure. Each vehicle was allowed to coast down from 55 miles per hour with the transmission in neutral. The total drag is defined by

$$D_T = D_a + D_m = M \frac{\Delta V}{\Delta t}$$

where D_a and D_m are the aerodynamic and mechanical contributions to the drag, M is the vehicle mass, and Δt is the time it takes for the truck to decrease its speed by an amount ΔV. Measurements were taken for each 5-mi/h (8.05-km/h) interval. The effects of mechanical drag were calculated by using standard models and were subtracted to determine the aerodynamic drag. At 55 mi/h, the drag coefficient was 0.74 for the low-drag configuration as compared to 1.17 for the unmodified (baseline) vehicle.

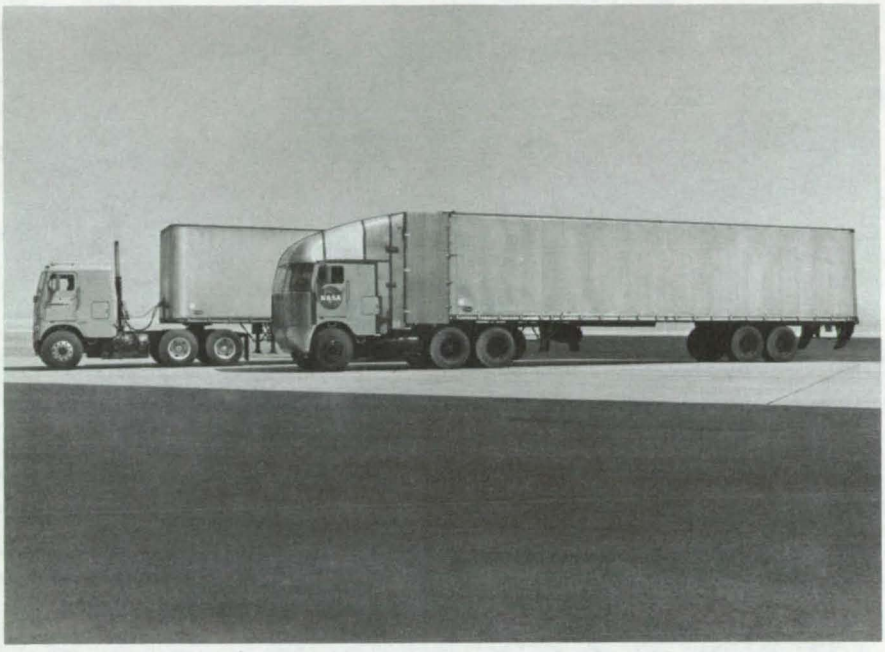

Fuel Consumption is Reduced by modifying the forebody aerodynamics of this tractor-trailer. The unmodified vehicle is shown at the left. The modified vehicle at the right has larger corner radii and a sheet-metal fairing extending from the modified tractor top and sides to the trailer.

Fuel-consumption tests were conducted along a 312-mi (502-km) stretch of open road with one vehicle following the other by 1/2 mile (0.8 km). During the tests, radio communications were maintained so that the crews could coordinate shifting, engine start and stop times, and even the opening and closing of windows. Fuel consumption was lowered by between 18.0 and 24.4 percent for the low-drag-configuration truck.

Although the tests were conducted in lightly (but equally) loaded vehicles in calm or near-calm wind conditions, one can confidently extrapolate the qualitative trend to operational applications. It is expected that the improvements would decrease somewhat with increased wind velocities and would be affected by factors such as the terrain, driving techniques, and mechanical condition.

This work was done by Louis Steers of **H. L. Dryden Flight Research Center.** *For further information, Circle 44 on the TSP Request Card.*
FRC-11015

Combination Force and Angular-Deflection Indicator

Tool measures force-to-deflection curve for rudder and for brake pedals on aircraft.

Lyndon B. Johnson Space Center, Houston, Texas

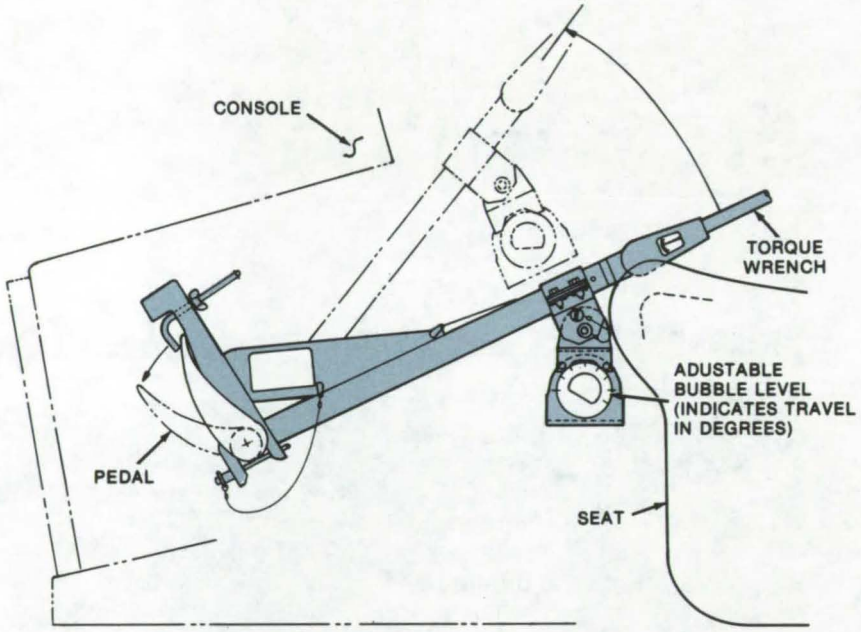

Figure 1. A **Combination Force and Angular-Deflection Indicator** is shown in the brake-pedal checkout position. As the lever arm is rotated, torque readings are taken at various angular increments to verify the deflection-versus-force relationship.

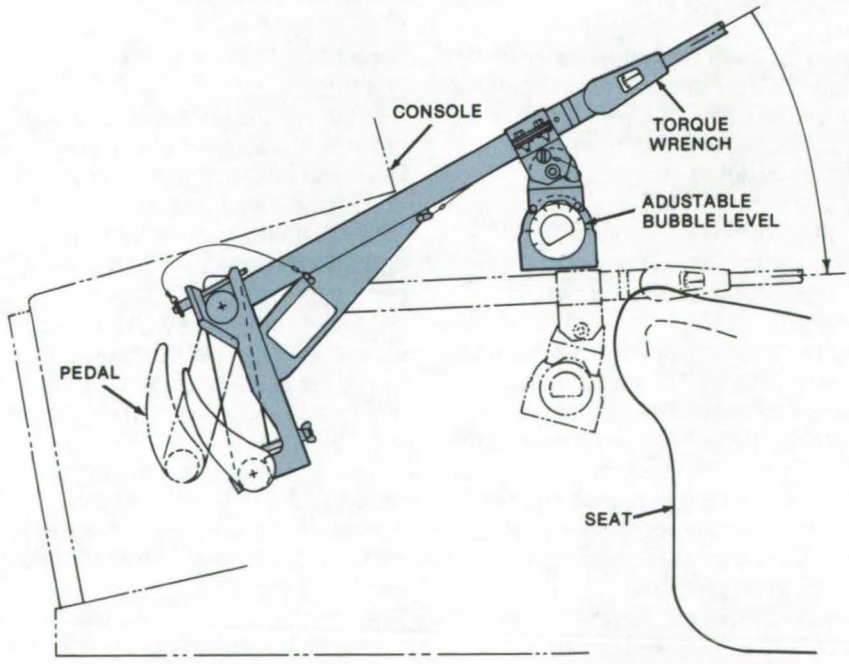

Figure 2. **Tool is Inverted** for rudder-pedal checkout.

Aircraft brake and rudder pedals are often rather inaccessible, making it difficult to verify proper operation. Precision push/pull scales, along with auxiliary tools may be used to check pedal force; however, these do not indicate angular displacement, nor can they be used to check the deflection-versus-force relationship. Protractors are sometimes used in conjunction with spring scales, but it is usually difficult to manipulate both tools for accurate readings, due to the limited accessibility of the pedals.

Verification of pedal operation is possible with a new tool that measures force and angular displacement. With the tool, one can check both rudder- and brake-pedal operation.

The new tool has a lever arm with fittings for quick attachment to the pedal at one end, a torque wrench at the other end, and an adjustable bubble-level degree indicator. To check brake-pedal angular deflection and force, the pedal is positioned full aft, and the tool is secured to the pedal as shown in Figure 1. With no brake force applied to the pedal, the bubble level is set at 0°. Then the torque wrench is engaged, and the lever arm is rotated through breakout and various angular increments to full travel, as indicated on the bubble. Torque readings are taken at each increment to verify the proper force/deflection relationship. Rudder-pedal angular deflection and force are incrementaly verified in the same manner except that the tool is inverted by 180° to impart rudder-pedal deflection force, as shown in Figure 2.

This work was done by Jerome F. Kauppi of Rockwell International Corp. for **Johnson Space Center.** *For further information, Circle 45 on the TSP Request Card.*
MSC-16155

Noncontact Measurement of Angular Deflection

Optical and electromechanical components are incorporated into a feedback system.

Langley Research Center, Hampton, Virginia

A new technique developed at Langley Research Center for measuring the instantaneous angular deflection of an object requires no physical contact. Previous noncontacting methods involved modulation of a light beam by a variable-density or a polarized disk, followed by intensity measurements using a light sensor. These and other methods suffer accuracy limitations due to light-intensity changes, motional interaction, and nonlinear response.

The new technique, illustrated in the figure, utilizes two flat refractors, a converging lens, and a differential photocell. Light is transmitted through the first flat reflector to the lens, which focuses it through the second flat refractor to an image on the differential photocell. The two flat refractors are identical, and they are placed an equal distance from the converging lens, as are the light source and the photocell. The output of the photocell, which is a function of image displacement, is fed to an amplifier that drives a galvanometer that rotates the second flat refractor.

This refractor is rotated so that the image displacement is very nearly zero, making the galvanometer current a measure of the deflection of the driven galvanometer. Geometrically, it is evident that the rotation of the driven refractor is proportional to and nearly equal to the rotation of the first, or "object," refractor, yielding an accurate measurement of the rotation of the first refractor via the galvanometer current.

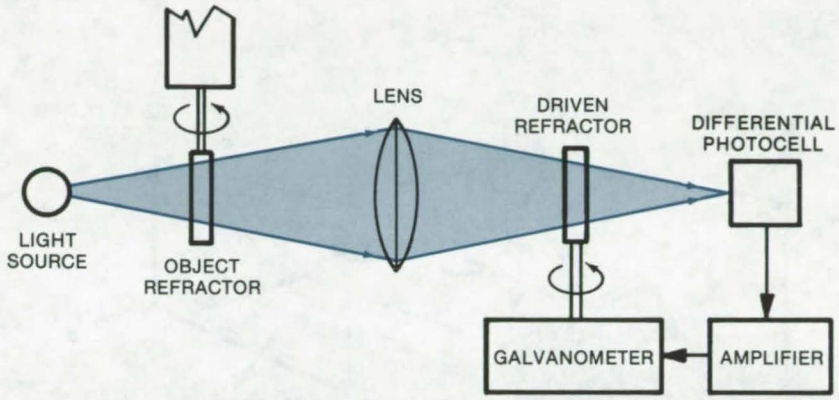

Angular-Deflection Measurement Technique is "noncontacting" in that only a refractor needs to be attached to the sensed object. As the object refractor rotates, the focused image of the light source shifts. This shift causes a photocell output proportional to the change in light intensity. This amplified output is used to drive a galvanometer that rotates the "driven" refractor until the differential photocell output returns to zero. The galvanometer deflection corresponds to the rotation of the object refractor.

This technique is capable of fast response (>10 Hz) and can measure relatively large angles (>±30°) without contact. The system is relatively insensitive to extraneous light (insensitivity can be further enhanced by use of a modulated beam), and the accuracy and linearity limitations of previous methods are virtually eliminated. The distinction of this method is its combination of optical and electromechanical components into a feedback system in which measurement error is made to approach zero. Application is foreseen in the measurement of torsional strain.

This work was done by Emmett L. Bryant of **Langley Research Center.** *No further documentation is available.*

Inquiries concerning rights for the commercial use of this invention should be addressed to the Patent Counsel, Langley Research Center [see page A8]. Refer to LAR-12178.

Calibrated Method for an Ultrasonic Gray-Scale Recorder

A calibrated method for ultrasonic C-scanning is based on direct correlation of gray-scale response to the electronic signal used. In the new procedure, the optical density of a reference recording is measured to generate a curve of reflective intensity versus transmission.
(See page 20.)

Modified Chemiluminescent NO Analyzer Accurately Measures NO_X

Chemiluminescent analysis of nitrogen oxides in gas samples containing carbon monoxide has been inaccurate. Based on new test findings, a chemiluminescent analyzer with a molybdenum NO-to-NO_X converter and an air purge can accurately measure NO and NO_X in sample gases containing up to 30 percent CO.
(See page 54.)

Low-Intensity X-Ray and Gamma-Ray Imaging Device

A new low-intensity X-ray image scope (Lixiscope), developed for X-ray astronomy applications, makes fluoroscopy and radiography at low dosages possible. The X-ray or gamma-ray shadow image of an object is converted to a visible-light image that is intensified and amplified for direct viewing or recording.
(See page 67.)

Low-Cost Ultrasonic Lamb-Wave Transducer

Cast-and-bond method is used to fabricate inexpensive Lamb-wave transducers in many sizes and shapes.

Lyndon B. Johnson Space Center, Houston, Texas

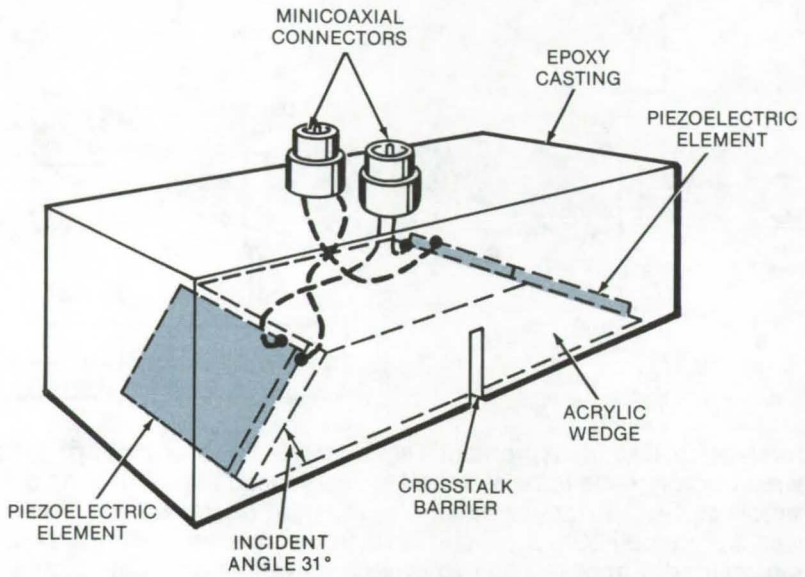

A Contact Ultrasonic Transducer propagates a Lamb wave through thin aluminum sheet material. This model includes two elements that measure the effects of damping and loading which, in turn, are indirectly equated to bond integrity. The transducer has been used to evaluate the bond integrity of an aluminum facing 0.010 inch (0.254 mm) thick, adhesively bonded to an aluminum facing 0.016 inch (0.406 mm) thick.

Lamb-wave transducers are used in evaluating the bond integrity of thin materials. Compared to conventional ultrasonic transducers, they produce greater changes in signal amplitude and phase response. To date, however, Lamb-wave transducers have been fabricated by extensive machining of housings and brackets, a costly procedure. This expense can be avoided by using cast-and-bond construction that results in a more reliable and less expensive transducer.

Cast housing and fixed-element angle bonding in the new transducer, as illustrated, produce a better piezotransfer function that, in turn, gives a better signal-to-noise ratio. Such transducers may be fabricated in many sizes and shapes. Because of this versatility, it is now possible to inspect many objects of different configurations that could not be reached with earlier transducers.

This work was done by Calvin C. Kammerer of Rockwell International Corp. for **Johnson Space Center.** *No further documentation is available.*
MSC-16333

Quick-and-Easy Shear-Load Testing

Simple device for applying shear loads can be rapidly assembled and disassembled, without damaging the test specimen.

Lyndon B. Johnson Space Center, Houston, Texas

A device for applying shear loads to test specimens can be attached and removed without damaging the specimen surface. The device consists of two mating Velcro strips, one of which adheres to the specimen surface and the other to a shear-load strap (see figure). A vacuum bag covers the device to increase the shear-load carrying ability of the Velcro.

Previously, it was necessary to bond rubberized metal straps to the surface to be loaded in shear. The procedure was time consuming and messy, and the specimen often was damaged when the bonded straps were removed. The new device was developed to apply drag loads to the Space Shuttle Orbiter nose gear doors. Because it is quick, clean, and inexpensive, the new method is expected to be useful in commercial testing laboratories for applying shear loads to smooth surfaces on which there is no provision for conventional attachments and which could be easily damaged.

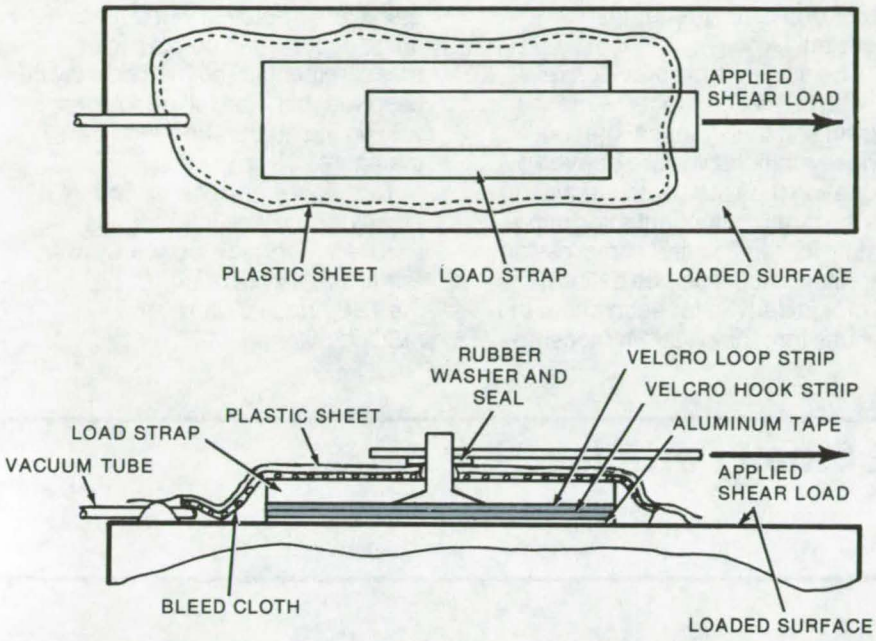

Shear Loads are applied to a test specimen via Velcro strips, which can be easily separated and removed when testing is over.

To make a shear-load test, the user cleans the surface to be loaded and applies a strip of adhesive aluminum tape. The user attaches a Velcro strip (the hook side) with pressure-sensitive adhesive, attaches another Velcro strip (the loop side) to a load strap with a similar adhesive, and mates the Velcro strips. Next, a plastic sheet is placed over the assembly and is sealed to the surface with chromate paste. A 1/4-inch (0.63 cm) plastic tube is inserted under the sheet and is connected to a vacuum source. The vacuum is at least 10 to 12 psi (0.069 to 0.083 N/m^2) below atmospheric pressure. The maximum recommended working load is the pressure differential on the vacuum bag multiplied by the Velcro surface area.

To disassemble and remove the device, the user removes the shear load, takes off the plastic sheet (the zinc chromate merely provides a pressure seal, not an adhesive bond), unzippers the Velcro strips, and peels away the aluminum tape from the specimen surface.

This work was done by John A. Gustafson and James K. Neary of Rockwell International Corp. for **Johnson Space Center.** *No further documentation is available.*
MSC-16765

Improved Strain-Gage Calibration

Accuracy of tension strain measurements above 1 percent is considerably improved.

Lyndon B. Johnson Space Center, Houston, Texas

A new method for calibrating strain gages improves the accuracy of tension strain measurements. Strains in the range of 1 to 10 percent are often encountered in modern structural practice; however, current techniques for calibrating bridge-type gages result in tension strain values significantly lower than the actual strains.

In the calibration of a quarter bridge (see figure), insertion of the calibration shunt results (with $\Delta R = 0$) in an output voltage (E) that is always positive. When the bridge is in use (calibration switch open), the variation in sensor resistance (ΔR) will be positive or negative since the actual strain can be either a tension or compression. Moreover, for a

(continued next page)

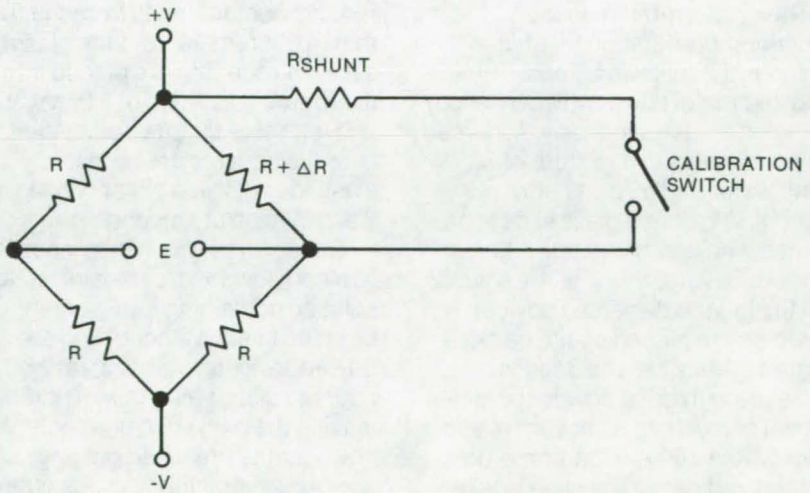

The **Accuracy of This Quarter-Bridge Strain Gage** is improved by accounting for the nonlinearity of the bridge output for equivalent compression and tension strains (in which ΔR, the resistance of the strain sensor, has the same magnitude but opposite signs).

given ΔR the magnitude of the output voltage will be different depending on whether ΔR is positive or negative. Current techniques for gage calibration do not take this into account and have generally used the compression strain-calibrating factor when measuring either compressions or tension strains. For small strains the error is small, but this can lead to a serious error for tension strains greater than 1 percent.

The new method provides relationships that connect the measured strain and the shunt calibration. These relationships are derived by equating the shunt output equation to the strain output equation separately for tension and compression strains. Since a unique calibration factor is derived for each case, the results for tension strain measurements are improved without sacrificing accuracy in compression measurements. The method may be used with half and full bridges as well as the quarter bridge shown in the figure.

This work was done by Robert W. Troke of Rockwell International Corp. for **Johnson Space Center.** *For further information, Circle 46 on the TSP Request Card.*
MSC-16852

Surface Examination of Small Particles

Specimen-preparation technique for electron microscopy

Lewis Research Center, Cleveland, Ohio

The surfaces of freshly-produced small (micron size) particles are very reactive, usually resulting in the formation of various coatings due to the reaction of atmospheric gases on these particle surfaces. The coating on a metal powder, for example a layer formed by reaction with an oxidizing environment, may be examined in minute morphological and crystallographic detail by first coating the oxidized powder with vacuum evaporated carbon, dissolving the metal in a suitable solvent, and then examining the residue by electron microscopy with both transmission and electron diffraction modes.

The electron-microscopy specimen-preparation technique includes the following steps. The oxidized metal powder (NiCrAl alloy) particles are ultrasonically dispersed for ten minutes in a mixture of 50 parts water and 50 parts ethyl alcohol. A cleaned glass slide is precoated with approximately 100 Å of carbon. Several drops of the solution containing the dispersed powder particles are placed on the carbon-coated glass slide and dried in air. The slide with dried powder particles is then placed into a vacuum evaporator where 100 Å of carbon is deposited vertically. The slide is taken out and floated on the carbon side with 0.25 percent of Mowital resin (or equivalent) in chloroform and air dried in a tilted position to remove the excess solution. A low-melting [318 K (113° F)] wax is heated and applied on top of the Mowital film and left to solidify at a thickness of no more than 0.004 in. (0.1 mm).

The carbon/Mowital/wax film is then scored into 1/8-in. (3-mm) squares and held over an HF solution, in order to loosen the carbon film from the glass slide. The HF vapor loosens the film within ten seconds, and the slide is immersed in water to float off the carbon/Mowital/wax film squares. To remove contaminants from the film that might remain from the glass slide, the squares are placed into a five-percent solution of HF in water and left there for one hour. After this, the squares are repeatedly washed in distilled water with a final wash in absolute alcohol.

The squares with the composite film and powder are transferred to a solution containing four-percent bromine in ethyl alcohol and are covered and left standing for 16 hours to dissolve the metal particles, leaving the oxide film unaffected. The squares are taken out and washed several times in absolute alcohol, placed on electron microscope grids, and left floating on almost-boiling water for about 30 minutes to remove the wax. The carbon/Mowital film, now securely attached to the microscope grid, is placed on several layers of filter paper and saturated with chloroform to dissolve away the Mowital. After about 30 minutes, the grid with the carbon film is dried and is ready to be examined by transmission electron microscopy.

This surface preparation and examination technique for small particles can be used to study catalysts (determination of the cause of "poisoning"), to study the nucleation and growth of metal oxides, and to determine the chemical nature of lubricated surfaces after wear has occurred.

This work was done by Bruno C. Buzek and Thomas K. Glasgow of **Lewis Research Center.** *Further information may be found in NASA TM-X-71749 [N75-30262], "A Study of the Oxide Dispersion and Recrystallization in NiCrAl Prepared from Preoxidized Powder," a copy of which may be obtained at cost from the New England Research Application Center* *[see page A7].*
LEW-12842

Thermocouples Measure Very-Hot Gas Temperatures

Heating rate of cooled thermocouple is extrapolated to determine temperatures above thermocouple melting point.

Lewis Research Center, Cleveland, Ohio

In using thermocouples to measure the temperature of a high-temperature gas, the limit of measurement is primarily determined by the melting point of the thermocouple material. Secondary limits are also imposed by oxidation or chemical attack by constituents in the gas that destroy the material or effect a change in thermocouple calibration. Recently, it has been demonstrated that a pulsed thermocouple system can compute gas temperatures above the melting point of the thermocouple material by short term exposure of the thermocouple to a heating cycle.

A thermocouple probe has been designed that incorporates a small jet of inert gas to cool the thermocouple well below the temperature of both the gas it has been immersed in and the melting point of the thermocouple material itself. During this time, the thermocouple is protected from the oxidation and chemical attack that would have taken place if it were allowed to remain at the higher temperatures normally imposed by the gas stream.

When a measurement of gas temperature is to be made, the cooling jet is turned off momentarily, allowing the thermocouple to heat up to near its melting point, at which time the cooling is reapplied. The heating curve (temperature change with time) is recorded by a high speed digital system. The final temperature that the thermocouple would have attained, if it were capable of surviving at the high gas temperature, is then calculated by extrapolating an exponential curve fit to the recorded data, by use of a modern high-speed computing system.

This system has been developed and evaluated in a laboratory burner apparatus, and has been applied to research combustor testing. In the research combustor application, the jet coolant solenoid valve cycling operation and thermocouple output were controlled by the test facility minicomputer, which was connected to a high-speed data-acquisition system. The FORTRAN computer program used is presented in the reference listed below. Data must be obtained for about 60 percent of the total heating step (leaving 40 percent for computing) in order to obtain adequate accuracy (error less than 3 percent). An added benefit in the research combustor application was that the cooling jet protected the thermocouple from melting during inadvertent temperature excursions occurring during startup and shutdown.

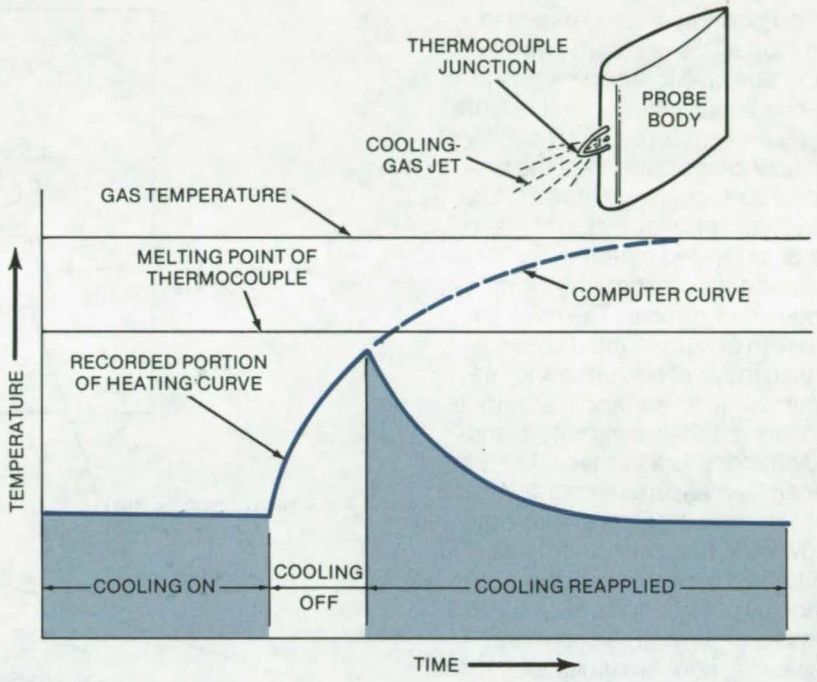

Extrapolated High Temperature Measurements in a hot gas are made with a cooled thermocouple. A cooling gas, which keeps the thermocouple temperature below its melting point, is turned off and the thermocouple heating rate is recorded. This information is then used to compute the temperature of the hot gas.

This work was done by George E. Glawe, Lloyd N. Krause, and Herbert A. Will of **Lewis Research Center.** *Further information may be found in NASA TM-X. 71883 [N76-18408], "A New Approach to the Pulsed Thermocouple for High Gas Temperature Measurements," a copy of which may be obtained at cost from the New England Research Application Center [see page A7].*

LEW-12843

Infrared Scanners for Temperature Measurement in Wind Tunnels

Computer data reduction allows use of high-rate remote IR scanners.

Langley Research Center, Hampton, Virginia

Temperature measurement in wind tunnels is one of the most important physical parameters in aerodynamic testing. Temperature measurement is required not only of the flow gases but also of the test model surface, since temperature may affect strength, stability, and life of the tested material. Surface temperature sensors may be either mounted or remote. The main limitation with either mounted sensors (which may not be suitable for attachment to all surfaces) or remote sensors (such as pyrometers and radiometers) is that these devices generally measure temperatures at predetermined points and do not allow wide-field measurements. Wide-field measurements may be made by using a number of surface sensors or several radiometers. However, there are limitations to the number of surface sensors that can be used before the surface is affected by the measurement, and the use of many radiometers is costly and takes up space.

Therefore, a remote technique for wide-field measurements with good spatial resolution, good thermal response, and high-frequency response is essential when the researcher cannot determine the best place to mount surface sensors or cannot mount them at all. The infrared scanners, such as that outlined in Figure 1, are now available on the market and can fill this need. Figure 2 illustrates the entire recording and data-reduction format of the IR scanner.

In application, the energy from the test surface captured by the scanner is attenuated by a selectable optical stop, a filter, and an optical window in the path of the beam. The data stored on the FM tape are digitized and fed into the computer for processing. Since the voltage output from a radiometer may not always be a linear function of the radiance of the surface, the instrument calibration is transformed to relate output voltage to surface radiated energy. In addition, corrections must be made for the window and the filter. The radiated energy is then calculated and corrected for the emittance of the surface.

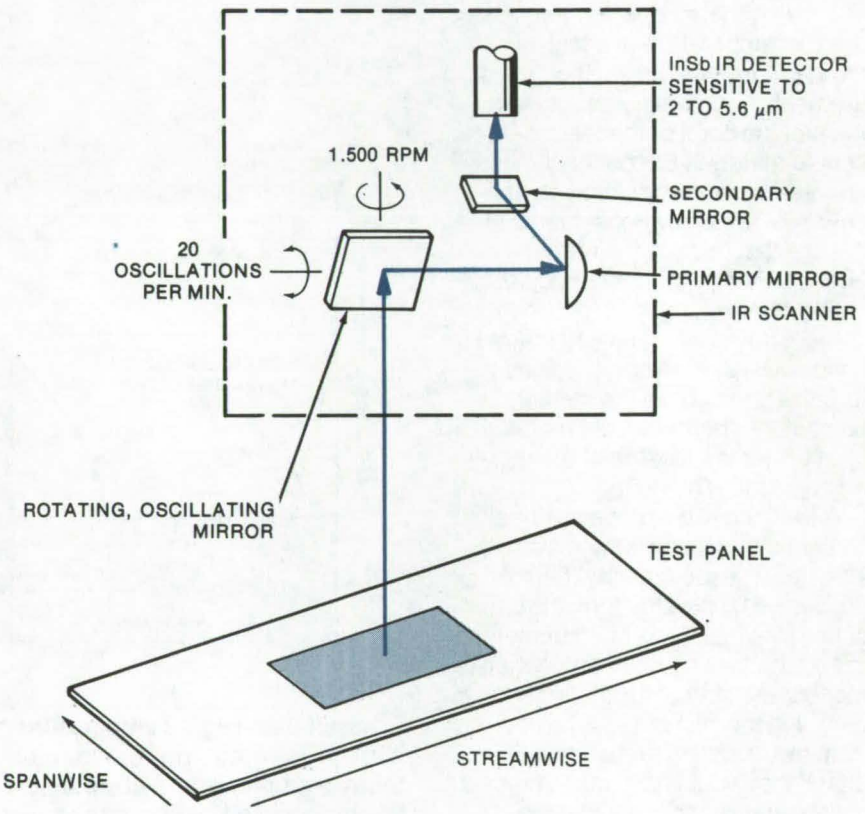

Figure 1. An IR Scanner Optical Head is used at Langley Research Center to measure surface temperatures of test models. Energy is radiated from the test panel to a rotating, oscillating mirror that undergoes a two-dimensional sweep across the test surface. A primary spherical mirror reflects it to a secondary flat mirror and thence to the detector. A varying dc voltage is generated by the vertical motion of the mirror, and a pulse voltage is generated by its horizontal motion. These voltages are monitored to determine location of the scan. a 20° by 20° field is swept every 5 seconds, generating 150 sweep lines per frame. Traverse time of each sweep line across the 20° field of view is approximately 2 milliseconds.

Spectral emittance, which is required for accurate temperature measurements, is determined by a self-emission comparison method as a function of both temperature and wavelength.

The volume of data generated by these systems makes standard plots of temperature vs. time vs. position impractical. A multiscan plot relating deflection height to temperature can be used, or data can be plotted in three dimensions as temperature vs. streamwise vs. spanwise directions or as isotherms as functions of these directions. Figure 3 shows the

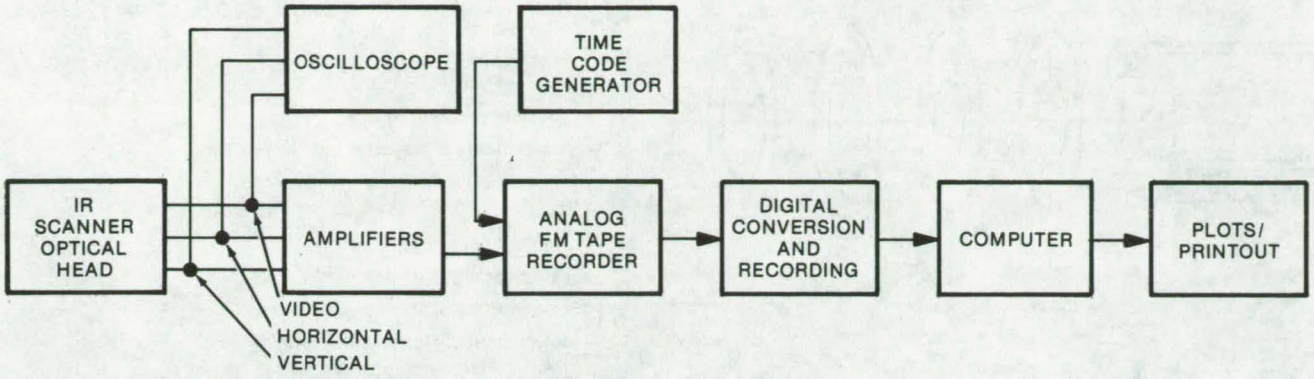

Figure 2. The **IR Scanner Data Production and Reduction** begins with three signals: the horizontal pulse, vertical position voltage, and detector output (video) with a time-code pulse. These are recorded simultaneously on four channels of an instrument-quality, 80-kHz band-pass, FM tape-recording system. Data are also sent to an oscilloscope display for parallel monitoring. Data recorded can be viewed on the display and ultimately digitized, computer processed, and printed out in final form.

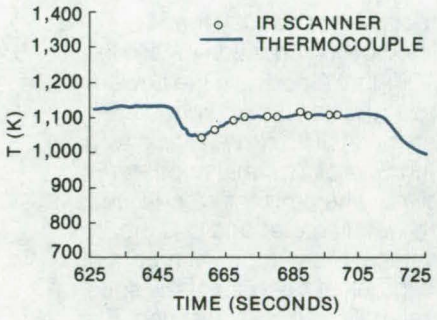

Figure 3. **Thermocouple and IR Scanner Data** are compared for a test panel in a wind tunnel.

correlation between data obtained with this technique and with surface-mounted thermocouples.

The IR scanner has proved to be a valuable temperature-measuring tool in aerodynamic testing of large panels, since large surfaces can be scanned without disturbing the model and without extensive sensor installation as would otherwise be required. Computer techniques have eliminated the greatest difficulty encountered with the use of IR scanners, that being the large quantity of data generated for processing. Data are accurate to within better than ±5 percent.

Langley researchers are employing IR scanners not only for surface temperature measurements in wind tunnels but also for such uses as tracking and diffusion studies of rocket exhausts, nondestructive testing of rocket motor nozzles and composite materials, and for the detection of nonuniformity in home insulation.

This work was done by Andronicos G. Kantsios of **Langley Research Center.** *For further information, Circle 47 on the TSP Request Card.*
LAR-12171

Noise Calculation on the Basis of Vortex Flow Models

New treatment of a well established phenomenon results in computational simplification.

Langley Research Center, Hampton, Virginia

Many theories of the origin of aerodynamic noise have been advanced. In these theories, which have been shown to be fundamentally equivalent, an expression for the far-field sound radiation from a body of flow is generally given in terms of an integral of a source distribution over the volume of flow, as well as a surface integral of the flow-induced pressures over any surfaces which may be present. The source distribution is further expressed in terms of temporal fluctuations of various flow parameters. Thus, the crux of the aeroacoustic analysis problem is the determination of the dynamic behavior of the flow.

Previously, mathematical treatment, for even limited regions of three-dimensional time-dependent flow, has been extremely difficult and complex. A new flow-modeling technique yields a relatively simple method for calculating sound radiation involving planar, cylindrical, or spherical surfaces. The flow model employs potential flow theory with the action of viscosity on the flow-field described in terms of point vortices. The presence of surfaces in the flow is analyzed by way of the classical method of images, and the sound is calculated through a reformulation of previous theory for sound generation in the presence of stationary and rigid surfaces.

This new technique simplifies calculation of noise for vortices in

(continued next page)

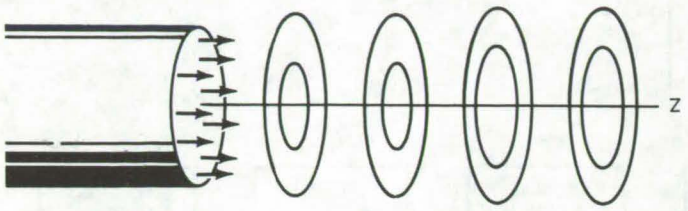

$$\varrho_a(\vec{x},t) \cong -\frac{\varrho_o}{4\pi a_o^4}\frac{x_i x_j}{x^3}\left(\frac{d^2}{dt^2}\int_V y_i L_j \vec{dy}\right)^* + \frac{1}{4\pi a_o^4}\frac{1}{x}\left(\frac{d^2 e}{dt^2}\right)^*$$

Where

ϱ_a = acoustic density

ϱ_o = ambient density

$\vec{x}$ = observer position vector

x_i = components of observer position vector

$x = |\vec{x}|$

t = time

a_o = ambient speed of sound

$\vec{y}$ = source position vector

y_i = components of source position vector

L_j = component of Coriolis acceleration

V = volume

e = total solenoidal kinetic energy

and the asterisk (*) indicates evaluation at the retarded time $t - x/a_o$.

Figure 1. The **Jet Model** above is used to calculate the far-field sound radiated by the large-scale structure of a circular jet.

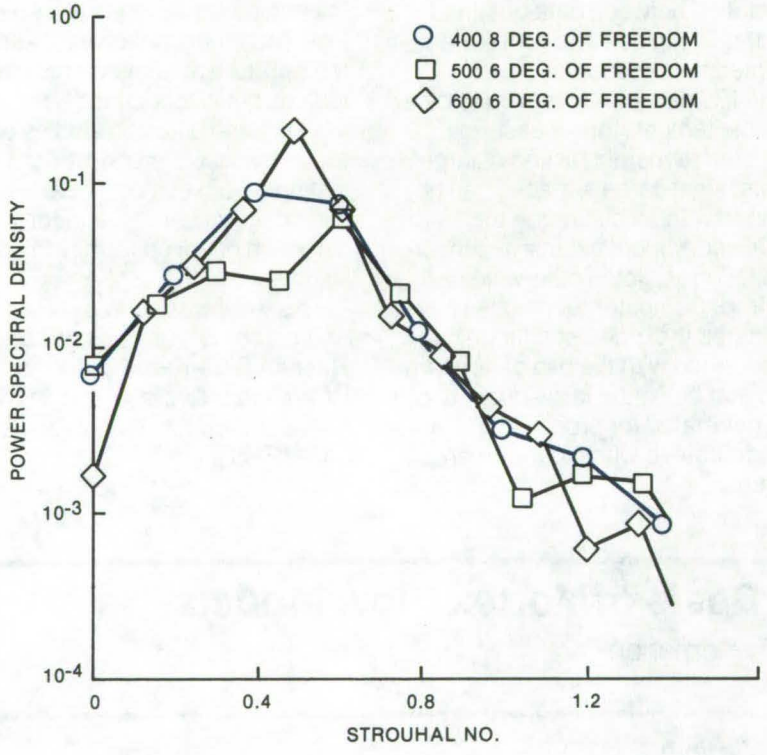

Figure 2. The **Noise Spectrum** is shown as predicted for sound radiated 90° to the jet axis.

free space and in the presence of surfaces. For example, the technique can predict the sound radiated by the large-scale structure of a circular jet. The jet structure was modeled as a train of toroidal rings as shown in Figure 1. The rings are shed at equal time intervals from the jet exit and propagate downstream under the influence of their own self-induced convection velocity, the velocity induced by the other vortices present, and the source velocity of the jet. The model is started from rest and allowed to reach a steady-state condition. The far-field radiated sound may then be calculated by the equation in Figure 1.

Figure 2 portrays the power-spectral density of the radiated sound at 90° to the jet axis as a function of Strouhal number (St = fD/U where f is the frequency, D is the jet diameter and U is the jet velocity) for various numbers of degrees of freedom of the spectral estimate and vortices shed. The spectrum is continuous even though the vortex shedding rate is periodic and peaks at the Strouhal number observed experimentally.

The methodology of the current mathematical treatment is applicable to a wide variety of flow regions and geometries. The reflection principle is extended to the whole class of potential flows that may be solved through the method of images. This allows the sound radiation to be computed solely through a volume integral over the exterior and interior of any surfaces which may be present. The source distribution is then rewritten in terms of the vorticity within the flow: a computationally efficient formulation of the aeroacoustic theory.

This work was done by Jay C. Hardin of **Langley Research Center.** *For further information, Circle 48 on the TSP Request Card.*
LAR-12271

Thermal-Control Canister

Fixed- and variable-conductance heat pipes accurately control the temperature of an instrument package.

Goddard Space Flight Center, Greenbelt, Maryland

A canister that uses heat pipes to control its temperature is an ideal container for heat-dissipating equipment in extreme thermal environments. By using a variable-conductance heat-pipe link together with a fixed-conductance system, the canister temperature can be varied over a wide range yet held stable to ±1° C. The system is superior to heaters and thermostats, fluid transfer loops, and other thermal control methods since it has fewer parts and requires considerably less power. One model, designed for installation in the Space Shuttle Orbiter, can handle up to 300 watts of heat generated within the canister. Its temperature can be set to any value between zero and 30° C. In this application, the external conditions vary from direct exposure to the Sun, to the darkness of outer space, to temperatures of up to 100° C developed in the payload bay during reentry.

As shown in the figure, an assembly of conventional heat pipes absorbs the heat generated by the instruments within the container and transfers it to a variable-conductance heat pipe. The variable-conductance pipe is in thermal contact with a heat-pipe array on an aluminum radiator above the canister. The canister, which is made out of a good thermal conductor, such as aluminum, is surrounded by a thermally insulating blanket.

In addition to the usual components present in a conventional heat pipe, the variable-conductance heat pipe has a noncondensable, low thermal-conductivity gas contained in a reservoir that is attached to the condenser end of the pipe. When this gas is heated, it expands to occupy a larger volume. This decreases the effective area of the condenser and the number of active radiator heat pipes. If the gas is cooled, it decreases in volume and increases the effective area of the condenser.

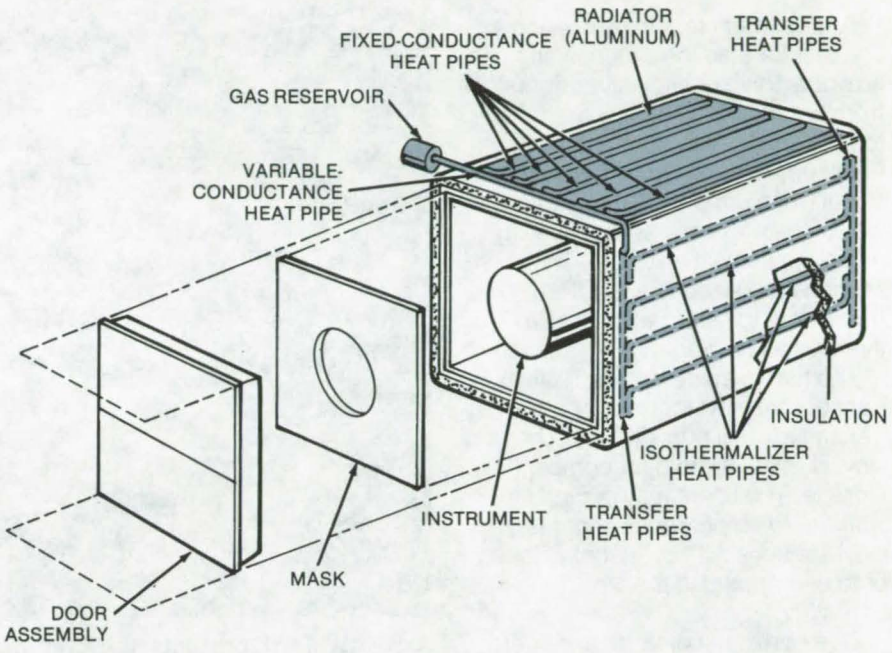

Fixed- and Variable-Conductance Heat Pipes stabilize the temperature of this instrument canister. Temperature control is provided by regulating power to a heater in the gas reservoir of the variable-conductance heat pipe. The cover is fitted with a thermally insulating mask to reduce heat loss through the end of the package.

The conductance is controlled by a temperature sensor, such as a thermistor, located on the instrument or on the canister wall. A signal from the sensor is coupled to a control circuit, along with a preset reference signal. The controller generates an error signal that adjusts power to a heater in the reservoir of the variable-conductance heat pipe. An increase in canister temperature will decrease the power to the heater; this increases the conductance of the system and allows its temperature to drop. If the temperature decreases more heater power is applied and the conductance is lowered.

Various modifications of the basic design are possible. For example, a programable controller can be added to change the temperature-set point, or the canister can be partitioned, with separate controllers for each section. The system operates best, with the widest range of set points, if the reservoir is isolated from direct heat exchange with its environment. It can be shielded with radiation reflectors, reflecting paint, or an insulating blanket.

This work was done by Stanford Ollendorf of **Goddard Space Flight Center.** For further information, *Circle 49 on the* TSP Request Card.

This invention is owned by NASA, and a patent application has been filed. Inquiries concerning nonexclusive or exclusive license for its commercial development should be addressed to the Patent Counsel, Goddard Space Flight Center [see page A8]. Refer to GSC-12253.

Cryostat Safety Tent

Transparent tent encloses a cryostat for maximum safety.

Goddard Space Flight Center, Greenbelt, Maryland

A new safety tent for enclosing a cryostat located inside a building prevents toxic or explosive vapors from entering the building area. The tent as shown is supported by sectional framework, using lightweight metal (for example, aluminum), and is designed for easy assembly with minimum use of handtools. The sections are sized to allow the framework to be stored as a relatively small package.

The tent is made from a clear transparent vinyl for maximum transmission of outside light. The vinyl is relatively thin for compact storage. The users may decide whether to employ snap-together vinyl sections with overlapping joints or to use zippers in the tent assembly.

One horizontal or vertical zipper opening is used at the tent entrance. The height of the zipper opening is 72±1 in. (183±2.5 cm) and is reinforced to prevent tearing. A metal rust-free 12-in. (30-cm) collar adapter is mounted on the side of the tent. This collar is attached to a round flexible hose connected to the explosionproof airblower.

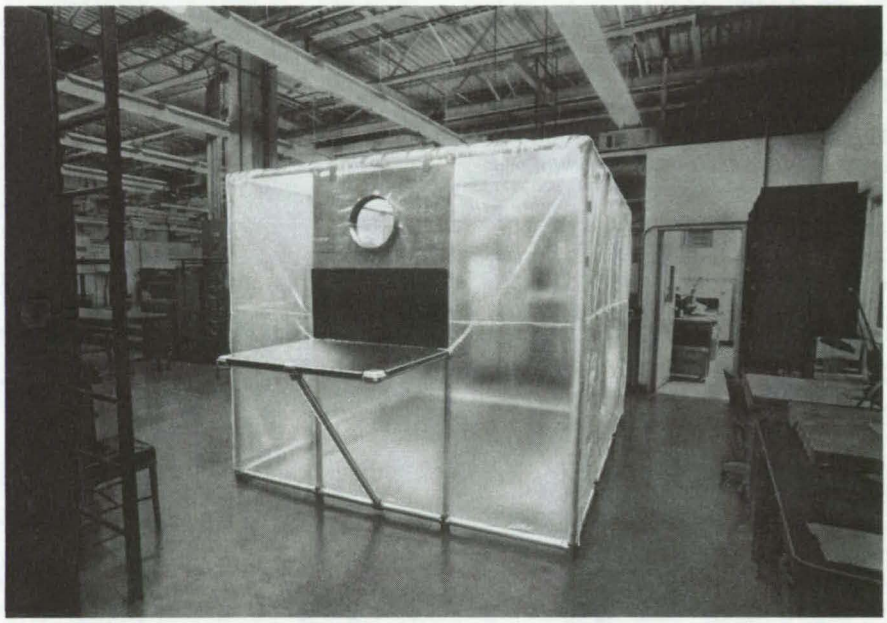

A Safety Tent protects the cryostat. The frame posts are mounted on casters for easy moving of the tent from one area to another. The tent bottom is 3 in. (7.5 cm) off the ground.

This work was done by John L. Millman of **Goddard Space Flight Center.** *For further information, Circle 50 on the TSP Request Card.*
GSC-12206

Film Adhesive Enhances Neutron Radiographic Images

Modified adhesive helps test adhesive bonds more reliably.

Lyndon B. Johnson Space Center, Houston, Texas

Adhesive bonds are often inspected nondestructively by neutron radiography. In contrast to X-ray analysis, in which only metal components are imaged, neutron radiography yields information about the adhesive and other nonmetals in a bonded structure.

The resolution of neutron radiographic images of thermally conductive film can be increased by replacing approximately 5 percent of the aluminum powder normally used to provide thermal conductivity by gadolinium oxide. Neutron radiographs of test structures in which the gadolinium oxide had been added had significantly better resolution than those obtained on conventionally mixed samples. Problems such as poor distribution, omission, filleting, overlay inclusions, and discontinuities in the adhesive were easily discerned. Thermal and structural properties were equivalent to those made by using the unmodified adhesive. The oxide also has the advantage of being chemically stable.

This work was done by Madison W. Reed of Vought Corp. for **Johnson Space Center.** *No further documentation is available.*
MSC-18061

Thermal Compensator for Helium Refrigerators

Feedback circuit reduces temperature fluctuations at the cold tip of a closed-cycle helium refrigerator.

Goddard Space Flight Center, Greenbelt, Maryland

High-resolution infrared spectroscopy requires a source with a very stable output frequency. Semiconductor diode lasers have been used as high-resolution infrared sources; however, since the output frequency of these devices is extremely sensitive to thermal fluctuations, they must be used with some type of temperature-stabilizing system.

One method that has frequently been used is to mount the diode on the cold tip of a closed-cycle helium refrigerator. However, these refrigerators have a small inherent temperature oscillation that is troublesome in applications that demand high stability. The usual method of control is to attenuate the oscillations by inserting insulating materials between the cold tip of the refrigerator and the load.

A new system that requires only a few components substantially reduces the amplitude of these fluctuations. As shown schematically in the figure, a temperature-sensing diode and a heating diode are mounted on a heat sink that provides a good conductive path between the load (shown as a laser diode) and the cold tip of the refrigerator. The sink has a small volume and low thermal capacitance so that the sensor is at substantially the same temperature as the heater and virtually no thermal phase lag exists between them. The sensor generates negative-feedback control signals that drive the heating diode to maintain temperature stability. With this arrangement, temperature excursions of the cold tip have been reduced to within 1.6×10^{-4} K.

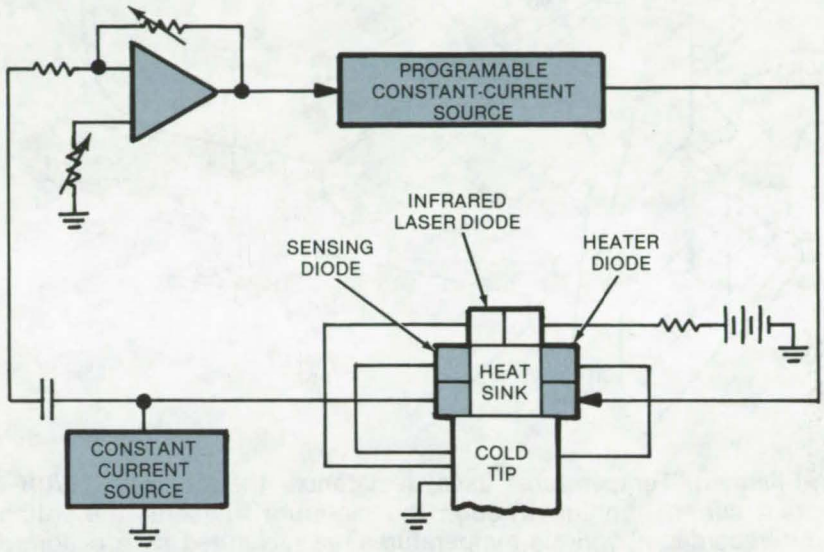

A Negative-Feedback System controls the temperature at the cold tip of a closed-cycle helium refrigerator. The refrigerator has an inherent temperature oscillation at about 3 Hz that is converted to voltage changes across the sensing diode. These are used to regulate the current that drives the heater diode and stabilizes the temperature.

The method is applicable to other temperature-control applications, especially in crowded systems. Examples are laser equipment, electronic instruments, and computer systems.

This work was done by John J. Hillman and Donald E. Jennings of **Goddard Space Flight Center.** *For further information, Circle 51 on the TSP Request Card.*

This invention is owned by NASA, and a patent application has been filed. Inquiries concerning nonexclusive or exclusive license for its commercial development should be addressed to the Patent Counsel, Goddard Space Flight Center [see page A8]. Refer to GSC-12168.

Calibration Target for Temperature Radiometer

Convenient technique for measuring temperature/voltage drop characteristics of a very thin filament.

Langley Research Center, Hampton, Virginia

A technique has been developed for measuring the temperature of extremely thin filaments heated to between 600 and 1,400 K. In this specific case, it was desired to measure the temperature of a 0.001-in. (0.0254-mm) platinum filament that was to be used as a calibration target for a noncontact temperature-measuring radiometer. The radiometer had been modified

(continued next page)

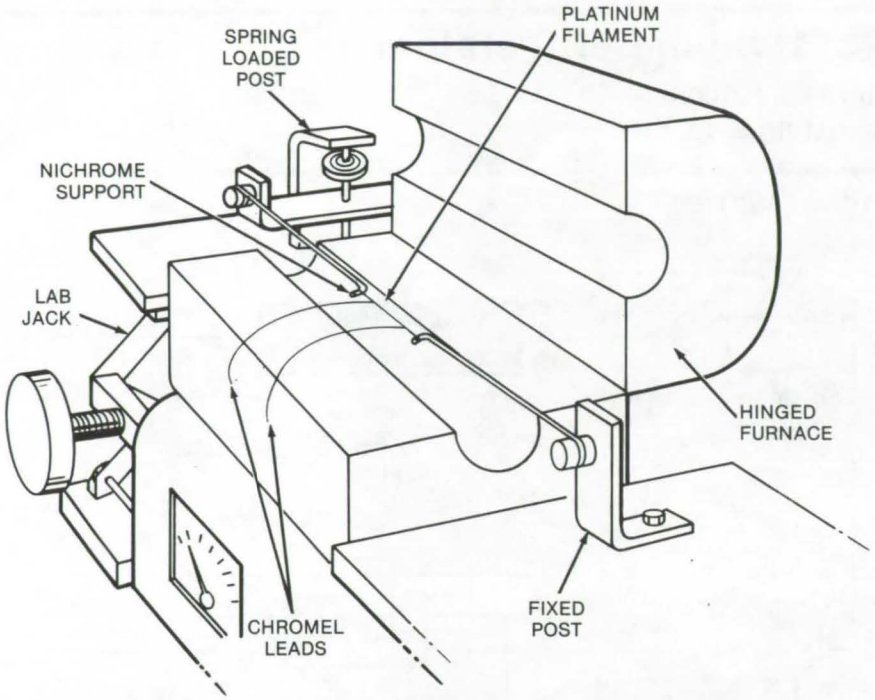

Thin-Filament Temperature uses resistance thermometry. With a constant current running through the platinum filament, the voltage drop is recorded at various temperatures, as measured by a calibrated thermocouple. The now-calibrated filament is used as a calibration target for a temperature radiometer.

so that its field of view was filled by the unusually-small 0.001-in. filament.

In this technique, the platinum filament is both the temperature source and the temperature sensor. The platinum filament is welded to Nichrome support wires, as shown in the figure. One support wire is fixed, and the other is spring-loaded to keep the tension on the thermally expanding filament constant. Chromel leads are welded to the platinum filament, which then becomes the sensing element of a resistance thermometer.

The platinum thermometer is lowered into a tube furnace from which all leads are electrically insulated. A calibrated thermocouple is positioned inside the furnace near the filament. The furnace is then heated while maintaining constant current through the platinum filament. Temperatures measured by the calibrated thermocouple are related to the voltage drops in the filament measured via the Chromel leads, establishing a temperature-resistance relationship over the desired 600 to 1,400 K range.

The filament is then removed from the furnace and used as the target for the radiometer. The filament is heated through the use of known currents, and the voltage drops are measured via the Chromel leads while the output voltage of the radiometer is read. By deriving the filament temperature from the current and voltage readings, the correlation between temperature and radiometer output is determined, and calibration curves are established for the radiometer.

This work was done by S. Franklin Edwards, William F. Stewart, and David S. Vann of **Langley Research Center.** *No further documentation is available.*
LAR-12239.

Rapid Leak Detection With Liquid Crystals

Simple test procedure is inexpensive and accurate.

Lyndon B. Johnson Space Center, Houston, Texas

In a novel application of liquid crystals, small leaks in vacuum lines are detected by applying a temperature-sensitive coating, warming the suspected area, and observing a color change due to differential cooling by the leak jet. The technique is fast, accurate, and requires no complex leak-detection equipment. It works for leaks on either the inside or outside walls of vacuum-jacketed lines. All of the materials required for using the technique could easily be packaged and marketed as an inexpensive kit.

To make a leak check, an alcohol-soluble liquid-crystal coating is applied to the exterior of the vacuum line. A black water-soluble coating is applied under the liquid-crystal coating to give a uniform background for the irridescent color change. Next, the surface around the suspected leak area is warmed with a heat gun. When the heat gun is removed, localized cooling caused by a leak jet produces a color change that pinpoints the location of the leak. The leak can be in the exterior wall or at an adjacent point on the interior wall (see figure).

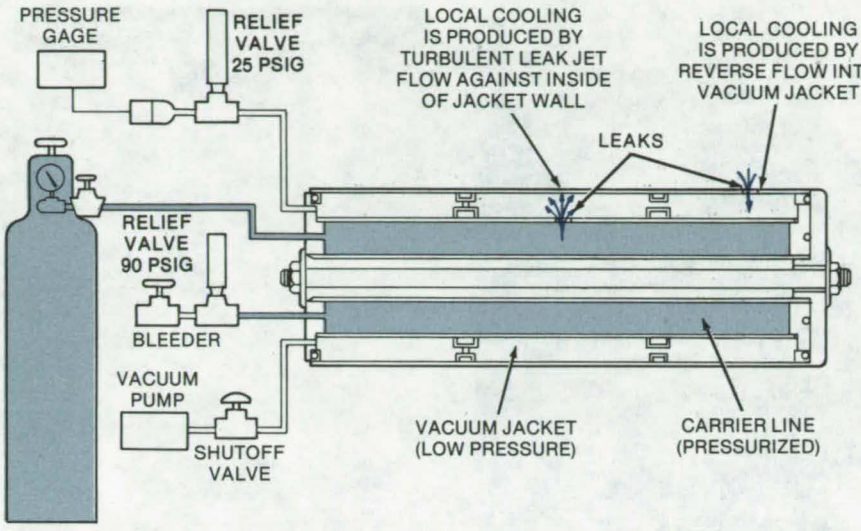

Tiny Leaks Can Be Detected by applying a liquid-crystal coating and heating the wall. Color changes indicate local cooling by the leak jet. Liquid crystals that respond at temperatures just above ambient with a sensitivity of 0.1 ° C can be used.

In a test of the technique, a 0.0015-in. (0.0038-mm) leak on the interior wall of a vacuum-jacketed fluid line produced a thermogram that located its position to within 1/4 in. (0.65 cm). A liquid crystal that changed color in the range 33° to 36° C was used for the test. The carrier line was pressurized to 50 psig (340×10^3 N/m^2), and the jacket was at approximately 15 psig (100×10^3 N/m^2).

This work was done by Robert M. Heisman, William F. Iceland, and Emil P. Ruppe of Rockwell International Corp. for **Johnson Space Center.** *No further documentation is available.*
MSC-16804

Thermal-Leak Analyzer for Vacuum-Jacketed Lines

Infrared scanner
detects small gas leaks.

Lyndon B. Johnson Space Center, Houston, Texas

A technique for detecting small leaks inside vacuum-jacketed carrier lines does not require access into the enclosed vacuum area. The method was developed for maintenance of the liquid hydrogen and liquid oxygen lines for the Space Shuttle; in this application it was not permissible to introduce helium into the lines for conventional leak testing.

A water-soluble black coating is applied to the exterior of the vacuum jacket in the area of the suspected leak (Figure 1). After the carrier line is pressurized, atmospheric pressure is introduced into the jacket to intensify any leak jet and thus to improve the sensitivity of the test. The painted area is warmed with a heat gun, and an infrared scanner is used to detect a cooled spot on the exterior of the jacket (Figures 2 and 3). This "cool spot" is caused by the impingement of the jet from a small leak in the carrier line across the

(continued next page)

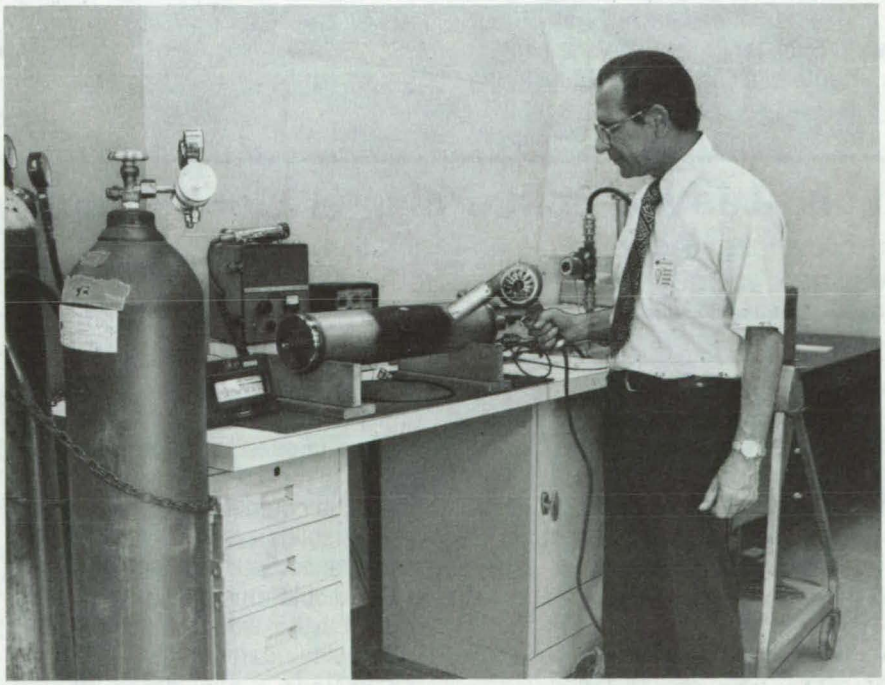

Figure 1. The **Leak Test on a Vacuum-Jacketed Line** is performed by coating the suspected area with a water-soluble black paint that gives even, infrared emission. The area is being warmed with a heat gun so that the leak jet will create a cooler spot.

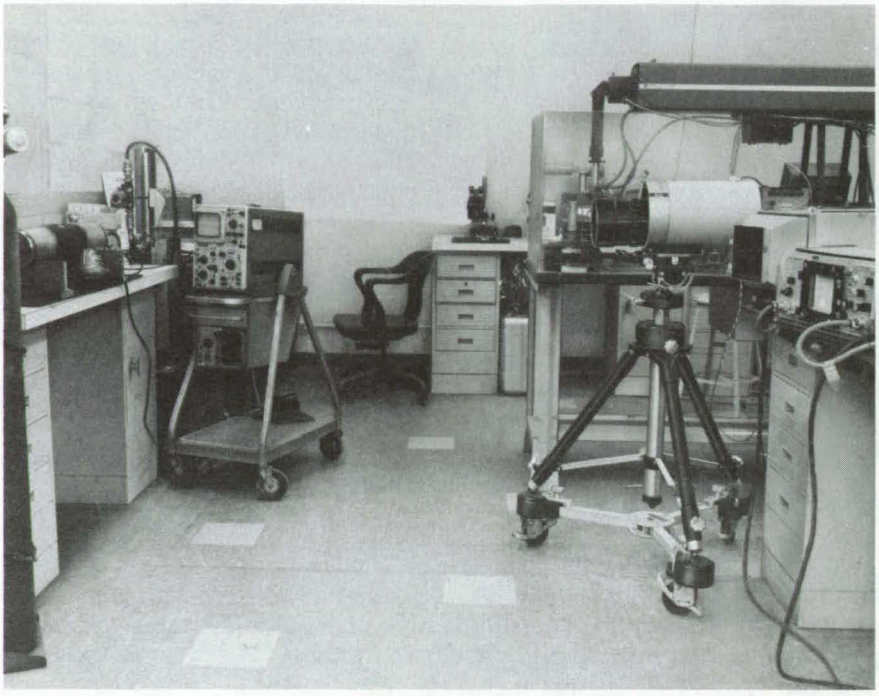

Figure 2. An **Infrared Scanner** unit with color television is shown at right aimed toward the test chamber at the left of the picture.

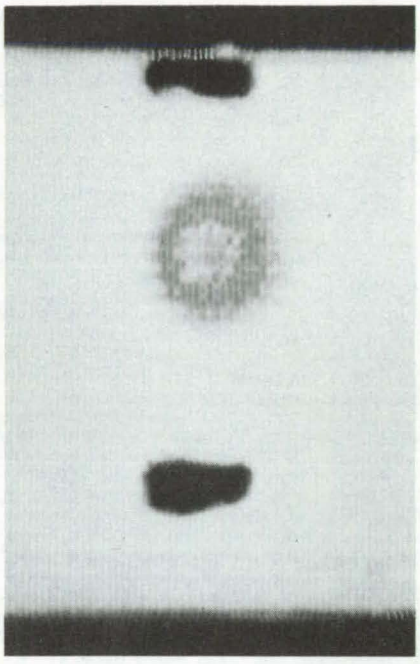

Figure 3. The **Leak Is Detected on an IR Scanner** as a color spot indicating the jet-cooled area. The actual image is in color and pinpoints the spot center more exactly than the black-and-white photo above.

jacket space or by the cooling around a leak orifice in the exterior jacket.

It may be possible to extend the sensitivity of the test to yet smaller leaks and to determine the effects of elongated orifices angled in the tube wall. Such leaks produce elliptical patterns that can be studied for analysis of leak patterns.

This work was done by Robert M. Heisman, William F. Iceland, and Emil R. Ruppe of Rockwell International Corp. for **Johnson Space Center.** *No further documentation is available.*
MSC-16802

Long-Lasting Solid-Polymer Electrolytic Hygrometer

Hollow tube made of oxidation-resistant material absorbs and quantizes moisture from air sample.

NASA's Jet Propulsion Laboratory, Pasadena, California

Many hygrometers make use of an electrolytic cell through which moist gases are drawn. The water vapor content of the gas is absorbed at the surface of a polyphosphoric acid film and is electrolyzed to gaseous hydrogen and oxygen by means of closely-spaced noble metal electrodes. However, polyphosphoric acid is a liquid that can move under high g loads and would tend to evaporate, particularly under prolonged exposure to the hard vacuum of deep space. Hygrometers using a solid to absorb water from an air sample have had limited use; all solids used so far can be oxidized, so that they decompose rather quickly and must be replaced frequently.

A new hygrometer that overcomes these problems uses an oxidation-resistant sulfonated fluorocarbon polymer (Figure 1) as a solid-state sensor. The critical element of the hygrometer (Figure 2) is a hollow tube made of the polymer placed in a chamber where the sample gas passes over the inner and outer surfaces of the tube. The tube material absorbs the moisture from the air passing across it and changes conductance. Spiral-wound platinum wire electrodes, in contact with both surfaces of the tube, are connected to a dc voltage

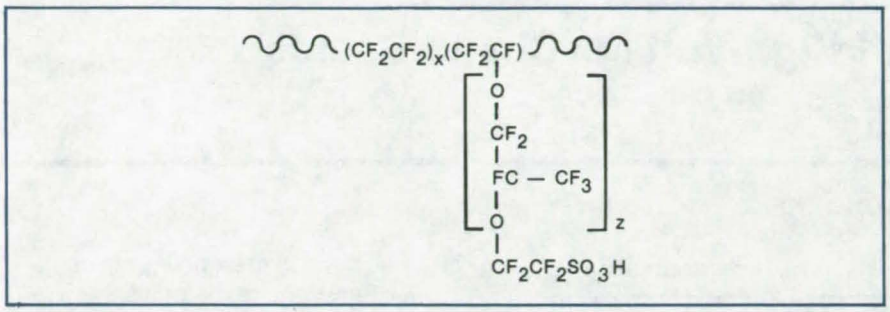

Figure 1. **Sulfonated Fluorocarbon Polymer** is chemically stable, and it can be used in electrolyzers that pass currents as high as 10 A/cm^2 at a temperature of 130° C for periods up to 5 years. The wet polymer has an electrical resistance of about 1 ohm-cm (20 percent water content). Molecular weight is about 1,000; thus vapor pressure is close to zero.

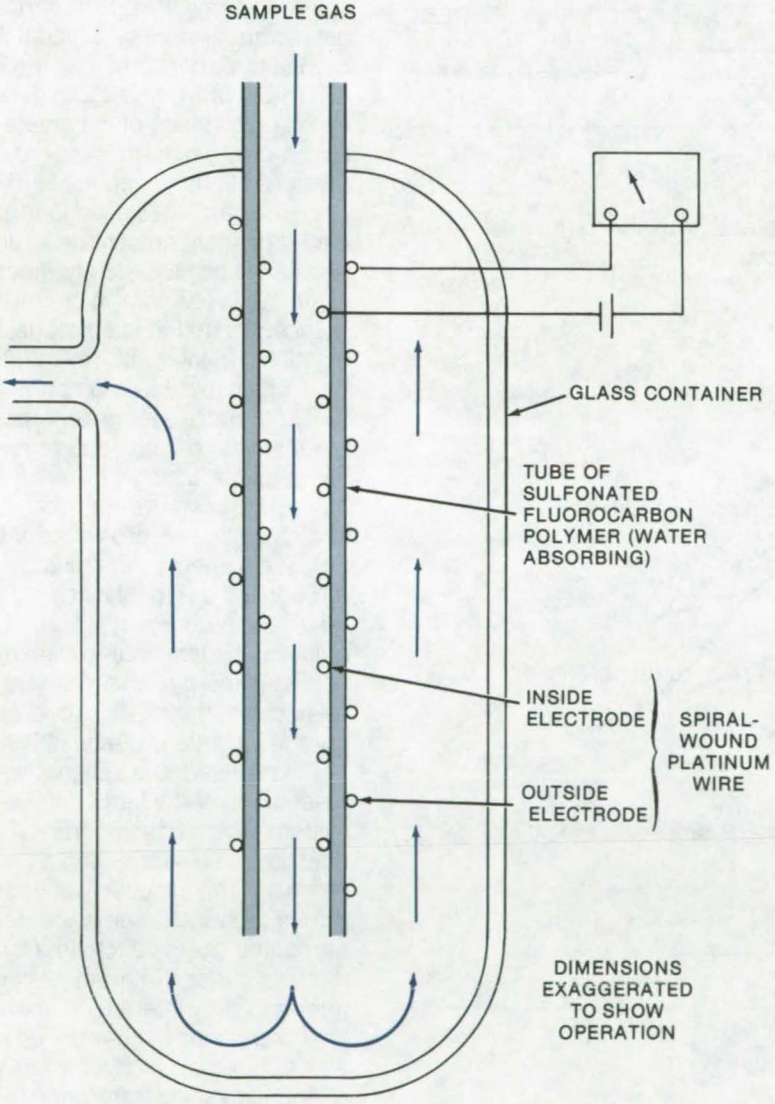

Figure 2. **Solid-State Electrolyte Hygrometer** consists of a hollow tube (made from sulfonated fluorocarbon polymer) within a chamber through which a sample gas passes. The tube absorbs moisture from the air passing across both its inner and outer surfaces, causing a change in the conductance of the polymer. This change, recorded with suitably calibrated instrumentation, is related to the change in water content in the gas sample.

and suitable calibrated instrumentation for recording the change in conductance. This change is a measure of the water content in the gas sample.

This work was done by Daniel D. Lawson of Caltech for **NASA's Jet Propulsion Laboratory.** *For further information, Circle 52 on the TSP Request Card.*

This invention is owned by NASA, and a patent application has been filed. Inquiries concerning nonexclusive or exclusive license for its commercial development should be addressed to the Patent Counsel, NASA Resident Legal Counsel-JPL [see page A8]. Refer to NPO-13948.

Ultrasonic Evaluation of High-Voltage Circuit Boards

Ultrasonic transmission indicates resistance to corona formation.

Lewis Research Center, Cleveland, Ohio

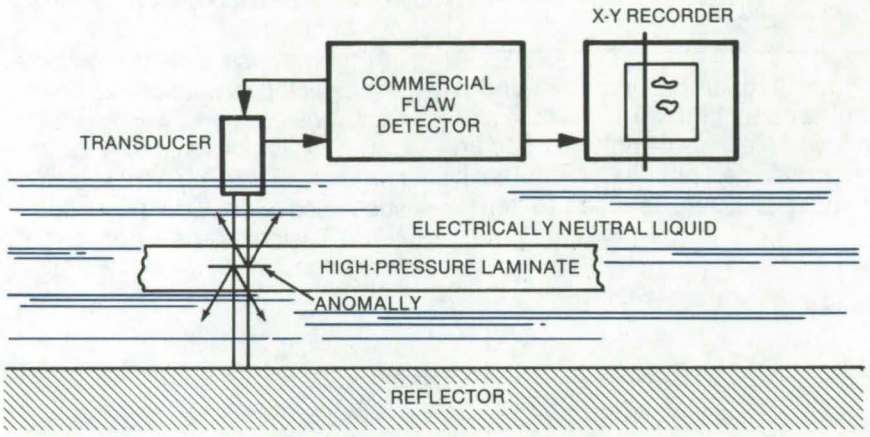

Figure 1. **Ultrasonic Scanning System** detects variations in fiber layup and internal voids in printed circuit boards.

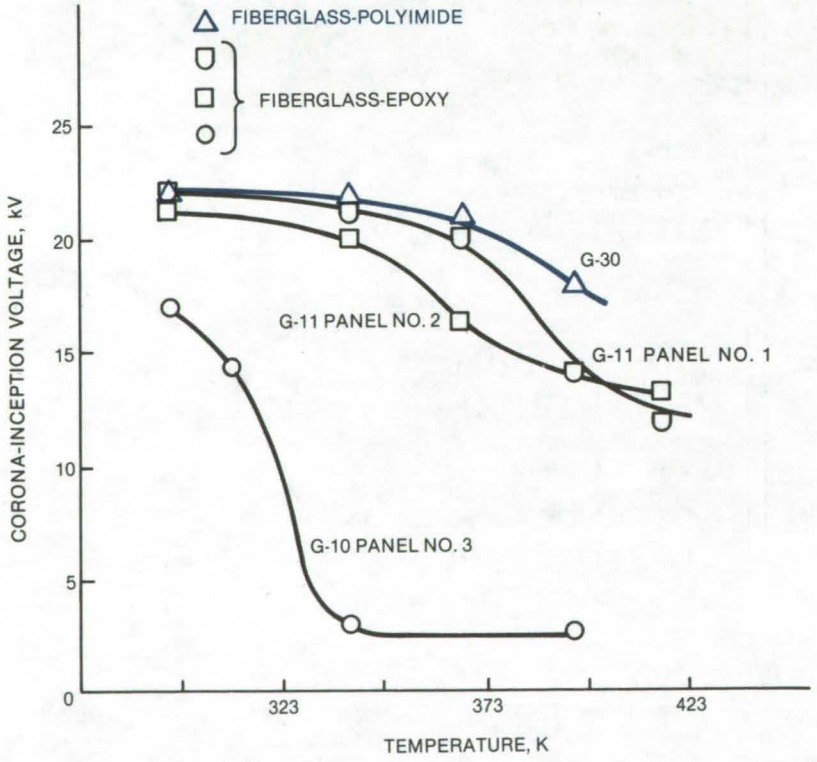

Figure 2. **Corona-Onset Voltage** shown is that required to initiate 5-picocoulomb discharges between two 4.7-mm-diameter solder balls bonded with epoxy to one surface of test specimen. Distance between electrodes was 51 mm. Tests were performed in air. Data points represent single measurements.

Advanced power electronics systems require materials that are capable of withstanding increasingly severe operating environments in the form of high voltage, high temperature, and high vacuum. These conditions encourage corona discharges that can jeopardize the reliability and long life performance of the electrical system. Standard corona tests performed according to ASTM-D-1868 and D-2275 measure corona resistance of candidate circuit-board materials only at discrete locations. Since the high-pressure laminates used to fabricate circuit boards can contain structural anomalies due to porosity, fiber layup, and variations in chemistry, it is essential that these materials be evaluated in their entirety before building up a critical component.

By utilizing a system incorporating a transmission technique with a reflector plate, a single transducer can be used to scan the high-pressure laminates and record variations in ultrasonic energy transmitted through the board thickness. The result is a permanent record of the ability of the laminate to transmit acoustic energy, which can be correlated with the relative level of corona inception voltage (CIV).

Figure 1 shows a schematic representation of the immersion test system. The ultrasonic transducer acts both as a sender and a receiver. The acoustic waves pass through the specimen twice, losing part of the energy each time by virtue of surface interactions and attenuation by internal microstructure. Variations in fiber lay-up as well as internal voids are causes of attenuation and scatter, and they result in loss of signal intensity received by the transducer. Different specimen materials can also result in different degrees of attenuation.

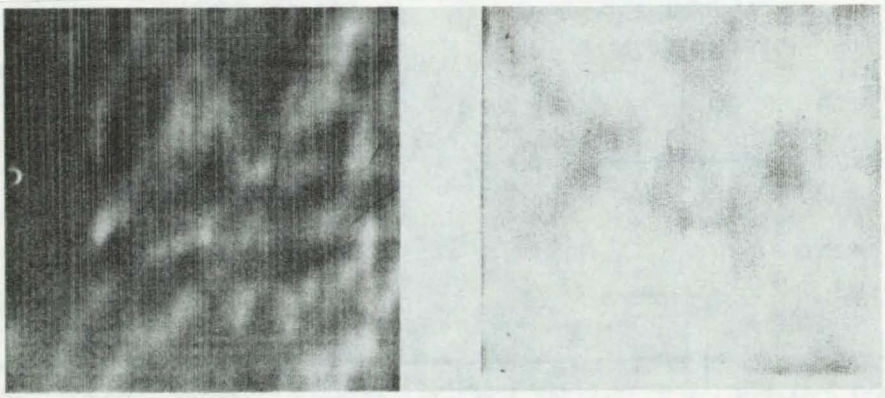

(a) Panel No. 1. NEMA Specification G11: Relatively-good ultrasonic transmission.

(b) Panel No. 3. NEMA Specification G10: Relatively-low ultrasonic transmission.

Figure 3. Ultrasonic C-Scans show varying levels of ultrasonic transmission through 2.36-mm fiberglass/epoxy high-pressure laminates. The darkness of the scan lines is proportional to the level of transmitted energy.

Figure 2 shows results of CIV tests performed at temperatures up to 284° F (413 K). The materials tested were high pressure laminates being considered for use in the high-voltage section of the power unit in the transmitter experiment package for the Communications Technology Satellite (CTS). The power unit operates in the range of 11 to 13 kV at 194 to 248° F (363 to 393 K). The laminates were fabricated to National Electrical Manufacturers Association (NEMA) grades G-11 and G-30 specifications; G-10 is unacceptable.

The materials were ultrasonically scanned over their entire area to measure the ultrasonic transmission characteristics. Typical results in the form of power sensitive graytone recordings, presented in Figure 3, indicate that better ultrasonic transmission correlates with higher CIV values. The scans also show that significant variation in the degree of ultrasonic transmission exist within a given panel. Thus, possibly the greatest value of the ultrasonic scanning technique is when used as a tool for mapping specific panels to permit selecting the best areas of the laminate for circuit board use. This technique was used to help select all flight-quality fiberglass/polyimide circuit-board panels for the power supply on the CTS launched in January 1976. The ultrasonic evaluation procedure is relatively safe, fast, and inexpensive, and can be performed with commercially available equipment.

This work was done by Stanley J. Klima and Thomas J. Riley of **Lewis Research Center.** *Further information may be found in NASA TM-X-73432 [N76-27475], "Ultrasonic Evaluation of High Voltage Circuit Boards," a copy of which may be obtained at cost from the New England Research Application Center [see page A7].*
LEW-12781

Fuseholders Allow Fast System Checkout

Test cable connects circuits to analyzer via hole drilled in each fuseholder cap.

Lyndon B. Johnson Space Center, Houston, Texas

Engineers working on the power distribution network of the Space Shuttle Orbiter vehicle have come up with a simple and timesaving technique for checking circuit continuity and isolation from other circuits in the system. Such checkout is necessary to safeguard against costly equipment damage that could occur if power were turned on in the presence of faulty circuit connections.

The caps on the standard cartridge fuseholders in each of the circuits have been modified to allow each circuit to be connected readily to an automatic circuit analyzer. The results have been impressive. A system with 200 fused circuits has

(continued next page)

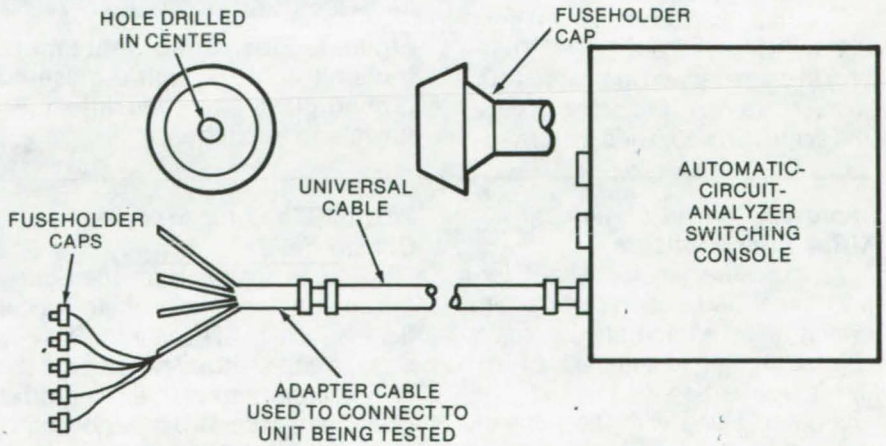

Modified Fuseholder Cap with a hole drilled through its center allows leads from an automatic circuit tester to be inserted into each circuit of many separately fused circuits. In an application, a 100-wire cable was divided into 20 groups of 5 wires each to connect to 100 circuits.

been tested in 1 hour. Previously, it took 1 hour to test just one circuit because, after each fuse was removed, the tester had to be connected manually to each circuit.

A hole drilled in the center of each cap, as shown in the figure, is the means by which the automatic tester is connected to the system. With the fuses removed, wires belonging to a special cable connected to the automatic tester are inserted into each fuse cap. The tester, which is a commercially-available continuity tester used for checking out wiring harnesses, then sequentially steps from one circuit to the next, testing each one automatically. Not only is the test accuracy greatly increased over that obtained with manual testing but the test results can be printed out as well.

This work was done by Robert L. Wooters of Rockwell International Corp. for **Johnson Space Center.** *No further documentation is available.*
MSC-16856

Window Flaw Detection by Backscatter Lighting

Tiny scratches can be detected with a portable fiber-optic probe.

Lyndon B. Johnson Space Center, Houston, Texas

An array of fiber-optic light emitters in a portable mounting block can pinpoint tiny flaws, cracks, and scratches in transparent materials. The probe assembly, shown in Figure 1, transmits light through the surface to illuminate the interior of the material by backscattering off its edges.

As seen in Figure 2, cracks that are a considerable distance from the illuminated edge are clearly distinguished by this method. The scratch in the foreground is only 0.0008 in. (0.002 cm) deep. The technique, which was originally developed to locate cracks in spacecraft windows after their installation, can be used with light-sensitive contact paper to give a permanent record of the scratch pattern. It can also be used for rapid visual checks.

The four fiber-optic light emitters shown in Figure 1 are 1/8 in. (0.32 cm) in diameter and are canted 10° to the horizontal. The screw allows the angle to be adjusted for curved

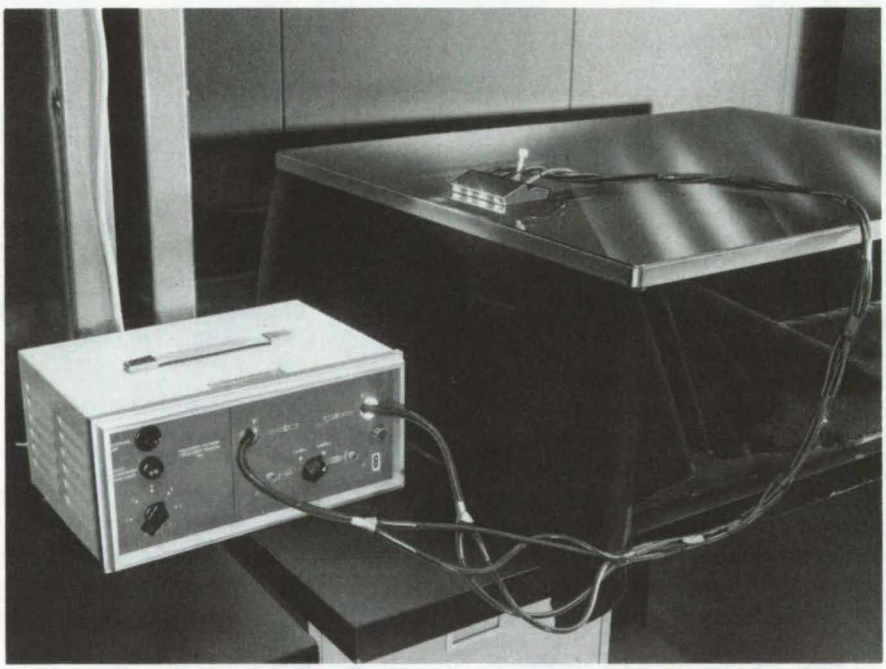

Figure 1. **Fiber-Optic Light Emitters** are mounted in a portable holder to transmit light through a glass surface. The light backscatters off the ground glass edge and into the interior of the glass to pinpoint tiny flaws and scratches.

Improved Control of Medical X-Ray Film Exposure

An exposure sensing system for a light-intensified motion-picture X-ray system uses an aperture or adjustable diaphragm to sample light from the image region of interest. This approach, along with the appropriate optics, can optimize the exposure sensitivity.
(See page 69.)

Video Method for Studying Optical Fields

A clever approach for measuring the intensity distribution in an optical field records the pattern with a vidicon and then displays it on an oscilloscope, using the vertical sweep as a trigger. Single horizontal lines in the field can be isolated by using the sweep delay feature of the oscilloscope.
(See page 44.)

Automated Tester for MOS Devices

An automated system can rapidly diagnose MOS integrated circuits. Its programed electronics investigate transistor and cell characteristics to compile the data needed for screening. The program can be changed rapidly to alter the test procedures, test duration, and precision.
(See page 3.)

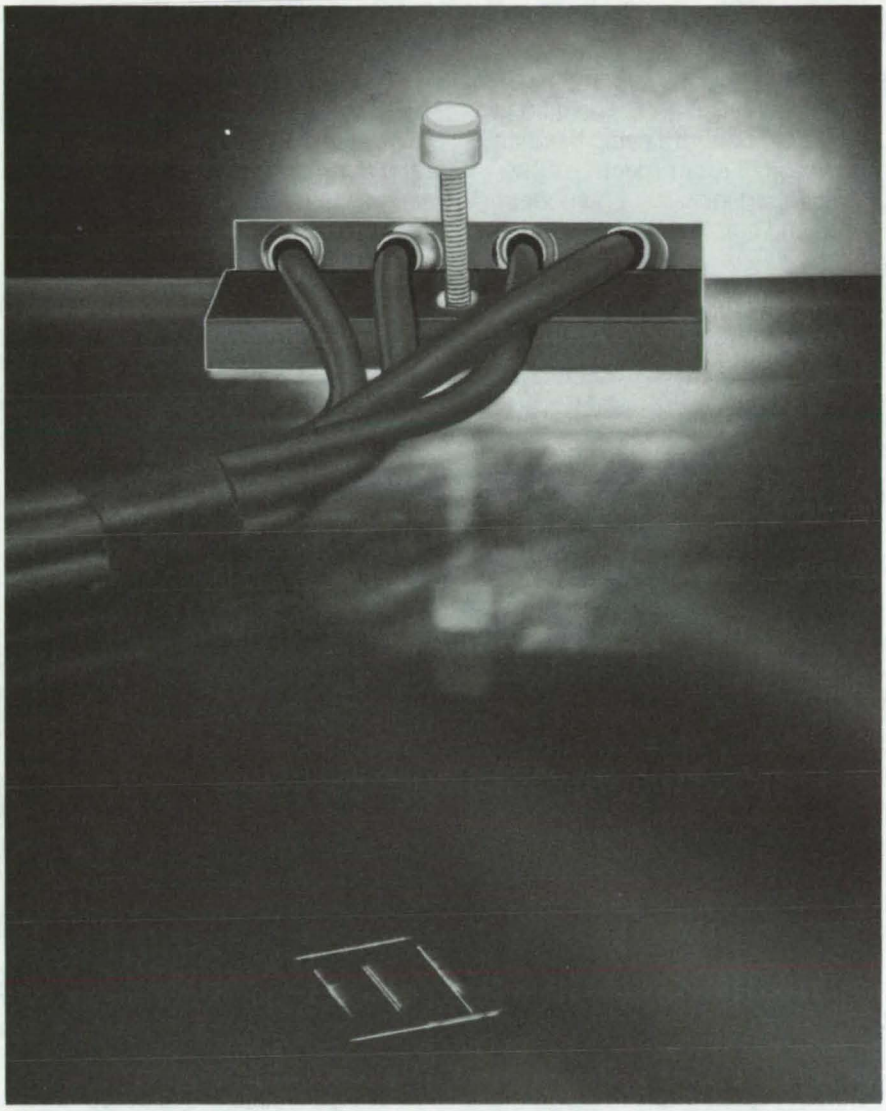

Figure 2. **Scratches Are Seen Clearly** against a dark background. A light-sensitive paper can be placed against the glass surface to provide a permanent record of the scratch pattern.

windows. The flexible fiber optics can be used safely in potentially explosive or flammable areas; they present no hazard of breakage or contamination in controlled environments.

The technique was tested on a 1- by 30- by 40-in. (2.5- by 76- by 102-cm) spacecraft window that had been scribed with scratches that had depths ranging from 0.0006 to 0.001 in. (0.0015 to 0.0025 cm). The holder was placed 3 to 4 in. (7.6 to 10 cm) from the window edge, and light was directed through the surface. Scratches 20 in. (51 cm) from the edge were clearly illuminated with this setup.

This work was done by Leroy K. Crockett and Fred R. Minton of Rockwell International Corp. for **Johnson Space Center.** *For further information, Circle 53 on the TSP Request Card.*
MSC-16605

Books and Reports

These reports, studies, and handbooks are available from NASA as Technical Support Packages (TSP's) when a Request Card number is cited; otherwise they are available from one of NASA's Industrial Application Centers or the National Technical Information Service.

Predicting Surface Heat Flux

Single embedded thermocouple used to predict flux and temperature.

Surface heat fluxes for high- or low-conductivity materials that have temperature- and pressure-dependent properties are predicted, using a numerical method based on data from a single embedded thermocouple. The method is presented in a report.

The technique solves for heat rate and temperature at a given surface at each time step rather than for the entire history. Initially the Newton-Raphson technique is used for temperature solutions; then a quadratic fit is employed.

Numerical difficulties can arise in determining the surface heat rate or

(continued next page)

the surface temperature from data based on interior thermocouples. This difficulty is due to the timelag between the surface and the thermocouple location. Another factor is the damping of surface changes at the thermocouple location.

The numerical technique has been verified, using a single thermocouple embedded in low-conductivity material; and the same approach has been used to verify results for high-conductivity material. The accurate results demonstrate the capability to compute surface conditions; i.e., heat flux and/or temperature using the data from a single experiment.

The report includes a number of tables and graphs to present the study.

This work was done by Donald M. Curry of **Johnson Space Center** *and Stanley D. Williams of Lockheed Electronics Co., Inc. Further information may be found in NASA TM-X-58176 [N76-20410], "Determination of Surface Heat Flux Using a Single Embedded Thermocouple" [$4.50] and NASA TM-58204 [N77-27349], "Surface Heat Flux Determination" [$4.50]. Copies may be purchased [prepayment required] from the National Technical Information Service, Springfield, Virginia 22151. MSC-16095*

Computer Programs

These programs may be obtained at very reasonable cost from COSMIC, a facility sponsored by NASA to make new programs available to the public. For information on program price, size, and availability, circle the reference letter on the COSMIC Request Card in this issue.

Approach and Landing Simulation

Evaluation and Integration of avionics topics

The program, VALT (VTOL Approach and Landing Technology), integrates avionics research in navigation, guidance, controls, and displays with a realistic aircraft model. An overall simulation program, VALT evaluates and integrates various areas of avionics research. It gives researchers the capability of evaluating an avionics area independently from other research areas and thus allows more flexibility in time schedules.

The various measurement sensors and avionics functions are represented by separate modules, allowing new algorithms to be included into the simulation with little impact on the overall program structure. For each module, the user can choose one of the supplied models or add other models as they are developed. The program currently includes a six-degree-of-freedom helicopter model. This program should prove very useful in the design and evaluation of avionics systems, particularly for VTOL type aircraft.

The program comprises many independent modules that represent specific hardware onboard an actual aircraft (such as rate gyros), external navigational aids, and physical functions such as winds. In general, the helicopter model calculates and feeds back perfect signals, such as linear and angular velocities, accelerations, positions, and angles. The sensor models use as inputs the helicoper-derived signals, and they generate appropriate output variables to represent the measurements. The user may select perfect measurement, where the output is equivalent to the input, or models with errors, where the output is a corrupted version of the input. The outputs from the inertial-measuring-unit sensors feed into a navigation computer module. The current module represents an error model, but the module could easily accommodate actual navigation computer equations. All of the measurement data are fed into an estimator module. The current estimator module has the output being a duplicate of the input, but a Kalman filter or any type of estimator could be included.

The guidance computer and external guidance commands are composed of several modules. Guidance commands can be generated internally by stored nominal trajectory data and automatic guidance steering laws. External guidance commands are generated by the pilot or by air traffic control. The guidance outputs generally represent some type of perturbation errors and are fed into the control computer. The control computer uses these commands to generate equivalent control-stick commands.

The helicopter module consists of several submodules. The main sections include actuator and rotor nonlinearities and dynamics, force and moment calculations, equations of motion, and an update section to calculate all of the variables that are fed to the sensor modules.

The use of this program has been simplified as much as possible because of the various disciplines that will be running the program. NAMELIST type data input is used, and only the data associated with the particular simulation being run are required as input. This feature is accomplished by a series of defaults that the user can set to select modules for the overall simulation. Output consists of time-iterative listings of requested simulation variables over a particular time period for which initial conditions are given.

This program is written in FORTRAN and COMPASS for the FTN compiler and has been implemented on a CDC 6000 series computer with a central memory requirement of approximately 60K (octal) of 60-bit words. The program is overlayed and is supplied in NOS MODIFY Program Library Format.

This program was written by Aaron J. Ostroff of **Langley Research Center.** *and R. Brian Wood of Vought Corp. For further*

information, Circle A on the COSMIC Request Card.
LAR-12060

Stability Characteristics of Elastic Airplane

Static and dynamic analyses of flexible aircraft.

The FLEXSTAB system of programs uses linear theories to evaluate static and dynamic stability, trim state, inertial and aerodynamic loading, and elastic deformations of aircraft configurations at subsonic and supersonic speeds. The distinctive features of the FLEXSTAB system are:

- It is based on unified linear aerodynamic, structural, and dynamic analytical methods valid for a wide variety of aircraft configurations.
- It can incorporate empirical and theoretical corrections in aerodynamic and stability analysis.
- It merges the low frequency dynamics of a flexible body with low-frequency unsteady aerodynamics for aircraft dynamic stability analysis.

The FLEXSTAB system solves a wide variety of problems; primary emphasis has been placed on analyzing the stability and control characteristics of flexible aircraft. As a consequence, the unsteady formulation is restricted to low-frequency analysis. The system also solves simple rigid aerodynamic problems conveniently and efficiently. Byproducts of these analyses include the calculations of aerodynamic load distributions and, for elastic solutions, the calculation of net loads (aerodynamic plus inertial) at the structural nodes (grid points), and structural deformations. As in all aerodynamic potential flow programs, the flow is considered to be attached and inviscid; that is, separation and viscous flow effects are neglected.

FLEXSTAB is essentially an open-ended program in that the number of aerodynamic segments and structural degrees of freedom used to describe an aircraft configuration are generally limited by economic considerations rather than size limitations of the FLEXSTAB system. Dual code is provided in the matrix operational subroutines for efficient in-core and out-of-core calculations. Assembly language code has been written into subroutines where speed is essential, such as the matrix vector inner product computations.

Configurations to be analyzed may be made up of multiple wings, bodies, tails, nacelles, and like units. Structures are represented as being rigid, static-elastic, or residual-elastic; in the latter case the dynamic stability analysis uses the lower-frequency free-vibration-mode shape amplitudes as structural degrees of freedom while retaining the static effects of all modes. Data describing the geometric and structural characteristics and the specific flight condition to be analyzed are input. The user can define a beam-like structural model within FLEXSTAB itself, or he can input a more general finite-element flexibility matrix created from an outside structures program such as NASTRAN. The program uses this input data to form aeroelastic matrices for the unrestrained vehicle and then calculates the aerodynamic and stability characteristics and structural loads of the aircraft.

Aircraft stability and control analysis is performed at prescribed flight conditions defined by Mach number, altitude, angle of bank, pitch, yaw, and roll rates, and either flightpath angle or thrust. If the perturbation equations of motion are nonlinear (as a consequence of the user supplying nonlinear aerodynamic data or wanting to investigate large perturbations), or if discrete gust disturbances are input, dynamic stability characteristics are evaluated from the time histories plots.

Lifting-pressure distributions on the aircraft can be calculated in the course of the solution of any stability analysis problem. Structural loads, deflections, and rotations are calculated at aerodynamic panel centroids in the execution of any stability analysis problem. The FLEXSTAB system can be used to calculate either the jig shape or design-point shape of an elastic aircraft.

The effects of configuration changes, such as planform, camber shape, and structural elasticity can be evaluated by performing any of the above analyses for each configuration change. Present FLEXSTAB capabilities can be extended through interfacing or linking with computer programs outside the FLEXSTAB system. An example is taking the loads or elastic deflections at the structural grid points calculated by FLEXSTAB and inputting them into the NASTRAN Structural Analysis Computer Program to calculate internal structural stresses at specified flight conditions.

The CDC version of FLEXSTAB (ARC-11086) is designed to operate on CDC 6000 or 7000 series computers. CDC 6000 series computers must have a minimum of 131K word central memory. CDC 7000 series computers must have a minimum of 65K word small memory and 512K word large memory. The minimum configuration of either series must contain a card reader, a printer, a card punch, one tape transport, and a disk system with at least a 2.5-million word capacity for limited problem capability and a 12-million word capacity for general problem capability. FLEXSTAB is designed to run under control of the SCOPE 3 or KRONOS 2 operating systems on 6000 series computers or SCOPE 2 on 7000 series computers. The FORTRAN Extended compiler (Version 3.0 or 4.2) and the COMPASS assembler (Version 3.0) are used by FLEXSTAB. Calcomp basic software routines are required by plotting programs.

The IBM version of FLEXSTAB (ARC-11144) is designed to operate on the IBM 360 series computer. The IBM 360 must be a Model 75 or larger and have 408K of central memory available. The minimum configuration must contain a card reader, a printer, a card punch, two magnetic tape drives, and up to 4.6 megabytes of disk storage for scratch use during execution. The

(continued next page)

source code is written in FORTRAN G, FORTRAN H, and OS ASSEMBLER. Calcomp basic software routines are required by plotting programs.

This work was done by Larry L. Erickson of **Ames Research Center.** *For further information, Circle B [CDC Version, ARC-11086] or C [IBM Version, ARC-11144] on the COSMIC Request Card.*
ARC-11144

WAKE and WASH

Prediction of light aircraft horizontal tail onset flows

Two computer programs, WAKE and WASH, can be used to determine onset flow in the vicinity of the horizontal tail of light aircraft. The primary function of a horizontal tailplane is to balance the pitching moment that arises when the lift force developed by the wing is applied at a moderate distance from an aircraft center of gravity. The horizontal tail must be sized and positioned for good performance and for acceptable longitudinal stability and control.

The passage of the wing through the air ahead of the tail compounds the problem by producing a downward inclination, or downwash, in the air approaching the tail and, if the tail is directly in the wing wake, a lower air velocity at the tail due to the wing drag force. The WAKE and WASH programs aid the light-aircraft designer by predicting the downwash and velocity profiles in the vicinity of the horizontal tailplane.

The downwash computer program employs the deflected vortex approach. In this approach the wing is replaced with a series of horseshoe vortices representing both the wing lift and the vorticity shed by the wing. The downwash is taken as the result of the interaction of the flow due to these horseshoe vortices with the freestream flow. The trailing vortices are allowed to deflect both spanwise and vertically so that their paths become streamlines. These streamlines define the wake centerline position. This downwash method includes a treatment of the effects of fuselage interference on the wing lift distribution, but does not include the effect of the diminishing fuselage size or the boundary layer on the aft fuselage. Also neglected is the modification of the downwash field of the wing due to the upwash created by the horizontal tail. A lifting-line representation of the wing is used in the program and should be acceptable for the design of light aircraft.

In the profile program the vertical variation in flow magnitude is determined by a quasi-three-dimensional solution based on solving the two-dimensional boundary layer equations along various streamlines displaced spanwise. These two programs can be used to determine the downwash angles, wake-sheet location, and velocity profiles in the wing wake.

These programs are written in FORTRAN and have been implemented on the IBM 360 series computer with a central memory requirement of approximately 100 K of 8-bit bytes.

This program was written by Frederick O. Smetana and Delbert C. Summey of North Carolina State University for **Langley Research Center.** *For further information, Circle D on the COSMIC Request Card.*
LAR-12262

Flow Velocities and Streamlines

For midchannels of axial, radial, or mixed-flow turbomachines or annular ducts

A computer program has been developed for calculating the subsonic or transonic flow on the hub-shroud, midchannel, stream surface of a single-blade row of a turbomachine. The program uses both the finite-difference and the quasi-orthogonal (velocity-gradient) methods, combined in a way that takes maximum advantage of both. The finite-difference method is used to obtain a subsonic-flow solution. The quasi-orthogonal method is then used, if necessary, to extend the range of solutions into the transonic regime.

A solution can also be obtained for an annular duct without blades. The flow must be essentially subsonic, but there may be local areas of supersonic flow. The solution is for two-dimensional, adiabatic shock-free flow. The blade row may be fixed or rotating, and the blades may be twisted and leaned. The flow may be axial, radial, or mixed. Upstream and downstream flow conditions may vary from hub to shroud, and provision is made for an approximate correction for loss of stagnation pressure. Viscous forces are neglected along solution mesh lines running from hub to tip.

This program is a revision of and supersedes a previous program published as NASA Tech Brief B74-10130, "Computer Program for Calculating Velocities and Streamlines on Mid-Channel Flow Surface of Axial or Mixed-Flow Turbomachine" (LEW-12129). The capabilities of the earlier program have been extended to handle nonaxial flows without restriction, to handle annular ducts without blades, and to allow for any specified streamwise loss distribution. Numerous detailed improvements have been made for more accurate and efficient calculations.

The design of blades for compressors and turbines ideally requires methods for analyzing unsteady, three-dimensional, turbulent viscous flow through a turbomachine. Such solutions are impossible at the present time, even on the largest and fastest computers. The usual approach at present is to analyze only steady flows and to separate inviscid solutions from viscous solutions. Three-dimensional inviscid solutions are just beginning to be obtained with the present generation of computers, but they require excessive computer time. At present, inviscid analyses usually involve a combination of several two-dimensional solutions on intersecting families of stream surfaces to obtain what is called a quasi-three-dimensional solution.

Since there are several choices of two-dimensional surfaces to analyze

and many ways of combining them, there are many approaches to obtaining a quasi-three-dimensional solution. Most two-dimensional solutions are either on a blade-to-blade surface of revolution or on the meridional or midchannel stream surface between two blades. However, when three-dimensional effects are most important, significant information can often be obtained from a solution on a cross-sectional surface of the passage normal to the flow.

With this program, a solution to the equations of flow on the meridional surface can be carried out. This solution surface is chosen when the turbomachine under consideration has significant variation in flow properties in the hub-shroud direction, especially when input is needed for use in blade-to-blade calculations. The solution can be obtained either by the quasi-orthogonal method, which solves the velocity-gradient equation from hub to shroud on the meridional stream surface, or by a finite-difference method, which solves a finite-difference equation for a stream function on the same stream surface.

The quasi-orthogonal method is efficient in many cases and can obtain solutions into the transonic regime. However, there is difficulty in obtaining a solution when blade-aspect ratios are above 1. Difficulties are also encountered with curved passages and low hub-tip-ratio blades. For such cases, the most promising method is the finite-difference solution, but this solution is limited to completely subsonic flows.

The program can be used both for analysis and design and is reported in two volumes: Part I is the User's Manual, and Part II is the Programmer's Manual. Part I contains all the information necessary to use the program as it is written. It explains the equations involved and the method of solution, and it gives a numerical example to illustrate the use of the program. Part II includes the complete program listing and a detailed program procedure.

This program is written in FORTRAN IV for use on IBM TSS/360-67 equipment.

This program was written by Theodore Katsanis and William D. McNally of **Lewis Research Center.** *For further information, Circle E on the COSMIC Request Card.*
LEW-12966

Hydraulic Dynamic Analysis

Modular program for analysis of entire system

ROHDA (Rockwell Hydraulic Dynamic Analysis) is a new program that mathematically describes complete hydraulic systems to study their dynamic performance. Previous simulations of hydraulic systems employed computer models of individual system elements and used the method of characteristics to simulate the connecting lines. ROHDA can be used to conduct dynamic simulations of an entire hydraulic system (or individual segments), providing physical insight into problems that are obscured by previous approaches.

This new program calculates the pressures, flows, and component variables throughout a hydraulic system. Thus, the designer can study the dynamic response of any system parameter, such as actuator-piston velocity, pump output pressure, or line pressures. ROHDA should prove a valuable tool to engineers working with detailed performance results of aircraft, spacecraft, or similar hydraulic systems.

As a general purpose hydraulic simulation program, ROHDA employs a building-block approach in the form of subroutines that simulate the various components of a hydraulic system. These subroutines are then controlled by a main program. Component modules available include pumps, pressure lines, flow lines, flow-reversing and pressure-reversing lines, orifices, sinks and sources, regulators, fittings, reservoirs, accumulators, filters, valves, and actuators.

The structure allows users to include additional component modules as they are developed. The hydraulic system functional arrangement is defined by input data. The order of the elements in the data deck determines the order of system evaluation. The input to the hydraulic system is normally an actuator demand that causes a disturbance to propagate through the model. Outputs are time histories of pressure and flows at any point in the system and component variables of interest, such as actuator velocity, position, and load.

This program is written in FORTRAN IV and has been implemented on an IBM 360 series computer with a central memory requirement of approximately 280K of 8-bit bytes. This program requires a link library which can be supplied only as an IBM IEHMOVE unloaded data set.

This program was written by Robert L. Gale, Ardell W. Nease, and Desmond J. Nelson of Rockwell Internation Corp. for **Johnson Space Center.** *For further information, Circle F on the COSMIC Request Card.*
MSC-16795

Performance Optimizing

Program for dynamic systems subject to transient loadings.

PERFORM is a system of computer programs developed for determining the optimal behavior of a structural-mechanical system subject to transient disturbances or loadings. It provides characteristics of the "theoretically best" or limiting design concept according to response criteria dictated by design requirements. Equations of motion of the system in first and second order form include incompletely specified elements with characteristics determined in the optimization of one or more performance indexes. These indexes are subject to the response criteria in the form of constraints.

(continued next page)

The constraints typically are formed from displacements, stresses, forces, velocities, or accelerations that cannot exceed certain prescribed values. The performance indexes are optimized using linear programing techniques in which the performance requirements become objective functions.

PERFORM makes it possible to approach a design problem directly from the design criteria without a prior commitment to a particular design concept. With this limiting-performance capability, the designer can determine the feasibility of a proposed design on the basis of the specifications alone. Using PERFORM, the evaluation of proposed designs can be made without a multitude of analyses for each design candidate.

PERFORM is a collection of programs that are part of a four-phase problem-solving system. The first phase is the preprocessing of the input data and the setting up of the linear programing problem of the limiting-performance problem. The output from the first phase consists of:

- The Diagnostic File: a listing of errors detected in the input data;
- The Post-Processor Data File: containing arrays needed to compute specific limiting-performance responses from the linear programing solution;
- The Linear Programing Problem Data File: containing data for the linear programing problem;
- The Report Generator Language File: containing the program used by OPTIMA to write the linear programing problem solution; and
- The Application Control Language Program File: containing the program used by OPTIMA to describe the steps and parameters necessary to solve the linear programing problem.

The second phase is a sort phase. The records of the Linear Programing Problem Data File must be processed further before becoming usable by OPTIMA. The third phase is the solution of the linear programing problem. To do this, PERFORM uses the CDC OPTIMA system. The final phase is the post-processing phase. Using the solution of the linear programing problem and the arrays computed in the first phase, the post-processor programs compute the desired responses of the limiting performance problem. These responses and trade-off plots are printed as solutions.

The programs in this package are written in FORTRAN IV and COMPASS for the CDC FTN compiler. These programs can operate in batch or interactive mode and have been implemented on a CDC 6000 series computer with a central memory requirement of approximately 36K (octal) of 60-bit words. To use the PERFORM program, one must have access to the CDC OPTIMA linear programing system.

This program was written by B. Clark, W. D. Pilkey, and B. P. Wang of the University of Virginia for **Langley Research Center.** *For further information, Circle G on the COSMIC Request Card.*
LAR-11930

Dynamics of Gas-Thrust Bearings

Load coefficients calculated up to third harmonic.

In recent years, gas-bearing technology has been a key factor in many industrial applications. Gas operating systems have a ready supply of lubricant and eliminate the costly addition of oil reservoirs, pumps, and lines. Gas lubricants offer less friction, are not susceptible to temperature extremes, and exhibit greater reliability than conventionally lubricated bearings. A computer program was developed to calculate the load coefficients, up to the third harmonic, for hydrostatic gas thrust bearings. Average load capacity, stiffness, and damping are determined as functions of squeeze number, amplitude of oscillation, supply pressure, and restrictor coefficient. The program should prove useful in the identification of industrial situations where gas-thrust bearings have potential applications.

The computer program can be used to carry out a theoretical analysis of the effects of high-amplitude oscillation, induced by a periodic load disturbance, on the dynamic behavior of an inherently compensated, infinitely long strip gas-thrust bearing. The Reynolds equation, a nonlinear time-dependent parabolic partial differential equation, is applied to the bearing for the analysis. The Reynolds equation is numerically approximated using finite-difference techniques. The time-dependent load-carrying capacity is represented by a Fourier series up to and including the third harmonic. The space and time derivatives are represented by central and backward difference expressions respectively. Solutions are calculated in terms of design curves for the stiffness, damping, and load capacity of the bearing.

This program is written in FORTRAN V and has been implemented on a UNIVAC 1100 series computer with a central memory requirement of approximately 29K decimal of 36-bit words.

This program was written by A. Kent Stiffler and Ricardo R. Tapia of Mississippi State University for **Lewis Research Center.** *For further information, Circle H on the COSMIC Request Card.*
LEW-12754

Machinery

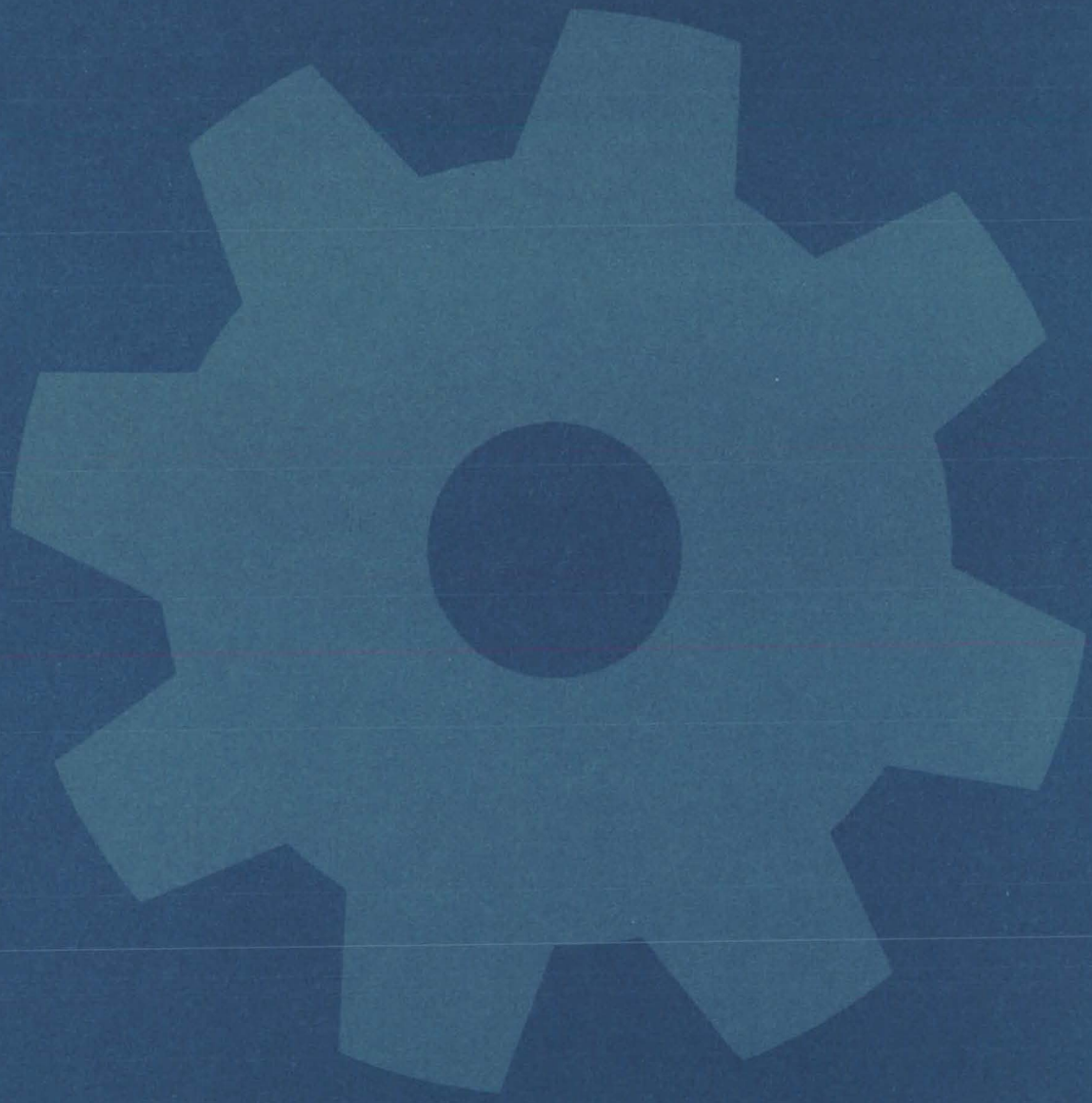

Hardware, Techniques, and Processes

Rigid Coupling Is Also Flexible

Spring-loaded coupling is rigid under light loads and swivels under higher loads.

Lyndon B. Johnson Space Center, Houston, Texas

A spring-loaded swivel coupling that is rigid under light- or no-load conditions becomes flexible when subjected to higher loads. The coupling automatically switches between its rigid and flexible modes. The breakout point can be set at any desired value by selecting the appropriate preload springs.

The coupling, shown in the figure, was originally designed to secure a payload to the payload bay in the Space Shuttle Orbiter. Powered mechanical latches had previously been used to perform the same function. Since the new coupling is a passive device, it is less expensive and considerably more reliable. These same features should make it useful in other applications that use flex couplings.

In the Shuttle application, the coupling was inserted in the arm used to erect, move, and deploy the payload. The coupling remains rigid while the payload is stowed or when the arm is rotated; it flexes to permit relative motion between the stowed payload and the payload bay when higher stresses are applied under in-flight conditions.

Figure (a) shows the coupling in its rigid mode. The central shaft connects to the payload; the flange at the right is attached to a clevis on the support structure. An axial tensile or compressive force that exceeds the spring preloads will compress one or the other spring, as in (b). A lateral force (c) will tilt the coupling around the structure flange. In this mode, the device acts as a circular hinge.

The coupling requires no cushions or elastomeric joints that might limit its temperature range. This feature plus its relatively-large displacement capability and preload feature should give it wide utility in load-limiting devices, relative-motion compensation, and other applications.

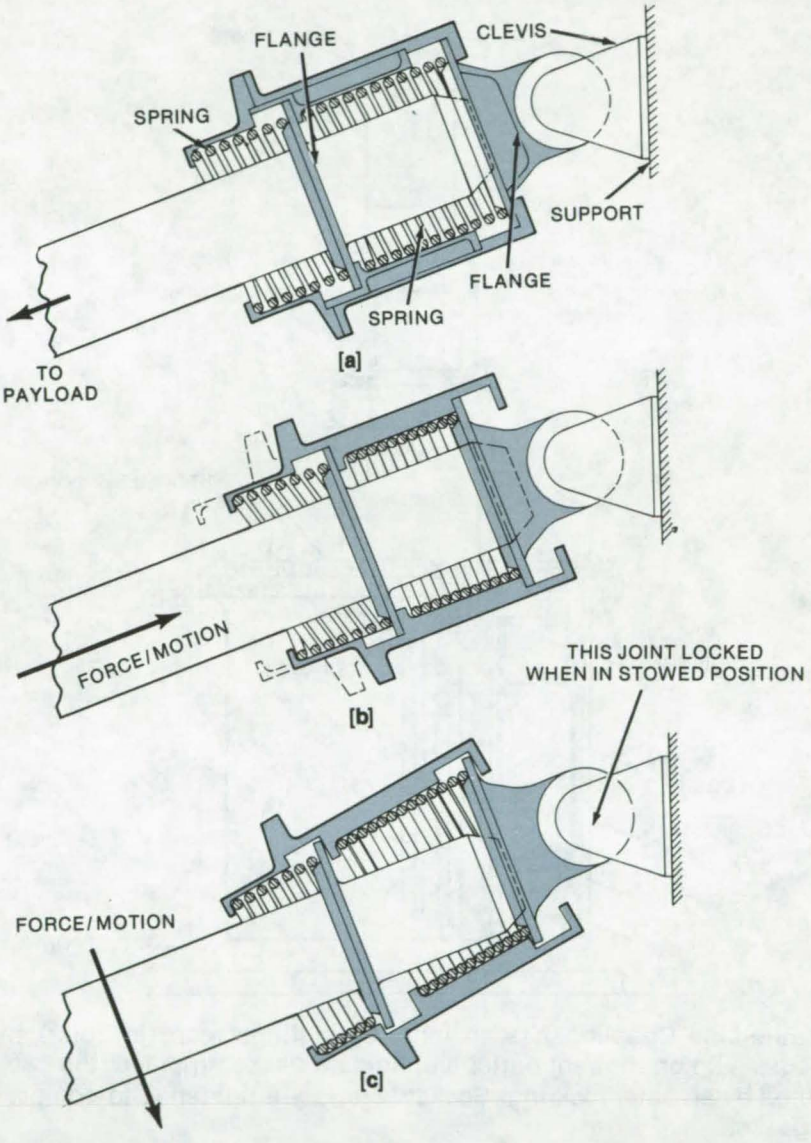

Spring-Loaded Coupling Remains Rigid (a) when applied forces are less than the spring preloads. It flexes, acting as a circular hinge when subjected to larger axial forces, as in (b), or lateral forces, as in (c).

This work was done by Walter T. Appleberry of Rockwell International Corp. for **Johnson Space Center.** *For further information, Circle 54 on the TSP Request Card.*
MSC-16488

Compact Pressure-Line Coupling

A coupling joins lines of different diameters without threaded fittings.

Lyndon B. Johnson Space Center, Houston, Texas

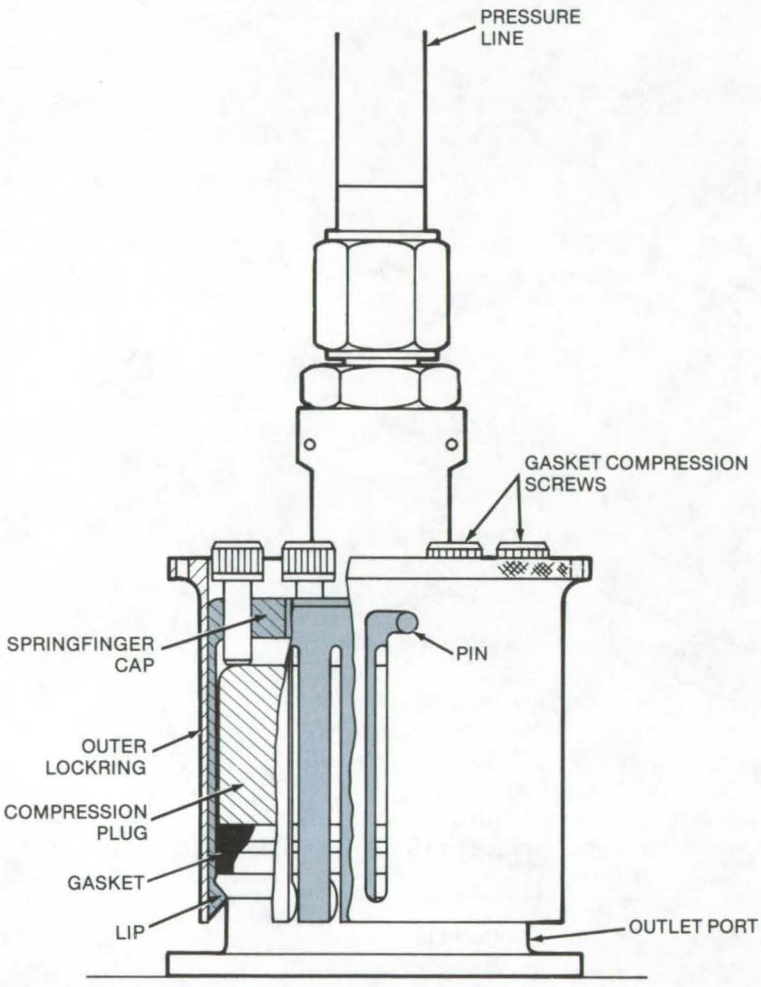

Pressure-Line Coupling has an inner springfinger cap (in color) that engages a lip on the vent outlet and holds a gasket in place; the cap is secured by an outer lockring. Socket screws are tightened to compress the gasket.

A new pressure-line coupling saves space by using socket screws rather than threaded fittings to compress a gasket. The compact coupling, shown in the figure, can be used to attach a pressure line to an outlet that has a large diameter. The outlet side requires only a small smooth nozzle with an outwardly flared lip; a lockring is installed on the line side of the coupling. Since a socket wrench is used to tighten the seal, the coupling can be installed in hard-to-reach locations that would be inaccessible if an adjustable wrench or other bulky tool were required.

To connect the pressure line, the gasket and gasket compression plug are positioned over the outlet. A springfinger cap is placed over the gasket and plug so that its fingers engage the underside of the lip on the outlet rim. The lockring is then placed over the cap and is rotated onto the locking pin. Finally, the socket screws are then tightened against the compression plug to seal the gasket. The process is carried out in reverse to remove the pressure line.

This work was done by John W. Guest of Rockwell International Corp. for **Johnson Space Center.** *No further documentation is available.*
MSC-16893

Plasma Igniter for Internal-Combustion Engines

Electromagnetic forces inject a plasma into the combustion zone at supersonic speed.

NASA's Jet Propulsion Laboratory, Pasadena, California

A hot ionized gas (a plasma) may ignite the air/fuel mixture in internal-combustion engines more effectively than a spark. In conventional ignitions, combustion begins as a small kernel that expands at the speed of the flame front. The plasma igniter, in contrast, rapidly injects large amounts of energy throughout the combustion chamber. This gives much higher engine efficiency, particularly when igniting lean

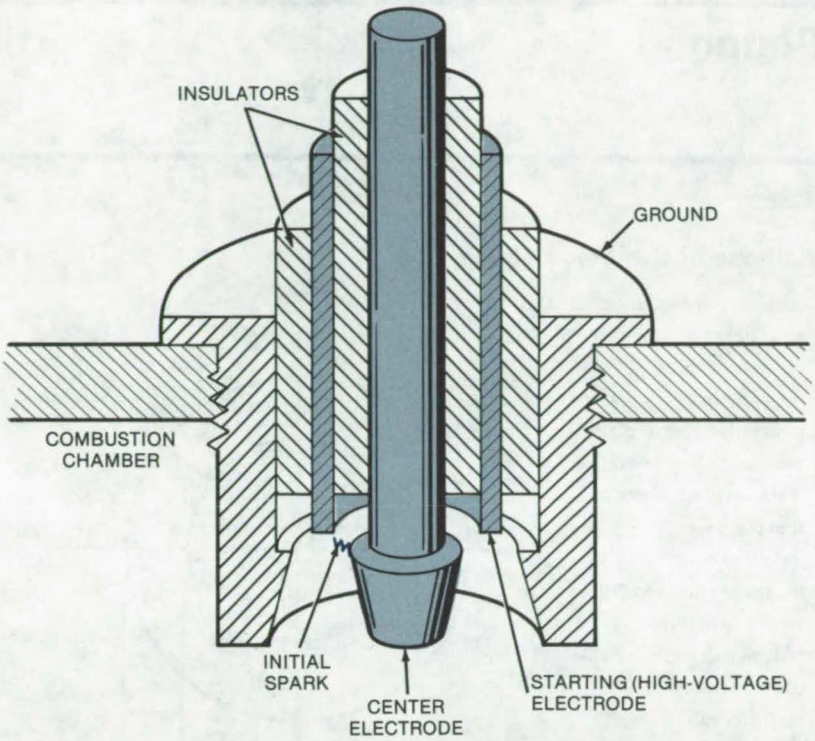

Figure 1. Plasma Igniter has center and high-voltage electrodes and a grounded outer shell. The spark can be generated by a conventional ignition system.

mixtures for which the flame-front speed is relatively slow.

In a proposed plasma igniter, the hot gas is propelled into the combustion zone by electromagnetic forces. Estimates indicate that the plasma may reach supersonic speed by this method. Since the rate of combustion is not limited by the flame-front speed, energy is delivered quickly and uniformly.

In one version of the plasma igniter, shown in Figure 1, a center electrode is connected to the ignition capacitor and a cylindrical electrode is connected to a conventional spark source. The outer shell of the igniter is grounded. When a spark is initiated between the two electrodes, the ionized gas in the spark path discharges the ignition capacitor into ground and creates a small toroidal plasma, as seen in Figure 2(a). The (radial) plasma current interacts with the circulating magnetic field around the center electrode. This electromagnetic force pushes the plasma toroid down [Figure 2(b)] and out of the igniter at high speed [Figuure 2(c)]. The large volume occupied by the plasma, as compared with a conventional spark, allows about 10 times as much energy to be injected.

The use of a starting electrode is not absolutely necessary. An alternative is to discharge a higher-voltage (30-kV) ignition capacitor with an external spark gap. This voltage would be transferred to a resistor between the center electrode and ground, producing the spark that initiates the plasma.

This work was done by Robert R. Breshears and Dennis J. Fitzgerald of Caltech for **NASA's Jet Propulsion Laboratory.** *For further information, Circle 55 on the TSP Request Card.*

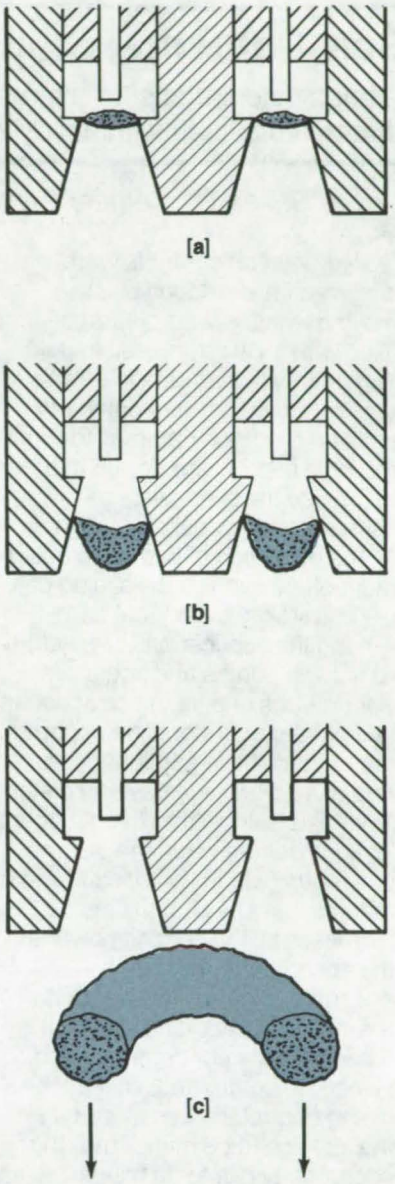

Figure 2. Plasma Toroid (a) expands (b) and is pushed out of the igniter (c) by the electromagnetic force between the discharge current and the magnetic field surrounding the center electrode.

This invention is owned by NASA, and a patent application has been filed. Inquiries concerning nonexclusive or exclusive license for its commercial development should be addressed to the Patent Counsel, NASA Resident Legal Office-JPL *[see page A8].* *Refer to NPO-13828.*

Self-Centering Stepped Piston

Design calculations for piston that centers itself within a cylinder.

Lewis Research Center, Cleveland, Ohio

Hydrodynamic effects were analyzed for a stepped piston moving within a tight-clearance tube filled with an incompressible fluid. Together with hydrostatic effects previously analyzed, a complete solution has been obtained for optimizing a piston-step design in order to provide the piston with a self-centering capability.

The operation of hydraulic equipment often involves the sliding of a piston within a cylindrical bore. Among the applications are hydraulic valves, pumps and actuators, viscometers and timing devices, and hydrostatic extruders. An important factor in all these applications is the rate of fluid leakage past the piston. Test results show that the minimum leakage occurs when the piston is concentric within its conduit, and that the leakage past the piston increases as the second power of the eccentricity. For a fully-eccentric, plain-cylindrical piston the leakage is two-and-one-half times that of a concentric piston. Hence, to control the leakage, one has to control the eccentricity. For the leakage to be minimized, the eccentricity has to be minimized as well.

A stepped cylindrical piston in a cylindrical tube is shown in Figure 1. The tube is filled with a fluid, and the piston moves with a velocity U relative to the stationary tube. The leading edge of the piston has the smaller diameter, so that the hydrodynamic pressure buildup around the piston produces a centering force.

The desired minimum eccentricity can be achieved by proper selection of the design parameters α and β where they are defined as:

$$\alpha = \frac{C_M}{C_m} \tag{1}$$

$$\beta = \frac{x_s}{L} \tag{2}$$

Definitions of Symbols Used in Text

C_M	larger radial clearance, $(D - D_2)/2$
C_m	smaller radial clearance, $(D - D_1)/2$
D	diameter of tube
D_1	major diameter of piston (see Figure 1)
D_2	minor diameter of piston (see Figure 1)
g	gravitational acceleration
H	distance piston falls
h	film thickness
L	length of piston
x_s	length of step (see Figure 1)
μ	viscosity of fluid
ϱ_f	fluid density
ϱ_p	piston density
R	radius of tube

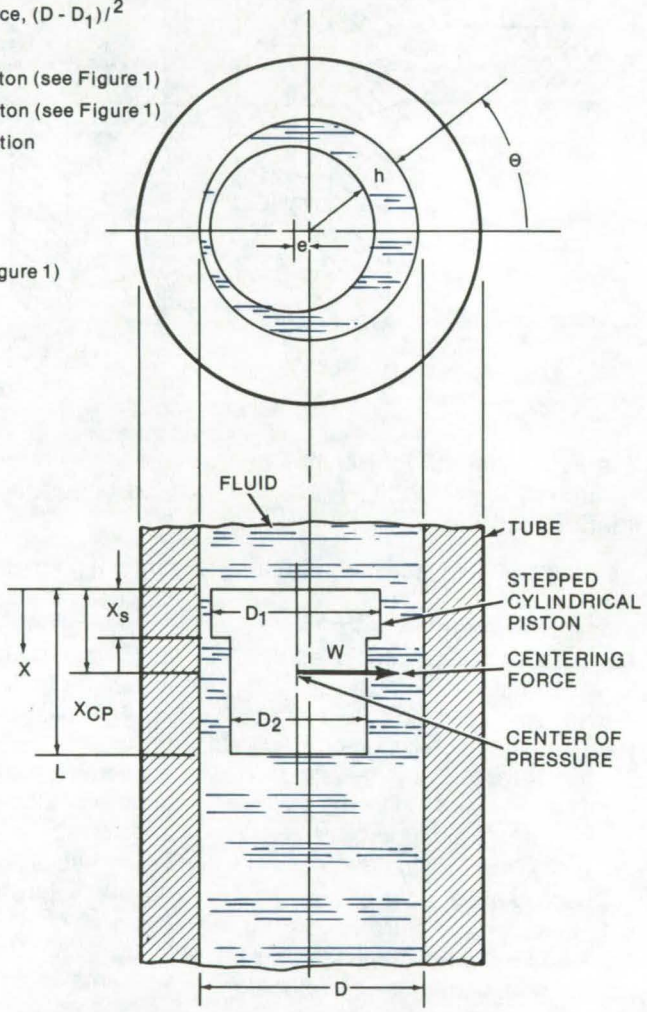

Figure 1. **Stepped Cylindrical Piston** in a cylindrical tube can be designed to center itself within the tube and thus minimize "leakage" past the piston.

The optimum step design is achieved by finding the parameters α and β so as to maximize the nondimensional centering force which is defined as:

$$\overline{W}_h = \frac{W_h}{9\pi\mu UR(L/C_m)^2} \tag{3}$$

In Figure 2, the nondimensional centering force $\overline{W}_h$ is plotted against the step-length parameter β for various step height ratios of α. From this graph, the optimum step geometry of $\alpha = 1.6$ and $\beta = 0.26$ is found for a maximum nondimensional centering force $\overline{W}_h$.

Assuming the stepped piston in the tube is at a constant velocity, the time it takes the stepped piston to fall a distance H can be written as:

$$t = \frac{6\mu RH}{C_m^3 g(\varrho_p - \varrho_f)\overline{Q}_g} \tag{4}$$

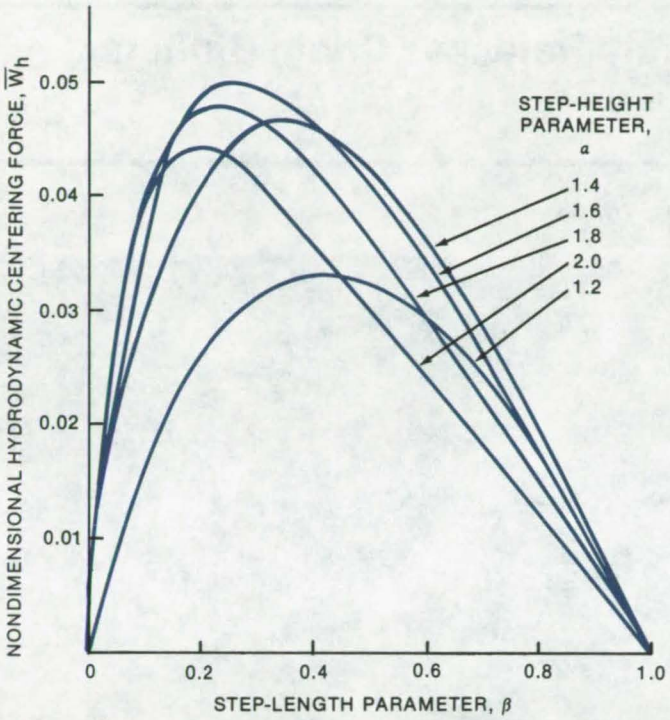

Figure 2. **Centering Force** is shown for various step configurations.

where:

$$\overline{Q}_g = \frac{a}{1 + \beta(a^3 - 1)} \qquad (5)$$

Experimental results for pistons falling in a water-filled tube showed that plain pistons wobbled as they fell down the tube while stepped pistons moved smoothly without any wobble. The agreement between theory and experiments was good.

This work was done by Izhak Etsion and Bernard J. Hamrock of **Lewis Research Center.** *Further information may be found in NASA TN-D-8345 [N77-11402], "Optimum Step Design for Centering of Pistons Moving in an Incompressible Fluid," a copy of which may be obtained at cost from the New England Research Application Center [see page A7].*

Inquiries concerning rights for the commercial use of this invention should be addressed to the Patent Counsel, Lewis Research Center [see page A8]. Refer to LEW-12997.

Compact Piston-Position Sensor

Strain gage measures the position of a spring-loaded piston without interfering with its motion.

Lewis Research Center, Cleveland, Ohio

To measure the position of a spring-loaded piston without affecting the piston's dynamic response characteristics, strain gages are attached to a fitting at the spring end. The fitting occupies a very small space in the end of the piston's cylinder.

The fitting is installed in the end of the cylinder, as shown in the figure. The washer has four arms pointing inward with the spring resting on the inner ends of the arms. The arms are stiff when compared to the piston spring. Mounted on both sides of one arm is a strain gage. When connected to a conventional strain-gage bridge circuit, the strain gage measures the force in the spring. If the spring force is linear, the bridge circuit readout is a direct measurement of the piston position.

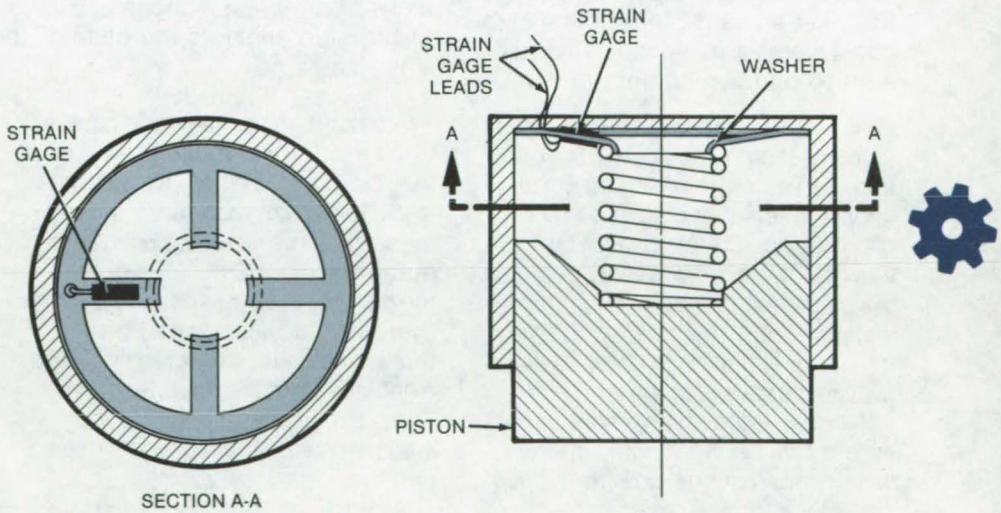

A **Strain Gage** installed on a special washer in contact with the piston spring records the spring force; if the force is linear, it measures the piston position.

This work was done by Miles O. Dustin of **Lewis Research Center.**

No further documentaiton is available.
LEW-12392

Modified Pipe Extension Safely Releases Chain Binders

A pipe, cupped and notched at one end, acts as safety device when releasing tiedown chains.

Lyndon B. Johnson Space Center, Houston, Texas

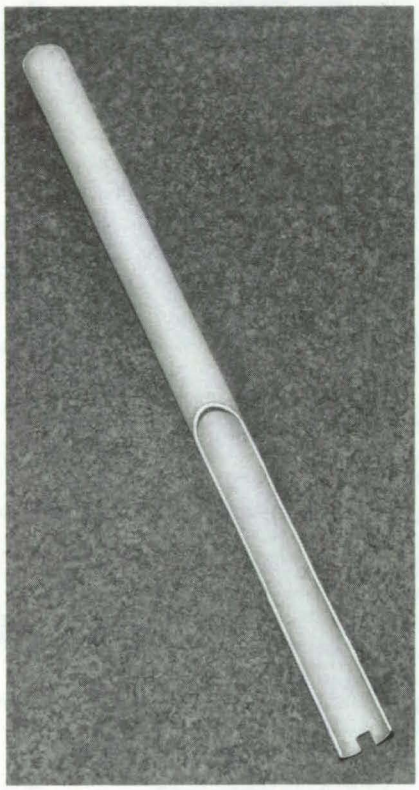

Figure 1. This **Pipe Extension** fits over a chain-binder handle to add leverage when applying tension to tiedown chains.

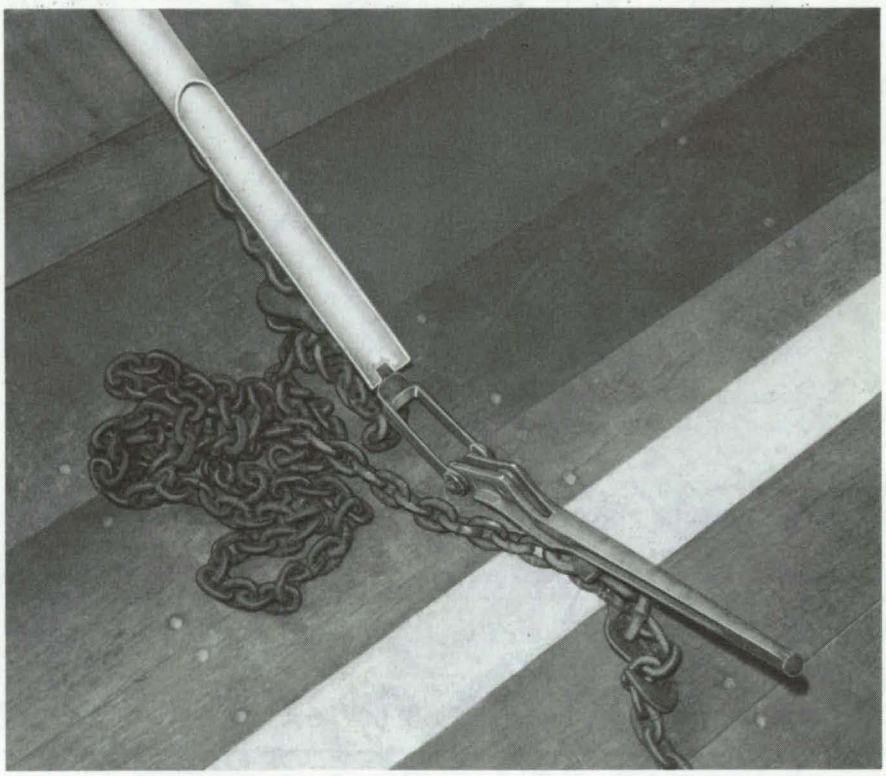

Figure 2. The **Open Cup** of the pipe extension allows the handle to move freely when it snaps to the no-tension position. A notch at the end of the pipe engages the base of the handle.

A length of pipe, cut partly in half along its length and notched at one end, can safely release tension in chain binders that cinch tiedown chains around truck loads. The easily fabricated accessory prevents the binder-handle from being thrown violently during the release. It thus can reduce injuries to personnel and prevent damages to the load.

Normally, the chain binder handle is kept short in order not to interfere with the load or protrude from the side of the truck. To gain extra leverage when rotating the handle to cinch or release the chains, truck-drivers will often fit a length of pipe over the handle.

A hazard arises when the handle is released since significant force may be required when, for example, a 150-lb (68-kg) man must release the tension previously applied by a man weighing 250 lb (113 kg). As the handle is raised and reaches the overcenter position, it may be thrown violently, wrenching the pipe extension from the driver's grasp. When this happens, the pipe may be slammed against the driver or load or thrown from the truck.

A simple modification of the pipe extension eliminates this hazard. The pipe, typically a 3-ft (0.91-m) length of steel pipe 2 in. (5.08 cm) in diameter, is cut in half for a distance equal to the length of the chain-binder handle, as seen in Figure 1. This part of the pipe then forms a cup for the handle. In addition, the pipe is notched at its end so that it may engage the base of the handle.

To release the binder, the cupped section of the pipe is placed under the handle, and the pipe is pushed upward. The handle is rotated upward until it slams open (Figure 2.) Since the handle rotates up and away from the cupped end, there is no danger of it catching the pipe and throwing it.

This work was done by Dale W. Haw of Rockwell International Corp. for **Johnson Space Center.** *No further documentation is available. MSC-16937*

Magnetostrictive Valve

Electromagnetically cycled valve would require no moving parts.

NASA's Jet Propulsion Laboratory, Pasadena, California

Electrically-activated solenoid valves are often used to inject small quantities of gas in pressure-control systems. However, the moving parts and close tolerances required for these valves limit their reliability under continuous use. The necessary reliability might be obtained by using a proposed valve that requires no moving parts and has less stringent tolerances. The proposed valve, which has response times on the order of 1 to 10 milliseconds, would use a magnetostrictive powered metal and electromagnets, rather than a solenoid. As in conventional valves, cycling would be controlled by applying a current.

When a polycrystalline nickel sample is placed in a magnetic field, it contracts along the field direction by about 30 parts per million and elongates in the transverse direction by about half that amount. Further experiments were to be considered using some kind of porous bonding material to the nickel to achieve stability. These dimensional changes (magnetostriction) are a characteristic of ferromagnetic metals and vary with the material, temperature, and magnetization state. In the proposed valve, the volume contraction of the ferromagnetic powder that occurs when a field is applied "opens" the valve. When the field is removed, the gas flow is cut off.

Two designs have been proposed. In one (see figure), a quantity of powdered nickel is inserted into a chamber in the valve housing and is compacted. An electromagnet is wound around the chamber to produce a longitudinal field (in the direction of gas flow). Finally, the gas fittings are assembled, preferably with a wire-mesh screen to contain the powder. In the second design, a rectangular powder chamber is sandwiched between two electromagnets that produce a transverse field.

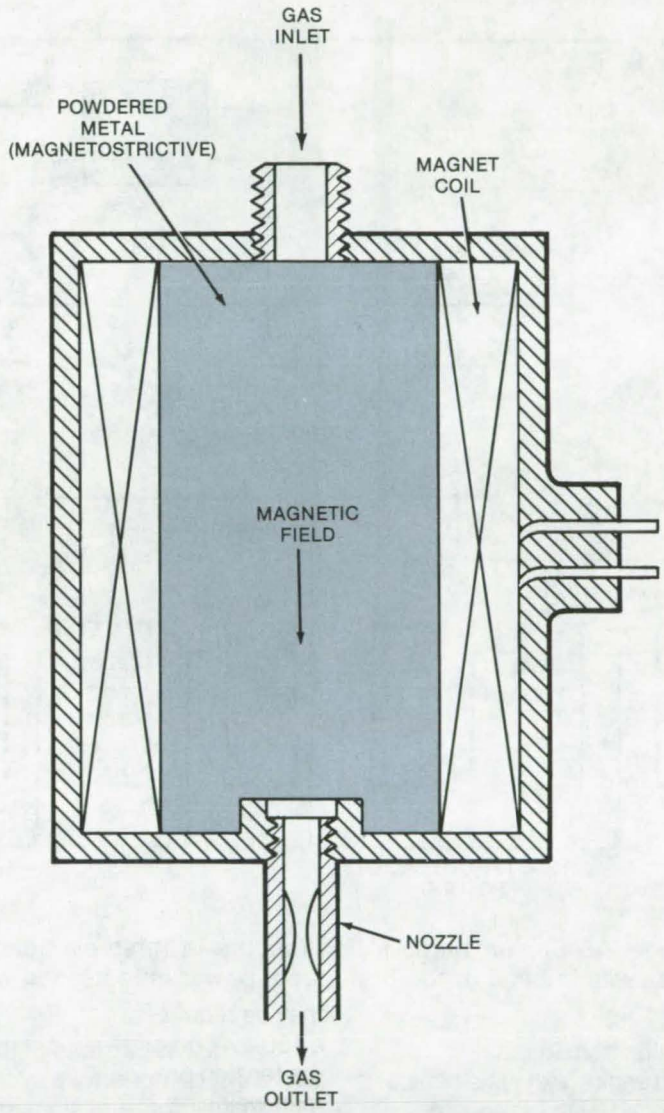

Proposed Magnetostrictive Valve would have powdered magnetostrictive material compacted in a chamber surrounded by a magnet coil. When the magnetic field is applied, the powder decreases in volume, allowing the gas to flow; the flow is cut off when the field is removed.

Some feasibility data have been obtained for the first design by using nickel powder and pressurized nitrogen gas at the flow inlet. The preliminary tests showed an inlet-gas pressure drop from 15 to 12 psi (1.03×10^6 to 0.82×16^6 N/m^2) upon the application of the magnetic field. The escaping gas could be heard at the flow outlet. Powdered iron was also tested in the chamber and gave some gas flow, although less than the nickel powder.

This work was done by Clifford C. Casabianca of Caltech for **NASA's Jet Propulsion Laboratory.** *For further information, Circle 56 on the TSP Request Card.*
NPO-14235

Boosting the Power of Two-Stage Engines

Low-pollution advantages are retained and power output is increased if the first stage operates on a two-stroke cycle.

NASA's Jet Propulsion Laboratory, Pasadena, California

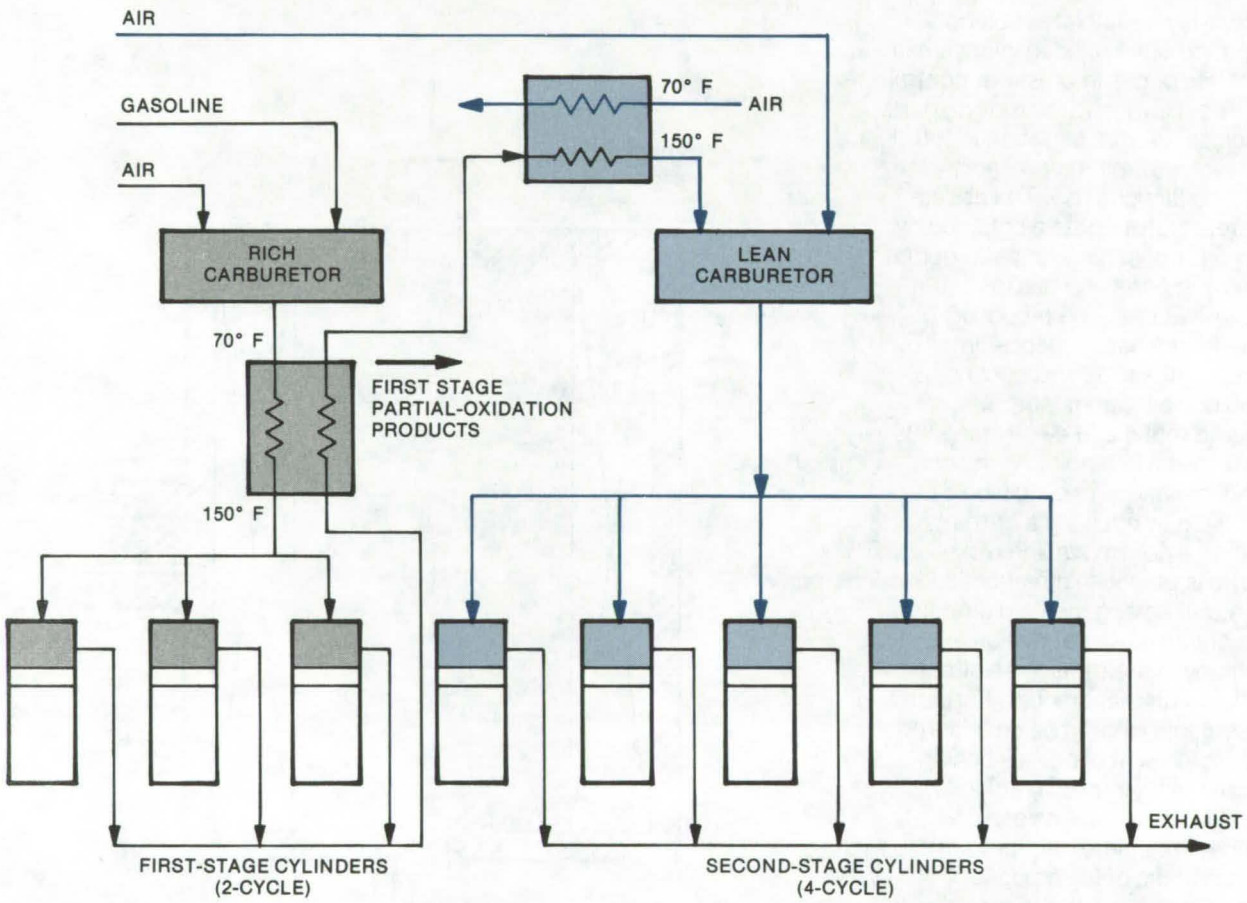

A **Two-Stage V-8 Engine** burns a rich mixture in three cylinders and a lean mixture in five cylinders. If a two-stroke cycle is used in the first stage, power is increased without adding to pollution.

Air pollution from internal-combustion engine exhausts can be greatly reduced by using engines that burn fuel in two stages, with the exhaust (including potential pollutants) from the first stage serving as the fuel for the second stage. The drawback of this scheme is that the maximum power of a two-stage engine is significantly less than that of an equivalent one-stage engine.

This disadvantage may now be eliminated by an engine concept in which the first stage operates on a two-stroke cycle instead of the more conventional four-stroke cycle. The two-stroke-cycle first stage may increase the overall maximum-power output of the engine by about 12 percent.

In the proposed engine, a fuel-rich mixture is burned in the first stage. Since there is not enough air in the mixture, the first-stage exhaust contains partially oxidized fuel. This is mixed with more air and is burned as an air-rich mixture in the second stage. Little or no nitric oxide pollution is produced in the process because, in the first stage, all the available oxygen is consumed by the fuel, and in the second stage, the combustion temperature is below the 2,800° F (1,538° C) temperature at which nitric oxide forms. Hydrocarbon pollution is also low because the hydrocarbons that are passed to the second stage from the first-stage exhaust are already in the gaseous state (instead of the usual droplets from a carburetor) and are easily burned to completion.

A two-stroke engine, in which compression, combustion, expansion, and exhaust are performed in two strokes of a piston instead of four, produces more power per turn of the crankshaft than an equivalent four-cycle engine. Ordinarily, a two-stroke engine is wasteful and polluting because it exhausts unburned fuel, but this is not a problem if the exhaust is passed on to a second stage.

A large portion of the first-stage exhaust consists of carbon monoxide. It is important that the first-stage combustion be controlled so that enough energy is left in the exhaust to raise the temperature of the second-stage combustion enough to completely oxidize the carbon monoxide to carbon dioxide (but not so high as to form nitric oxides).

In addition, it is important to control soot formation. If the first-stage combustion is too rich, soot will form. For a given air/fuel ratio, soot can be minimized by vaporizing and mixing the first-stage fuel with preheated air before the mixture is inducted into the cylinder. This precaution ensures a uniform air/fuel ratio throughout the cylinder and avoids extra-rich pockets that could produce soot.

One design for a two-stage, two-cycle/four-cycle process employs a V-8 engine (see figure). A carburetor supplies a rich air/fuel mixture to a heat exchanger to vaporize the fuel. The homogeneous rich mixture then enters three of the eight cylinders. The exhaust gas from these three cylinders is cooled and mixed with additional air in a carburetor and then burns to completion in the other five cylinders.

This work was done by John Houseman of Caltech for **NASA's Jet Propulsion Laboratory.** For further information, *Circle 57 on the* TSP Request Card.
NPO-14057

Precision Fluid-Pressure Regulator

Reshaping of the metering orifice improves pressure control and stability.

NASA's Jet Propulsion Laboratory, Pasadena, California

A concept intended to improve the stability and lifetime of fluid regulators suggests redesigning the metering orifice so that the poppet must move a greater distance to maintain the same pressure drop. By increasing the linear motion by a factor of eight or more, the regulator is made more stable and is capable of more precise pressure control.

In a conventional regulator (see figure) high-pressure fluid enters a chamber, passes through a metering orifice into a second chamber, and leaves the regulator at a lower pressure. A diaphragm in the second chamber acts as a feedback mechanism by moving a poppet in response to changes in the outlet pressure. The motion of the poppet varies the effective area of the orifice and adjusts the pressure drop.

Since the range of movement of the poppet in a small industrial regulator may be only 0.010 in. (0.025 cm) for a change from no flow to full flow, the operation of the valve is very sensitive to seat wear, aging, and trapped dirt particles. Also the poppet is susceptible to vibratory modes that can cause oscillations in the flow rate and can shorten the life of the regulator.

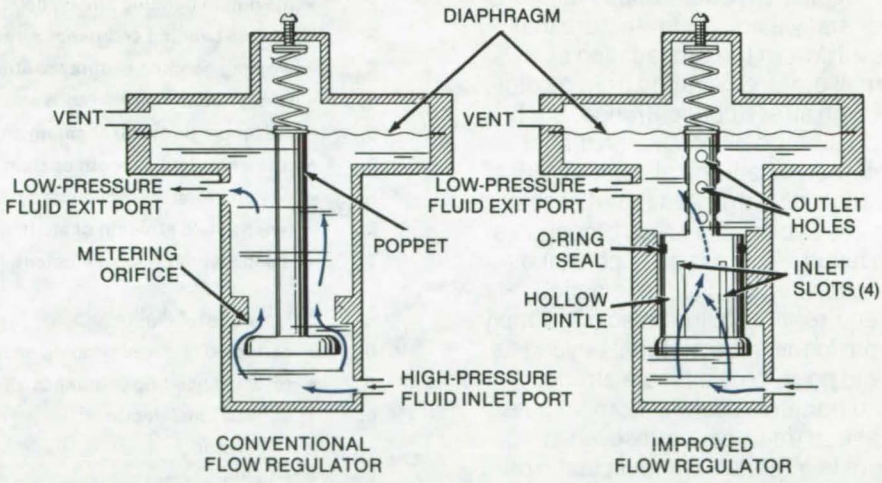

The Stability of a Fluid Regulator is improved by redesigning its flow-metering orifice. In a conventional regulator (left) the flow is controlled by the linear motion of a poppet; in the improved regulator (right) a slotted hollow pintle would replace the poppet to increase the linear motion required to obtain a given pressure drop.

In the proposed design four narrow metering slots in a hollow pintle replace the poppet. As shown in the figure, the fluid flows into the exposed area of the slots, through the pintle, and out of the holes in its top. The position of the pintle is controlled by a diaphragm as in the conventional regulator. If the slots are one-eighth of the circumference of the poppet, the poppet must move eight times the linear distance to cause the same pressure change.

This work was done by Allan R. McDougal of Caltech for **NASA's Jet Propulsion Laboratory.** *For further information, Circle 58 on the TSP Request Card.*
NPO-13370

Design of Transmission Shafting

Shafts meet load demands without excess material.

Lewis Research Center, Cleveland, Ohio

A formula for the design of transmission shafting has been developed which considers the flexure fatigue characteristics of the shaft material under combined cyclic bending and static torsion stress. This new formula permits selecting shaft sizes that meet common loading conditions without adding on excessive shaft material simply to accommodate large safety factors and low working stresses. The formula is applicable to the design of rotary power or torque transmission shafting external to machine elements.

One of the principal limitations of previous formulas for the design of shafting was that they did not consider fatigue as the predominant shaft failure mode. Fatigue failure is generally a complete fracture that results from the propagation of a small crack emanating from a point of high stress concentration, such as a surface discontinuity or an internal metallurgical defect. With a sufficiently large number of repeated stress cycles, the crack propagates to failure. There is an important distinction between static (elastic) fracture, i.e., failure resulting simply from loading the material beyond its yield point to its ultimate strength, and fracture resulting from fatigue. Fatigue fracture occurs even in ductile materials without plastic deformation; that is, at stresses below the yield point. There is no warning of impending failure.

Most rotating shafts are subjected to combined stresses of different types: a fully reversing bending moment combined with static torsion load and with negligible axial load. "Static" torsion load means only that the torque load is not fluctuating significantly.

Most industrial shafts transmit torque either in an overhung configuration, like the shaft of a cantilevered pulley, gear, or sprocket, or while loaded as simply supported beams, like a sprocket, pulley, or gear between bearing supports. They are in bending and torsional shear simultaneously.

Less common are shafts in configurations with a superimposed axial load, such as shafts for propellers, extruders, agitators, and those with thrust loads generated by transmission components like uncompensated helical or bevel gears.

The shaft design formulas (1) through (5) in the figure are applicable to rotating solid shafts under

$$\left(\frac{S_b}{S_{ew}}\right)^2 + \left(\frac{S_s}{S_{syw}}\right)^2 = 1 \qquad (1)$$

S_{ew} (working endurance strength factor) $= S_e/FS$ (2)

S_{syw} (working torsional yield strength factor) $= S_{sy}/FS$ (3)

$S_b = 32M/\pi d^3$ (4)

$S_s = 16T/\pi d^3$ (5)

$S_{sy} = S_y/\sqrt{3}$ (6)

$$d = \left[\frac{32(FS)}{\pi}\sqrt{\left(\frac{M}{S_e}\right)^2 + \frac{3}{4}\left(\frac{T}{S_y}\right)^2}\right]^{1/3} \qquad (7)$$

d = shaft diameter, in.
FS = factor of safety
k = fatigue modifying factor
M = maximum bending moment, lb-in.
S_b = maximum bending stress, psi
S_e = reverse bending endurance strength of shaft, psi
S_{ew} = working bending endurance strength of shaft, psi
S_{re} = reverse bending endurance strength of test specimen, psi
S_s = maximum torsional shearing stress, psi
S_{sy} = torsional yield strength of shaft material, psi
S_{syw} = working torsional yield strength of shaft material, psi
S_y = tensile yield strength of shaft material, psi
T = mean static torsional moment, lb-in.

$S_e = k_a k_b k_c k_d k_e k_f k_g S_{re}$ (8)

S_e = corrected reversed bending endurance strength of shaft
S_{re} = reversed bending endurance strength of rotating beam specimen
k_a = surface finish factor
k_b = size factor
k_c = reliability factor
k_d = temperature factor
k_e = duty cycle factor
k_f = fatigue stress concentration factor
k_g = miscellaneous effects factor

Expressions for Design of Transmission Shafts

the most common variety of loading conditions, namely, fully reversed bending in combination with static torsion, less than torsional yield, with negligible axial loading. Equations (4) and (5) are the classical design equations for bending and torsional stress.

For most steels, the tensile yield strength divided by the square root of 3 is approximately equal to the torsional yield strength [equation (6)]. This relationship and equations (2) through (5) are substituted into equation (1) to yield expression (7).

Equation (7) gives the required solid shaft diameter for known conditions of torque, bending moment, and shaft material. It is the basic shaft design equation proposed for a new shaft standard now being developed.

In equation (7), the reversed bending endurance strength S_e is generally different from the endurance strength found from rotating-beam specimens made from the same material, S_{re}. Many factors have been identified that can affect endurance strength in real service. To account for application differences, modifying factors may be applied to the uncorrected bending endurance strength of test specimens, as shown in equation (8).

Values for some of the fatigue-modifying factors for equation (8) can be found in several of the more recent machine design texts.

This shaft design formula embodies the following features:

- The design formula is predicated on a fatigue failure relation which consists of an elliptical variation of reversed bending endurance strength with static torsional stress.
- The design formula is of simple form and can be readily used with generally available specimen test data to compute the diameter of rotating shafts under the common shaft loading condition of cyclic bending and static torsion.
- Fatigue modifying factors have been incorporated into the design formula to adjust endurance strength test data published for rotating beam specimens for design differences between the shaft in actual service and that experienced by the test specimen.

This design formula has been proposed as the basis for a new standard to replace the withdrawn ASME Code for the Design of Transmission Shafting, ASA-B17C.

This work was done by Stuart H. Loewenthal of **Lewis Research Center.** *Further information may be found in NASA TM-X-73639 [N77-20482], "Fatigue Criterion for the Design of Rotating Shafts Under Combined Stress," which may be obtained at cost from the New England Research Application Center [see page A7].*
LEW-12965

"Nonfloating" Universal Joint

Modified crowned-spline joint transmits rotary motion without axial play.

Lyndon B. Johnson Space Center, Houston, Texas

A new "nonfloating" universal joint uses a ball and socket within a crowned-spline joint to transmit rotary motion with high axial and radial stability. The new design is lightweight and durable and requires a minimum of parts. Compared to most crowned-spine joints, which permit varying amounts of axial play, this joint is exceptionally tight. It does not use rubber cushions to limit play and is therefore useful over a wide temperature range.

The new joint has a conventional crowned (spherical) spline that engages straight spline teeth on the torque tube (see figure). The crown permits limited misalinements between the drive and driven shafts. A monoball bearing is installed at the center of rotation of the crowned spline. The ball may be staked,

(continued next page)

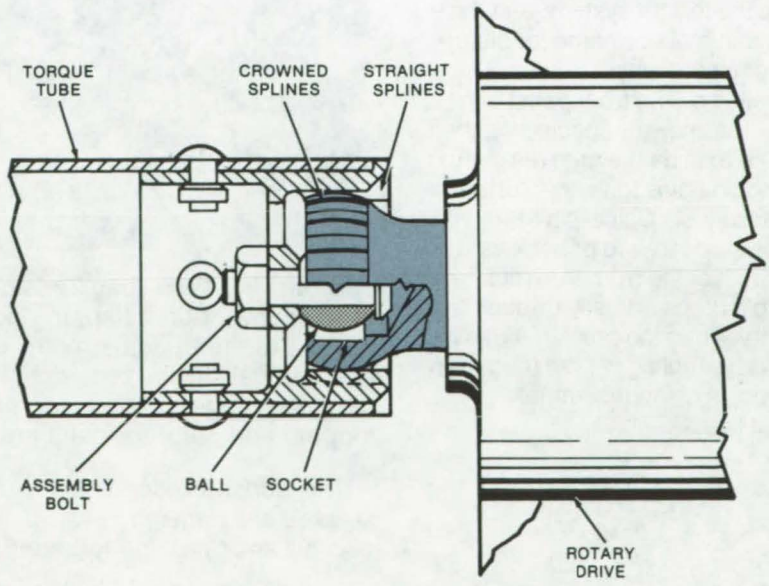

Universal Crowned-Spline Joint has an inner ball and socket to provide a rigid connection with virtually no axial play. The joint can attach a drive shaft to a torque tube, as shown here; or it can be adapted to form a pinned connection between segmented torque tubes.

pressed, or screwed in place, or the spline fitting can be swaged around the ball before the crowned-spline teeth are cut. A bolt through the ball and the female spline fitting holds the assembly together.

The joint can also serve as a universal joint between two torque tubes. The joint forms a pinned connection, and the ends of the tubes are able to "float." To make the pinned connection, the shaft on the crowned spline is formed into a straight spline that engages a female socket in the connecting part. This joint can be held in a bulkhead or other fixed structural support. The pin joint saves weight and facilitates assembly and disassembly.

This work was done by Walter T. Appleberry of Rockwell International Corp. for **Johnson Space Center.**

For further information, Circle 59 on the TSP Request Card.

This invention is owned by NASA, and a patent application has been filed. Inquiries concerning nonexclusive or exclusive license for its commercial development should be addressed to the Patent Counsel, Johnson Space Center [see page A8]. *Refer to MSC-19546.*

Flicking-Wire Drag Tensioner

A simple drag helps to reduce wire bonding rejects caused by uneven looping and clubfoot balls.

Lyndon B. Johnson Space Center, Houston, Texas

A new wire-drag system for a thermosonic gold-ball bonder improves the wire profile and applies a more consistent drag to the wire. The modified wire-drag equipment, based on a flicking-wire system, consists of alinement spacing washers, an adjustment guide-pin bracket, two adjustable tension washers, and a tension arm. The wire drag, installed in place of the former wire tensioner, is continuously adjustable from zero drag to the tensile strength of the wire. The no-sag wire drag is easier to thread than in the former system, and it requires minimal downtime for cleaning and maintenance.

Installed on the front panel of a bonder (as shown), spacing washers are used to aline the grooves in the Teflon guide pins to the centerline of the transducer. Guide-pin brackets are adjusted forward or backward so that wire feeding from the front guide pin drop vertically through the capillary. Then the bracket angle is adjusted, enabling wire to feed from the spool in an approximately straight line.

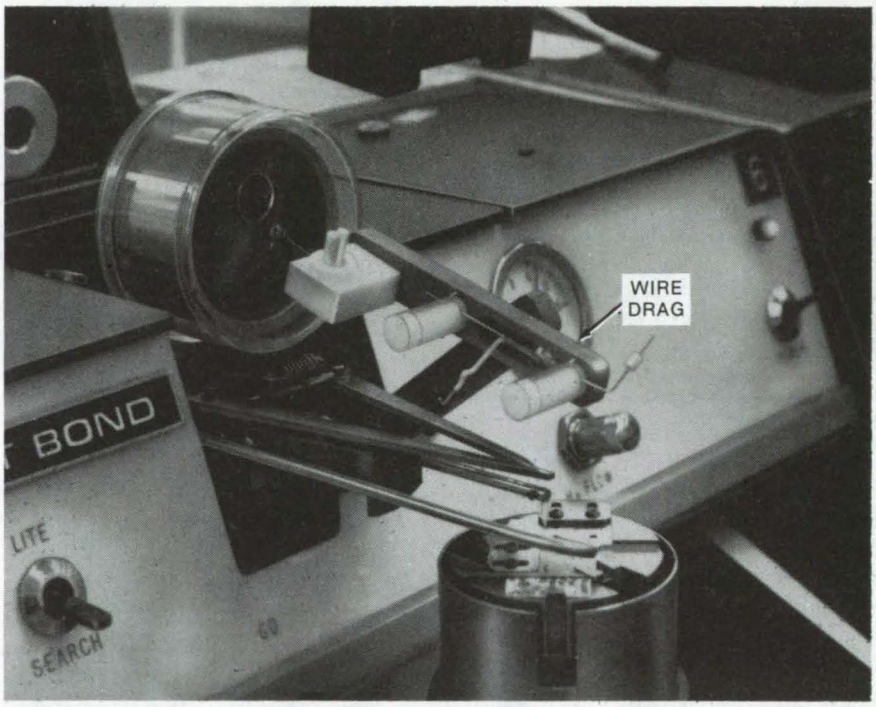

The Flicking-Wire Drag Tensioner is attached to a wire bonder in place of the conventional flapping-door system. Unlike the latter system that offers little drag adjustment, the flicking-wire system can be adjusted continuously from zero drag to the tensile strength of the wire. By reducing drag-tension inconsistencies, bond rejects caused by uneven looping and clubfoot balls are reduced.

This work was done by Michael A. Dassele and Harleigh Fairall of Sperry Rand Corp. for **Johnson Space Center.** *For further information, Circle 60 on the TSP Request Card.*

MSC-16367

Simple Air-Piston Gas-Sampling System

System traps contaminant-free samples without using mechanical pumps.

Lewis Research Center, Cleveland, Ohio

An air-piston gas-sampling system has been developed to obtain a low pressure gas sample without contaminating the sample with pressurizing gas. The design eliminates the need for mechanical pumps that may contaminate or overheat the gas sample. This system was designed into a condensation nuclei counter for use in the NASA's Global Atmospheric Sampling Program (GASP).

A low pressure gas sample is drawn into the system as illustrated in step 1. The exhaust port is connected to the static line from a pitot-static tube of an airliner; in other applications, the exhaust port could be connected to a vacuum pump. Clean pressurizing air is introduced into the system in step 2 and traps the sample at the inlet end. The pressurized gas sample is now drawn from the inlet side for analytical purposes in step 3.

The required volume of pressurized sample and the pressure ratio determine the tube length required to prevent the pressurizing air from contaminating the pressurized gas sample. The equation used was:

$$\text{tube length} = 4\,\frac{\left(\begin{array}{c}\text{pressure}\\ \text{ratio}\end{array}\right)\left(\begin{array}{c}\text{required}\\ \text{sample volume}\end{array}\right)}{(\text{tube cross-sectional area})}$$

The equation accommodates for dead volumes from fittings and the mixing region between the pressuring and sample gas. For example, for a pressure ratio of 4 to 1, a required sample volume of 1.2 in^3 (19.67 cm^3), and a tube inside diameter of 0.43 in. (1.09 cm), an 11.0 foot (3.37 meter) length of tubing is used with a spiral strip inserted in the center of the tube for boundary layer mixing.

This system can be used for sampling rates of 0.3 to 3.0 $in.^3$/sec (5 ot 50 cm^3/sec) and pressure ratios of 4 to 1 or less.

This work was done by Ted W. Nyland of **Lewis Research Center.** *No further documentation is available.*
LEW-12922

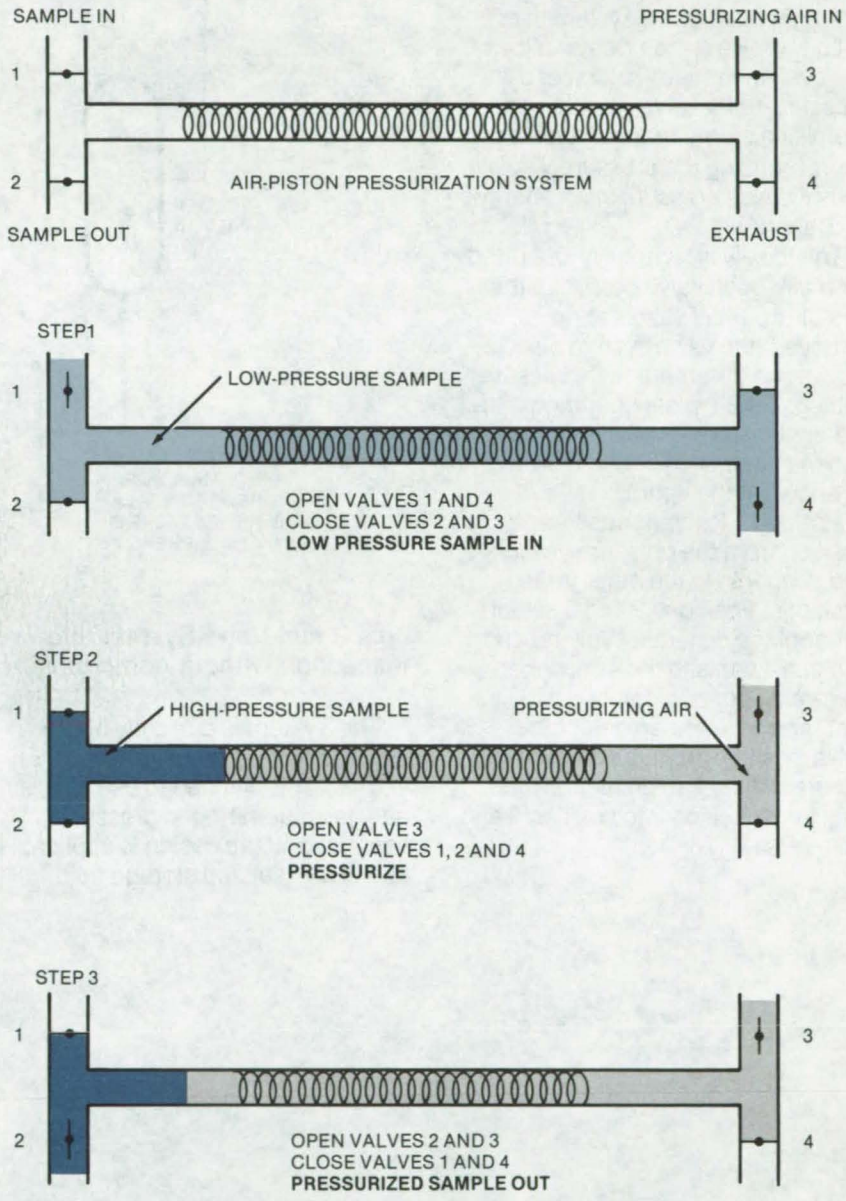

Air-Piston Pressurization System traps a gas sample in three steps. Pressurized sample is withdrawn from port 2 following step three.

Dual Relief-Valve System

Pressure-relief valve can be removed without depressurizing system.

Langley Research Center, Hampton, Virginia

A dual relief-valve system in use at Langley Research Center allows removal and recertification of a pressure-relief valve without compromising safety requirements or depressurizing the pressure vessels. Thus it saves pressurization energy and labor.

The four-way, manually-operated, normally-open valve permits either one of two relief valves to be removed; the valve system also allows two different relief-pressure settings for a typical operation. Off-the-shelf readily-available components are used to build the valve as shown in the figure.

Position 1 is the normally-open position from the pressure vessel and connects to the other three positions. Positions 2 and 3 select either of the dual relief valves, and position 4 vents to the atmosphere. This vent acts as a safety device in that the operator can detect the valve-position change across it to ensure that he has, in fact, switched fully from position 2 to position 3 and vice-versa.

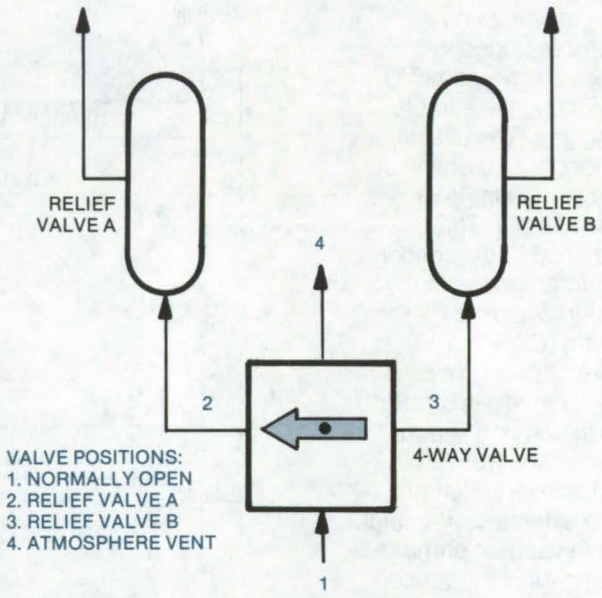

Dual Relief-Valve System allows pressure-relief valve to be removed for inspection without compromising system safety.

This system is currently in use with methane-storage pressure vessels. It is planned to use it for air and gaseous-nitrogen pressure vessels, and the design is applicable to any pressurized storage field, whether gaseous or liquid.

This work was done by John R. Karns and William R. Latta of **Langley Research Center.** *No further documentation is available. LAR-12267*

Fabrication Technology

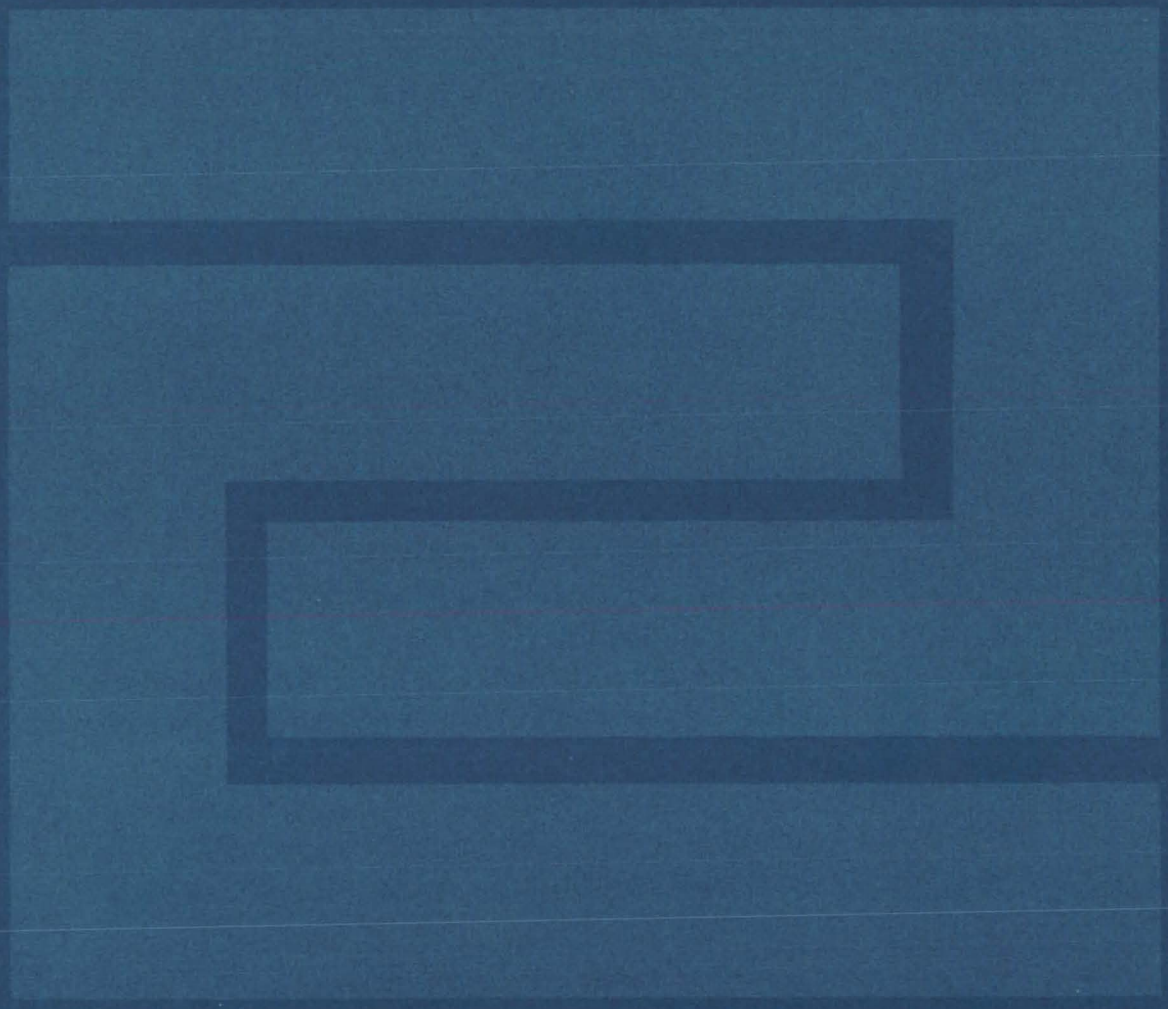

Hardware, Techniques, and Processes

Books and Reports

Computer Programs

High-Temperature Brazing of Stainless Steel

Prevention of iron contamination of platens and other process improvements lower cost and improve effectiveness.

Lyndon B. Johnson Space Center, Houston, Texas

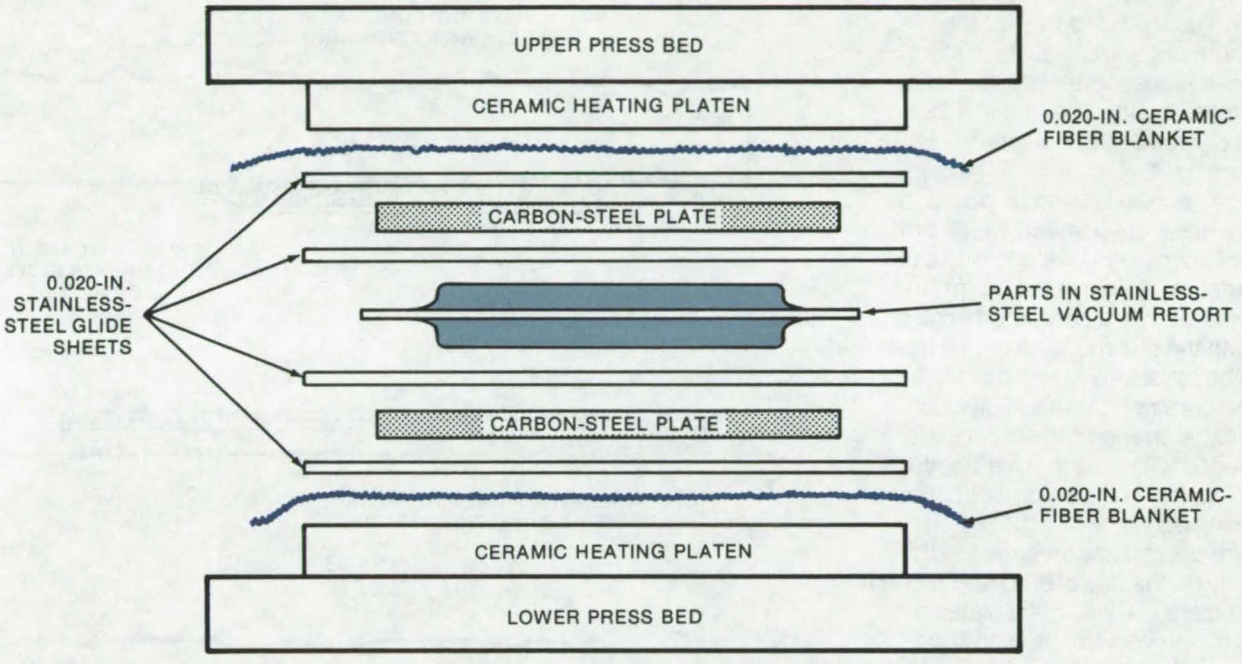

Platen Press Layup for vacuum brazing incorporates ceramic blankets to prevent iron contamination.

High-temperature high-pressure vacuum brazing has not generally been used as a method of fabricating stainless-steel parts, because of costs and technical problems with the process. Recently, several innovative tools and procedures were developed for high-temperature brazing of stainless-steel cold plates for NASA's Space Shuttle. These are described in this and three other articles in this issue of *NASA Tech Briefs* (see references at the end of this article). With these improvements, the process can now be considered as an effective and economical method of fabricating stainless-steel parts.

Previously, vacuum brazing of stainless steel had been limited to a combined pressure and temperature of around 200 psi (1.4×10^6 N/m^2) and 1,100° F (590° C). Under these conditions, the temperature was not high enough to insure a strong braze. Yet, if the temperature were raised, the fused silica platens would become contaminated with iron and would fail.

The problem of iron contamination has been eliminated by modifying the brazing setup. As shown in the figure, alumina/silica ceramic-fiber blankets are placed between the platens and the carbon-steel plate.

The carbon-steel plates are used to provide rigidity and improve heat transfer. Using only the carbon-steel plates and the ceramic blanket, some iron contamination still occurred. The thin stainless-steel glide plates were added, and the fused silica platens have been used at 2,000° F and 200 psi (1,090° C and 1.4×10^6 N/m^2) for 50 cycles without damage.

This work was done by Charles S. Beuyukian, Robert M. Heisman, and Mike J. Mitchell of Rockwell International Corp. for **Johnson Space Center.** *Related articles in this issue of NASA Tech Briefs are:*

"Form Die and Glide Plates for Vacuum Brazing" [MSC-16549],
"Internal Grid for Release of Brazing Retorts" [MSC-19472], and
"Vacuum Control for Brazing Stainless Steel" [MSC-19457].

For further information, Circle 61 on the TSP Request Card.
MSC-19459

Form Die and Glide Plates for Vacuum Brazing

Two innovations that lower cost of vacuum brazing

Lyndon B. Johnson Space Center, Houston, Texas

Two new procedures for the vacuum brazing of stainless steel lower the cost of this process and improve results. The first is a low-cost plywood form die for the retorts.

The new die is used to form pans in stainless-steel sheet, which are then folded and welded to make the retorts. As shown in the figure, the female die has a contoured edge to fit with the punch. A die of this type can be made easily and quickly by using commercial-grade plywood. For extra strength, the plywood is surfaced with an adhesive-bonded steel facing that also protects the forming edges.

The second improvement in the brazing is the use of smooth-finished glide plates. These glide plates are used when vacuum brazing stainless-steel cold plates; with a standard (rms 64) finish, the glide plates were found to partially bond to the stainless-steel parts.

Investigation showed this to be due to "washout" through even the slightest surface openings of a stop-off material used as a release agent. By finishing the glide plates to around rms 32 and by controlling their flatness, it is possible to insure full contact under platen-press pressure and to prevent washout of the release agent. Thus, the smooth finish will prevent the partial bonding of the glide plates to the stainless-steel part, an unexpected result since a smooth finish usually increases bonding.

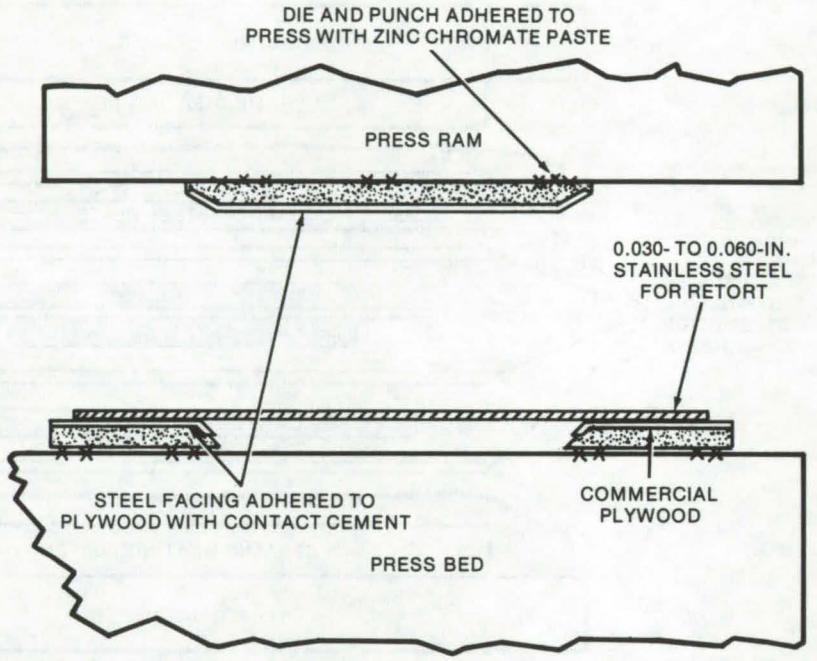

Form Die for fabricating steel retorts used in vacuum brazing is made from commercial plywood with a steel facing. Setup on the press is made with zinc chromate paste or double-backed adhesive tape.

This work was done by Charles S. Beuyukian and Mike J. Mitchell of Rockwell International Corp. for **Johnson Space Center.** *Related articles in this issue of NASA Tech Briefs are:*

"High-Temperature Brazing of Stainless Steel" [MSC-19459],
"Internal Grid for Release of Brazing Retorts" [MSC-19472], and
"Vacuum Control for Brazing Stainless Steel" [MSC-19457].

For further information, see the TSP reference at the end of "High-Temperature Brazing of Stainless Steel" on page 121.

MSC-16549

Low-Chromium Stainless Steels

Two modified stainless-steel formulations, with only two-thirds the chromium content found in conventional type 304, have mechanical and chemical properties that are comparable to type 304. The low-chromium stainless steels have potential uses in heat exchangers, transfer lines for chemicals, automobile trim, and other applications.
(See page 53.)

Fire-Retardant Foams

Foams being developed from a new family of polyimide resins have exceptional fire-retardant properties and are potentially useful in air and ground applications. These thermally stable foams release virtually no smoke or toxic products when exposed to high temperatures. Additional research to optimize their mechanical properties for commercial use is underway.
(See page 59.)

Ultra-High-Strength Boron Fibers

Boron-on-tungsten fibers with tensile strengths and strain-to-failure values increased by 50 percent over commercial grades are produced by a controlled chemical-etching process. The improved fibers have potential applications as lightweight composites in ground vehicles, spacecraft, and rotors for energy storage.
(See page 57.)

Internal Grid for Release of Brazing Retorts

Internal wire grid reduces thermocouple damage.

Lyndon B. Johnson Space Center, Houston, Texas

Another improvement in the vacuum brazing of steel parts (see the references at the end of this article) is the design of an internal wire grid that facilitates release of the retorts. A pattern of wires 1/8 in. (0.32 cm) in diameter is attached to the skirt area.

The grids permit the retorts to be opened more quickly after brazing. Formerly, it was necessary to machine through partially bonded areas when opening them, which often damaged thermocouples in the retorts. The grid also aids purging and evacuation and allows better control of the vacuum in the part area. [See "Vacuum Control for Brazing Stainless Steel" (MSC-19457) in this issue.]

The grid wires are shown in the figure installed in a stainless-steel retort just prior to closure for edge welding. The wires keep the sides of the vacuum retort separated even though they soften at the 2,000° F (1,090° C) brazing temperature.

Without the grid, the vacuum brings the internal skirt areas into localized contact, where partial welding occurs. The grids are coated by brushing on an amount of white stopoff.

In the figure it can be seen how the thermocouple leads are protected by the grid. These leads are sealed through the folded edge of the retort and can be easily removed, when cutting is not required to open internally welded areas.

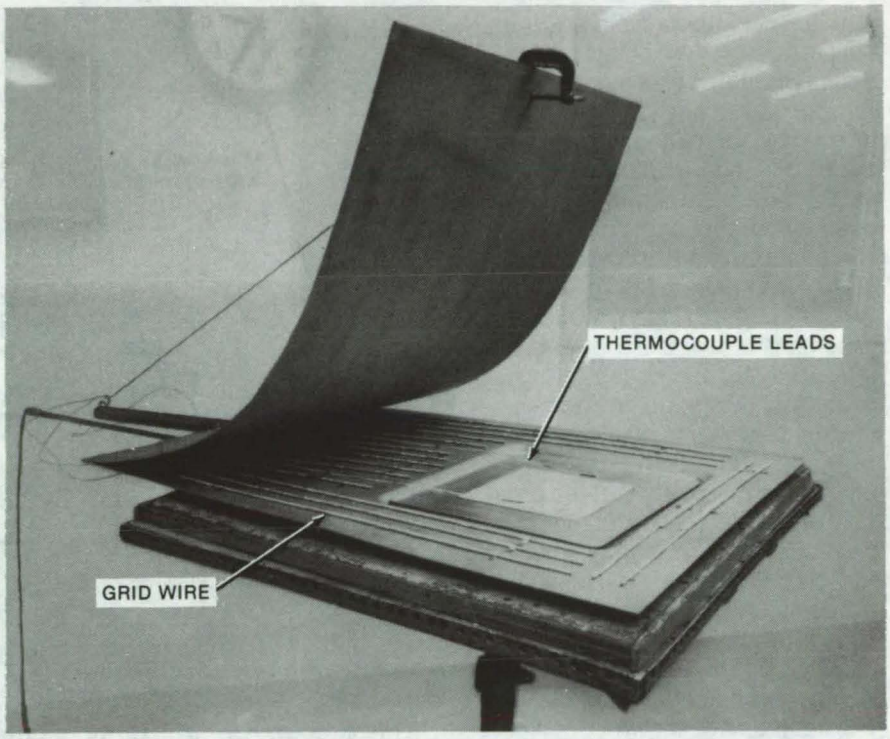

Wire Grid for Brazing Retort is made of 1/8-in. 347 alloy stainless-steel welding rod. It is held in place by stainless-steel foil clips attached with a portable spotwelder.

The grid of wires aids vacuum exhaust by forming channels leading to the vacuum exhaust tube in the rear (folded side) of the retort. These channels have been found to allow better control of the internal vacuum.

This work was done by Charles S. Beuyukian and Mike J. Mitchell of Rockwell International Corp. for **Johnson Space Center.** *Related articles in this issue of NASA Tech Briefs are:*

"High-Temperature Brazing of Stainless Steel" [MSC-19459],
"Form Die and Glide Plates for Vacuum Brazing" [MSC-16549], and
"Vacuum Control for Brazing Stainless Steel" [MSC-19457].

For further information, see the TSP Reference at the end of "High-Temperature Brazing of Stainless Steel" on page 121.

MSC-19472

Vacuum Control for Brazing Stainless Steel

Low-temperature outgassing improves braze quality.

Lyndon B. Johnson Space Center, Houston, Texas

When constructing pin-fin stainless-steel cold plates for the Space Shuttle, it was found that reliable nonleaking joints could be insured by controlling the outgassing during brazing. An improved vacuum-retort system was developed for purging, inert-gas filling, and controlling the absolute pressure of the vacuum retort. This vacuum-control system reduces the vaporization of braze-alloy and release-agent components, resulting in a significant improvement in the brazing quality.

The vacuum-control system utilizes the discovery that the pressure of the inert gas (argon) should be kept at about 25 microns of Hg (3.3 N/m²) both during the initial evacuation for inert-gas backfill and during the initial low-temperature heating. This increases outgassing to a level needed for quality brazes. The controls are shown in the figure.

The lines from the vacuum source were increased from 3/8 to 1 in. (0.95 to 2.5 cm), and internal retort grids were installed to control the pressure at the braze area more accurately. [See "Internal Grid for Release of Brazing Retorts" (MSC-19472) in this issue.]

The initial low temperature and "high" vacuum do not degrade the braze alloy and stopoff materials. Contamination during the 2,000° F (1,095° C) brazing cycle can be prevented by increasing the inert-gas pressure to about 200 microns Hg (27 N/m²).

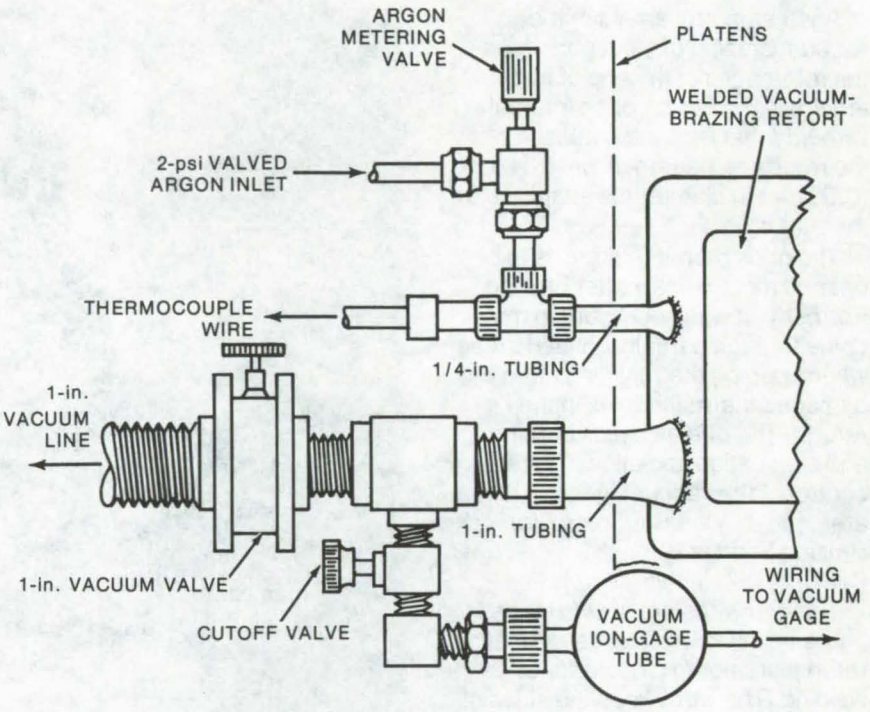

The Vacuum-Control Components for improved vacuum-retort brazing of stainless steel combine enlarged vacuum lines with bypass valving for intermittent exposure of the vacuum sensor. A needle valve controls the argon inlet to allow the pressure to be increased during the high-temperature brazing period.

Another problem with the 2,000° F brazing, the short life (usually one cycle) of the vacuum sensor, was also solved. The sensing unit is damaged by outgassing material, and merely teeing the sensor out of the main flow line does not solve the problem. In the new system, contamination is prevented by using a valved sensor that is closed during the initial heavy outgassing, except for intermittent brief readings.

This work was done by Charles S. Beuyukian and Mike J. Mitchell of Rockwell International Corp. for Johnson Space Center. *Related articles in this issue of NASA Tech Briefs are:*

"High-Temperature Brazing of Stainless Steel" [MSC-19459],
"Form Die and Glide Plates for Vacuum Brazing" [MSC-16549], and
"Internal Grid for Release of Brazing Retorts" [MSC-19472].

For further information, see the TSP reference at the end of "High-Temperature Brazing of Stainless Steel" on page 121.

MSC-19457

Process Fabricates Flat Panels at High Temperatures

Panel contours are precisely recorded on a compression grid for compensating machining operations.

Lyndon B. Johnson Space Center, Houston, Texas

The thickness of large flat panels at high temperatures can be controlled within 0.012 inch (0.03 cm) by an improved process that precisely records the panel contour on a special grid.

The grid compression procedure was originally developed for fabricating flat aluminum cold plates for the Space Shuttle. The plates are made by brazing aluminum sheets to a honeycomb structure while the assembly is held between the platens of a hot press. At the brazing temperature of 1,200° F (649° C), the platens tend to warp, so that the flatness of the panels is not within specifications. With the new procedure, a compensating contour plate can be machined to ensure that the cold plates are flat when they are brazed.

The compression grid contains an array of square pads, or "nodes." (The nodes are more densely concentrated at the extremities of the grid, where the distortion is most severe; see figure.) This grid, which is made of aluminum, measures 2 by 3-1/2 feet (0.61 by 1.06 m). After the grid has been pressed in the platens at the brazing temperature, the height of each node is carefully measured and recorded. From the measured data, a tape is prepared for a numerically-controlled machine tool that adjusts the contours of the copper heat sinks 1/4 inch (0.64 cm) thick used in the heated-press brazing process.

If plates having even greater flatness are required, the procedure can be repeated. That is, the platens can be used to compress a second grid. When the grid has been measured, a new tape can be prepared, and the heat sinks can be further machined.

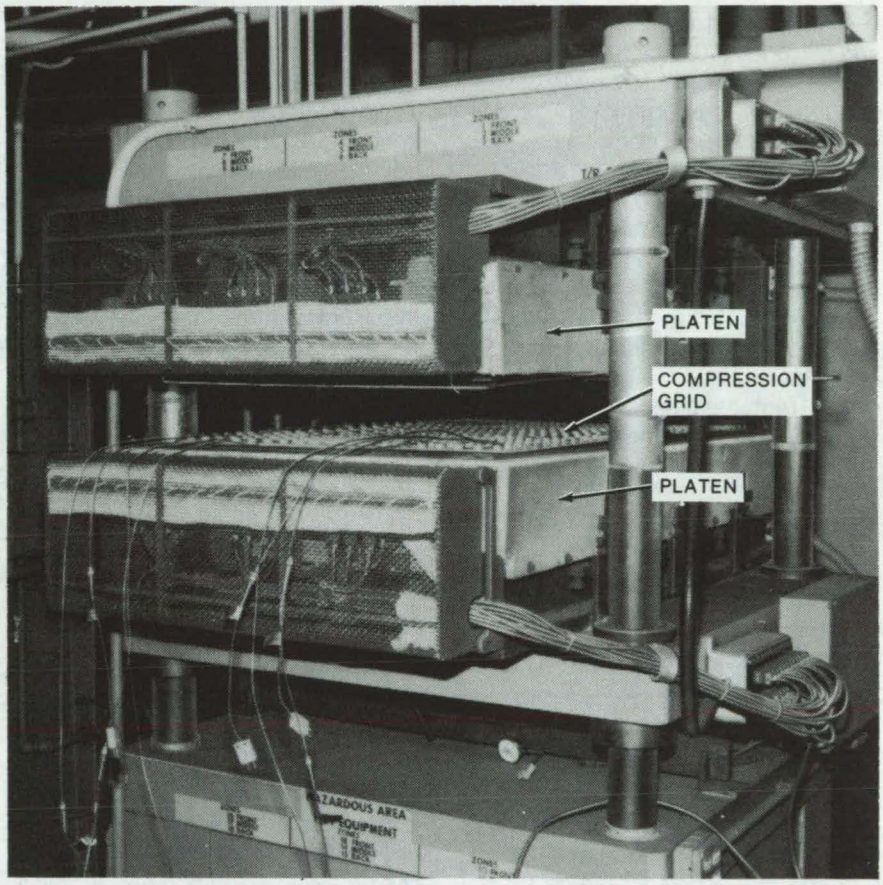

The Compression Grid Is Sandwiched between hot-press platens at 1,200° F. Grid "nodes" provide a permanent record of the platen contour for machining compensating plates used in high-temperature brazing operations.

This work was done by Charles S. Beuyukian, Robert M. Heisman, and Mike J. Mitchell of Rockwell International Corp. for **Johnson Space Center.** *No further documentation is available. MSC-16969*

Two Braze Alloys for Thin-Wall Components

Two braze alloys are compatible with high-temperature heat treatment of thin-wall components.

Marshall Space Flight Center, Alabama

A 1,900° F (1,045° C) braze alloy and a 1,800° F (990° C) second-cycle alloy have been developed for brazing iron/nickel/chromium thin-wall components. The alloys stay very strong up to 1,500° F (820° C) and are compatible with the base metals.

The first alloy has a brazing-temperature range of 1,900° to 1,925° F (1,045° to 1,060° C) and has a nominal composition by weight of 35 Au, 10 Pd, 14.5 Ni, 9.5 Mn, 0.1 La, with the balance Cu. The second, with a brazing temperature range of 1,775° to 1,825° F (975° to 1,005° C), is 38 Au, 2.5 Pd, 4.3 Ni, 8.0 Mn, 0.1 La, and the balance Cu. The densities are 0.46 lb/in.^{3} (0.62 kg/cm^3) and 0.47 lb/in.^{3} (0.63 kg/cm^3), respectively.

Both alloys are ductile and are not subject to hydrogen or cryogenic embrittlement. During the brazing operation both alloys demonstrate excellent wetting, flow, and gap-filling capabilities. Each resists oxidation and salt-spray corrosion.

The new alloys are producible as foils, tape, wire, and powder and may be brazed in either an argon or a hydrogen atmosphere. They are less dense and less expensive than other commonly used alloys in the same braze-temperature range and may be used to join stainless steels, precipitation-hardened stainless steels, and nickel and cobalt high-temperature alloys.

This work was done by Alexander Brennan and Ross D. McKown of Rockwell International Corp. for **Marshall Space Flight Center.** *For further information, Circle 62 on the TSP Request Card.*
MFS-19206

Laser Wire Stripping

Bench-mounted and hand-held laser units cut insulation from wires without nicking or scraping the conductor.

Lyndon B. Johnson Space Center, Houston, Texas

Using a laser beam to remove insulation from a wire is cost-effective for production operations that require the stripped wire to be completely undamaged. A recent report, "Selected Developments in Laser Wire Stripping" (NASA SP-5107), describes various equipment, techniques, and applications of this process. Both bench-mounted and hand-held laser stripping units are in operation, and in some applications a single CO_2 or YAG laser can provide the cutting beams for several of the units.

A laser beam can cut through the insulation on a wire without damaging the conductor because the focused laser radiation that vaporizes the insulation is merely reflected by the underlying metal. Therefore a wire stripper that uses a laser beam eliminates the quality-control problems of nicked, scraped, or cut conductors; moreover, the process is fast, clean, precise, and repeatable.

The laser beam cuts insulation by the process of ablation — i.e., by melting and vaporization; this mechanism requires absorption of roughly 100 kW/in.^{2} (15 kW/cm^2) at the surface of the insulation. For high-power density, a short wavelength is favored; however, in some cases the short waves may be reflected from the insulation instead of being absorbed by it, so a longer wavelength can often be more effective. For example, Teflon absorbs the 10.6-μm radiation from a CO_2 laser, but reflects the 1.06-μm beam from a YAG laser.

A bench-model laser wire stripper, built for Space Shuttle production manufacturing, uses a CO_2 laser and an optical system that deflects the beam. Stripping is initiated by inserting the wire into a collet, which positions it directly in line with the laser beam. A shutter is actuated, and the focused laser beam impinges directly on the wire surface; the beam rotates about the wire and then moves along the desired length to remove the insulation. A gas jet and vacuum system remove the vapors and debris produced during the stripping. Several stripping stations can be operated either simultaneously or on a time-sharing basis from a single laser beam by using beam splitters to distribute the beam to each stripper.

A hand-held wire stripper that contains a compact 2.5-W CO_2 laser is connected to a control cabinet by cables and hoses that carry high-voltage power, the CO_2 gas mixture, and cooling water to the laser, as well as power, oxygen, and vacuum to the rotating optical assembly. However, another hand-held unit leaves the laser in the control

cabinet; the light beam is carried to the stripper head by a fiber-optic cable. The laser used in this system cannot be a CO_2 type, because no fiber-optic transmission guides exist for the 10.6-μm infrared radiation from such lasers. Instead, a Nd:YAG laser that emits coherent radiation at 1.06 μm is used.

The beam from the Nd:YAG laser can also be fed into a bench-type laser stripper in place of the beam from the CO_2 laser, and a single Nd:YAG laser can drive several hand-held and/or bench-type wire strippers on a time-sharing basis.

The report, NASA SP-5107, "Selected Developments in Laser Wire Stripping," describes the development of laser-beam wire strippers for Space Shuttle production. The desired performance quality and operating speed are defined, and the advantages of laser stripping over conventional strippers for meeting these standards are discussed. Then the system parameters are established: laser power, optics, mechanical arrangements, and controls. The bench-mounted and hand-held units are described in detail, and step-by-step procedures for their operation are given.

The report concludes with a chapter on additional variations and modifications for the laser, the rotating optical system, the control elements, and cutting techniques for various types of wires. An appendix lists further references and sources.

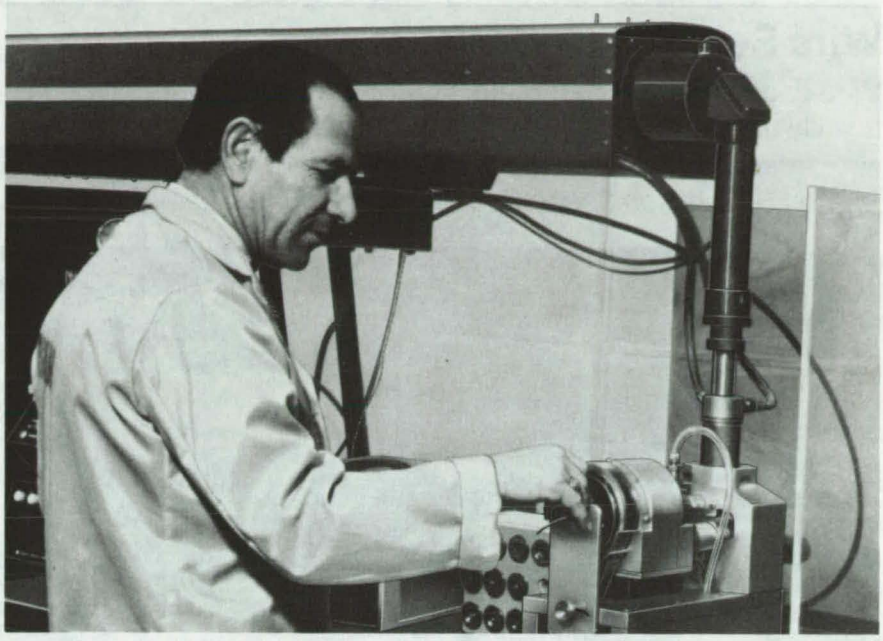

A Laser Wire Stripper is used in the production of wiring assemblies for the Space Shuttle. The CO_2 gas laser is at the top of the photo, and its beam is deflected down into the rotating optical assembly where the wire is automatically stripped upon insertion into a collet.

This work was done by Robert M. Heisman, William F. Iceland, Andrew R. Keir, Lester A. Small, and Floyd R. Yearian of Rockwell International Corp. for **Johnson Space Center.** *To obtain a copy of NASA SP-5107, "Selected Developments in Laser Wire Stripping," Circle 63 on the TSP Request Card.*
MSC-18000

Calculating Wire-Bundle Diameter

Diameters are estimated accurately, allowing rapid determinations of clamp sizes.

Lyndon B. Johnson Space Center, Houston, Texas

The outside diameters of wire bundles can be calculated rapidly and accurately by using a table of empirical factors — called "bundle factors" (BF). This technique allows closer sizing of the brackets and clamps needed to hold wire harnesses in place and allows more rapid determinations of the clamp sizes.

The table is constructed by using the empirical formula:

$$BF = \sqrt{1.49n}$$

where n is the number of wires in the bundle. The formula holds for n greater than 1; for n = 1, the bundle factor is 1.00.

If the wires in a bundle all have the same outside diameter (OD), the estimated wire-bundle diameter will be (OD)(BF). If the wires in the bundle have different outside diameters, the number and OD of each type are multiplied; then the sum of these products is divided by the total number of wires, and the result is multiplied by BF (for the total number of wires) to obtain the estimated bundle size.

This work was done by Eugene J. Stringer of Rockwell International Corp. for **Johnson Space Center.** *For further information, Circle 64 on the TSP Request Card.*
MSC-16378

Wire Selector/Calculator

Wire gage and other parameters can be quickly determined, using a circular calculator.

Lyndon B. Johnson Space Center, Houston, Texas

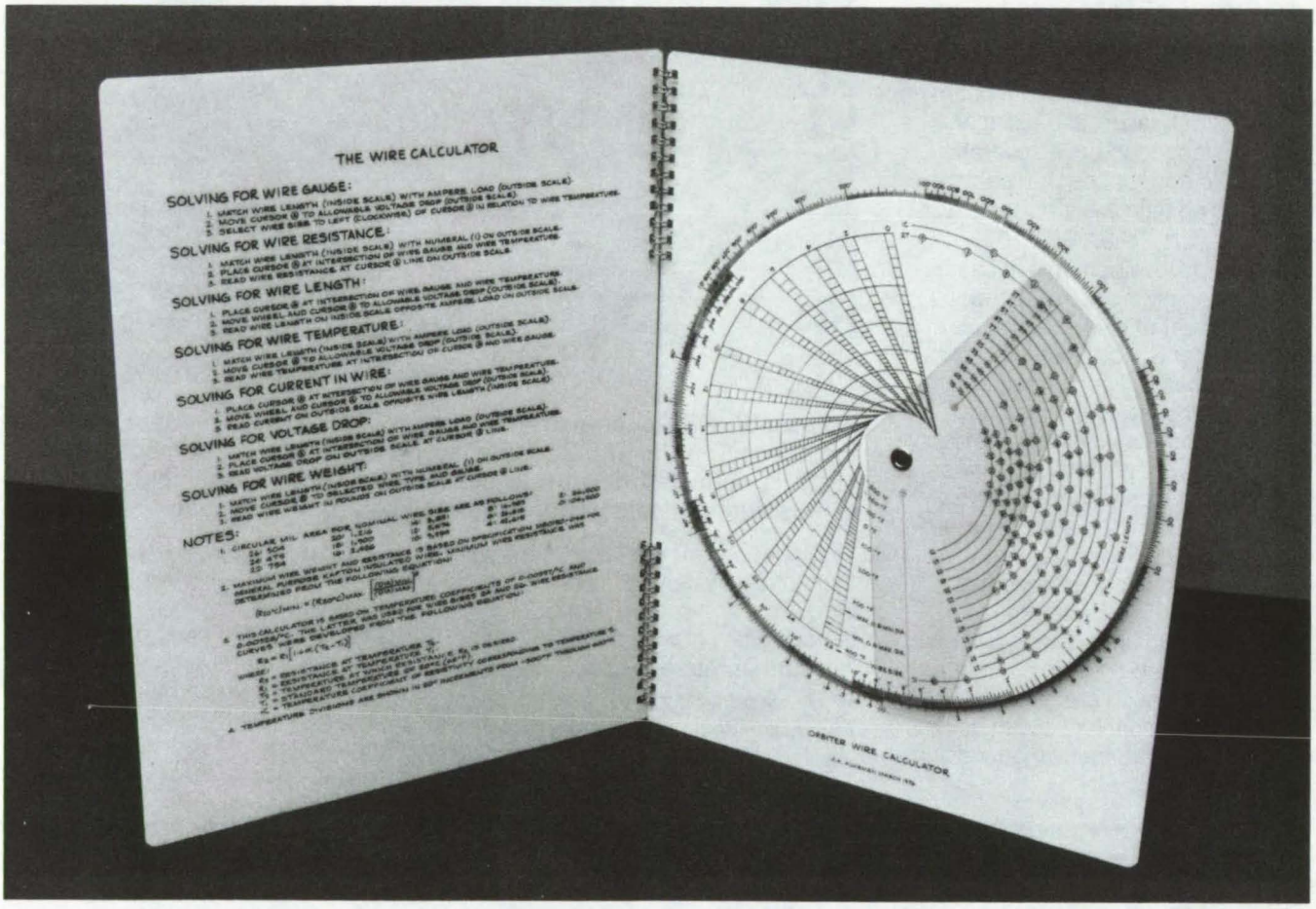

A laminated folder encloses the Wire Calculator and displays instructions for wire calculations. Useful data are tabulated on the other side of the folder.

A slide-rule type calculator helps engineers design — but not over-design — electronic wiring. For instance, given the wire length, current, allowable voltage drop, and temperature rise, an engineer can select the proper wire gage with the calculator; or given the wire length, wire gage, and temperature rise, the engineer can quickly calculate the resistance of the wire. The cost and weight of wire are reduced, and design time is saved.

The calculator has a circular disk containing five scales that rotate in relation to a fixed scale (see figure). A precision bearing pin holds the disk and the clear plastic cursor. The calculator is held in a folding booklike enclosure that gives step-by-step instructions and presents useful tables — for example, data on standard circuit breakers.

To determine wire weight, the user matches wire length on the disk with the number "1" on the outside scale, moves cursor line B to the selected wire type and gage, and reads the wire weight in pounds on the outside scale at cursor line A.

The calculator was developed for use in designing the Space Shuttle, the electrical/electronics systems of which contain about 16,000 voltage-sensitive circuits with 40,000 separate wires. The calculator has allowed these wires to be selected rapidly, accurately, and according to uniform standards. The calculator can be used without modification for systems employing the same aircraft-grade wire; it can be adapted for use in other systems that require optimum wire sizing.

This work was done by James R. Fuhrman of Rockwell International Corp. for **Johnson Space Center.** *For further information, Circle 65 on the TSP Request Card.*
MSC-16632

Bench-Top Soldering Aid for PC Boards

A rack for holding pc boards combines several features that help speed up production.

Lyndon B. Johnson Space Center, Houston, Texas

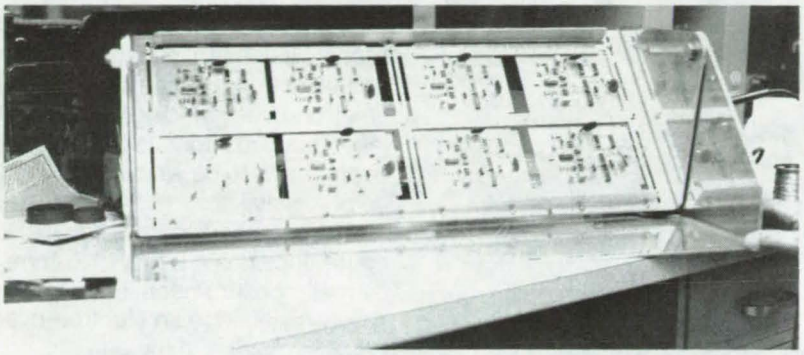

(a) LOADING POSITION

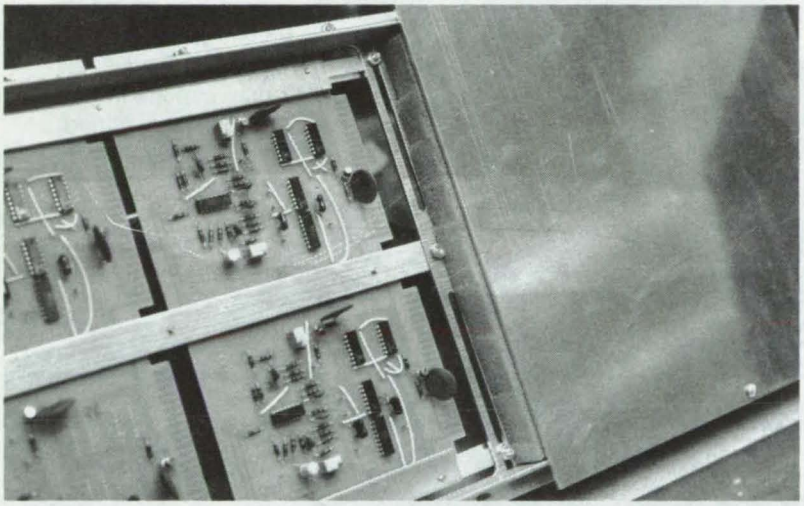

(b) COMPONENT CLAMPING

(c) SOLDERING POSITION

The **Bench-Top Soldering Rack** is shown in the loading position (a), with one retainer plate in place (b), and in the soldering position (c).

Large-scale or small-scale production can be speeded up with the multiple-board rack shown in the illustrations. When neither wave soldering nor dip soldering are appropriate or available, this frame allows a technician to insert components into several boards, flip them all with a single motion, and then systematically solder the leads on the reverse side.

The rack is relatively inexpensive to construct and combines several features that make it more efficient than conventional soldering frames. Two adjustable crossbars allow boards of any size up to 10 by 24 in. (25 by 61 cm) to be clamped in place. After the components are inserted, two foam-backed plates are used to hold all the boards and components firmly in place. The rack can then be rotated to present the reverse side for soldering. The angle of the boards can be varied for work from a standing or sitting position.

This work was done by Noel R. Manton and Richard A. Schroff of Rockwell International Corp. for **Johnson Space Center.** *No further documentation is available.*
MSC-16274

Laser Beam Assists in Precision Welding

Electron-beam welding is made more precise by using laser-aiming.

Marshall Space Flight Center, Alabama

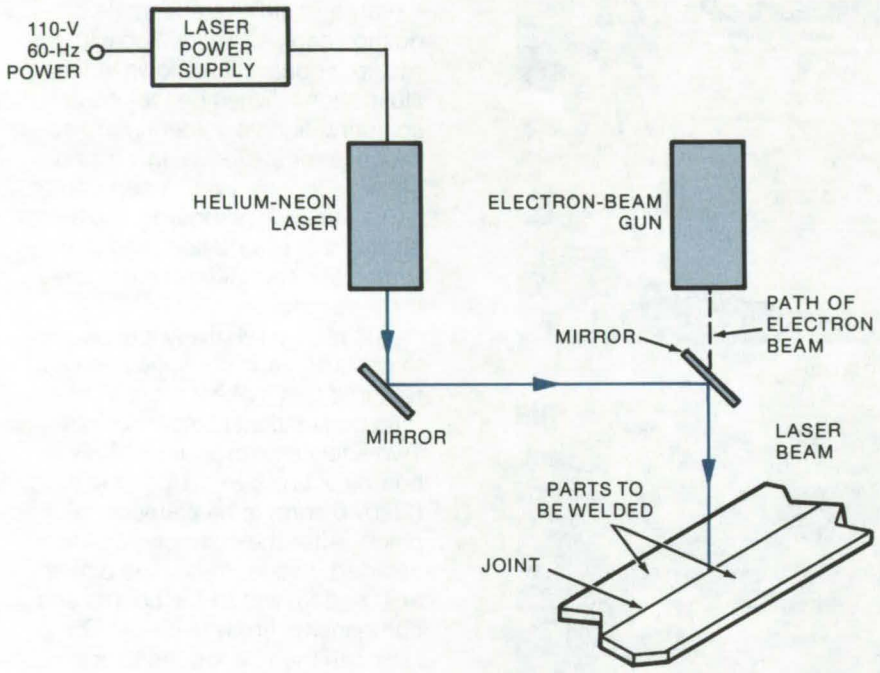

A Helium-Neon Laser Is Used to aline parts for electron-beam welding. A standard 2-mW laser with a 1.5-mm beam may be used.

An improved aiming method that uses a laser beam eliminates trial-and-error beam alinement in electron-beam welding. By using the laser beam to simulate the electron beam, parts to be welded are lined up precisely.

One proposed setup, shown in the figure, includes a 2-mW, 1.5-mm-diameter helium-neon laser that is rigidly fastened to an electron-beam gun. The laser and the gun are alined with their beams parallel. With the electron beam off, the light beam is transmitted by mirrors to the spot that will be welded. The electron-beam gun is turned on once the parts are correctly alined.

This work was done by Vincent R. Tolmei of Rockwell International Corp. for **Marshall Space Flight Center.** *For further information, Circle 66 on the TSP Request Card.*
MFS-19319

Tool Simplifies Weld Preparation of Aluminum

Cutting tool that mounts in a riveting gun removes material quickly and safely.

Lyndon B. Johnson Space Center, Houston, Texas

A special cutting tool prepares aluminum for welding quickly, easily, and cleanly. The tool, a chisel that can be installed in a pneumatic riveting gun, has a V-shaped cutting end that slopes slightly to the rear for easy penetration of the material and contains a tunnel through its middle for efficient removal of the cuttings (see figure).

The tool can be used to cut a V-groove that allows the weld zone to penetrate into the base material. It also removes cracked or porous material — from an improper weld, for example, ensuring integrity in a new weld. Furthermore, the tool can get at hard-to-reach areas, such as the inner parts of I-beams.

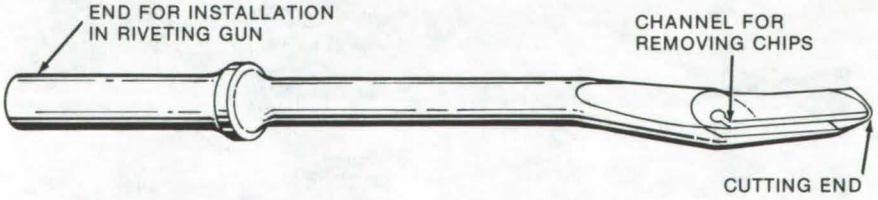

Weld-Preparation Chisel fits into a standard riveting gun. The midsection is bent slightly for easier access to the work, and the cutting end is V-shaped for faster removal of material.

Previously, weld preparation was done with a hand chisel; or, an abrasive grinding wheel was used. The wheel, however, invariably grinds some of its own material into the base metal and contaminates it.

The tool can be machined from 3/4-inch (1.9 -cm) tool-steel round stock, or it can be made from a long rivet by heating and forming the cutting end.

This work was done by Hershel C. LaRue and Edwin L. Shropshire of **Johnson Space Center.** *No further documentation is available.*
MSC-16992

High-Vacuum, Low-Temperature Bond for Second-Surface Mirrors

Indium solder reliably bonds second-surface mirrors to radiant coolers in cryogenic environments.

Marshall Space Flight Center, Alabama

A very-reliable mounting technique for second-surface mirrors in cryogenic environments uses indium solder to attach the mirror to a metal surface (for example, a radiant cooler for a quartz-crystal microbalance). Organic silicone cements have been used in the past for this application; however, they have been found to be unreliable at cryogenic temperatures. In high-vacuum applications, the silicones also have poor out-gassing characteristics.

First, the mirror is tinned with pure indium solder having a melting point of 157° C. Indium is a highly ductile metal that can absorb any thermal stress caused by expansion of the mirror. Next, the metal radiator to which the mirror is to be attached is tinned with an indium eutectic quaternary (In, 21 percent; Bi, 49 percent; Pb, 18 percent; and Sn, 12 percent) with a melting point of 58° C.

The mirror is attached to the metal structure in an oven that is heated to 75° C. At this temperature, the eutectic solder on the metal surface turns liquid, and the mirror with its indium-tinned surface is floated on the surface and positioned. Next, the oven temperature is slowly lowered to ambient, and the bonded component is removed.

Tests have shown that the bond does not deteriorate during temperature cycling between 300 and 100 K. In one application, the strength of adhesion was demonstrated when the metalized coating on the back of the mirror was pulled off before the indium solder fractured.

This work was done by D. McKeown and G. Sonnenschein of Faraday Laboratories Inc. for **Marshall Space Flight Center.** *For further information, Circle 67 on the TSP Request Card.*

Inquiries concerning rights for the use of this invention should be addressed to the Patent Counsel, Marshall Space Flight Center [see page A8]. Refer to MFS-23405.

Inspection of Adhesive-Bonded Radiators

Adhesive-bond thickness in honeycomb-sandwich radiators is verified by visual inspection.

Lyndon B. Johnson Space Center, Houston, Texas

A nondestructive method has been developed for the verification of the tube-to-facesheet bond in honeycomb-sandwich radiators. These radiators include a facesheet 0.011 inch (0.28 mm) thick adhesively bonded to a set of flow tubes. During the curing process, pressure from an autoclave creates a visible markoff of the tube through the facesheet. Through several years of experience, it was determined that this markoff is directly related to the 0.003- to 0.004-inch (0.076- to 0.102-mm) adhesive thickness necessary for the minimum heat-transfer properties of the adhesive-bonded radiators.

Now, this markoff through the facesheet is being used as an inspection aid to verify the critical adhesive thickness. The method is inexpensive and may be considered in verifying bond thicknesses in solar converters, collectors, and concentrators.

This work was done by Madison W. Reed of Vought Corp. for **Johnson Space Center.** *No further documentation is available. MSC-18062*

Glass Tubes for Protecting Solar Cells

Protecting solar cells against environmental effects might be accomplished more easily and cheaply by putting them inside glass tubes instead of hermetically sealing them between a pair of flat glass sheets. If the cells are coupled with a storage battery integrated into the tube, a freestanding power source could be built.

(See page 38.)

Measuring Oxide Trapping Parameters in MOS Structures

A system for controlled injection of electrons or holes into the oxide layer of a MOS capacitor can be used to measure oxide trapping parameters. Since trapping mechanisms can cause degradation and ultimate failure of MOS elements exposed to ionizing radiation, the system can be helfpul in predicting device tolerance.

(See page 4.)

Wrought Nickel-Base Superalloy

A new wrought nickel-base superalloy for advanced temperature use, is suited to cost-saving powder-metallurgy manufacturing methods and has improved phase stability during longtime heating. A wide variety of applications exists where stainless steels are used for oxidation and/or corrosion resistance.

(See page 53.)

Match-Mold Process for Foam Insulation

Newly-available fast-curing materials
greatly reduce production time and costs.

Lyndon B. Johnson Space Center, Houston, Texas

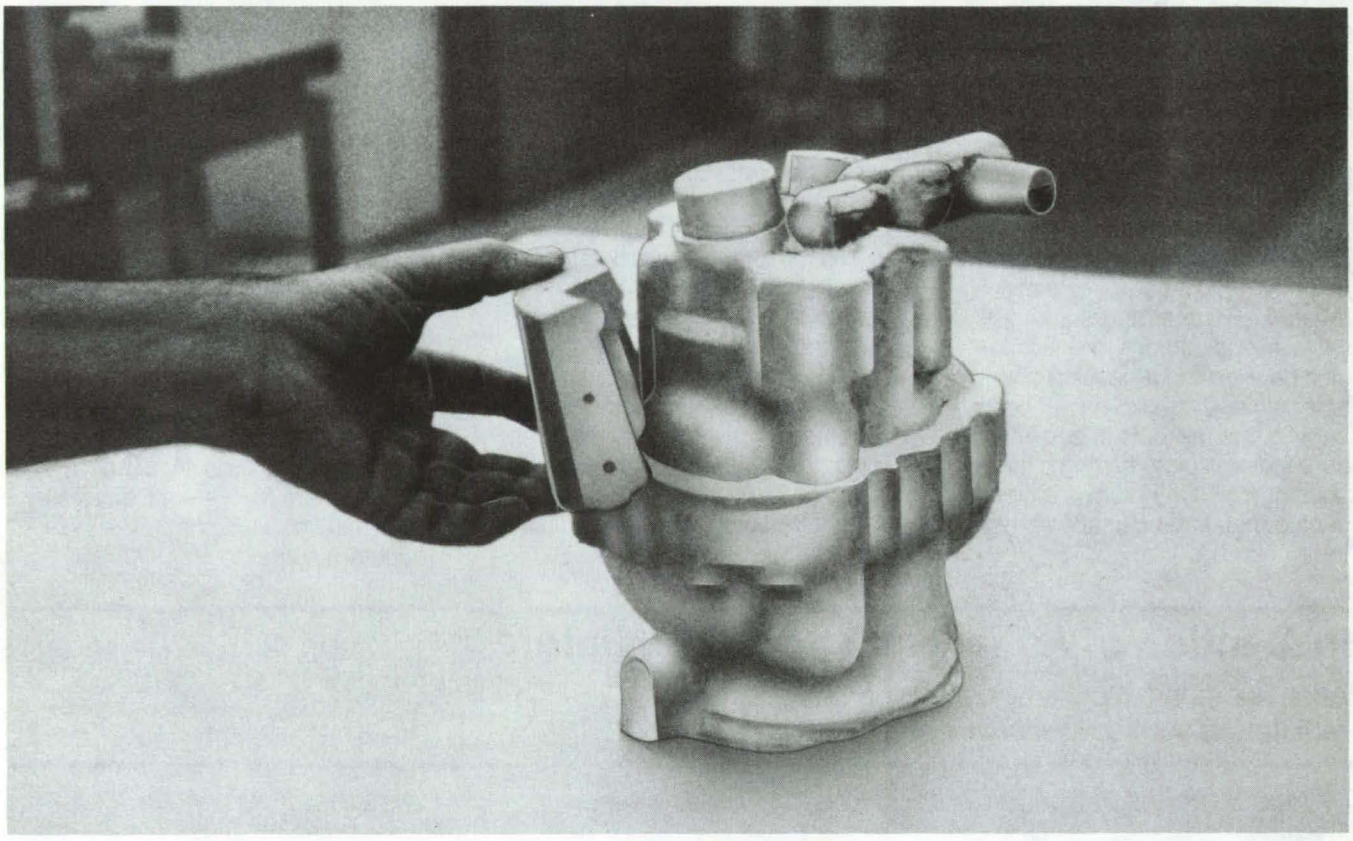

A **Segment of Foam Insulation** produced with the match-mold process is shown next to the mold for a valve to be insulated.

An improved process for the manufacture of foam insulation segments uses a newly-available fast-setting putty-type thixotropic epoxy material. It eliminates the need for leakproof enclosures that were required previously for splash-molding master patterns with low-viscosity water-based plasters. The method reduces cure time from 15 to 4 hours, and the epoxy masters are stronger and do not require special coating for storage.

The newly-available urethane-based high-strength fast-curing resins have been also used to cast reusable production molds from the master pattern. These molds can be made in approximately 25 percent of the time that was required to lay-up and oven-cure the previously-used fiberglass-reinforced plastic-laminated molds. This results in an estimated 50 percent cost savings over the standard approach.

For flameproofing, a fluorocarbon-based coating is applied to the production mold faces and is allowed to cure for 12 hours; a compatible urethane material is then used to adhere knit Kevlar (or equivalent) fabric onto the cured coating for abrasion resistance. The molds are assembled and filled with the pour foam. As the foam cures, the fabric bonds to the foam segment with the exact contour required for installation.

To facilitate removing finished segments from the mold, a simple "remove/release" technique has been devised. The facing is allowed to cure on the mold and is then stripped away from it. The facing is then put back on the mold and serves as an integral release facing. By separating the facing before pouring the foam, any release-agent or vacuum adhesion to the mold face is broken, and the cured foam is later removed easily.

Manufacturers who produce match-molded items of plastic, such as form-fitted insulation or packaging forms, could find the process to be of interest in several applications.

This work was done by Harold E. Rumenapp, Geza G. Liskay, and David S. Wang of Rockwell International Corp. for **Johnson Space Center.** *For further information, Circle 68 on the TSP Request Card.*
MSC-16631

Void-Free Foam Insulation

Partial filler sections produce large void-free foam parts.

Lyndon B. Johnson Space Center, Houston, Texas

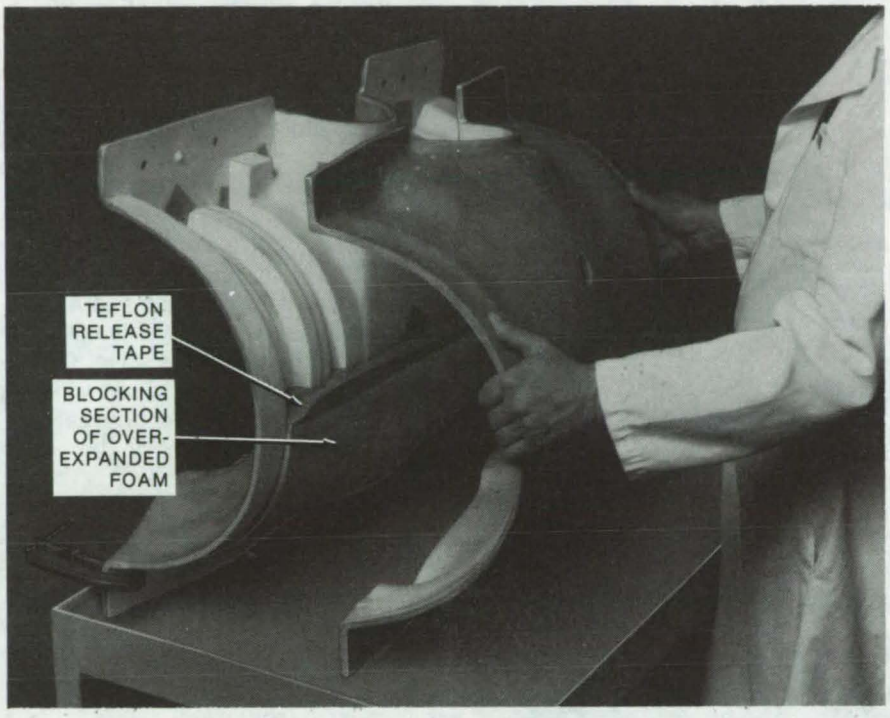

Sequential Casting of void-free foam insulation is possible by using a blocking piece for the first pour. This limits the pour height to 12 inches, as required to produce a void-free foam.

When using the match-mold process for strap-on foam insulation described in the preceding article, it is difficult to pour large sections without voids. This is particularly so when the foam is poured into molds to heights exceeding 12 inches (30 cm). Under these circumstances the foam expands, creating unacceptable voids.

To fabricate void-free insulation pieces higher than 12 inches, it was decided to make smaller parts and bond them together. This could have been done by making new partial and smaller molds. However, a more efficient procedure was developed by using the full-sized molds.

The method used is sectional casting. An overexpanded section of insulation is used to "fill up" enough of the mold so that the remaining height is less than 12 inches. As shown in the photograph, the mold is assembled, and void-free insulation can be cast in the unfilled portion. After setting, the overexpanded blocking section is taken away. The blocking section is made easily separable from the void-free section by taping the interface edge of the blocking section with Teflon release tape. The insulation part is completed with a second pour that adheres to the first via adhesive bonding.

With this technique, which may be repeated for even larger parts, void-free segments of strap-on foam can be made more economically than by using partial molds or by other sequential casting steps.

This work was done by Geza G. Liskay and David S. Wang of Rockwell International Corp. for **Johnson Space Center.** *No further documentation is available.*
MSC-16805

High-Rise Foam-In-Place Process

Large polyurethane parts are molded by sequential pouring without waiting for the foam to cure.

Lyndon B. Johnson Space Center, Houston, Texas

An alternate method for pouring void-free foam insulation may be superior for some users. [See the preceding articles "Match-Mold Process for Foam Insulation" (MSC-16631) and "Void-Free Foam Insulation" (MSC-16805) for a description of the foam and a foam pouring procedure]. By dividing the mold into sections and pouring foam for the second section directly onto the rising foam surface of the first, void-free parts that are 12 in. (30 cm) high have been produced. When fabricated in this way,

(continued next page)

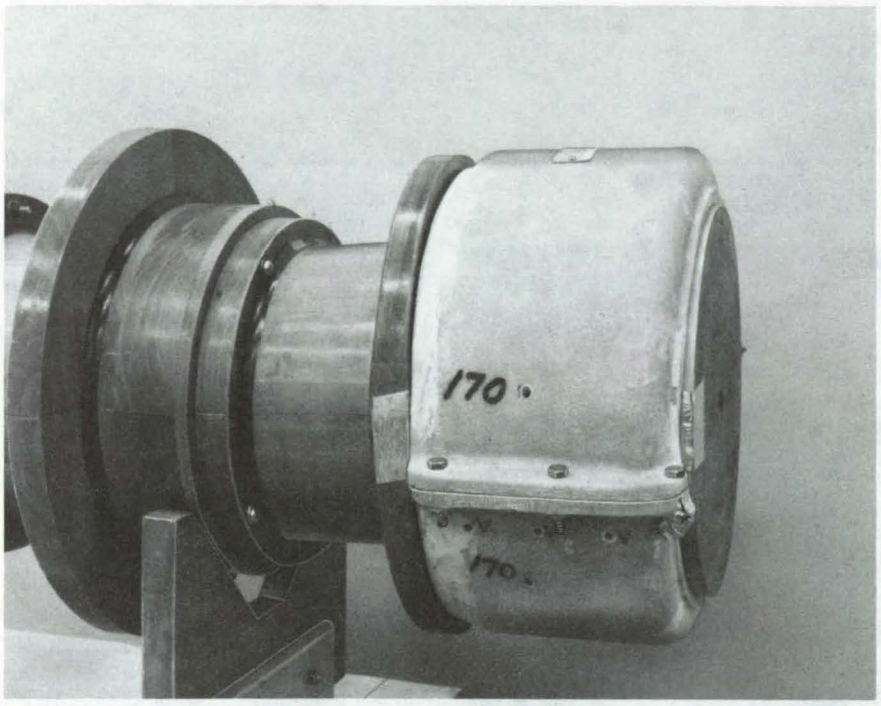

Figure 1. **Fillholes and Ventholes** (labeled "170" and "V" respectively) are used to mold a foam-in-place part made of polyurethane. Foam is poured through the lower fillhole first (identical holes are at the other side of the mold). When foam begins exuding from ventholes, they are taped, and a second pour is made through the upper fillhole.

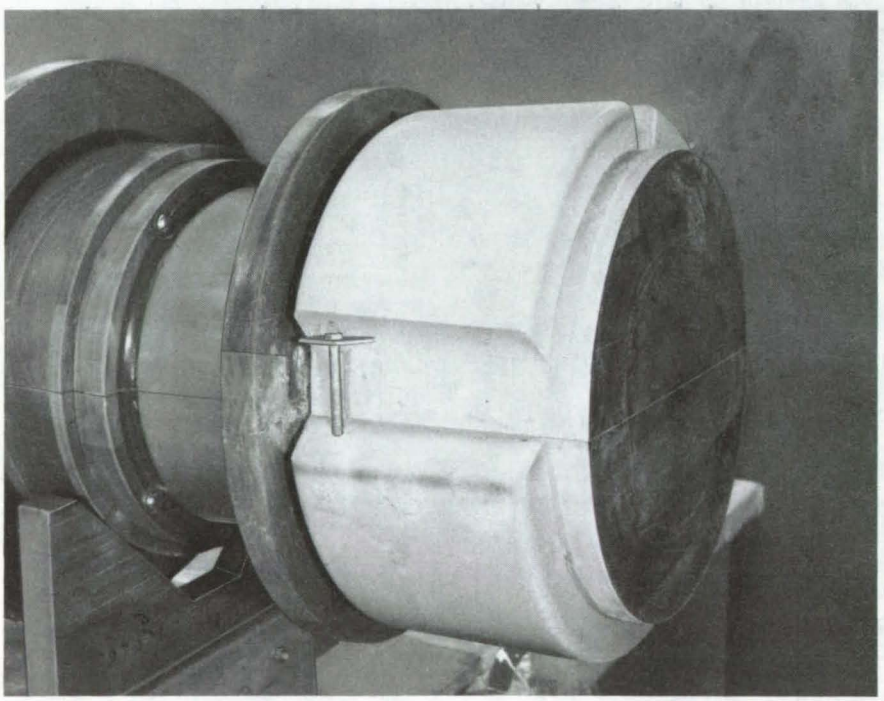

Figure 2.**Void-Free Insulation** is produced by the double-pour process, as shown in this photo of a cut section through the finished foam part.

the joints between pours and the tops of the parts are free of voids and need no trimming.

Thus far, simple, open, cylindrical shapes have been made; however, manufacturers interested in fabricating large foam parts for other applications could find the method useful. The most important specification appears to be that the depth of each pour be limited to between 10 and 12 in. (25 and 30 cm).

The photograph in Figure 1 shows an arrangement made for the double pour. Shown are two fillholes (labeled "170") and three ventholes (labeled "V"). The ventholes are about 8 to 10 in. (20 to 25 cm) above the bottom of the part and about 2 in. (5 cm) above the lower fillhole. The upper fillhole is about 5 in. (13 cm) above the vents. Not shown in the photograph is an identical set of pourholes and ventholes on the opposite side of the mold.

A first pour is made by injecting freshly mixed foam into the lower fillholes on both sides of the mold. When the rising foam begins to exude from the ventholes, the vents are immediately covered with tape. A second batch of foam is then injected into the upper fillholes.

Figure 2 shows a cut section through the finished foam insulation. There are no voids in the material, including the joint between the double-poured sections. (The projecting clip and bolt simulate parts of the hardware and are not related to the tooling for the pour.) Several other parts were also successfully made by using the specified heights for the fillholes and ventholes.

This work was done by Geza G. Liskay of Rockwell International Corp. for **Johnson Space Center.** *No further documentation is available.*
MSC-16931

Reclaiming Hybrid Integrated Circuits

Loose particles — normally a cause for rejection — can be shaken out of a circuit package.

Lyndon B. Johnson Space Center, Houston, Texas

By the time a hybrid integrated circuit is packaged and sealed, it can represent a sizable investment in time, effort, and materials. However, it is not uncommon for small particles — usually tiny bits of solder — to become entrapped in the circuit package. Such particles are so small that they escape detection during visual inspection. When the particles are finally detected during vibration testing, it is too late to do anything about them since the package is already sealed. It is possible to delid the package, remove the particles, and reseal, but this may introduce additional particles and requires the repetition of screening tests on the resealed unit. Since the particles can interfere with normal circuit operation, the IC usually must be scrapped.

A new method makes it possible to reclaim these circuits without exposing the hybrid circuit chip to a hostile environment or further contamination. The method is simple and fast and therefore adds little to the cost of the circuit. It does not seriously disrupt production schedules. Moreover, another round of screening tests is not required.

Essentially, the reclamation method consists of opening a very small hole in the package and shaking out trapped particles through the hole, while listening (with the aid of instruments) for the sound of rattling particles until it is certain that there are none left.

The procedure is performed in a dry box through which an inert gas is flowing at about 4 ft^3/min (0.51 m^3/min) to insure that room air cannot enter the package when it is opened. The dry box already holds the necessary tools (which have been cleaned previously) and the integrated circuit to be repaired.

An operator wearing rubber gloves punches a small hole [0.020 in. (0.05 cm)] in the lid of the circuit package. The operator applies a dab of acoustic couplant to the lid and places the package hole-side down on a vibrator in the dry box, positioning the hole so that it is clear and unobstructed. The operator turns on the shaker, operating it at 30 to 40 Hz, and adjusts the amplitude so that the acceleration varies from 0 to 6 g.

An acoustic transducer monitors the sounds of vibrating particles as the package is shaken, and an amplifier produces audio and oscilloscope output. Random noise bursts indicate loose particles; periodic noise bursts are caused by loose wires.

When the random noise stops, the package has been emptied of particles. Still manipulating tools in the dry box, the operator seals the package hole by covering it with a solder form and heating it.

This work was done by George Ebel and Henry Grossbard of The Singer Co. for **Johnson Space Center.** *For further information, Circle 69 on the TSP Request Card.*
MSC-16463

Bonding Kovar Pins to an Alumina Substrate

Assemblies for cryogenic applications are shockproof and vibrationproof.

Lyndon B. Johnson Space Center, Houston, Texas

Gold-plated Kovar pins can be mounted in a 94-percent alumina substrate by a cementing technique that provides a stress-free bond particularly well suited to the construction of sensors or instrumentation for very-low-temperature environments. Hence the method is likely to be of interest in wetted sensors or instrumentation for liquefied natural or petroleum gas production, storage, or distribution.

The mechanical bonding is accomplished by limiting bond-line thicknesses to between 0.001 and 0.003 inch (0.025 and 0.075 mm) for a nominal pin diameter of 0.028 inch (0.711 mm). Both the internal diameter of the locating hole and the outer diameter of the pin are wetted with refractory cement (Sauereisen No. 78, or equivalent). The pin is then inserted in the substrate, and the assembly is allowed to air-dry at room temperature for 1 hour. Final curing of the bond is at 170° F (77° C) for 2 hours. Each assembly is subjected to a 5-pound axial proof test as part of its inspection.

Use of the prescribed bond-line thickness and method of application extends the useful range of the bonding material into cryogenic temperatures. Thermal shock tests from + 68° to -320° F (+ 20° to -196° C) and vibration tests at temperatures from + 500° to -320° F (+ 260° to -196° C) have been conducted with no failures of the bond.

This work was done by George D. Bennett of Simmonds Precision, Instrument Systems Division for **Johnson Space Center.** *No further documentation is available.*
MSC-16828

"PC Fabrication" for Silicon Solar-Cell Arrays

Printed-circuit fabrication is proposed for mounting and interconnecting solar cells

NASA's Jet Propulsion Laboratory, Pasadena, California

Many of the structural materials potentially useful for fabricating the housing for silicon solar-cell modules poorly match the expansion coefficient of silicon. In addition, the often-used interconnection techniques of silk screening and hand wiring are expensive. An alternate technique, batch bonding a number of solar cells to a preconfigured printed-wiring board, is potentially inexpensive and may reduce the assembly and setup time of multi-element solar-cell power units.

As can be seen in the figure, the technique begins with a single-sided clad laminate, e.g., a phenolic or a glass epoxy, to which a copper layer has been laminated, in a fashion similar to printed-circuit art. After patterns are formed in the copper foil to delineate conductor regions, holes are drilled through appropriate portions of the patterns, and stakes are driven into the board.

Collars are then placed around the individual stakes to define the locations of the individual silicon cells in the form of round wafers. After the cells are assembled on the board, suitable clips are forced down over the stakes to hold the silicon wafers in place during the solder reflow. This staking/clip sequence (a technique that is potentially inexpensive and susceptible to automation) electrically interconnects the backs of one set of cells to the fronts of a second set. By allowing rows of wafers to be connected in series, the output voltage of the module is increased.

The entire assembly is next passed through a heat-cycle/wave soldering operation that solders the stakes to the copper circuit and bonds the solder-clad clips to the stakes and to the faces of the wafers in appropriate metalization regions. The entire module is covered with a suitable transparent plastic or glass

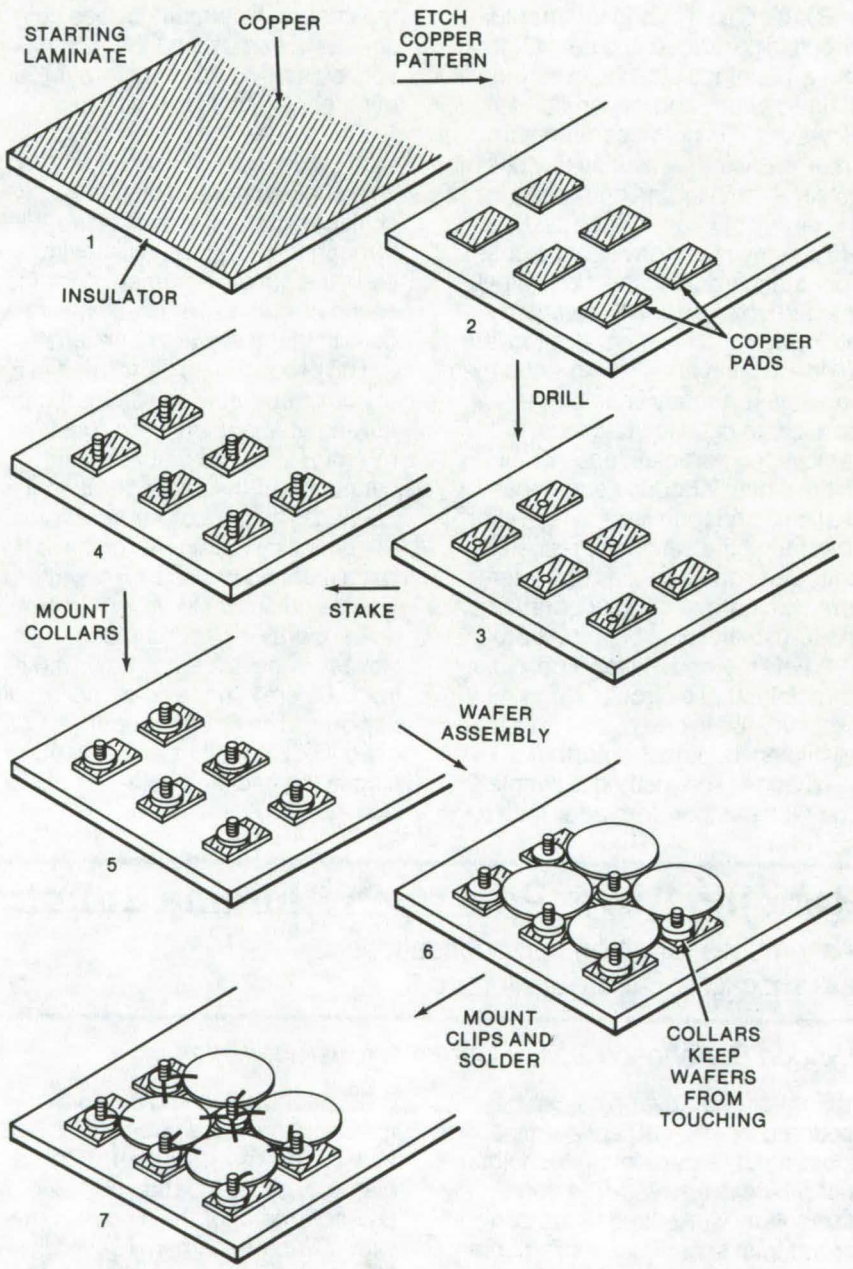

The **Mounting and Interconnecting of Silicon Solar Cells** proceed by a series of steps as outlined above. Printed-circuit board technology is used for the copper patterns and stakes on which the clips are pressed. The clips are constructed in a manner similar to that used in mounting power transistors. The stakes and clips inexpensively interconnect the fronts and backs of appropriate wafers by a technique that is susceptible to automation. The clips and collars define the areas between adjacent round wafers, so that registration of the wafers with one another is automatic.

for mechanical and environmental protection. Terminations are brought out of the cell by any suitable bus technique.

This technique limits the area of contact between the back of the individual cells and the underlying copper pattern to no more than 0.250 by 0.250 in. (0.635 by 0.635 cm) and preferably holds it to 0.100 by 0.100 in. (0.254 by 0.254 cm) to reduce distortion of the wafers and the sheet support material due to thermal expansion mismatch.

It is assumed that the metalization on the silicon cell is suitable for solder-reflow mounting and bonding and that the metalization on the front surface of the wafers registers with the clips. Conducting clips are solder clad; nonconductive clips are held in place on the stake following solder reflow either by a suitable thermoplastic bonding agent or by overlying soldered-down conducting clips.

This work was done by James A. Amick of RCA Corp. for **NASA's Jet Propulsion Laboratory.** *For further information, Circle 70 on the TSP Request Card.*
NPO-13991

Continuous Process Fabricates Battery Plaque

Fast coating/drying/sintering line produces high-quality nickel plaque for Ni/Cd cells.

Goddard Space Flight Center, Greenbelt, Maryland

A continuous process for making battery plaque for nickel-cadmium cells is much faster than batch processes. Plaque made by the continuous process has uniform, reproducible characteristics and carefully controlled thickness — essential for reliability and long life in batteries.

In the process, nickel-wire screen is drawn through a slurry containing nickel carbonyl powder and becomes coated with the slurry. The coated substrate is dried and sintered to produce finished plaque (see figure).

The slurry consists of alcohol and water, in addition to the nickel carbonyl powder in an organic binder. The alcohol makes the slurry more homogeneous by totally solubilizing the binder; later during drying, the alcohol is easily evaporated by gentle heat so that it quickly stabilizes the slurry-coated plaque and prevents running and sloughing of the wet material. The water prevents fissuring and cracking during the drying phase, which might occur as a result of too rapid removal of the alcohol solvent.

Motor-driven rollers pull the nickel-wire substrate through the slurry while doctor blades wipe off excess. The blade openings are adjusted to give the desired thickness of finished plaque. The wire screen is supplied from a reel; when a reel runs out, the leading edge of a new reel is stapled to the trailing edge of the old one, and the process continues without interruption.

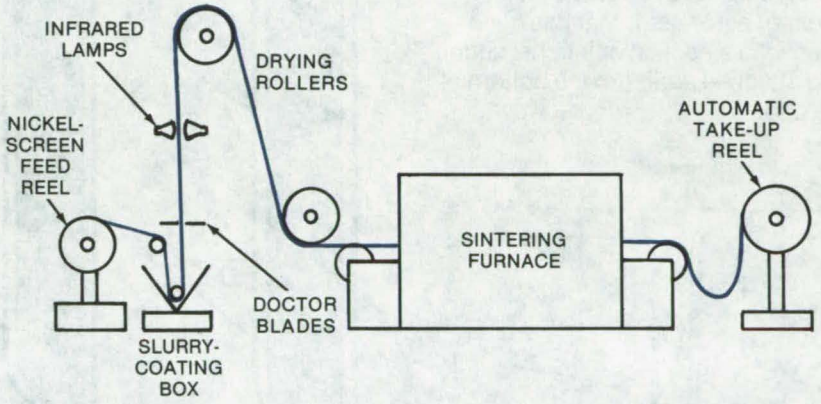

Continuous Process for Fabricating Battery Plaque gives uniform, reproducible physical characteristics. Coating of the nickel-screen substrate, drying, and sintering proceed without interruption. Thickness is checked at the "wet" (after coating), "green" (after drying), and finished stages.

The slurry-coated screen (the "wet" plaque) passes under infrared lamps for partial drying and over large rollers for further slow drying. At this point the thickness of the "green" plaque is measured. If necessary, the doctor-blade setting can be changed.

The green plaque proceeds through a three-zone sintering furnace, fueled by cracked "city gas" (producing H_2 and CO). The time-and-temperature profile can be varied to suit the plaque thickness. The median parameters subject the plaque to the equivalent of 30 minutes at 900° C. The finished plaque is checked for porosity and thickness, and any necessary changes in the doctor-blade setting or speed through the furnace are made.

As it emerges from the furnace, the finished plaque is taken up by an automatic reel. The material is then coined, tabbed, impregnated, and used in nickel-cadmium batteries.

This work was done by Michael J. Turchan of Tyco Laboratories, Inc., for **Goddard Space Flight Center.** *For further information, Circle 71 on the TSP Request Card.*
GSC-12054

Improved Thermal-Tile Barrier

New filler design, laser processing, and a new tool improve thermal tile.

Lyndon B. Johnson Space Center, Houston, Texas

There have been three new developments as a result of work with a thermal barrier that serves as a tile-gap filler in a thermal protection system. One of these is a new barrier design made from a ceramic woven fabric (AB312 or equivalent) folded over a thickness of alumina mat (see Figure 1). The barrier is precision-cut and sealed by a laser. The finished barrier is inserted into the gap between two tiles and is secured inside by a steel Velcro hook, or equivalent, that has been bonded to a section of Inconel spring and attached earlier to the bottom of the gap.

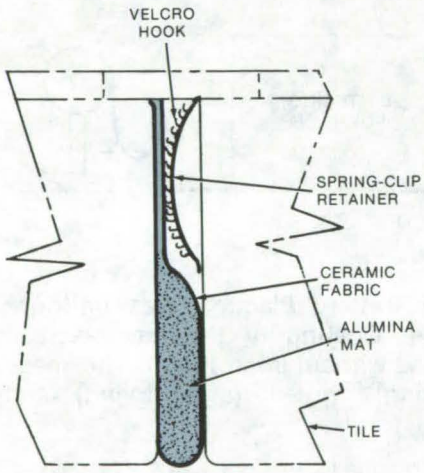

Figure 1. Side view of the **New Thermal Barrier** is shown filling the tile gap.

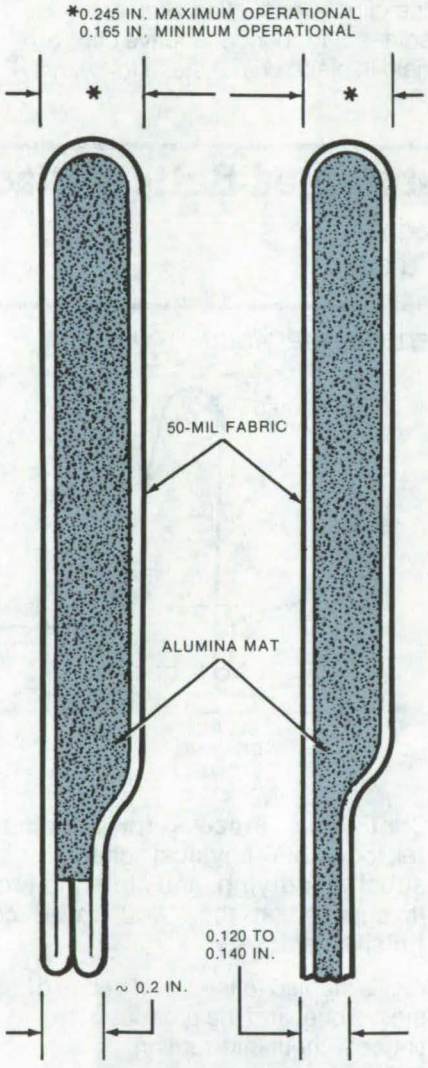

Figure 2. **Laser-Cut and Fused Barrier** (right) is compared with conventionally fabricated barrier (left). The extra thickness of the folded and sewn section makes it more difficult to fit into the gap. Laser cutting is accomplished with a sharply focused beam that is later defocused to produce a fused edge.

Another development is the laser fusing process used to seal the ceramic fiber. Figure 2 compares the earlier barrier fabricated by the cut-and-sew method to a new method using a CO_2 laser to cut and fuse the barrier. The latter produces a neater and more compact filler that forms a better fit in the tile gap.

Finally, a tool has been developed for sliding the barrier into the tile gap. The tool is made of a thin folded metal plate and has two spacers that slide above slots cut in the plates. Before the tile gap is filled, an empty tool is inserted into the gap to measure its depth. As the depth is measured, the spacers are adjusted to the proper height and are fixed in position with wingnuts. Next, the thermal barrier is positioned inside, flush against the spacers, and the metallic retainers are slipped into place with the retainer tongs lying over the bottom edge of the tool.

The tool then is slipped into the gap again until the spacers contact the top faces of the tiles. The wingnuts are loosened, and with the spacers held flush against the tile surfaces, the tool is raised, releasing the barrier inside the gap.

This work was done by Dale H. Cade, Richard N. Sidric, and Milo Surbat of Rockwell International Corp. for **Johnson Space Center.** *For further information, Circle 72 on the TSP Request Card.*
MSC-16929

Tile-Bonding Tool

Device applies uniform, constant, precise pressure to hold tiles in place during bonding.

John F. Kennedy Space Center, Florida

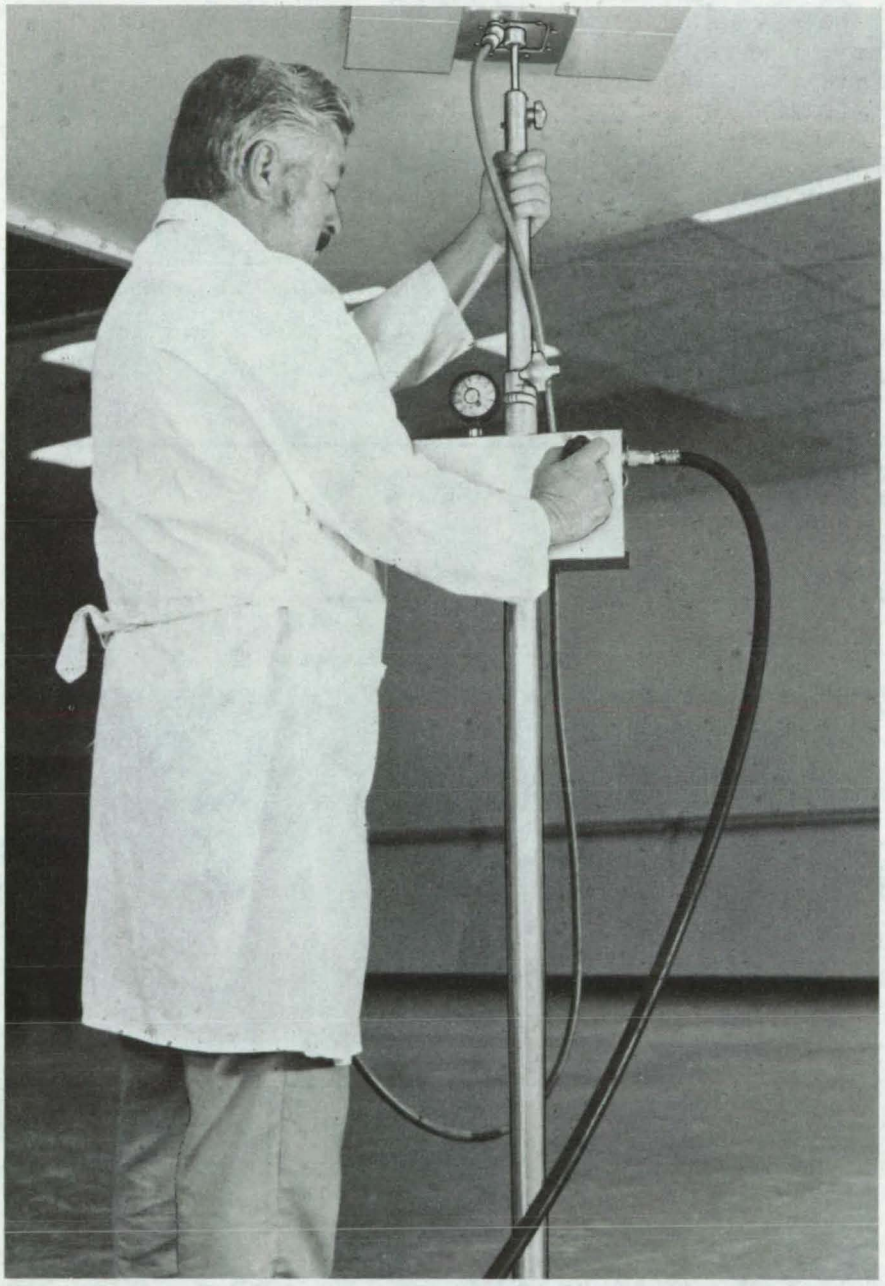

The **Tile-Bonding Tool** is being used by an operator who adjusts the pressure on a bladder mounted on an extended pole. The bladder applies a controlled uniform pressure over the surface of flat or contoured tiles. Only one bladder is shown here, but several can be used to bond many tiles simultaneously.

A simple tool holds tiles in place for bonding at precisely the right pressure for the tile material/adhesive combination. Designed for replacing the approximately 350 surface-insulation tiles that are expected to be damaged on a Space Shuttle during flight, the tool should be useful in other applications where holding or positioning fragile materials is necessary.

The tool consists essentially of pressure bladders supported by an adjustable pole. The pole, which has an antiskid foot, is placed on a floor or work surface and is extended until tiles on the uninflated bladders just touch the surface to which they are to be bonded. The user then opens a valve to a pressurized air supply to inflate the bladders to the desired pressure, which can be maintained within 1/2 psi (3.5×10^3 N/m^2). Each bladder applies a uniformly distributed force.

The pole can accommodate a single bladder to bond a single tile or multiple bladders to bond many tiles at once. Multiple bladders can be pressurized individually. Tiles can be flat or contoured. The pole can be used in any orientation as long as a solid reaction surface is available.

This work was done by Cyrus C. Haynie and Jack W. Holt of Rockwell International Corp. for **Kennedy Space Center.** *For further information, Circle 73 on the TSP Request Card.*
KSC-11053

High-Temperature Waterproofing for Tiles

Vapor-deposited coating protects silica tiles against water vapor up to 800° F.

Lyndon B. Johnson Space Center, Houston, Texas

Silica HRSI (high-temperature reusable surface insulation) tiles developed for the Space Shuttle are also expected to find commercial use as a high-temperature insulation. A waterproofing system recently developed for these tiles should be useful not only with commercial applications of the tiles but for composite materials, friable ceramics, and other materials that must be protected from moisture degradation at high temperatures.

The coating is formed by reacting methyl trimethoxy silane vapor with active hydrogen sites on the silica-fiber surface. Using acetic acid as a catalyst, the reaction produces a hexamethyldisilazane silicone-based polymer. The coating formed maintains its waterproof characteristics after 15 hours exposure to 800° F (427° C) at 1 atmosphere pressure.

This particular coating has the additional desirable property that degradation products formed do not affect the optical properties of the coating. Furthermore, the vapor-deposition method of applying the coating makes it particularly suitable for fragile components.

This work was done by E. B. Bahnsen and Y. D. Izu of Lockheed Missiles & Space Co., Inc., for **Johnson Space Center.** *For further information, Circle 74 on the TSP Request Card.*
MSC-16773

Simplified Tooling for Spray Masking

Magnetically-coated plastic masks are easily positioned around parts to be spray coated.

Lyndon B. Johnson Space Center, Houston, Texas

Setting up tiles that are to be spray coated can be done faster and more easily by positioning them within acrylic plastic masking frames that attach magnetically to the holding fixture. The plastic is "magnetized" with adhesive magnetic-rubber strips.

Originally developed for spraying ceramic coatings on insulation tiles destined for the exterior of the Space Shuttle, the tooling technique is simpler and less expensive than the conventional approach that calls for mechanically clamping down stainless-steel masks. The L-shaped masks are easily cut and altered to provide a low-cost and flexible approach. They should be useful in industrial applications in which spray-mask coatings are applied either manually or automatically.

For the Shuttle applications, the tiles were mounted on a turntable, shown in Figure 1, that is supported on a pin bearing. The photograph in this figure shows the side view of a tile with its masks held magnetically

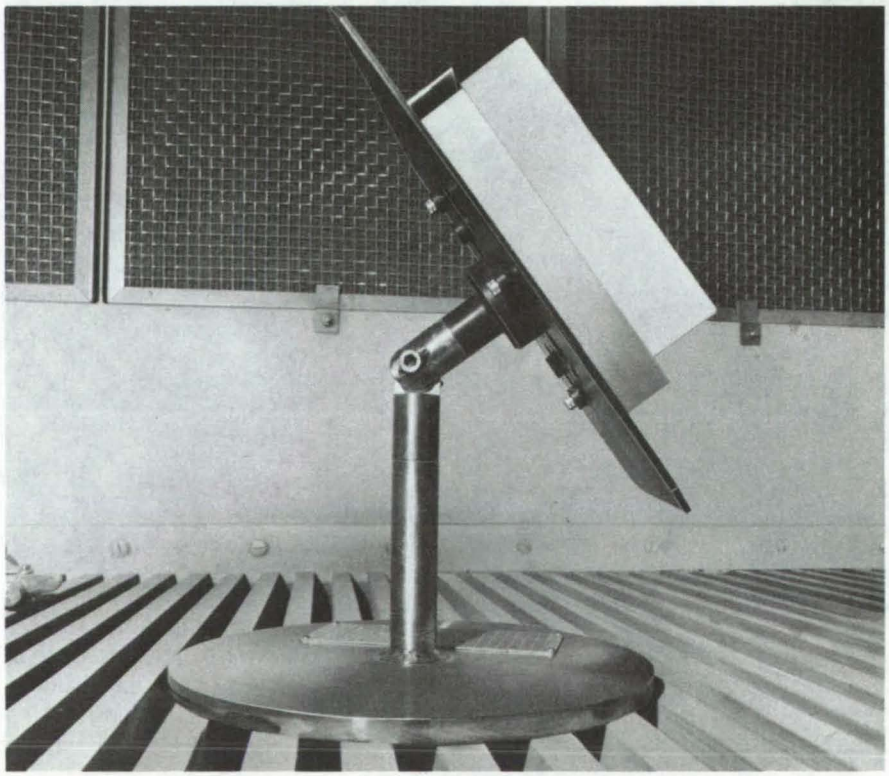

Figure 1. A **Turntable Supported on a Pin Bearing** holds a tile to be spray coated. Plastic masks, attached magnetically to the turntable, hold the tile in place.

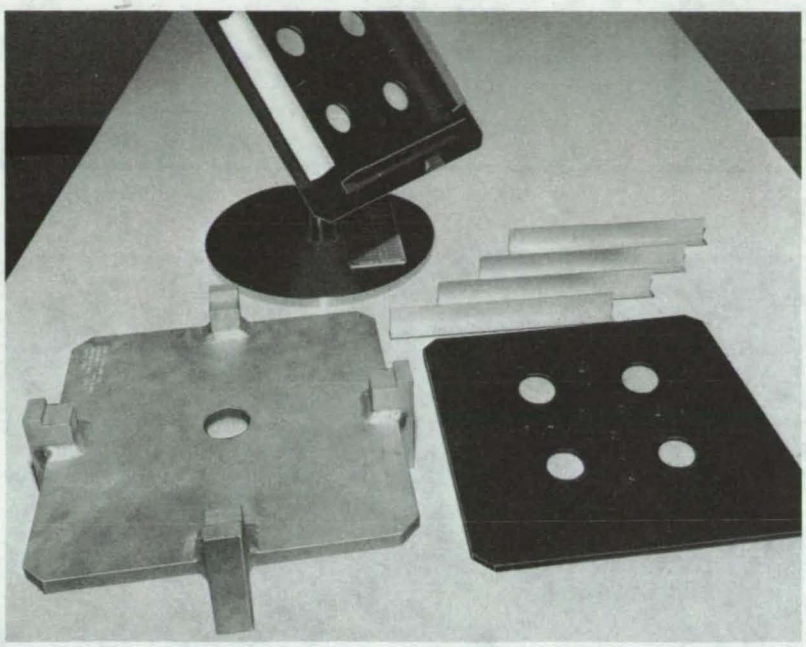

Figure 2. **L-Shaped Masks** are mounted on the turntable; an additional set is lined up beneath it, next to a plate that will carry the tiles to be sprayed. Special holding jigs like the one at lower left were also designed for the system.

to the turntable. The photograph of Figure 2 shows a front view of the turntable fixture. One set of four spray masks is shown on the turntable, while another set of four is lined up below, next to an extra tile-holding plate. These masks can be set up on the extra plate, which is then attached to the special jig shown at the lower left.

The complete fixture also includes a tile-removal plate that fits between the tile that is to be sprayed and the tileholding plate on the turntable. It allows the tile to be lifted from the plate with a minimum of handling.

This work was done by Bonnie J. Dunbar and Richard E. Hammons of Rockwell International Corp. for **Johnson Space Center.** *For further information, Circle 75 on the TSP Request Card.*
MSC-16927

Ladle for Pouring Hot Melt

A ladle with a detachable handle is designed for safe, convenient handling.

Lyndon B. Johnson Space Center, Houston, Texas

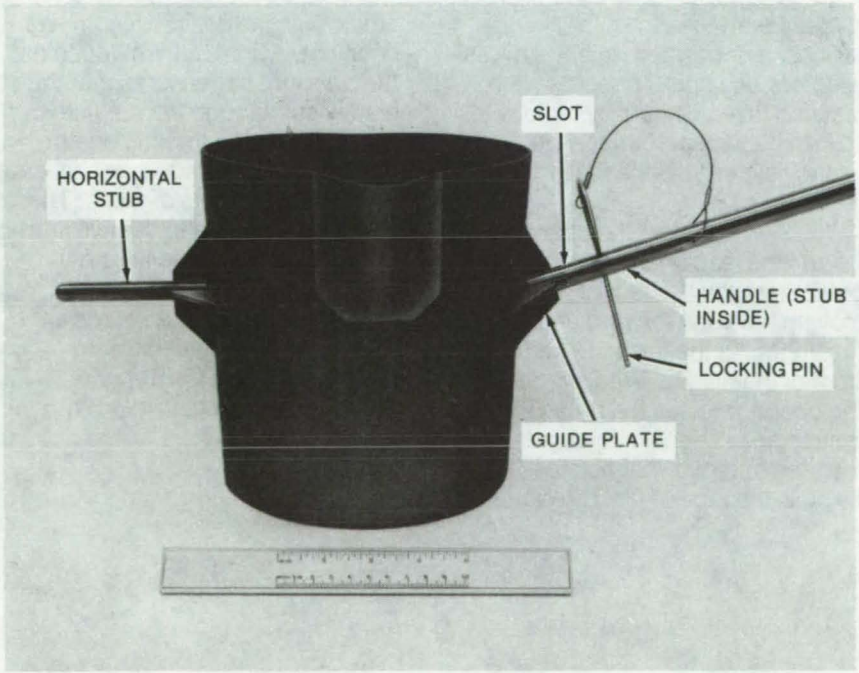

The **Improved Ladle,** as shown with the handle in position, includes two stubs that allow a choice of handle positions. The handle is inserted and locked with a pin. The pin has a large ring for easy gripping.

Lightweight melted materials are normally contained in relatively small ladles designed to be handled by one man. The ladles have tapered sides to rest in a holding ring attached to a handle. This is not a very convenient arrangement, because the ladle must be lifted by tongs to be placed onto the holding ring.

An improved ladle (see figure) includes two weld-attached stubs that include guide plates. One stub is positioned to accept a handle horizontally; the other accepts the handle at an angle. The handle end is slotted to slide into the guide plates. A pinlock secures the handle to the stub.

This work was done by Emil P. Ruppe and Kuni Teramura of Rockwell International Corp. for **Johnson Space Center.** *No further documentation is available.*
MSC-16974

"Space Slitter" for Film or Tape

Device cuts title strips for schedule boards quickly and accurately.

John F. Kennedy Space Center, Florida

A device that cuts film or tape into strips is a convenient, fast, and accurate way to trim titles for planning and scheduling boards. Developed for use in the Space Shuttle and other space programs, the cutter could also be used in graphics businesses — advertising, commercial art, publishing — and by any organization that relies on charts to establish goals and monitor progress.

The cutter is intended for 35-millimeter film or paper tape containing titles printed by a composing machine. The titles — which may be as much as 4-1/2 feet (1.5 meters) long — are trimmed, are attached to magnetic bars by an adhesive, and are mounted on a magnetic wall chart.

Formerly, the titles were trimmed by hand shears, pivoted-blade papercutter, or rotary-blade paper trimmer. These tools were generally unsatisfactory because they were slow, inaccurate, and uneven. The papercutter particularly was hazardous because it was necessary for the operator to hold slippery film with fingers close to the cutting edge.

The new cutter (see figure) eliminates these disadvantages. It guides the film or tape in a channel under cutting blades. It is fast, cutting two or three strips at a time at rates of 10 feet (3.3 meters) per minute. It is accurate, maintaining a margin as small as 0.01 inch (0.25 mm) above and below the title characters; and the cut edges are straight and parallel.

In its first version, the cutter was improvised from readily available materials — scrap wood, coathanger wire, and replacement blades for an Exacto knife. Nevertheless, it performed reliably. It was used, for example, to repeat a job that had taken 5 hours by hand with scissors and papercutter. The "space slitter" did the job in 15 minutes.

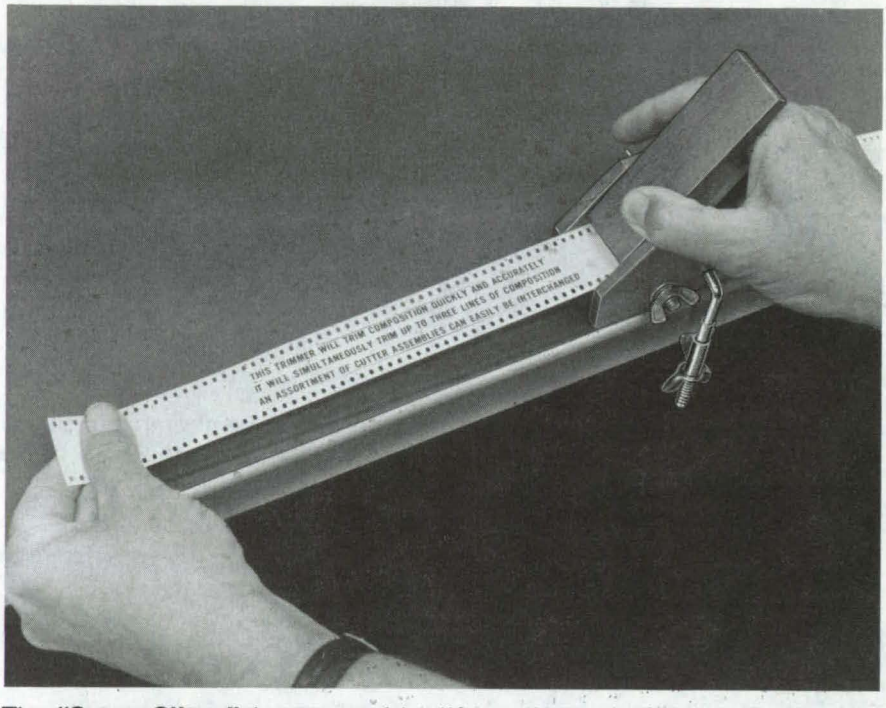

The "Space Slitter" is operated by lifting the end of a pressure bar to insert blades into film. The film is then pulled through the blades. An L-clamp holds the cutter securely on a table.

To use the cutter, the operator inserts the leading edge of the tape or film through the rear of the unit, moving the edge forward until the first letters in the titles are just in front of the blades. With one hand, the operator raises the pressure bar, embedding the tips of the blades into the tape or film. With the other hand, he pulls the tape or film through the cutter until the desired length has been cut. A light but firm touch on the pressure bar ensures that the blades cut through the medium. There is no need to bring one's fingers near the blades, so there is little chance of cuts or nicks. The device is designed to cut two lines of 24-point type or three lines of 14-point type simultaneously.

This work was done by William H. Johnson of The Boeing Co. for **Kennedy Space Center.** *For further information, Circle 76 on the TSP Request Card.*
KSC-10894

Portable Fluorescent-Dye Inspection Device

Device renders dyes visible for in situ inspection of parts.

Marshall Space Flight Center, Alabama

Onsite Fluorescent-Dye Inspection is possible with this portable shield. An ultraviolet light source and a magnifier are contained within the bellows.

Fluorescent penetrant-dye inspection of material surfaces, such as machined parts or forgings, normally requires a background of reduced lighting in order to examine the object carefully with ultraviolet light. For small objects, which can be placed in booths or darkrooms, this may not pose any special problems. However, many large objects are not easily transported and thus are not conveniently shielded from background lighting.

A new inspection device blocks ambient light from the area to be inspected and can be used to examine sections of large objects without requiring that they be moved or placed in a darkroom. The portable, hand-held device (see figure) consists of a bellows-type flexible shield having foam ends that seal the surface to be inspected. A small ultraviolet lamp and a magnifier mounted within the bellows permit the light to be localized and focused on a selected area. A rigid eyeshield hood extending to the operator's forehead further reduces background light and allows the surface to be inspected in situ.

This work was done by Frank E. Sugg of Rockwell International Corp. for **Marshall Space Flight Center.** *For further information, Circle 77 on the TSP Request Card.*
MFS-24019

New Adhesive Withstands Temperature Extremes

A new adhesive, developed for high-temperature components aboard satellites, is useful at both high and low temperatures and exhibits low-vacuum volatility and low shrinkage. The system uses a polyfunctional epoxy resin with high aromatic content, low equivalent weight, and a more compact polymer than the conventional bisphenol A type.
(See page 50.)

Boron Trifluoride Coatings for Plastics

Tough, durable coatings of boron trifluoride can be deposited on plastic optical components to protect them from the destructive effects of abrasion, scratching, and the environment. The coating material can be applied simultaneously with organic polymers, using plasma glow-discharge methods, or it can be used as a base material for other coatings to increase adhesion.
(See page 51.)

Partial Interlaminar Separation for Composites

Epoxy-matrix composites with improved fracture toughnesses, tensile strengths, and impact resistances are fabricated by using a perforated film to break part of the bond between laminae. The separation diffuses local stress concentrations near cracks, inhibiting their ability to propagate. Tests on modified panels showed a 50-percent increase in fracture strengths.
(See page 58.)

Books and Reports

These reports, studies, and handbooks are available from NASA as Technical Support Packages (TSP's) when a Request Card number is cited; otherwise they are available from one of NASA's Industrial Application Centers or the National Technical Information Service.

Handbook for Estimating Fabrication Costs

Guide helps design engineers determine total cost of fabricating electronic equipment.

A "Handbook of Estimating Data, Factors, and Procedures" gives engineers the information they need to estimate fabrication costs. The handbook consists largely of detailed standards for operations performed in making electronic equipment. It contains tables of "factors" for determining the costs associated with fabrication, such as the costs of production engineering, inspection, quality control, and special tooling.

The section on "standards" includes estimations of the time required for procedures ranging from machining, to wiring, to printed-circuit board fabrication. For example, the subsection on machining covers cutting, lathe operations, milling, drilling, and broaching. The lathe operations are typical: Minutes per job are listed for setup, teardown, and run time; and these jobs are further divided into subtasks — even to the level of filling in a timeslip (1.00 minute), analyzing blueprints (1.00 minute), walking to the toolcrib and back (5.00 minutes), and positioning the coolant jet on the workpiece (0.05 minute per inch).

For machining operations, time values are given for both "soft" materials (aluminum, magnesium, plastics) and "hard" materials (stainless steel, drill rod, beryllium, copper). The user who needs values for intermediate materials such as brass, bronze, and medium steel can interpolate between the extremes.

Standards for the fabrication of printed-circuit boards are another example of the information available in the handbook. Standard times are given for such operations as stamping, drilling, silk-screening, cleaning, plating, and epoxy-coating circuit boards.

The standards were developed over a period of years through time-studies and methods analyses. They are based on the level of efficiency that can be attained by a job shop turning out 1 to 1,000 units per order.

The "factors" section of the handbook furnishes data for several unidentified government contractors on cost elements (direct labor, indirect costs, and the like) as a percentage of total cost, data on typical contractor overhead rates, and data on allowances (above and beyond the standards) for learning, fatigue, and unavoidable delays — even for coffeebreaks and trips to restrooms. With the information in the factors section, an estimator can adjust costs derived from standards to make the total estimate realistic and competitive.

The factors are based on information published in magazines and journals by recognized professionals and on proposals prepared for the U.S. Government.

This work was done by Leonard M. Freeman of **Marshall Space Flight Center.** *Further information may be found in NASA TM-X-73397 [N77-27248], "Handbook of Estimating Data, Factors, and Procedures," a copy of which may be obtained at cost from the New England Research Application Center* *[see page A7]*.
MFS-23795

Scale Parachute Fabrication

Design, fabrication, and testing of scale drogue and scale pilot parachute models

A published report describes highlights in developing six 12.5-percent scale drogue parachute models, three of which had 16 percent porosity and the other three 24 percent porosity, and also two 12.5-percent scale pilot models, each with 24 percent porosity. Deployment bags were also fabricated for each model.

During the fabrication some design changes were necessary to maintain the specified geometric porosity of the parachutes because the width of supplied ribbons necessary for the parachute body was short of the specified 0.25 in. (0.64 cm). The modifications involved the use of a larger number of horizontal ribbons and changes in gap width and in the length of the gores.

Four newly-developed tooling aids are mentioned that have helped in constructing the gores for various parachutes. These aids allowed quick, accurate, and uniform fabrication of parachute gores in which the handling of short lengths of ribbon is minimized.

Step-by-step parachute fabrication was carefully controlled by using process cards. Qualified parachute material cutters, sewing-machine operators, parachute fabricators, and parachute riggers were all involved in the fabrication.

A series of measurements was made on the finished product to meet the dimensional and porosity requirements. Results of these measurements are tabulated in the report.

This work was done by David Bacchus of **Marshall Space Flight Center** *and Daniel Henke of*

Goodyear Aerospace Corp. Further information may be found in NASA CR-120719 [N76-18055], "Scale Drogue Parachute Model," a copy of which may be obtained at cost from the New England Research Application Center.
MFS-23139

CMOS Bulk-Metal Design Handbook

A user's guide to CMOS LSI chip design

A comprehensive handbook describes techniques for generating precision mask artwork for complex CMOS integrated circuits, starting from a logic diagram. The techniques are based on the standard-cell approach, which uses computer programs and a standard-cell library to assemble custom designs.

To use the system, the designer provides a logic circuit that can be partitioned into simpler, frequently-used logic combinations (standard cells). The input for the artwork computer program is derived from the partitioned logic. This input includes a list showing the connectivity between cells, the sequential numbering of the logic elements, and the initial cell placement (this can be arbitrary at the beginning).

The program automatically generates the metalization and tunnels to interconnect the standard cells into the required function. It accepts the user's input and produces a magnetic tape that stores instructions for driving a pattern generator. The pattern generator, in turn, configures the seven-level mask artwork that is necessary to fabricate a CMOS integrated circuit.

The standard-cell library is a collection of basic logic circuits implemented with CMOS technology. All standard cells have been designed, topologically configured, analyzed, and stored on magnetic tape. The library is extensive and is designed to meet present and anticipated requirements. It is open ended to allow the user to define new cells.

The library includes data sheets and a pictorial representation of the artwork along with the function and performance of each cell. Characteristics such as unique drive capabilities, undefined output states, and influences of output loading on clock rate are also given along with data for estimating intercell wiring capacitance and propagation delays.

The handbook also includes user guidelines for designing efficient CMOS arrays. These include discussions of intercell layout, input protection, guard bands, bonding-pad design, and interconnection and packaging methods.

This report was prepared by Teddy M. Edge of **Marshall Space Flight Center.** *Further information may be found in NASA TM-78126 [N77-86193], "C-MOS Bulk Metal Design Handbook," a copy of which may be obtained at cost from the New England Research Application Center* *[see page A7]*.

Inquiries concerning rights for the commercial use of this invention should be addressed to the Patent Counsel, Marshall Space Flight Center *[see page A8]*. *Refer to MFS-23856.*

Improved Electron-Beam Welder

New monitoring procedures and circuit changes enhance welder performance.

The results of a comprehensive test-and-evaluation program to improve the performance of a 7.5-kW electron-beam welder at Marshall Space Flight Center are described in a report that is now available. The report describes the existing unit and 17 changes that were incorporated to improve performance, ranging from new monitoring and maintenance procedures to component and circuit changes.

The improved unit is now equipped with monitoring equipment that measures its critical parameters. New seals were added to prevent temperature-related gas leaks and vacuum grease was eliminated on seals inside the electron gun to prevent clogging of the gas orifice. The previous all-aluminum cathode was replaced by a titanium/aluminum configuration to improve and retain pilot-arc performance. Electrically stressed surfaces were polished to a mirror finish, and all sharp edges were rounded to reduce electron accumulation and dielectric breakdown. The anode material, originally copper, was changed to titanium.

Other measures include pressure-testing of the gun and its high-voltage cable assembly, fine cone-point adjustment of the cathode gas vents, use of a micron-range vacuum gage to preset pilot-arc operating pressure, regular cleaning of the gun pilot-arc cavity, and reduced ionization-gas flow rate to avoid dielectric breakdown.

This work was done by R. A. Smock, R. A. Taylor, and W. A. Wall of **Marshall Space Flight Center.** *Further information may be found in NASA TM-X-73390 [N77-23491], "Investigations For the Improvement of Space Shuttle Main Engine Electron Beam Welding Equipment," a copy of which may be obtained at cost from the New England Research Application Center* *[see page A7]*.
MFS-23772

Computer Programs

These programs may be obtained at very reasonable cost from COSMIC, a facility sponsored by NASA to make new programs available to the public. For information on program price, size, and availability, circle the reference letter on the COSMIC Request Card in this issue.

Pneumatic Servomechanisms

Dynamic analysis program

DYNAPS, a generalized computer program, can analyze almost any kind of pneumatic servomechanism and the system it is controlling. The system and device to be modeled can contain up to twenty ullage chambers, twenty moving parts (e.g., pistons and poppets), and forty flow lines. The program can be easily modified to model larger systems.

DYNAPS calculates, as a function of time, the position of all moving parts within the system and servomechanism, pressures within the internal chambers of the servomechanism and in any ullage chambers in the complete system, and flow-rates in each line of the system, including sensing lines and main flow passages. DYNAPS has been used in the Space Shuttle Program to make analytical assessments of the dynamic behavior of a regulator controlling the pressure in a tank that has liquid flowing into or out of it. It should also prove useful in the analysis of other pneumatic servomechanisms including pressure regulators, relief valves, pneumatic actuators or positioning devices, shock absorber systems, and surge chambers.

The DYNAPS program comprises five major parts. The first is the main routine that handles all input/output functions and has the "logic" to model the system from the input data. Moving parts, such as pistons, are assumed to be subjected to pressure-area forces, spring forces, breakout friction, dynamic friction, viscous damping, flow drag, and vibration. Every volume is assumed to comprise a multispecies gas and to be connected to other volumes by one or more lines. Each volume may do work on a piston, the piston being either the surface of a moving part or moving liquid surface.

The second and third components of the program set up the necessary rate and position equations and perform the time integration using a Runge Kutta integration algorithm. A fourth component solves the flowrate, mass, and energy equations to determine the rate of change of the pressures, temperatures, and gas composition within each chamber and the flowrate in connecting lines. The fifth component solves the force-balance equations and determines the acceleration history on all moving parts in the system.

The DYNAPS program is written in FORTRAN V and has been implemented on a UNIVAC 1108, under control of EXEC 8, with a central memory requirement of approximately 27K decimal of 36-bit words. DYNAPS can produce plots of the line histories of the sytem variables being studied. Plotting is accomplished on a SC-4020 plotter.

This work was done by T. E. Bailey and G. M. Joseph of Martin Marietta Corp. for **Marshall Space Flight Center.** *For further information, Circle J on the COSMIC Request Card.*
MFS-23295

Mathematics and Information Sciences

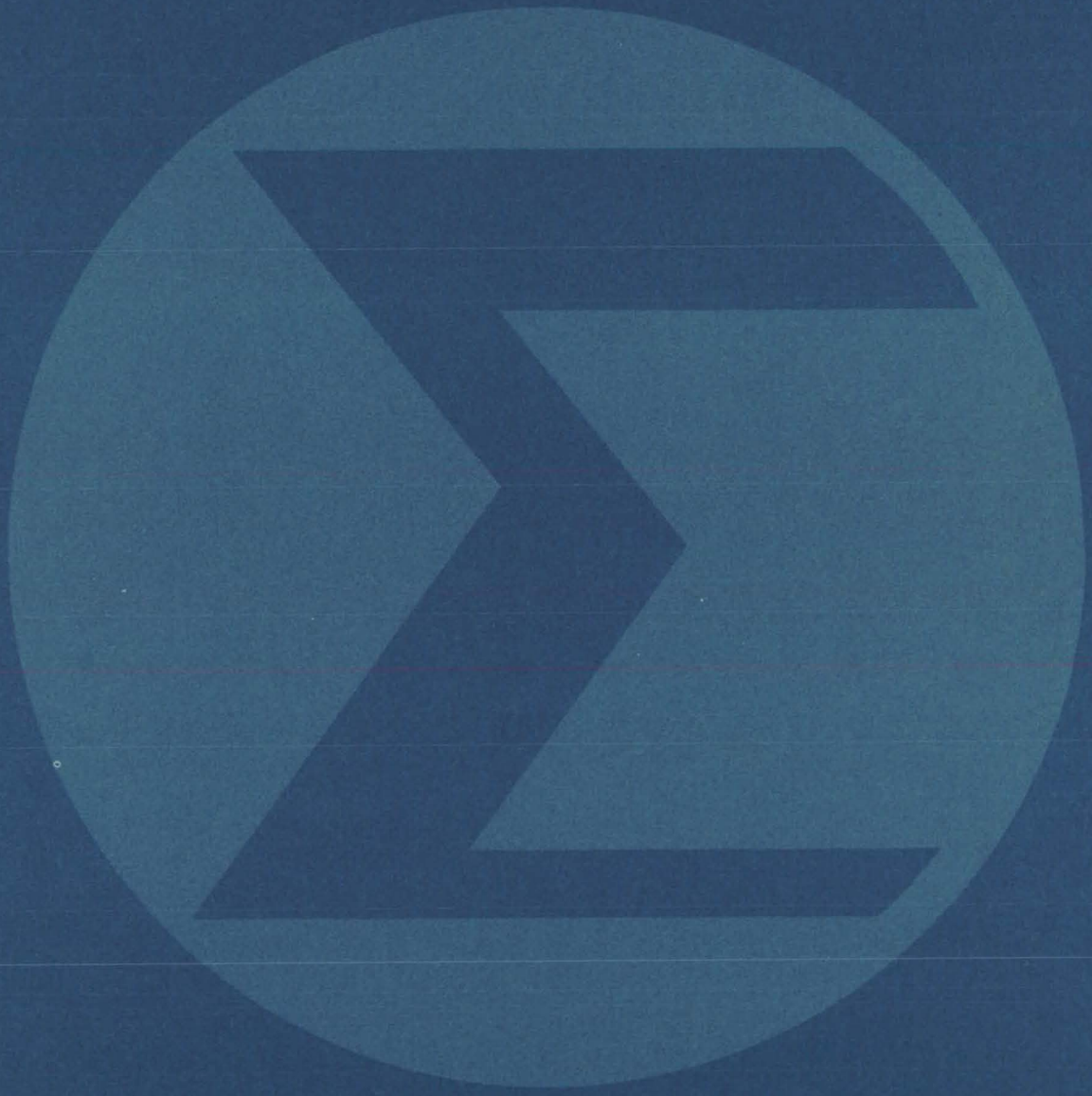

Verification of Redundancy Management Design

A statistical method checks designs by simulating system operating conditions and adding error factors.

Lyndon B. Johnson Space Center, Houston, Texas

Electromechanical systems that must operate unattended for long periods are often designed with redundant subcomponents. Redundancy allows the system to sustain a number of failures and still achieve its objective, or at least avoid a catastrophic accident. Such systems also require a supervisory unit (called a redundancy management system) that processes the redundant signals, detects failures, and reconfigures the system when a failure is detected.

The verification of redundancy management design before its implementation in hardware is a complex problem. Any analytical model should include the complete system dynamics along with all possible error-producing factors. Often, so many simplifying assumptions must be made that key factors are omitted.

A new method for verifying redundancy management design uses a statistical analysis to check system performance without making oversimplifying assumptions. The method considers requirements such as avoiding nuisance failures, detecting faults, and reducing transients incurred as a result of failures. It also verifies the choice of the signal "trip levels" at which components are judged to have failed.

A time history of redundant sensor inputs is developed using a closed-loop model of the system dynamics, sensors, and control system. This "forcing function" is then applied to an open-loop model of the redundant channels to include noise and other failure-inducing effects. The simulation of the open-loop model is repeated many times with a random set of errors selected each time. A "Monte Carlo" statistical analysis is performed, and the data are used in a routine that computes the probabilities of failure over a range of trip-level settings.

This method, which was adopted as the preflight verification sequence for the Space Shuttle Orbiter, has potential commercial and industrial applications where a redundancy management system is used to detect and isolate failed components. It should be particularly useful in applications where signals from redundant channels are compared using trip-level detection as the criterion for failure.

In analyzing the Shuttle system, the method accounted for random noise and the corruption of the redundant channels by vehicle bending caused by turbulence and actuator motion.

This work was done by Hendrik C. Gelderloos and David V. Wilson of Honeywell Inc. for **Johnson Space Center.** *For further information, Circle 78 on the TSP Request Card.*
MSC-16713

Books and Reports

These reports, studies, and handbooks are available from NASA as Technical Support Packages (TSP's) when a Request Card number is cited; otherwise they are available from one of NASA's Industrial Application Centers or the National Technical Information Service.

Model for Redundant-Sensor Signal Errors

Order statistics improve the analysis of system behavior and failure situations.

A report that describes the application of order statistics to the analysis of failure modes in redundant systems should be useful to designers of critical-process control systems. While redundancy management has usually been associated with manned and unmanned flight control and long-term interplanetary missions, its techniques are also relevant to many terrestrial processes that demand high reliability, such as the manufacture of dangerous chemicals and control systems for mass transit.

The order-statistics approach can be applied to a standard redundant system in which the outputs of several sensors are used to monitor the same function. In the lateral accelerometer of the Space Shuttle, for example, four sensors are installed, and one median-selected signal is used for input to the control electronics. If one sensor fails, the redundancy management unit switches to a different median-selected value from among the three remaining units. The decision input for detecting real failures and changing from one sensor to another depends upon the differences between the signals from the redundant sensors.

The premise of the order-statistics concept is that while the redundant signals are independent samples, their distributions are nonnormal and dependent. That is, they tend to keep the same order over longer periods than the sampling rate; the signals having low, middle, and high

(continued next page)

error values will usually remain in the same channels.

On this basis the probabilities and sizes of the maximum signal differences that could cause first and second failures, and the change in selected-sensor output due to a failure, can be calculated from the distribution of transients for each sensor, ordered according to the magnitude of their median values. For many applications, this approach represents the most realistic assessment of the system performance.

The report gives a detailed mathematical discussion of the approach, with relevant graphs and equations. In addition to a presentation of background material, the report discusses the order-statistics formulation of a quad-redundant system, including the cases of first and second failures and estimates of their maximum size. A summary of the failure modes for other switching situations, including triplex redundancy, is also given.

This work was done by Delroy J. Sowada of Honeywell Inc. for **Johnson Space Center.** *To obtain a copy of the report, Circle K on the TSP Request Card.*
MSC-16715

Computer Programs

These programs may be obtained at very reasonable cost from COSMIC, a facility sponsored by NASA to make new programs available to the public. For information on program price, size, and availability, circle the reference letter on the COSMIC Request Card in this issue.

Body-Fitted Coordinate Systems Transformations

Programs for solving partial differential equations

Two new programs, TOMCAT and FATCAT generate two-dimensional body-fitted coordinate systems and coordinate transformations. TOMCAT provides for the automatic numerical generation of a general multiconnected, two-dimensional region containing any number of arbitrarily shaped bodies. The body-fitted coordinate system generated is very useful for numerical solutions of partial differential equations representing physical systems where boundary conditions are the dominant influence on the character of the solution. After a coordinate system has been generated, FATCAT generates the scale factors for use in solving any partial differential equation transformed to the rectangular transformed plane. This package should find use in many fields where accurate numerical representation of boundary conditions and accurate numerical solutions of partial differential equations are desired.

A general method used to generate boundary-fitted coordinate systems is to let the curvilinear coordinates be solutions of an elliptic partial differential system in the physical plane, with Dirichlet boundary conditions on all boundaries. One coordinate is specified to be constant on each of the boundaries, and a monotonic variation of the other coordinate is specified around each boundary. The transformed coordinate system generated has a coordinate line coincident with each boundary, is rectangular in the transformed plane, and has a square mesh in the transformed plane. Thus, in the transformed plane, the numerical solution of a partial differential system may be computed on a fixed rectangular field with a square mesh with no interpolation required regardless of the shape of the physical boundaries, regardless of the spacing of the curvilinear coordinate lines in the physical plane, and regardless of the movement of the coordinate system in the physical plane in problems with time-dependent boundaries.

The coordinate system generated by TOMCAT is not necessarily orthogonal. The lack of orthogonality only requires that the partial differential system to be solved on the coordinate system must be transformed directly through implicit partial differentiation. Not requiring the body-fitted coordinate system to be orthogonal allows arbitrary spacing of the coordinate lines, with the capability for concentrating coordinate lines so that the accuracy of numerical solutions is enhanced. All necessary calculations for making transformations from the physical plane to the transformed plane are performed by FATCAT.

These programs are wirtten in FORTRAN IV for the CDC FTN compiler and have been implemented on a CDC 6000 series computer with a central memory requirement of approximately 216K (octal) of 60-bit words. FATCAT can generate plots of the transformed coordinate system in the physical plane. For plots, the program references the LRCGOS plot library, which is supplied as relocatable code. A Calcomp plotter is required for plotted outout.

This program was written by C. Wayne Mastin, Frank C. Thames, and Joe F. Thompson of Mississippi State University for **Langley Research Center.** *For further information, Circle L on the COSMIC Request Card.*
LAR-12307

SUBJECT INDEX

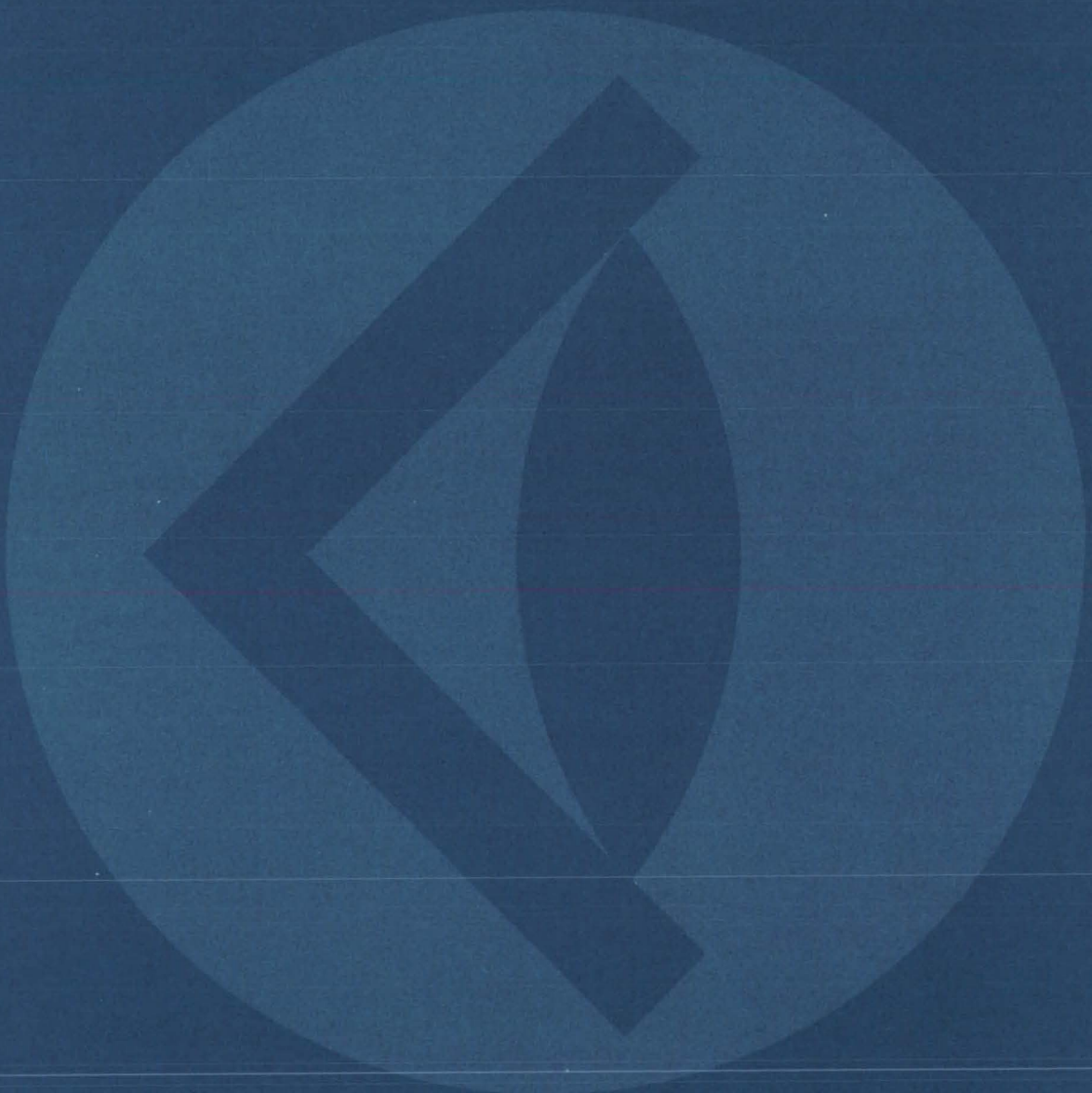

National Aeronautics and
Space Administration

Washington, D C
20546

Official Business
Penalty for Private Use $300

SPECIAL FOURTH-CLASS RATE
BOOK

FOURTH-CLASS MAIL
POSTAGE & FEES PAID
NASA
WASHINGTON, D.C.
PERMIT No. G 27

NASA

Filament-wound air bottles, developed for NASA's Johnson Space Center and Lewis Research Center, are used by scuba divers, firemen, and others. Each bottle is wrapped with 1,670 miles of filament to produce a lighter, stronger container that can hold more oxygen in a given volume.